Atomic Energy Control Board
P.O. Box 1046
Ottawa, Canada
K1P 5S9

Commission de contrôle de l'énergie atomique
C.P. 1046
Ottawa, Canada
K1P 5S9

INFO-0136-2

THERMAL AND HYDRAULIC BEHAVIOR OF CANDU CORES UNDER SEVERE ACCIDENT CONDITIONS - FINAL REPORT

VOLUME 1 - ANALYTICAL METHODS AND RESULTS

by

J.T. Rogers
Carleton University

A research report prepared for the
Atomic Energy Control Board
Ottawa, Canada

RESEARCH REPORT

June 1984

THERMAL AND HYDRAULIC BEHAVIOR OF CANDU CORES UNDER SEVERE ACCIDENT CONDITIONS FINAL REPORT

ABSTRACT

This report gives the results of a study of the thermo-hydraulic aspects of severe accident sequences in CANDU reactors. The accident sequences considered are the loss of the moderator cooling system and the loss of the moderator heat sink, each following a large loss-of-coolant accident accompanied by loss of emergency coolant injection.

Factors considered include expulsion and boil-off of the moderator, uncovery, overheating and disintegration of the fuel channels, quenching of channel debris, re-heating of channel debris following complete moderator expulsion, formation and possible boiling of a molten pool of core debris and the effectiveness of the cooling of the calandria wall by the shield tank water during the accident sequences. The effects of these accident sequences on the reactor containment are also considered.

Results show that there would be no gross melting of fuel during moderator expulsion from the calandria, and for a considerable time thereafter, as quenched core debris re-heats. Core melting would not begin until about 135 minutes after accident initiation in a loss of the moderator cooling system and until about 30 minutes in a loss of the moderator heat sink. Eventually, a pool of molten material would form in the bottom of the calandria, which may or may not boil, depending on property values. In all cases, the molten core would be contained within the calandria, as long as the shield tank water cooling system remains operational. Finally, in the period from 8 to 50 hours after the initiation of the accident, the molten core would re-solidify within the calandria.

There would be no consequent damage to containment resulting from these accident sequences, nor would there be a significant increase in fission product releases from containment above those that would otherwise occur in a dual failure LOCA plus LOECI.

RÉSUMÉ

Le présent rapport fournit les résultats d'une étude des caractéristiques thermohydrauliques des séquences d'accidents graves dans les réacteurs CANDU. Les séquences d'accidents à l'étude sont la perte du système de refroidissement du modérateur et la perte du modérateur comme source de refroidissement qui se produisent à la suite d'un accident majeur de perte de caloporteur accompagné d'une perte d'injection de caloporteur d'urgence.

Les divers facteurs retenus comprennent l'évacuation et l'ébullition progressive du modérateur, la mise à nu, le surchauffage et la désintégration des canaux de combustibles, le refroidissement subit des débris de canal, le réchauffage des débris de canal à la suite d'une évacuation totale du modérateur, la formation et l'ébullition possible d'une masse de débris du coeur en fusion, ainsi que l'efficacité du refroidissement de la paroi de la cuve par l'eau des boucliers thermiques, au cours des séquences d'accidents. Le rapport traite aussi des effets de ces séquences d'accidents sur l'enceinte de confinement du réacteur.

Les résultats indiquent qu'il n'y aurait aucune fusion à grande échelle du combustible lors de l'évacuation du modérateur hors de la cuve, ainsi que pendant une période de temps ultérieure considérable au cours de laquelle les débris du coeur refroidis subitement se réchaufferaient. La fusion du coeur ne commencerait qu'environ 135 minutes après le début d'une perte du système de refroidissement du modérateur, et qu'environ 30 minutes après le début d'une perte du modérateur comme source de refroidissement. Une masse de matières en fusion se formerait éventuellement au fond de la cuve et pourrait bouillir ou non, selon ses propriétés. Dans tous les cas, le coeur en fusion serait contenu à l'intérieur de la cuve aussi longtemps que le système de refroidissement des boucliers thermiques demeurerait opérationnel. Finalement, entre 8 et 50 heures après le début de l'accident, le coeur en fusion se solidifierait de nouveau à l'intérieur de la cuve.

Les séquences d'accidents susmentionnées n'endommageraient pas l'enceinte de confinement et l'augmentation des rejets de produits de fission de l'enceinte de confinement ne serait pas supérieure à celle qui se produirait dans le cas d'une défaillance double, c'est-à-dire une perte caloporteur et une perte d'injection du caloporteur d'urgence.

DISCLAIMER

The Atomic Energy Control Board is not responsible for the accuracy of the statements made or opinions expressed in this publication and neither the Board nor the author assumes liability with respect to any damage or loss incurred as a result of the use made of the information contained in this publication. This work was produced by Carleton University, with J.T. Rogers as principal investigator, under contract to the Atomic Energy Control Board; contract no. OSU82-00079.

TABLE OF CONTENTS

VOLUME 1. ANALYTICAL METHODS AND RESULTS

	Page
List of Figures	xi
List of Tables	xiii
Nomenclature	xiv
1. INTRODUCTION	1
2. BACKGROUND AND APPROACH	2
3. SELECTED ACCIDENT SEQUENCES	4
3.1 Accident Sequences S11 and S12 - Loss of Moderator Cooling System (LOMCS)	4
3.2 Accident Sequences S13 and S14 - Loss of Moderator Heat Sink (LOMHS)	5
3.3 Accident Sequences S15 and S16 - Failure to Shut Down	5
4. ASSESSMENT OF ACCIDENT SEQUENCES S11 AND S12: LOCA + LOECI + LOMCS	6
4.1 Analytical Flow Chart for Accident Sequences S11 and S12	6
4.2 Initiation of Accident Sequences S11 and S12	6
4.3 Heat Source to the Moderator as a Function of Time	7
4.4 Thermal-Hydraulic Behavior of the Moderator	10
4.4.1 SUBCOOL	12
4.4.2 MODBOILSUB	14
4.4.2.1 Sub-cooled Boiling and Onset of Bulk Boiling	14
4.4.2.2 Mass and Energy Balances For Bulk Boiling Conditions	14
4.4.2.3 Void Fractions For Bulk Boiling Conditions	17
4.4.2.4 Redistribution of Downward Flowing Liquid Among Slices	18
4.4.2.5 Pressure Gradients in Calandria and Relief Ducts	19
4.4.2.6 Uncovery of Calandria Tubes	20
4.4.2.7 Behavior of Fuel Channels after Uncovery of Calandria Tubes	21
4.4.2.8 Choked Flow in the Relief Ducts	25
4.4.3 MODBOILALL	26
4.5 Thermal Analysis of Uncovered Calandria Tubes - IMPECC-UCZ	26
4.5.1 Basic Model	26
4.5.2 Heat Transfer Coefficients	27
4.5.3 Zircaloy-Steam Reaction Heat Source	31

		Page
4.6	Thermal Behavior of Fuel Channel Debris	33
4.6.1	Transient Thermal Behavior of Solid Debris	34
4.6.1.1	Characteristics of Debris	34
4.6.1.2	Basic Heat Transfer Model and Property Values	34
4.6.1.3	Boundary and Initial Conditions	39
4.6.1.4	Computer Program DEBRIS	41
4.6.2	Effect of Molten Pool of Core Debris on Calandria Wall	41
4.6.2.1	Thermal Behavior of Heat-Generating Molten Pools	42
4.6.2.1.1	Non-boiling Pools	43
4.6.2.1.2	Boiling Pools	46
4.6.2.1.3	Computer Program MOLTENPOOL	47
4.6.2.2	Interaction of Molten Pool with Calandria Wall	48
4.6.2.3	Interaction of Vaporized Core Material with Calandria Wall	53
4.7	Behavior of Fuel Channel Debris in Shield Tank	59
4.8	Interaction of Molten Core Material with Concrete	60
4.8.1	Probability of Molten Core Interaction with Concrete	60
4.8.2	Behavior of Concrete Exposed to Molten Core Material	60
4.8.3	Analytical Model of Molten Core Material - Concrete Interaction	62
4.9	Containment Pressurization	69
4.9.1	Causes of Containment Pressurization	69
4.9.2	Analytical Model of Containment Pressurization	69
5.	RESULTS OF ASSESSMENT OF ACCIDENT SEQUENCES S11 AND S12: LOCA + LOECI + LOMCS	71
5.1	Heat Source to Moderator	71
5.2	Thermal-Hydraulic Behavior of Moderator and Thermal Behavior of Uncovered Fuel Channels	72
5.2.1	Moderator Behavior Before Channel Uncovery	73
5.2.2	Moderator Behavior With No Channel Disintegration After Uncovery	76
5.2.3	Thermal Behavior of Uncovered Fuel Channels	76
5.2.3.1	Method of Approach	76
5.2.3.2	Calandria Tube and Fuel Temperatures	77
5.2.3.3	Prediction of Delay Time to Channel Disintegration	81

Page

5.2.4 Moderator Behavior With Channel Disintegration 84

5.2.4.1 Reference Conditions 84

5.2.4.2 Sensitivity Assessment 86

5.2.5 Effect of Steam Superheating 88

5.2.6 Effect of Deuterium Production in the Calandria 90

5.2.7 Summary and Conclusions on Moderator Expulsion and Uncovered Fuel Channel Behavior 95

5.3 Thermal Behavior of Fuel Channel Debris in Bottom of Calandria 97

5.3.1 Thermal Behavior of Solid Debris Bed in Bottom of Calandria 97

5.3.2 Thermal Behavior of a Molten Pool of Core Debris 102

5.3.2.1 Internal Characteristics of a Molten Pool 102

5.3.2.2 Interaction of Molten Pool of Core Debris with Calandria Wall 106

5.3.2.2.1 Interaction of Liquid Pool Itself with Calandria Wall 106

5.3.2.2.2 Interaction of Vaporized Core Material with Calandria Wall 109

5.4 End Point for Accident Sequences S11 and S12 110

5.5 Containment Pressurization and Effects in Accident Sequences S11 and S12 112

6. ASSESSMENT OF ACCIDENT SEQUENCES S13 AND S14: LOCA + LOECI + LOMHS 117

6.1 Introduction 117

6.2 Initiation of Accident Sequences S13 and S14 118

6.3 Moderator Discharge Rate Through Ruptured Outlet Pipe 118

6.3.1 Description of Accident Sequences 118

6.3.2 Analytical Model for Moderator Discharge Through Pipe Break 119

6.3.3 Criterion for Channel Disintegration 124

7. RESULTS OF ASSESSMENT OF ACCIDENT SEQUENCES S13 AND S14: LOCA + LOECI + LOMHS 125

7.1 Heat Source to Moderator 125

7.2 Discharge of Moderator from Calandria 125

7.3 Behavior of Fuel Channel Debris 128

7.4 Thermal Behavior of Molten Pool of Core Debris 132

7.4.1 Internal Characteristics of the Molten Pool 132

7.4.2 Interaction of Molten Pool with Calandria Wall 134

		Page
7.4.2.1	Interaction of Liquid Pool Itself with Calandria Wall	134
7.4.2.2	Interaction of Vaporized Core Material with Calandria Wall	135
7.5	End Point for Accident Sequences S13 and S14	138
7.6	Containment Pressurization and Effects in Accident Sequences S13 and S14	138
8.	GENERAL CONCLUSIONS	140
References		143
Figures		153
Acknowledgements		203

VOLUME 2. APPENDICES

A.	MAJOR FEATURES OF IMPECC-Z COMPUTER PROGRAM	A1
B.	COMPUTER PROGRAM MODBOIL	B1
1.	Listing of MODBOIL	B2
2.	Sample Output of MODBOIL	
C.	VAPOR EXPLOSIONS	C1
1.	Introduction	C1
2.	Mechanisms and Characteristics of Vapor Explosions	C1
3.	Experimental Results with UO_2, Zirconium and Zr O_2	C8
4.	Application of Results and Criteria to Accident Sequences in CANDU	C10
4.1	Accident Sequences S11 and S12	C12
4.2	Accident Sequences S13 and S14	C13
5.	External Triggering of Vapor Explosions	C15
6.	Efficiency of Coherent Molten Fuel-Coolant Interaction and Calculated Effect on Calandria Vessel	C17
7.	Conclusion	C20
D.	COMPUTER PROGRAM DEBRIS	D1
1.	Listing of DEBRIS	D2
2.	Sample Output of DEBRIS	
E.	COMPUTER PROGRAM MOLTENPOOL	E1
1.	Molten Pool Property Values	E2
2.	Listing of MOLTENPOOL	E3
3.	Sample Output of MOLTENPOOL	

		Page
F.	AVERAGE CONDENSATION HEAT TRANSFER COEFFICIENT FOR VAPORIZED CORE MATERIAL ON THE CALANDRIA WALL	F1
G.	COMPUTER PROGRAM CONFILM	G1
	1. Listing of CONFILM	G2
	2. Sample Output of CONFILM	
H.	ANALYTICAL MODEL OF CONTAINMENT PRESSURIZATION	H1
I.	COMPUTER PROGRAM BLDG	I1
	1. Listing of BLDG	I2
	2. Sample Output of BLDG	

LIST OF FIGURES

Figure		Page
1.	CANDU LOCA Functional Event Tree, Accident Sequences	153
2.	CANDU Reactor Isometric Diagram	154
3.	Analytical Flow Chart for Accident Sequences S11 and S12	155
4.	Heat Production Rate by Zircaloy-Water Reaction. Bruce Maximum Power Channel Conditions	164
5.	Control Volume Used in MODBOIL	165
6.	Network Diagram for Radiation Heat Transfer From Uncovered Calandria Tube	166
7.	Determination of Configuration Factor for Calandria Tubes	167
8.	Analytical Model for Molten Material on Calandria Wall	168
9.	Map of Conditions for Melting of Calandria Wall	169
10.	Non-dimensional Unmelted Wall Thickness Diagram	170
11.	Non-dimensional Solidified Crust Thickness Diagram	171
12.	Geometry of Molten Pool of Core Material and Melted Concrete	172
13.	Reactor Vault Cooler Capacity	173
14.	Total Heat Input Rate to Moderator. Bruce-A Unit	174
15.	Calandria Pressure at Base of Relief Ducts. Reference Conditions	175
16.	Void Profiles Across Calandria	176
17.	Mass of Moderator Remaining in Calandria vs. Time. No Channel Disintegration	177
18.	Moderator Expulsion Rate. No Channel Disintegration	178
19.	Times of Row Uncovery. No Channel Disintegration	179
20.	Maximum Calandria Tube Temperatures for Top Row	180
21.	Maximum Calandria Tube Temperature for Rows 4 and 12	181
22.	Maximum Fuel Temperatures in Different Rows	182
23.	Maximum Fuel and Calandria Tube Temperatures. Sensitivity Study Results	183
24.	Moderator Expulsion Rate. Reference Conditions	184
25.	Times of Row Uncovery and Disintegration. Reference Conditions	185
26.	Mass of Moderator Remaining in Calandria vs. Time. Reference Conditions	186

		Page
27.	Effect of FRCMAS on Moderator Remaining in Calandria	187
28.	Effect of FRMELT on Moderator Remaining in Calandria	188
29.	Mass of Moderator Remaining in Calandria with Instantaneous Disintegration. Effects of Debris Temperature	189
30.	Heat Flow Rates from Uncovered Calandria Tubes to Steam for Various Conditions	190
31.	Estimated Steam Temperature at Uppermost Row of Intact Tubes. Reference Conditions	191
32.	Temperatures in Porous Bed of Solid Core Debris	192
33.	Temperature Profiles Across Porous Bed of Solid Core Debris. Reference Conditions	193
34.	Effects of Pore Size on Characteristics of Porous Debris Bed	194
35.	Core Debris Molten Pool Characteristics Property Sets 1 and 2	195
36.	Core Debris Molten Pool Characteristics Property Sets 3 and 4	196
37.	Effect of Heat Flux from Core Debris Molten Pool on Calandria Wall	197
38.	Containment Pressure and Temperature for Reference and Instantaneous Disintegration Conditions	198
39.	Containment Pressure and Temperature. Sensitivity Study Results	199
40.	Model for Moderator Drainage from Calandria. Accident Sequences S13 and S14	200
41.	Moderator Liquid Level in Calandria. Accident Sequences S13 and S14	201
42.	Volumetric Discharge Rates from Calandria. Accident Sequences S13 and S14	202

LIST OF TABLES

Table		Page
1.	Grouping of Channels and Characteristics of Each Group. Bruce-A Reactor Unit	8
2.	Data for IMPECC-UCZ Runs Used to Establish Equation for Fuel Channel Disintegration Times, Equation 16	82
3.	Average Deuterium Gas Production Rates and Steam Consumption Rates from Uncovered Calandria Tubes Established from IMPECC-UCZ Runs	93
4.	Maximum Effects of Deuterium Gas Production on Calandria Pressure. Reference Conditions	94
5.	Results of MOLTENPOOL Analysis for Reference Conditions	104
6.	Condensation of Vaporized Core Debris on Calandria Wall	111
7.	Characteristics of Solid Debris Bed in Bottom of Calandria at Initiation of Melting. Accident Sequences S13 and S14	130
8.	Results of MOLTENPOOL Analysis for Accident Sequences S13 and S14	133
9.	Condensation of Vaporized Core Debris on Calandria Wall. Accident Sequences S13 and S14	136
C-1	Composition of Corium, Atom Per Cent	C9
E-1	Molten Pool Properties	E1

NOMENCLATURE

A	- area
A_{cd}	- area of calandria wall exposed to vaporized core material, m^2
A_{CW}	- surface area of containment boundaries, m^2
A_p	- area of interface between molten pool and underlying concrete, m^2
A_p	- cross-sectional area of moderator inlet pipe to calandria, m^2
A_r	- rate constant, $cm/s^{\frac{1}{4}}$
A_T	$= \frac{T_H - T_C}{T_C}$
Bi	- Biot number
Bi_a	- defined by equation 43
Bi_{ac}	- defined by equation 45
C	- concentration, moles/mole
C	- coefficient in equation 16, = 0.17
C_C	- specific heat of moderator on contact with molten core materials, J/kgK
C_H	- specific heat of molten core materials, J/kgK
C_o	- void distribution parameter
C_p	- specific heat, J/kgK
C_{Va}, C_{VD}	- specific heat at constant volume of containment air and deuterium gas respectively, J/kgK
CI	- containment impairment
CON	- containment
D	- diffusion coefficient for steam through hydrogen, cm^2/s
DF	- dual failure
d_o	- outside diameter of calandria tubes, m or cm
d_p	- fuel pellet diameter, m
E_b	- emissive power of a black body, W/m^2
E_g	- activation energy for de-hydration or decomposition reaction in concrete, kJ/mole or k cal/mole
ECI	- emergency coolant injection
ECLT	- emergency cooling - long term

EXPN - exponent in equation 16, = 1.6

ΔE - activation energy for diffusion of O_2 in Zr O_2, J/gm-mole

F - factor to allow for thermal resistance of contacts between fragments in debris bed

F_N - factor to allow for reduced vault cooler capacity

F_{ij} - radiation configuration factor between surfaces i and j

FEPR(N) - average fuel element power rating in slice N, W/cm

FRCMAS - fraction of mass of uncovered, disintegrated channels which falls to bottom of calandria

FRMELT - fraction of Zircaloy in mass of falling channels which is initially molten

F_B - radiation interchange factor for cubical pore structure representing debris bed

F_T - radiation interchange factor between upper surface of debris bed and calandria wall

f_d - fraction of molten pool heat source which flows downward into concrete

f_o - constant coefficient in fission power decay heat equation, $f_o = 0.13$ for the ANS decay heat equation for long times

f(t) - fission power decay heat equation, defined by equation 71

g - acceleration of gravity, m/s^2

g_c - gravitational constant, $\frac{kg\ m}{N\ s^2}$

h_b - heat transfer coefficient from molten pool of core material to edge of pool, W/mK

h_c - convection heat transfer coefficient, W/m^2K

h_c - heat transfer coefficient of shield tank water on calandria wall, W/mK

h_D - mass transfer coefficient, cm/s

h_f - enthalpy of liquid

h_g - enthalpy of vapor

h_r - radiation heat transfer coefficient, W/m^2K

h_{cd} - condensation heat transfer coefficient, W/m^2K

h_{fg} - latent heat of vaporization

h'_{fg} - modified latent heat of vaporization to allow for sub-cooling of film in film condensation, defined by equation 104, J/kg

j_f - volumetric flux (superficial velocity) of liquid

j_g - volumetric flux (superficial velocity) of vapor

$j_{g\infty}$ - superficial vapor velocity at the upper surface of a boiling, heat generating pool, m/s

K_g - coefficient in reaction rate equation for gas evolution from concrete, sec^{-1}

K_R - Rosseland absorption coefficient, m^{-1} or cm^{-1}

K_T - total loss coefficient for flow in broken moderator inlet pipe

k - thermal conductivity, W/mK

k_B - effective thermal conductivity of debris bed, W/mK

k_C - thermal conductivity of moderator on contact with molten core material, W/mK

k_f - thermal conductivity, evaluated at the film temperature, W/mK

k_H - thermal conductivity of molten core materials, W/mK

k_M - weighted mean thermal conductivity of solid materials in debris bed, W/mK

k_m - thermal conductivity of molten wall material, W/mK

k_s - thermal conductivity of solidified crust of core material, W/mK

L - internal length of calandria, m

L_d - molten pool maximum depth, m

LOCA - loss-of-coolant accident

LOECI - loss-of emergency coolant injection

M - molecular weight

M_a - mass of air in containment, kg

M_C - mass of moderator mixing with molten core material, kg

M_D - mass of deuterium gas in containment, kg

M_f - mass of heavy water liquid in containment, kg

M_g - mass of heavy water vapor in containment, kg

M_H - mass of molten core material mixing with coolant, kg

MCS - moderator cooling system

MHS - moderator heat sink

δM_g, δM_f, δM_D - masses of D_2O vapor, D_2O liquid and deuterium gas discharged from calandria relief ducts in a time increment, kg

m - mass, kg

$\dot{m}_m$ - rate of discharge of moderator from calandria, kg/s

$m_f(N)$ - mass of liquid in slice N, kg

$m_g(N)$ - mass of vapor in slice N, kg

$\dot{m}_f(N)$ - mass flow of liquid entering slice N, kg/s

$\dot{m}_g(N)$ - mass flow of vapor entering slice N, kg/s

$\overline{\dot{m}_{D_2}}$ - average deuterium gas production rate per channel, lb_M/hr or kg/s

$\delta\dot{m}_f$ - net rate of liquid mass change in a slice ($\delta\dot{m}_f(N) = \dot{m}_f(N-1) - \dot{m}_f(N)$)

$\delta\dot{m}_g$ - net vapor mass generation rate in a slice ($\delta\dot{m}_g(N) = \dot{m}_g(N-1) - \dot{m}_g(N)$)

$\overline{\delta\dot{m}_{st}}$ - average steam consumption rate per channel from Zircaloy steam reaction, lb_M/hr or kg/s

N - slice (node) identification, numbered from top to bottom

N - conduction-radiation coupling parameter, equation 37

Nu - Nusselt number in a molten heat-generating pool allowing for both natural convection or boiling and for internal thermal radiation

Nu' - Nusselt number for a molten heat generating pool ignoring the effects of thermal radiation, defined by equation 33

n - index of refraction

n_g - exponent in reaction rate equation for decomposition of concrete, equation 58

Pr_f - Prandtl number evaluated at the film temperature

p_i - pressure over moderator surface, kPa or psia

p_∞ - reactor vault pressure, kPa or psia

Q_o - initial reactor power, W

Q_H - heat loss to boundaries of containment in a time step, Joules

Q_R - heat removed from containment atmosphere by vault coolers in a time step, Joules

$Q(\theta_g, \theta_b)$ - geometric factor governing core material vapor average condensation coefficient on the calandria wall, defined by equation 52

$\dot{Q}_{gz}$ - rate heat generation in fuel by fission product decay and Zircaloy-steam reaction of cladding, W/m

$\dot{Q}_i(N)$ - power into slice N from the fuel channels, W

$\dot{Q}_o(N)$ - rate of heat flow from slice N to the calandria wall, W

$\dot{Q}_s(N)$ - rate of heat storage in slice N, W

q_r - heat transfer rate by radiation, W

q_v - actual core-average volumetric heat source in fuel material, or average volumetric heat source in molten pool, W/m^3

q_{vB} - effective volumetric heat source in debris bed allowing for dilution effect of structural material and for porosity of bed, W/m^3

q'' - heat flux, W/m^2

q''_{mC} - heat flux into concrete from molten pool of core debris and concrete, W/m^2

R - inner radius of calandria, m

R_e - radius of a hypothetical calandria without calandria tubes with a free volume equal to that of the actual calandria, m

R_o - universal gas constant, 8.3202 J/gm. mole K.

Ra - Rayleigh number for a molten heat-generating pool based on pool depth and volumetric heat source, defined by equation 34

Re_{max} - Reynolds number for steam flow over a row of calandria tubes, based on the mass velocity at the smallest cross-flow area for the row

RTB - correction factor to allow for reduced cross-flow heat transfer coefficients in the first few rows of a tube bank

r - radius, cm or m

r_o - radius of melt front in concrete, m

r_{cm} - maximum radius of molten pool in concrete, m

r_p - $p_i/(p_i + \rho_f \frac{g}{g_c} z_m)$

S - Stefan number for concrete, defined by equation 75

Sc - Schmidt number, $\frac{\nu}{D}$

SD - shut down (special safety system)

SF - single failure

T - temperature, ^oC or K

T_B - average temperature of containment atmosphere, ^oC or K

T_{Bi} - initial temperature of containment atmosphere, ^oC or K

T_{BPU} - boiling point of molten core material, K

T_b - average temperature of pool of molten debris, ^oC

T_C - temperature of moderator on contact with molten core materials, ^oC

T_C - concrete temperature, ^oC

T_{C_m} - effective melting temperature of concrete, ^oC

$T_{C\infty}$ - concrete temperature remote from the molten pool of concrete and core debris, ^oC

T_c - temperature of shield tank water as coolant on calandria wall, ^oC

$\overline{T}_{Fa}$ - mean (weighted average) fuel temperature assuming adiabatic conditions, ^oC or K

T_f - freezing temperature of molten core material, ^oC

T_H - temperature of molten core materials on contact with moderator, ^oC

T_i - interface temperature on initial contact between molten core materials and moderator, ^oC

T_{MFB} - minimum film boiling temperature, ^oC

T_{MPU} - melting point of core material, K

T_m - melting temperature of calandria wall, ^oC

T_{SAT} - saturation temperature, ^oC

T_{SN} - spontaneous nucleation temperature, ^oC

T_{WB} - average surface temperature of containment boundaries, ^oC or K

TCT - calandria tube temperature, ^oC or K

TFl - fuel temperature, ^oC or K

TRS - steam temperature, ^oC or K

ΔT_C = $T_{Cm} - T_{C\infty}$, K

t - time, s, m or hr

t_e - total time to drain calandria, s or m

t_m - time at which maximum radius of molten pool in concrete is reached, s

$t_{uc}(N)$ - time to uncovery of calandria tubes in slice N, minutes

δt - time increment in computer program, s

$\delta t_d(N)$ - delay time after calandria tube uncovery until channel disintegration in slice N, minutes

U - overall heat transfer coefficient for the calandria wall and the shield tank water, defined by equation 56

U_e - internal energy of containment fluids, Joules

U'_e - new value of internal energy of fluids in containment at the end of a time step, Joules

U''_e - trial value of internal energy of fluids in containment used in trial and error analysis, Joules

U_H - heat transfer coefficient to containment boundaries, W/mK

δU_e - internal energy of fluids discharged from calandria in δt, Joules

u_{mC} - velocity of melt front in concrete, m/s = dr_o/dt

V - free volume in a slice, m^3

V_{gu} - volume of core material vapor in layer above boiling pool, m^3

V_u - total volume of UO_2 in core, m^3

V_z - total volume of structural material in fuel channels, m^3

$\dot{V}_f$ - volumetric flow rate of liquid moderator, ft^3/s or m^3/s

$\dot{V}_g$ - volumetric flow rate of air in slug counter flow, ft^3/s or m^3/s

v_{gj} - vapor drift velocity, m/s

$v_{s\infty}$ - slug rise velocity, m/s

v_∞ - bubble rise velocity, m/s

w - half-width of debris or molten pool surface in bottom of calandria, m

w_m - width of liquid moderator surface in calandria, m

x_C - distance into concrete from interface of molten pool, m

y_m - vertical distance between horizontal mid plane of calandria and surface of moderator at any time, m. (See Figure 40)

z - vertical distance from top surface of debris bed, m

$\bar{Z}$ - average depth of molten pool, m

z_o - difference in elevation between bottom of calandria and centre line of rupture in moderator outlet pipe, m

z_m - height of liquid moderator in the calandria, m

dz/dt - rate of growth of $Zr\,O_2$ layer in Zircaloy, cm/s

α - thermal diffusivity, m^2/s

α - constant exponent in fission power decay heat equation, $\alpha = 0.283$ for the ANS decay heat equation for long times

α - void fraction

α' - void fraction at previous time step

α_B - effective thermal diffusivity of debris bed, m^2/s

α_C - thermal diffusivity of concrete, m^2/s

β - volumetric coefficient of expansion, K^{-1}

β_g - concentration of gas evolved by heating of concrete, moles/mole

$\beta_1, \beta_2, \beta_3$ - parameters governing growth of solidified layer of core material under condensing film on calandria wall, defined by equations 55a to 55c

Γ - condensate film flow rate per unit length of film, kg/ms

δ - film thickness, m

δ_a - initial thickness of calandria wall, m

δ_m - value of $\delta(t)$ at t_m, m

δ_p - mean pore dimension, m

δ_s - thickness of solidified crust of molten core material, m

δ_w - ultimate steady-state thickness of solid portion of partially melted calandria wall, m

$\delta(t)$ - parameter related to the velocity of the melt front for a molten pool in concrete; the "thermal boundary layer" thickness in the concrete, m

ε - emissivity

ε_v - porosity of debris bed

η_M - maximum theoretical efficiency of an MFCI, eq. 94

θ - half-angle at calandria centre-line subtended by debris or molten pool surface, radians, or simply half-angle measured from bottom of calandria, radians

θ_b - half-angle at calandria centre-line subtended by upper surface of boiling pool, radians

θ_C - non-dimensional temperature of concrete, defined by equation 61

θ_g - half-angle at calandria centre-line subtended by upper boundary of vaporized core material, radians

θ_m - ratio of maximum temperature to surface temperature in a molten pool. Temperature in Kelvins

λ - latent heat of fusion of molten core material, J/kg

λ' - product of fraction of original fuel mass which arrives at a concrete surface and fraction of fission products remaining in the fuel mass which arrives at a concrete surface

μ - dynamic viscosity, kg/m s

μ_M = $M_C C_C / M_H C_H$

ν - kinematic viscosity, m^2/s

ρ - density, kg/m^3 or gm/cm^3

ρ_C - density of moderator on contact with molten core materials, kg/m^3

ρ_H - density of molten core materials, kg/m^3

ρ_m - weighted mean density of solid materials in debris bed, kg/m^3

ρ_s - density of solidified core material in sub-layer under condensing film layer, kg/m^3

$(\rho\lambda)_C$ - effective latent heat of fusion of concrete, per unit volume, J/m^3

σ - Stefan-Boltzmann constant, 5.669×10^{-8} W/m^2K^4

σ - surface tension, N/m

ϕ - defined by equations 42 or 44

Subscripts (Not defined elsewhere)

B - debris bed

BP - boiling point

b - boiling, or molten pool

C - concrete or cold fluid

c - calandria tube

cs - calandria wall above debris bed or molten pool

d - downwards

f - liquid

fg - vaporization

g - vapor

MP - melting point

s - steam

T - top surface of debris bed

u or U - fuel material

u - upwards

w - wall or surface

z - Zircaloy or $Zr O_2$

2 - calandria tubes surrounding a given calandria tube

THERMAL AND HYDRAULIC BEHAVIOR OF CANDU CORES UNDER SEVERE ACCIDENT CONDITIONS FINAL REPORT

1. INTRODUCTION

This report describes the results of a research study undertaken for the Atomic Energy Control Board under contract OSU82-00079 on the thermal and hydraulic behavior of CANDU cores under accident conditions more severe than those normally considered in the licensing process. This work was a continuation of one aspect of a study undertaken under a previous contract, OSU80-00237. For completeness, the results obtained on this aspect of the previous study, as reported in reference 1, are summarized here, as are relevant results from an earlier project, as reported in reference 2.

Certain results of the present study have been presented in reference 3.

The objective of the present study was to provide AECB with increased knowledge on the safety of CANDU reactors, in particular on the possible consequences of severe accident sequences so as to assist in establishing more extensive assessments of risk to the public and to facilitate examination of licensing submissions.

This investigation was not intended to be a comprehensive study of accident risks such as those of the Reactor Safety Study (the Rasmussen study)(4), the German Risk Study (5) or more recent PRA's (6). Only a single type of accident was selected for study, a large Loss-of-Coolant Accident (LOCA), and the study was confined mainly to thermal and hydraulic physical processes with no estimates of probabilities of accident sequences being included, nor calculations of fission product releases made. Manpower and budgeting constraints also prevented thorough analyses of all aspects of the selected accident sequences.

It must be recognized that the behavior of core components under the extreme conditions considered in this study is, in general, quite speculative since little experimental information on core component behavior and physical phenomena under these conditions are available. The approach used in the study has been to attempt to model physical behavior of core components and the moderator on a physically-sound basis, as far as possible, and to provide flexibility in the computer programs developed and used in the analyses. This flexibility has enabled the sensitivity of core behavior to various assumptions to be examined

and will permit improvements in the analyses as more experimental information becomes available. Obviously, the analyses at this stage have considerable uncertainties associated with them so that results must be treated with some caution.

2. BACKGROUND AND APPROACH

In the initial stages of the project, considerable thought was devoted to the approaches and methods to be used. An event tree for a large LOCA, as shown in Figure 1, was developed to identify potential event sequences following the LOCA. The code used to identify events in Figure 1 is defined in the Nomenclature. In the event tree, the upper branch for any event indicates success, the lower branch failure. In this event tree, the emergency cooling function has been divided into two stages, emergency coolant injection (ECI) and emergency coolant long-term recirculation (ECLT). Also, the unique safety feature of CANDU reactors, the moderator heat sink (MHS) with its cooling system (MCS), is recognized. Studies of severe accident conditions in CANDU reactors show that there will be no fuel melting even for a large LOCA combined with loss of emergency coolant injection (LOECI) provided that the moderator heat sink and the moderator cooling system are effective (1,2,7,8,9).

Accident sequence S1 in Figure 1 represents the conventional large LOCA single-failure (SF) accident, as analyzed in the Canadian licensing process, in which all the special safety systems function as intended. In this sequence, MHS and MCS are not generally needed and therefore no options are shown for these systems.*

The dual failures considered in the licensing process, i.e., LOCA plus containment impairment (CI) and LOCA plus LOECI are shown in accident sequences S2 and S9 respectively.

In Figure 1, success of the containment function is included as a possibility in each accident sequence. This option differs from that used in the Rasmussen

---

*In certain cases of LOCA's with early stagnation during blowdown, pressure tube ballooning may occur, which could require the MHS and MCS to assist the emergency cooling system in providing adequate cooling of the fuel (7). This accident sequence has not been considered directly in this study, and is not shown in Figure 1.

study, in which it was assumed that any core melt-down in a LWR resulted in containment failure, either by over-pressure or by core melt-through. Potential containment success is included here since it is not evident that severe core damage will result in consequent containment failure for a CANDU reactor.

Many theoretical accident sequences or events have been eliminated in Figure 1 because they are illogical or irrelevant. For example, it is assumed that failure to shut down the reactor results in core melt-down and makes the operation of the emergency cooling system and the moderator heat sink irrelevant. The only other event which may affect the outcome of this accident is the success or failure of the containment system, in the assessment of which the possibility of containment failure resulting from the failure to shut-down must be considered (i.e., a common-cause or consequent failure).

In Figure 1, we have assumed that failure of ECI also results in failure of ECLT, although this will not necessarily be true.

Failure of the moderator heat sink (e.g., by moderator coolant pipe rupture) makes the operation of the moderator cooling system irrelevant, so that no option is shown in Figure 1 for this event in the cases where MHS fails.

From the event tree of Figure 1, two accident sequences were selected for detailed study: S11, loss of moderator cooling system (LOMCS), and S13, loss of moderator heat sink (LOMHS). In addition, a brief assessment was to be made of S15, failure to shut down, if time permitted; unfortunately, no analysis of S15 could be undertaken, although some of the analytical tools developed could be applied to this accident sequence.

Actually, the study of accident sequence S11 will also apply to accident sequence S12 since no estimates of fission product releases to the environment were made, as mentioned earlier, so that success or failure of the containment function is irrelevant within the scope of the study. Similarly, the study of accident sequence S13 also includes accident sequence S14. However, the studies did include assessments of the effects on containment of the accident sequences, so that the likelihood of consequent containment failure because of the accident sequences has been evaluated.

The study has been undertaken using a Bruce-A reactor unit to represent a typical CANDU reactor. Data for a Bruce-A reactor unit were taken from references 10 and 11.

3. SELECTED ACCIDENT SEQUENCES

Brief, qualitative descriptions of the accident sequences selected for study are given in this section of the report. Following this section, detailed descriptions, methods and results for each accident sequence are given in turn. In the following descriptions, alternative outcomes at various stages of the accident sequences are included for generality, although the study itself has shown that some of these outcomes will not occur or are very unlikely.

3.1 Accident Sequences S11 and S12 - Loss of Moderator Cooling System (LOMCS)

In these sequences, following a stagnation-break LOCA with failure of emergency cooling, the moderator heat sink is present and effective, but the moderator cooling system fails, (e.g., by loss of service water to the moderator heat exchanger, moderator system pump failure, etc.). The moderator heats up and the pressure in the calandria increases as the vapor pressure of the moderator increases and as moderator swell compresses the helium cover gas in the relief ducts. See Figure 2. The rupture disks break, liquid overflows into the reactor vault and the moderator eventually begins to boil. Moderator is lost from the calandria as vapor and as entrained liquid. The void fraction in the moderator increases and eventually the upper rows of calandria tubes dry out or are uncovered. Following calandria tube uncovery, the fuel channels overheat and fuel, pressure and calandria tubes may melt or disintegrate. Melted or disintegrated channels fall into the remaining moderator. A vapor explosion may occur but, in any case, rapid quenching of the molten or solid debris will result in rapid vapor generation with resulting surges in calandria pressure and in two-phase flow discharges from the relief ducts. The pressure surges may damage the calandria. Fission products from the damaged fuel will escape from the calandria to the reactor vault, with a certain fraction released to the reactor vault atmosphere. Deuterium gas from the Zircaloy-water reaction will also escape to the reactor vault. The steam and deuterium discharges, and possible deuterium combustion, will cause pressure increases in the reactor vault.

Eventually, many fuel channels may disintegrate and the quenched debris will accumulate in the bottom of the calandria. As the moderator boils off completely

the debris will be uncovered and will begin to heat up again. The debris may melt and form a molten pool supported by the calandria wall, with the calandria wall cooled by the shield tank water. The calandria wall may melt or fail and the molten material mix with the shield tank water which may result in a vapor explosion and which will once again quench the debris. The shield tank water may boil off into containment and the debris may heat up and melt once more. Molten material may melt through to the fuelling machine duct and through the floor of the duct into the underlying rock. Interaction of the molten pool with concrete will generate non-condensible gases which will tend to increase containment pressure. Eventually, any molten material will solidify in the concrete or the underlying rock.

3.2 Accident Sequences S13 and S14 - Loss of Moderator Heat Sink (LOMHS)

These accident sequences are similar to those for LOMCS, except that the moderator heat sink itself is lost, e.g., by rupture of one of the moderator coolant pipes outside the shield tank. In this case, fuel channels will be uncovered much more rapidly and fuel melting is more probable. Molten or unquenched debris which will soon melt will probably accumulate in the bottom of the calandria much earlier than in the case of LOMCS. Subsequent events will be similar to those described above, but the consequences may be more severe. These accident sequences were assessed following the study of sequences S11 and S12.

3.3 Accident Sequences S15 and S16 - Failure to Shut Down

In these accident sequences, the reactor shut-down systems fail to function after a LOCA and the regulating system also fails to shut down the reactor. As mentioned earlier, operation of the emergency coolant system and functioning of the moderator heat sink and coolant system are irrelevant in this case and the fuel will melt rapidly. Pressure and calandria tubes will then rupture allowing molten material to mix with the moderator, which may result in a vapor explosion. The vapor explosion may rupture the calandria, as well as breaking the calandria rupture disks. Since these events will occur rapidly, steam generated by the vapor explosion as well as further steam generation from the moderator and shield tank water will probably add to pressurization of containment caused by steam flashing from the coolant discharging from the original pipe break. Hydrogen from the Zircaloy-water reaction will also pressurize containment and may result in additional pressurization from combustion. Missiles from the rupture of the calandria may cause damage to the containment.

Melting of the fuel and its mixing with the moderator will effectively cause reactor shut-down.

As in the previously-described accident sequences, molten debris will probably melt through to the fuelling-machine duct and eventually through the floor of the duct. Events related to these melt-throughs will be similar to those discussed earlier.

4. ASSESSMENT OF ACCIDENT SEQUENCES S11 and S12: LOCA + LOECI + LOMCS

4.1 Analytical Flow Chart for Accident Sequences S11 and S12

A detailed and comprehensive analytical flow chart was developed which identifies the various stages of the accident sequence, the analytical steps required for their assessment and relates the stages and analytical steps to each other. The analytical flow chart for this accident sequence is shown in Figure 3, which is divided into nine parts, Figures 3A to 3I. Connections between the parts of Figure 3 are indicated by corresponding numbers on the logic flow lines.

It should be noted that certain departures from the sequence of events shown in Figure 3 were found as the study progressed. Nevertheless, the results of the study indicated that Figure 3 still provided a reasonable description and basis for assessment and a reasonable guide to the inter-relations of various events.

As emphasized in Section 1., there are considerable uncertainties about some of the physical mechanisms and component behaviors in the various stages of these accident sequences, particularly in the disintegration of fuel channels and the behavior of the fuel channel debris. In such cases, bounding analyses and sensitivity analyses have been done and certain judgments have been applied as to the likelihood of a given behavior.

4.2 Initiation of Accident Sequences S11 and S12

In these accident sequences, it was assumed that the size and location of the primary system pipe rupture which causes the LOCA are such that stagnation occurs late in the period of the primary-coolant blowdown. With failure of emergency cooling injection, this occurrence results in sagging of the pressure tubes onto the calandria tubes (7,8). It was assumed that pressure tubes contact calandria

tubes when the pressure tube temperature reaches 1000°C (1,2)*. Contacts between the tubes provide effective heat flow paths to the moderator heat sink, which would prevent fuel melting provided that the moderator cooling system functions properly (7,8,9). In the present case, it is assumed that the moderator cooling system also fails. The sequence of events following these initiating events has been analyzed and the methods used and results obtained are described in the following sections.

4.3 Heat Source to the Moderator as a Function of Time

The steps contributing to the establishment of the heat source to the moderator as a function of time are listed in boxes 1 to 6 in Figure 3.

From an examination of channel power distributions in a Bruce-A reactor unit (e.g., 10), groupings of channels and appropriate average initial (full) powers for the groups were established, boxes 1 and 2. The objective of the grouping was to establish a heat source to the moderator that would account for the overall effect of all the fuel channels while also representing, to some extent, the channel power distribution, and hence, the different time behaviors of the heat sources from channels of different powers. Four groups of fuel channels were chosen with the full-power average fuel element power ratings (FEPR) and other data for each group as given in Table 1. A conservative approach has been taken in this study in that all fuel channels are assumed to be affected similarly in the accident rather than only those in the critical core pass.

To establish heat flow rates from the groups of channels to the moderator, the previously-developed computer program, IMPECC (1,2,8,9,12,13), was used as the basic analytical tool. However, IMPECC as originally developed, did not allow for heat generation resulting from the exothermic reaction between Zircaloy and heavy water vapor which will probably occur in a severe LOCA. As explained in references 2 and 12, a three-dimensional model of the fuel channel, rather than the two-dimensional model used in IMPECC, would be necessary for a realistic modelling of the effects of the Zircaloy-steam reaction, to allow for the

*Pressure tube sagging may occur at temperatures from 800°C to 1000°C (e.g., 7). At lower sagging temperatures, the stored heat released on contact will be less than at higher temperatures, so that use of the highest temperature within the above range will be conservative.

Table 1: Grouping of Channels and Characteristics of Each Group Bruce-A Reactor Unit

Group	No. of Channels	Full-Power Average FEPR, W/cm
1	40	30
2	160	27
3	160	21
4	120	18

temperature-dependent reaction rate, the heating of the steam as it flowed along the channel and the conversion of the steam flow to deuterium flow as the reaction proceeded. To avoid the necessity of developing such a complex three-dimensional computer program, a simplified procedure was used in which IMPECC was modified to allow for the effect of the Zircaloy-steam heat source in an approximate manner. (Box 3 in Fig. 3.).

Studies at WNRE using the computer program CHAN-2, have established the heat generation rate as a function of time resulting from the Zircaloy-steam reaction in a high-power channel in a Bruce-A reactor unit following a severe LOCA accompanied by a LOECI for late-stagnation conditions (14). The Zircaloy-steam heat generation rate as a function of time is shown in Figure 4. The heat generation rate shown in Figure 4 is that produced by a steam flow rate in the channel of 12 g/s, which results in the maximum temperature rises of the fuel sheaths and pressure tube because of the Zircaloy-steam reaction (e.g., 13).

The heat generation rate given in Figure 4 was incorporated as an additional heat source term into a modified version of the IMPECC program, IMPECC-Z. This heat source was distributed among the fuel rings in the model in proportion to the amount of Zircaloy sheath in each ring. The additional heat source for each ring is triggered in IMPECC-Z when the maximum sheath temperature in that ring reaches a specified value*, which is an input to the program. A temperature of 1050°C was used for the Zircaloy-steam reaction trigger temperature in the analyses described here.

The Zircaloy-steam heat source was distributed over the fuel sheaths only, rather than the fuel sheaths and the pressure tube for reasons of convenience in modifying IMPECC. This approximation is conservative, since the heat actually generated in the pressure tube, which is, of course, accounted for in the heat source term shown in Figure 4, is assigned to the fuel sheaths and thus must

*The three outer rings of a 37-element fuel bundle are represented in IMPECC by solid annular rings of fuel with annular Zircaloy sheaths on the inner and outer surfaces (12). The Zircaloy-water reaction heat source is triggered separately for the Zircaloy on each surface when its temperature reaches the specified value.

flow over larger thermal resistances to reach the moderator, resulting in predicted fuel and sheath temperatures higher than would occur in the real case. The predicted pressure tube temperature should also probably be somewhat conservative since, while the predicted heat flow rate from the pressure tube to the calandria tube will be reasonably correct, the predicted outer sheath temperature of the outer fuel ring will be somewhat higher than would actually be the case which will cause the inner surface temperature of the pressure tube to be somewhat higher than actual because of radiation heat transfer.

The major features of the modified IMPECC program are listed, for convenience, in Appendix A.

The program IMPECC-Z was run for each grouping of channels as listed in Table 1 and the heat flow rates to the moderator as functions of time were determined. Since the pressure tubes in each grouping are predicted to sag at somewhat different times, a simple computer program was developed to combine properly-weighted heat flow rates from the calandria tubes (Box 5 of Figure 3). The resulting moderator heat source is presented later in this report.

4.4 Thermal-Hydraulic Behavior of the Moderator

As discussed in section 3.1, with the failure of the moderator cooling system, the moderator will heat up and eventually begin to boil. Moderator will be lost through the relief ducts initially under single-phase liquid conditions and eventually under two-phase and single-phase vapor conditions. As the void fraction increases in the calandria, calandria tubes will dry out or be uncovered. The uncovered tubes may disintegrate and fall to the bottom of the calandria. Eventually, all the moderator may be lost from the calandria.

An explicit, finite difference computer program, MODBOIL, has been developed to analyze the thermal-hydraulic behavior of the moderator under these conditions. The steps associated with the thermal-hydraulic behavior of the moderator and related effects considered in MODBOIL are listed in boxes 7 to 17 and 24 to 28b of Figure 3. To facilitate use of MODBOIL, three sub-programs have been developed to cover different stages of the accident sequence, SUBCOOL, MODBOILSUB and MODBOILALL. The scopes of these sub-programs are as follows:

a) SUBCOOL models heating of the moderator under single-phase natural convection and sub-cooled boiling conditions up to the time when liquid spills from the ruptured relief ducts because of moderator swell resulting from its temperature increase and moderator displacement resulting from the sub-cooled boiling void fraction (Boxes 7 to 9b of Figure 3).

b) MODBOILSUB models heating of the moderator after liquid spills from the relief ducts and as bulk boiling develops in the moderator. It incorporates thermal-hydraulic analysis of moderator boil-off and allows for calandria tube uncovery and disintegration. (Boxes 7 to 17 and 24 to 28b of Figure 3).

c) MODBOILALL models heating of the moderator after bulk boiling has begun in all moderator slices. It incorporates the same thermal-hydraulic analysis and the same tube uncovery and disintegration features as MODBOILSUB. (Boxes 10 to 17 and 24 to 28b of Figure 3).

In all the sub-programs of MODBOIL, the moderator is divided into 24 horizontal slices, one for each row of calandria tubes. A typical slice is shown in Figure 5. Transient heat and mass balances for each slice are incorporated into each of the sub-programs.

In all the sub-programs, the time-dependent heat source for each slice is pro-rated from the overall heat source given later in Figure 14, taking into account the number of fuel channels in the slice and their average power rating. This method is approximate in that it apportions the heat source to each slice according to the total normal power rating of the fuel channels in the slice, ignoring the smoothing effect of the Zircaloy-water reaction heat source. The resulting slice power distribution will be less uniform than that which would be expected in reality, but the total power to the moderator will be correct and the overall moderator behavior should not be affected greatly by this simplification.

Properties of heavy water used in the programs were taken from references 15 to 17, while properties of light water were taken from references 18 and 19

(Appendix A-7). In general, each property is represented in the programs by fourth-order (or lower) polynomial curve fits to the tabulated properties.

Descriptions of the major assumptions and methods used in each sub-program are given in the following sections of this report. Further information on MODBOIL is provided in reference 20 and a listing and sample output of the program are provided in Appendix B.

4.4.1 SUBCOOL

As described earlier, this sub-program is used to simulate the initial heating of the moderator in the calandria from a uniform initial temperature until liquid moderator overflows from the relief ducts after the rupture disks break.

In SUBCOOL, transient heat balances are made on each moderator slice accounting for the pro-rated heat source, as described in the previous section, heat storage in the liquid moderator, heat transfer to the calandria walls*, heat storage in the calandria walls* and heat transfer to the shield tank water. Heat transfer coefficients from the moderator to the calandria wall and from the calandria wall to the shield tank water are predicted using conventional correlations for turbulent natural convection on vertical surfaces. Although the surfaces are in general not vertical, the natural convection circulation patterns near the walls will be similar to those for vertical walls and the predicted coefficients will not be sensitive to geometry for the high Rayleigh numbers encountered. Also, the heat transfer rate to the shield tank is relatively low throughout the transient so that the results are quite insensitive to the probable uncertainties in these heat transfer coefficients. In this study, the shield tank cooling system was assumed to function properly, so that the shield tank water temperature is set constant at its normal value. From the heat balances, at each time step the moderator and calandria wall temperatures are determined for each slice. An option in SUBCOOL permits zero, or complete mixing of the moderator among the slices at each time step.

From the temperatures of the moderator in each slice, the total thermal expansion of the moderator is determined at each time step. The pressure over the

*Heat transfer to, and storage in, the end walls of the calandria were ignored, which is a conservative assumption.

moderator, before rupture disk failure, is then determined allowing for the vapor pressure corresponding to the bulk average moderator temperature and the partial pressure of the helium cover gas allowing for the decreasing volume of gas and vapor space as the moderator swells. The pressure in each slice is then calculated allowing for the vapor-space pressure and the static head over each slice.

The onset of sub-cooled boiling in each slice is determined using the Saha-Zuber correlation (21). The program includes a factor to modify the OSV point as predicted by the Saha-Zuber correlation to permit evaluation of the sensitivity of the thermal-hydraulic behavior of the moderator to the predicted OSV point.

The sub-cooled void fractions in each slice are predicted by the Wallis drift-flux equation for the isolated bubble regime (22, equation 9.33) with zero liquid volumetric flux. The equivalent quality which is required to enable the sub-cooled void fraction to be predicted by the Wallis equation is determined using a method similar to that of Levy (23).

The program calculates the swelling of the moderator volume and the resulting rise of liquid level in the relief ducts resulting from the moderator expansion caused by heating in each slice and the additional expansion caused by the formation of sub-cooled voids in each slice. As described earlier, the program calculates the pressure over the moderator before the rupture disks break, accounting for the moderator vapor pressure and the compressed helium cover gas and predicts the time at which the rupture disks break. As discussed in reference 1, preliminary studies with earlier versions of SUBCOOL showed that the bulk moderator temperature was always below the saturation temperature corresponding to reactor vault pressure at the times of rupture disk failure because of the presence of the helium cover gas. Therefore, no flashing of moderator occurs at these times, so that moderator flashing is not allowed for in SUBCOOL when the rupture disks break. Runs with SUBCOOL have confirmed the validity of this approach.

Following failure of the rupture disks, the pressure over the moderator in the relief ducts is set to the reactor vault pressure, assumed in all cases to be normal atmospheric pressure.

The analysis in SUBCOOL terminates when liquid moderator begins to spill from the relief ducts.

4.4.2 MODBOILSUB

As described earlier, MODBOILSUB models heating of the moderator and other effects after liquid spills from the relief ducts and as saturated bulk boiling develops in the moderator. Initial conditions are obtained from the output of SUBCOOL.

4.4.2.1 Sub-cooled Boiling and Onset of Bulk Boiling

Slice heat balances under sub-cooled boiling conditions in MODBOILSUB are written in the same manner as those in SUBCOOL. Until bulk boiling begins in any slice the pressure over the moderator (since the rupture disks have failed) is assumed to be equal to the reactor vault pressure which has been assumed to be normal atmospheric pressure in all cases. Before bulk boiling begins in any slice, the pressures in all slices are calculated by adding the static head at the slice to the reactor vault pressure. The calculated pressure in each slice is then compared to the saturation pressure corresponding to the moderator temperature in the slice. As long as the calculated pressure is greater than the saturation pressure, sub-cooled conditions apply and the slice heat balance continues to be determined as described in section 4.3. When the calculated pressure in a given slice equals the saturation pressure, bulk boiling is assumed to begin and the method of analysis is changed to account for this effect as described below. The sub-program MODBOILSUB thus predicts the times and sequence of the onset of bulk boiling in the moderator slices and readily handles the situation in which some slices are undergoing bulk boiling while others are under sub-cooled boiling conditions.

4.4.2.2 Mass and Energy Balances For Bulk Boiling Conditions

After bulk boiling begins in a slice, MODBOILSUB uses transient mass balance and transient energy balance equations expressed in explicit finite difference form to determine conditions in a slice.

The mass balance on slice N* is given by:

$$\dot{m}_g(N) + \dot{m}_f(N) = \frac{\delta m_f(N)}{\delta t} + \frac{\delta m_g(N)}{\delta t} + \dot{m}_g(N-1) + \dot{m}_f(N-1) \qquad (1)$$

* Note that slices are numbered starting from the top of the calandria so that slice N-1 lies above slice N.

where the first and second terms on the left hand side represent the mass flow rates of vapor and liquid into the slice respectively, the first and second terms on the right hand side of the equation represent the change in stored liquid and vapor masses resulting from evaporation, liquid displacement by vapor void formation and liquid entrainment, if any, and the third and fourth terms on the right hand side represent the flow rates of vapor and liquid out of the slice, respectively. Equation 1 may also be written as:

$$\delta\dot{m}_g(N) + \delta\dot{m}_f(N) + \frac{\delta m_f(N)}{\delta t} + \frac{\delta m_g(N)}{\delta t} = 0 \qquad (2)$$

The rate of change of stored liquid in a slice is given by:

$$\frac{\delta m_f}{\delta t} = ((1 - \alpha) - (1 - \alpha')) \frac{V\rho_f}{\delta t} \qquad (3)$$

where the prime denotes that the variable is to be evaluated at the previous time step.

Similarly, the rate of change of stored vapor in a slice is given by:

$$\frac{\delta m_g}{\delta t} = (\alpha - \alpha') \frac{V\rho_g}{\delta t} \qquad (4)$$

The energy balance on slice N is given by:

$$\dot{Q}_i(N) + \dot{m}_g(N)\, h_g(N) + \dot{m}_f(N)\, h_f(N) =$$

$$\dot{m}_g(N\text{-}1)h_g(N\text{-}1) + \dot{m}_f(N\text{-}1)h_f(N\text{-}1) + \dot{Q}_o(N) + \dot{Q}_s(N) \qquad (5)$$

where the first term on the left hand side represents the heat flow rate from the calandria tubes, the second term represents the energy flow into the slice in liquid and the third the energy flow into the slice in vapor. On the right hand side, the first two terms represent the energy flow out of the slice

in vapor and liquid, respectively, the third term the heat transfer rate to the calandria wall from the slice and the fourth term represents the rate of energy storage in the slice.

Since property values change very slightly from slice to slice under all conditions, it has been assumed that $h_g(N) \approx h_g(N-1)$ and $h_f(N) \approx h_f(N-1)$.

Solving for the net vapor generation rate in a slice, we obtain:

$$\delta\dot{m}_g(N) = (\dot{Q}_i(N) - \dot{Q}_o(N) - \dot{Q}_s(N))/h_g(N) - \delta\dot{m}_f(N)\frac{h_f(N)}{h_g(N)} \qquad (6)$$

Substituting for $\delta\dot{m}_f(N)$ in equation 6 from equation 2, and simplifying, we obtain for the net vapor production rate in slice N:

$$\delta\dot{m}_g(N) = (\dot{Q}_i(N) - \dot{Q}_o(N) - \dot{Q}_s(N))/h_{fg}(N) + \left(\frac{\delta m_f(N)}{\delta t} + \frac{\delta m_g(N)}{\delta t}\right)\frac{h_f(N)}{h_{fg}(N)} \qquad (7)$$

The rate of change of stored energy in slice N is given by:

$$\dot{Q}_s(N) = \frac{\delta m_f(N)}{\delta t}u_f(N) + \frac{\delta m_g(N)}{\delta t}u_g(N) \qquad (8)$$

Substituting equation 8 into equation 7 and simplifying, we obtain, for the net vapor production rate in slice N:

$$\delta\dot{m}_g(N) = \frac{\dot{Q}_i(N) - \dot{Q}_o(N)}{h_{fg}} - \frac{\delta m_g(N)}{\delta t}\left(1 - \frac{p}{\rho_g h_{fg}}\right) + \frac{\delta m_f(N)}{\delta t}\frac{p}{\rho_f h_{fg}} \qquad (9)$$

In equation 9, the first term on the right hand side represents the vapor generation rate resulting from the net power input to slice N while the last two terms represent the net vapor out-flow rate from the slice because of the change of void fraction in the slice. Under most conditions, the last two terms, as

calculated from equations 3 and 4, are small compared to the other term. Only when the void fraction is changing very rapidly, such as when bulk boiling initiates in a slice, will the last two terms amount to more than 1% or 2% of the first.

An equation for $\delta\dot{m}_f(N)$, the net liquid "production" rate in slice N, can be derived in a manner similar to that used to find $\delta\dot{m}_g(N)$:

$$\delta\dot{m}_f(N) = -\frac{(\dot{Q}_i(N) - \dot{Q}_o(N))}{h_{fg}} - \frac{\delta m_f}{\delta t}\left(1 - \frac{p}{\rho_f h_{fg}}\right) + \frac{\delta m_g}{\delta t}\frac{p}{\rho_g h_{fg}} \qquad (10)$$

In equation 10, the first term on the right hand side represents the reduction in liquid flow rate in slice N because of evaporation while the last two terms represent the net liquid flow rate out of slice N because of transient void growth, calculated using equations 3 and 4. As bulk boiling develops in a slice, the last two terms dominate equation 10. Only when the void fraction is changing very slowly will the first term be significant compared to the last two.

4.4.2.3 Void Fractions For Bulk Boiling Conditions

The determination of void fractions as bulk boiling develops and for fully-developed bulk boiling requires recognition of the different two-phase flow regimes that may exist. Assessment of these situations resulted in the identification of two flow regimes of significance here: isolated bubble flow at low void fractions and churn-turbulent flow at high void fractions.

In the isolated bubble regime, as in SUBCOOL, the Wallis void fraction equation for zero liquid volumetric flux (22, equation 9.33) is used, even though in this case, unlike that of SUBCOOL, there will be a net liquid volumetric flux. However, the liquid flux under isolated bubble conditions will be small, so that no significant error will be introduced by this approximation. Therefore, the isolated bubble regime void fraction equation used is:

$$\alpha = 0.5 - \left(0.25 - \frac{j_g}{v_\infty}\right)^{\frac{1}{4}} \qquad (11)$$

where v_∞, the bubble rise velocity, is given by Harmathy's equation (22)

$$v_\infty = 1.53 \left(\frac{g\, g_c \sigma(\rho_f - \rho_g)}{\rho_f^2}\right)^{\frac{1}{4}} \qquad (12)$$

For high void fractions, the experiments of Ginsberg, et al., (24) on volume-heated boiling pools shows that the churn-turbulent flow regime exists. The boiling of the moderator on the calandria tubes can be assumed to approximate a volume-boiling situation.

Therefore, the Zuber-Findlay (25) void fraction equation for the churn-turbulent flow regime, as recommended by Ginsberg, et al., (24), is used for high void fractions:

$$\frac{j_g}{\alpha} = C_o j + v_{gj} \qquad (13)$$

In equation 13, the void distribution parameter, C_o, is normally 1.2 to 1.35 for vertical circular tubes and rectangular ducts, respectively. This range of values of C_o was found by Ginsberg, et al., to give reasonable results for the volume-heated void fraction in the churn-turbulent flow regime, with the higher value being somewhat better than the lower. However, since C_o has not been established for the flow geometry of the calandria, it has been treated as an input variable in MODBOILSUB. Values of C_o in the range of 1.1 to 1.6 have been used in the analyses. The vapor drift velocity in equation 13 is given by (22):

$$v_{gj} = v_\infty (1 - \alpha)^n \qquad (14)$$

where n, for churn-turbulent flow, equals 0.

From information given by Wallis (22), the boundary between the isolated-bubble regime and the churn-turbulent regime lies in the range of $\alpha = 0.25$ to 0.4. The boundary value is an input to be specified by the user in MODBOILSUB. In most of the cases run, a boundary value of $\alpha = 0.25$ has been used.

4.4.2.4 Redistribution of Downward Flowing Liquid Among Slices

Eventually, after all slices experience bulk-boiling conditions, decreasing heat generation rates will cause the void fraction in some of the slices near the top

of the calandria to decrease which may require liquid to flow downwards into these slices from higher slices or the relief ducts.* Also, when a slice is depleted of liquid, condensation of the vapor on the calandria wall is allowed for, using a conventional correlation for laminar film condensation on a vertical surface (e.g., 26, equation 9.13). In such cases, the liquid formed is assumed to be re-distributed to lower slices. To handle the redistribution of liquid among slices under such conditions, MODBOILSUB makes use of several different types of mass balance equations, in addition to the mass balance equations for normal isolated-bubble and churn-turbulent flow regimes, depending on the conditions in a slice and in the neighboring slices at a given time. These types of mass balance equations, are designated by the indicator ITYPE in MODBOILSUB. Values of ITYPE are printed out for each slice at each time step.

4.4.2.5 Pressure Gradients in Calandria and Relief Ducts

From the calculated vapor and liquid flow rates in each slice and in the relief ducts, the two-phase pressure losses in each slice and in the relief ducts are determined, allowing for friction, spatial momentum change and gravity or static head effects. Under all conditions, the rate of momentum change as a function of time was negligible. Appropriate equations for the component pressure drops were taken from reference 27. In these equations, the two-phase friction multiplier used was that of Martinelli-Nelson, as expressed by Jones and Dight, with the mass-velocity correction factor of Collier and Tremblay. The spatial momentum pressure change and the static head were determined from first principles using void fractions calculated as described above. In the relief ducts, the void fraction in churn-turbulent flow is predicted by equation 13 with $C_o = 1.2$. Results show that the only significant pressure changes within the calandria are those due to static head effects with significant friction and momentum change pressure losses occurring only in the relief ducts under all conditions. The pressure in each slice in the calandria is determined in MODBOILSUB by adding the total pressure loss in the relief ducts to the total static head in each slice. In all cases, the reactor vault pressure was assumed to be atmospheric.

---

*An estimate of the mass of heavy water in the moderator cooling system which could flow into the calandria as moderator boils off (See Boxes 12 and 26 of Figure 3) showed that it was not very significant compared to the mass remaining in the calandria throughout most of the transient, so that this effect has been ignored in the analysis.

In MODBOILSUB, the flow rate in the relief ducts during the development of bulk boiling in the calandria, i.e., from the time of initiation of bulk boiling in the top slice to the time of initiation of bulk boiling in the bottom slice (typically less than two minutes), is calculated as an average flow rate over the time from the start of bulk boiling in the calandria. This approach was used to avoid the large flow and pressure drop excursions which otherwise occurred during the development of bulk boiling.* It is not expected that this simplification results in any significant errors in the prediction of the mass of liquid moderator remaining in the calandria at any time in the long run. Once bulk boiling has developed in all the slices, this flow averaging procedure is no longer needed nor used, except as noted in section 4.4.2.8.

Under certain conditions, choked flow can occur in the relief ducts. The method used to predict relief duct and calandria pressures under these conditions is described in section 4.4.2.8.

4.4.2.6 Uncovery of Calandria Tubes

Eventually, as liquid moderator is lost through the relief ducts, calandria tubes in the top row will be effectively uncovered. As more liquid moderator is lost, lower rows of calandria tubes will be uncovered in turn. It is important to know the times of uncovery since calandria tubes will no longer be cooled effectively by the liquid moderator beyond these times, causing them and their pressure tubes and fuel bundles to heat up rapidly, eventually leading to possible break-up or melting.

While calandria tubes in a given slice will obviously be uncovered when there is no longer any liquid left in the slice, they will, in general, dry out or become effectively uncovered before complete disappearance of liquid from the slice.

Because of the importance of knowing the effective uncovery times, several criteria for calandria tube uncovery were considered: pool boiling critical heat flux on horizontal tubes, flow boiling critical heat flux over single horizontal tubes, critical heat flux in horizontal tube bundles, the flooding limit for two-phase flow in a large volume and change of flow pattern from churn-turbulent flow to dispersed or mist flow. After an extensive review of the literature and the

---

* Note that this procedure does not eliminate flow and pressure oscillations but only damps the oscillations.

conditions of concern, it was judged that none of critical heat flux criteria would be appropriate for these high-void bulk boiling conditions mainly because of the effect of vapor flows from the lower tubes for the first two CHF criteria, and the gradual initiation of boiling at the top of the "bundle", rather than uniform boiling throughout the "bundle" for the third CHF criterion.

Of the two remaining criteria, the flooding limit might appear to be the more appropriate as the uncovery point for the moderator in the calandria. However, the present conditions are quite different from those for which conventional flooding models and correlations (e.g., 22, Chapters 10 and 11) apply, so that this criterion could not be used here.*

Therefore, the criterion used is that of flow regime transition from churn-turbulent to dispersed or mist flow. With the dispersed droplets in mist flow, it is very unlikely that adequate cooling of the calandria tube by liquid could be maintained. From the work of Ginsberg, et al., (24), the criterion of Dukler and Taitel (28) for this flow regime transition seems to be the most appropriate for the present conditions. By this criterion, the transition from churn-turbulent to dispersed flow occurs at

$$\frac{j_g}{v_\infty} = 2.02\alpha \left(\frac{\rho_f}{\rho_g}\right)^{\frac{1}{4}} \qquad (15)$$

This equation was used in the analysis to predict the time of tube uncovery in each row.

4.4.2.7 Behavior of Fuel Channels after Uncovery of Calandria Tubes

Since uncovered calandria tubes in a given slice are no longer transferring heat to the liquid moderator after uncovery, the heat input to the slice is set to zero in the program.

The transient thermal behavior of the uncovered fuel channels has been analyzed by developing and applying a modification to the IMPECC program, called

*Note that application of conventional flooding correlations such as those in reference 22, Chapters 10 and 11, to the present situation results in the prediction that flooding will not occur in the calandria, because of the large vapor velocities required.

IMPECC-UCZ. A description of this program is given later in this report, in section 4.5.

MODBOILSUB incorporates four options to describe the behavior of fuel channels after uncovery of calandria tubes.

In one option the channels are assumed to remain in place, that is, not to break up. This is an optimistic assumption but may represent the actual behavior of certain channels after uncovery, depending on uncovery time and power rating.

In the second option, channels are assumed to disintegrate when calandria tube temperatures reach 1750°C, the nominal melting point of Zircaloy. Determinations of the times after uncovery for calandria tubes to reach this temperature were made using IMPECC-UCZ for various uncovery times, steam flow rates and fuel element power ratings, as will be presented later in this report, in section 5.2.3. From these results, an approximate 'empirical' equation was developed to predict the time after calandria tube uncovery in a slice at which the calandria tube temperature reaches 1750°C, and hence, the fuel channel disintegrates. The equation developed is:

$$\delta t_d(N) = C\left[\frac{t_{uc}(N)}{(FEPR(N))^{0.5}}\right]^{EXPN} \qquad (16)$$

where $C = 0.17$

$EXPN = 1.6$

For generality, C and EXPN are treated as inputs to the program, but the values given above have been used in all cases so far.

Equation 16 was established for a constant steam temperature of 100°C. Therefore, it does not account for the effects on calandria tube temperatures of superheating of the steam as it flows over the calandria tube and over uncovered calandria tubes in the rows below that being considered. The actual delay times to disintegration will thus be somewhat less than predicted by equation 16. This point is discussed in section 5.2.5.

In the third option, an arbitrary delay time after calandria tube uncovery can be specified as an input to the program. In this option, the same fixed delay time to disintegration applies to the fuel channels in each slice in the core.

In the fourth option, upon the disintegration of a row of channels under either of the two foregoing disintegration options, all uncovered rows under the disintegrating row are assumed to disintegrate also. This option allows for the probable fracture and breakup of any uncovered channel should it be struck by debris falling from above.

At channel disintegration in a given slice, an arbitrary fraction of the total mass of fuel, pressure tubes and calandria tubes in the slice is assumed to drop instantaneously into the bottom slice. The arbitrary fraction is an input value which can be varied from 0 to 1, to establish the sensitivity of moderator behavior to various assumed fractional disintegrations of fuel channels. Also, an arbitrary fraction of the Zircaloy mass in the slice can be assumed to be molten at the time of channel disintegration. Again, the fraction molten is an input value that can be varied from 0 to 1 for sensitivity studies. No allowance has been made for a molten fraction of the uranium oxide fuel material since, as we will see in section 5.2, no fuel melting is anticipated to occur after calandria tube uncovery.

In the program, the average temperatures of the fuel, solid Zircaloy and molten Zircaloy at the moment of channel disintegration are specified as input values. Values of these temperatures which have been used in the analyses have been estimated from the results of computer runs using IMPECC-UCZ.

As mentioned earlier, the mass of disintegrated material is assumed to fall instantaneously to the bottom slice in the calandria. In the computer program, the free volume in the bottom slice is reduced accordingly and the heat source in the bottom slice is increased to allow for decay heat and stored heat of the fallen debris. The stored heat considered in the program includes the latent heat of fusion of Zircaloy if a fraction of the Zircaloy is assumed to be molten. The disintegrated material is assumed to be quenched by the moderator in the bottom slice. The mechanisms of quenching heat transfer from the disintegrated

material considered in MODBOILSUB are film boiling, using the correlation of Breen and Westwater (29), plus the radiation contribution as given by Bromley (30), until the minimum film boiling temperature, which is predicted by the correlation of Bradfield (31), is reached. After this point, nucleate boiling is assumed to occur, with the correlation of McAdams, (32) as modified by the author (33, section 10.3) being used to predict the heat transfer coefficients. Surface areas of the disintegrated material per unit mass or per channel are specified as input values in MODBOILSUB. In all cases described in this report, the surface area of the fuel debris per channel was assumed to be the total surface area of all the pellets in the channel. Obviously, the fuel pellets would fracture and fragment during the severe transients considered here, increasing the surface-to-volume ratio and, hence, the rate of quenching of the pellets. The increased quenching rate would increase the steam generation rate in the bottom slice and thus the magnitudes of the steam discharge rate and calandria pressure surges. On the other hand, fuel pellets might remain within oxidized sheaths, decreasing the surface-volume ratio and the steam discharge rate. The surface area of the Zircaloy (or ZrO_2) debris per channel was assumed to be the total (inside and outside) surface areas of the sheaths, the pressure tube and the calandria tube for the cases in which Zircaloy is assumed not to melt. Break-up of the solid Zircaloy in these cases would not be expected to result in a significant increase in exposed surface area per channel. For the cases in which Zircaloy is assumed to melt, the probable exposed surface area was estimated as follows. In these cases, the molten Zircaloy would be expected to form droplets. Considering its surface tension and density, the probable mean size of droplets of molten Zircaloy would be in the range of 0.5 to 1.5 cm*. The area-to-volume ratio of spheres in this diameter range includes the area-to-volume ratio of the solid Zircaloy in a channel. Therefore, considering the many uncertainties in any estimation of the surface-to-volume ratio of molten Zircaloy, it was decided to assume that the surface-to-volume ratio of the molten Zircaloy was the same as that of the solid Zircaloy. In all cases, therefore, the surface area of molten Zircaloy per channel was assumed to be the same as for the cases in which no Zircaloy melting occurs.

---

* This estimate is based on information in reference 34, and on estimated property values of molten Zircaloy.

It should be noted that a vapor explosion is not expected to occur when disintegrated fuel channels fall into the moderator. An earlier assessment concluded that vapor explosions are very unlikely under the present conditions (1, section 3.5). Further examination of this question has reinforced the conclusion that vapor explosions will not occur following fuel channel break-up in this accident sequence, as discussed in Appendix C.

The surge of vapor generation which occurs when disintegrated channel debris falls into the lowest moderator slice will displace liquid upward in the calandria and may decrease the void fraction in some of the upper slices sufficiently to effectively cover, once again, previously uncovered calandria tubes in these slices. See section 4.4.2.6. However, it is assumed in these cases that the increased liquid flow does not rewet the calandria tubes, mainly because of the high temperatures which are rapidly reached by uncovered calandria tubes, as we will see. Also, the period of effective re-covering of these tubes has been found to be quite short as the surge of vapor generation in the lowest slice subsides rapidly as quenching of the debris proceeds.

4.4.2.8 Choked Flow in the Relief Ducts

In early runs with MODBOIL, it became evident from the two-phase flow discharge rates through the relief ducts that choked flow conditions would exist under certain conditions during the transient. Such conditions occurred when:

a) bulk boiling was developing in the moderator with a consequent rapid change in void fraction which resulted in rapid two-phase flow discharges through the relief ducts, and

b) large numbers of fuel channels disintegrated and fell into the bottom slice simultaneously.

Choked flow through the relief ducts is calculated in MODBOILSUB assuming homogeneous equilibrium two-phase flow.

The method used to calculate the conditions for choked flow in the program is to raise the relief duct exit pressure by a given increment (an input to the program) until the calculated choked flow discharge rate equals the average mass flow rate produced by vapor generation and liquid displacement in the calandria from the beginning of the existence of the choked flow condition. Typically,

the periods of choked flow last for a few tens of seconds only. The procedure of averaging the flow rates from the calandria in this manner is essentially the same as the procedure used when bulk boiling is developing in the moderator, and is done for the same reason i.e., to avoid the very high flow and pressure drop excursions that might otherwise occur.

4.4.3 MODBOILALL

MODBOILALL models heating of the moderator and other effects after saturated bulk boiling has developed in all the slices in the calandria. Initial conditions are obtained from MODBOILSUB or from other runs of MODBOILALL.

MODBOILALL is used simply for convenience, to avoid having to repeat the same calculations for the non-boiling, sub-cooled boiling and partial bulk boiling phases of the transient for each run, when conditions are changed which will affect the moderator behavior after bulk boiling is fully developed but will not affect behavior before this time. For example, changes in assumptions concerning the timing and extent of channel disintegration only affect moderator behavior after bulk boiling has developed in all the slices.

All procedures, assumptions and methods applying in MODBOILSUB after bulk boiling has developed throughout the calandria also apply in MODBOILALL and need not be repeated here.

4.5 Thermal Analysis of Uncovered Calandria Tubes - IMPECC-UCZ

4.5.1 Basic Model

The steps relating to the thermal behavior of uncovered calandria tubes are given in boxes 18 to 22 of Figure 3. This behavior is established by using a modification of the IMPECC program, IMPECC-UCZ. In this modification, analysis for a given row of fuel channels proceeds in the normal fashion in IMPECC until the specified uncovery time, which will have been established from MODBOIL for the given row and uncovery conditions. From this time on, a calandria tube in this row is assumed to be cooled only by convection and radiation to steam flowing over the tube, generated from the moderator surrounding lower fuel channels.*

*As described in sections 4.4.2.6 and 4.4.2.7, the sudden surges of steam generated by disintegrated channels in the bottom slice of moderator result in considerable increases in liquid flow rate into the upper slices. In effect, the upper tube rows are re-covered with liquid for a short time. However, as explained in section 4.4.2.7, it is assumed that calandria tubes are not rewet under these conditions, since their temperatures are very high at these times.

In IMPECC-UCZ, the steam flow rate is assumed to be constant. Of course, actual steam flow rates under these conditions will not be constant in these accident sequences; as we will see, MODBOIL results show that, for the periods over which calandria tube uncovery may be expected to occur, there is a general decrease of steam flow rate with time, but sudden surges occur as uncovered channels disintegrate. Therefore, a range of steam flow rates, established from MODBOIL runs, has been used in the study to determine the sensitivity of predicted results to steam flow rate. In IMPECC-UCZ, the steam temperature is also assumed to be constant. Again, the sensitivity of predicted results to a range of steam temperatures has been investigated.

4.5.2 Heat Transfer Coefficients

In IMPECC-UCZ, the convection heat transfer coefficient to the steam* is predicted using the correlation of Grimison for heat transfer to a flow over a bank of ten or more in-line tubes (26, section 6.4). For the pitch-diameter ratio of the calandria tubes, Grimison's correlation is:

$$\frac{h_c d_o}{k_f} = 0.269 \quad Re_{max}^{0.628} \quad Pr_f^{1/3} \qquad (17)$$

To allow for the lower heat transfer coefficients than those predicted by equation 17 which occur in the first few rows in a tube bank, a correction factor, RTB, also derived from the work of Grimison (26, section 6.4), is introduced on the right-hand-side of equation 17. The value of RTB used in the present study is 0.64, which applies for the first tube row in a bank. Correction factors for other tube rows are higher, so that the approach used is conservative.

Radiation from the uncovered calandria tube to its surroundings is an important heat transfer mechanism because of the high temperatures reached by the tube during the transient. Radiation heat transfer rates from the calandria tubes are difficult to predict in general because of the different surroundings of calandria tubes depending on the row in which they are located and whether or not the tubes can "see" bulk liquid, droplets suspended in vapor or simply vapor.

*No allowance is made for the presence of deuterium gas resulting from the Zircaloy-steam reaction. The deuterium gas would have a slight beneficial effect on convection heat transfer, but its flow rate is intermittent and quite low, so this effect is ignored here.

Also, while the steam environment absorbs and emits radiation, it is also partly transparent to thermal radiation. In addition, while calandria tubes are assumed not to re-wet under liquid flow surges, radiation heat transfer from the tubes will certainly increase in such circumstances. Finally, uncovered calandria tubes in and near the outer rows and columns will be cooled by radiation to the calandria wall which is well cooled at all times, and there will also be an axial dependence of radiation cooling of uncovered tubes since surfaces near the ends of the tubes will readily "see" the cooled end shields.

Because of the difficulty of allowing for all of these effects, several of which would change with time for a given tube row, a simplified model of thermal radiation cooling was established which is judged to be conservative for most conditions encountered. In this model, radiation is assumed to occur from a calandria tube to the steam atmosphere in its surroundings. Steam, having a heteropolar molecular structure, can absorb and emit thermal radiation in certain wave-length bands. Although the steam surrounding uncovered calandria tubes will, in general, have significant concentrations of water droplets under the conditions in the calandria, even when the steam is superheated*, the effect of the droplets, which would enhance radiation cooling of the calandria tubes, is ignored. All other possible heat sinks for radiation heat transfer from the calandria tubes, such as the bulk liquid, the cooled calandria wall and the cooled end-shields are also ignored. Thus, the model represents radiation cooling under the most adverse situation, for a calandria tube surface near the centre of the core remote from any bulk liquid and in the absence of liquid droplets. Consistent with this assumption, the model is assumed to be two-dimensional, with longitudinal effects ignored.

In the model, the partial transparency of the steam to thermal radiation is allowed for by recognizing that a portion of the thermal energy radiated by a given calandria tube will be intercepted by surrounding calandria tubes. It is assumed that all such intercepted radiation is absorbed completely by the surrounding calandria tubes, i.e., they are assumed to be black bodies. In reality, of course, some of this impinging radiation would be reflected and a

---

* In mist flows, there can be significant departures from equilibrium so that large populations of liquid droplets may exist even when the vapor is considerably superheated (e.g., 19, p.223; 35).

fraction of the reflected radiation would be absorbed by the steam, thus providing additional cooling of the calandria tube in question.

Additional assumptions are that the calandria tube surface temperature is uniform and that all surrounding calandria tubes are at the same temperature as the tube in question at any time. This assumption will be approximately correct for surfaces near the centre of the core.

This simplified radiation heat transfer model can be represented by the network diagram shown in Figure 6, in which node c represents a particular calandria tube, node 2 represents the total surface of the surrounding calandria tubes seen by node c and node S represents the steam around node c. The behavior of the steam as a partially-absorbing and partially-transmitting medium is represented in Figure 6 in the conventional manner for such a medium (e.g., 26).

Since there is no net heat flow from node c to node 2, since all neighboring calandria tube surfaces are assumed to be at the same temperature at all times, the net heat flow rate from a given calandria tube to the steam can be deduced readily from Figure 6. It is given by:

$$q_{r\ cs} = \frac{\sigma A_c (T_c^4 - T_s^4)}{\frac{1-\varepsilon_c}{\varepsilon_c} + \frac{1}{F_{cs}\varepsilon_s}} \tag{18}$$

From equation 18, the equivalent radiation heat transfer coefficient can be determined:

$$h_{r\ cs} = \frac{\sigma (T_c^4 - T_s^4)}{\left(\frac{1-\varepsilon_c}{\varepsilon_c} + \frac{1}{F_{cs}\varepsilon_s}\right)(T_c - T_s)} \tag{19}$$

The configuration factor between the given calandria tube and the steam, F_{cs}, was determined on the basis of the assumption that a portion of the radiation emitted by a calandria tube will be intercepted by the surrounding calandria tubes. Configuration factors for radiation from a calandria tube to the nearby calandria tubes were calculated by the string method of Hottel (e.g., 32) for

the 16 closest tubes that a given calandria tube can see, as shown in Figure 7. Tubes beyond those shown in Figure 7 were not considered because analysis showed that configuration factors for such tubes are very small. Also, it is unlikely that a significant fraction of radiation would penetrate to such tubes in any case because of absorption by the intervening steam, since the equivalent beam length for radiation in the steam for the given geometry of tubes is about 0.54 m. (36, Fig. 31-33, 32, Table 4-2) and the shortest distance to tubes beyond those considered in Figure 7 is about 0.77 m.

Using the string method, the configuration factors for tube c with tubes 2A, 2B and 2C in Figure 7 were determined in turn. The resulting values and the corresponding overall configuration factor between tube c and all tubes 2 are listed below:

$$F_{c2A} = 0.203$$

$$F_{c2B} = 0.142$$

$$F_{c2C} = 0.082$$

$$F_{c2} = 0.427$$

Since it has been assumed that all radiation emitted by a calandria tube impinges on either the steam or the surrounding calandria tubes, the configuration factor between a calandria tube and the surrounding steam is:

$$F_{cs} = 1 - F_{c2}$$

$$= 0.57$$

For the beam length of 0.54 m., assuming a mean steam pressure of one atmosphere*, the steam emissivity was determined using Figures 4-15 and 4-16 of reference 32. The resulting value of ε_s is 0.49.

*For much of the transient, the mean steam pressure in the calandria will be somewhat above one atmosphere and at certain moments it will be well above atmospheric pressure. Increased pressure will increase the absorptivity of the steam and thus improve radiation cooling of the calandria tubes. Such improvements are ignored in the analysis.

The dependence of the calandria tube emissivity, ε_c, on temperature is allowed for in the analysis as follows:

$$\varepsilon_c = 0.2 \quad , \quad T_c < 100^{\circ}C$$

$$\varepsilon_c = 0.2 + 7.146 \times 10^{-4}(T_c - 100), \quad 100^{\circ} < T_c < 800^{\circ}C$$

$$\varepsilon_c = 0.7 \quad , \quad T_c > 800^{\circ}C$$

4.5.3 Zircaloy-Steam Reaction Heat Source

As an uncovered calandria tube heats up, its temperature soon reaches a level at which the exothermic reaction rate between the steam and Zircaloy becomes significant, providing an additional heat source. IMPECC-UCZ incorporates equations to predict the heat generated by this reaction. The reaction rate is controlled by either solid-state diffusion of oxygen through the previously-formed layer of ZrO_2 (37) or mass transfer of oxygen from the steam flow through the deuterium gas layer which will form at the solid surface as the reaction proceeds (38), whichever is the slower mechanism.

For the solid-state diffusion reaction, it can be shown from the Fick diffusion equation and the Arrhenius rate equation that, for non-isothermal conditions as experienced in the present case, the rate of growth of the ZrO_2 layer is given by:

$$\frac{dz}{dt} = \frac{d}{dt}\left[\int_o^t \left(A_r \exp\left(-\frac{\Delta E}{2R_o T}\right)\right)^2 dt\right]^{\frac{1}{4}} \qquad (20)$$

The values of A_r and $\frac{\Delta E}{2R_o}$, where ΔE is the activation energy and R_o the universal gas constant, are given by Urbanic and Heidrick (37) as follows:

$$T < 1580^{\circ}C$$

$$A_r = 0.036 \text{ cm/sec}^{\frac{1}{4}}$$

$$\frac{\Delta E}{2R_o} = 6793 \text{ K}$$

$$T > 1580^{\circ}C$$

$$A_r = 0.144 \text{ cm/sec}^{\frac{1}{4}}$$

$$\frac{\Delta E}{2R_o} = 8007 \text{ K.}$$

The discontinuity in the Arrhenius rate equation indicated by the two sets of constants results from the change in oxide microstructure from tetragonal $Zr\ O_2$ to cubic $Zr\ O_2$ at temperatures greater than about 1580°C.

For the mass-transfer controlled reaction rate, the analogy between heat and mass transfer together with Grimison's equation for turbulent-flow heat transfer across a bank of cylindrical tubes arranged on an in-line pattern, as given previously in this section, have been used in the program. The resulting equation for the mass transfer coefficient is:

$$\frac{h_D\, d_o}{D} = 0.269\ RTB\ \ Re_{max}^{0.628}\ \ Sc^{1/3} \qquad (21)$$

The diffusion coefficient for steam through hydrogen is given by (13):

$$D = 0.6115\ \left(\frac{T}{273}\right)^{1.81} \qquad (22)$$

where T is the steam temperature and it has been assumed that the pressure is atmospheric.

It can be shown that the rate of growth of the $Zr\ O_2$ layer when controlled by mass-transfer is given by:

$$\frac{dz}{dt} = \frac{M_z}{2\rho_z}\,\frac{\rho_s}{M_s}\ h_D\ (C_s - C_w) \qquad (23)$$

In the program, C_s and C_w are input values, but in all cases considered so far, $C_s = 1.0$ and $C_w = 0$.

The logic in IMPECC-UCZ selects the lower of the two reaction rates at any time during the transient. When the mass transfer reaction rate is governing at certain calandria tube nodes at a given time, the program prints out this information.

The Zircaloy-steam reaction on the calandria tube is completed when the entire tube thickness has been oxidized.

It should be noted that the deuterium produced in the calandria during the Zircaloy-water reaction on the calandria tubes has been ignored in calculating the pressure drop in the relief ducts and the calandria pressure at any time. Errors in the predicted results arising from this assumption are negligible as will be discussed later in this report.

4.6 Thermal Behavior of Fuel Channel Debris

Debris that collects at the bottom of the calandria from fuel-channel disintegration is quenched by the remaining moderator, as discussed earlier. Eventually, however, the moderator will completely boil off*, so that the quenched debris will no longer be well-cooled and its temperature will start to rise again because of the heat generated by the remaining** fission products. Temperatures of the debris may reach the melting points of ZrO_2 and UO_2 and a molten pool of these materials may form at the bottom of the calandria.*** These events are covered in boxes 30 to 32 in Figure 3.****

To establish whether a molten pool of core material will form at the bottom of the calandria and to determine the times at which such a pool might begin to form under various conditions which might be encountered, a simple one-dimensional transient heat transfer model was developed and a computer program, DEBRIS, was written using this model. For cases in which a molten pool is predicted to form, its effects on the calandria wall, cooled by the shield tank water, were established from literature data on molten pools of core material with internal heat sources using a one-dimensional steady-state model of the calandria wall to determine whether wall melting would occur and if so, its extent.

---

*The debris will probably dry out, as a result of critical heat flux effects (e.g., 39) and begin to heat up before the moderator has completely boiled off. However, since the time at which the moderator completely boils off is uncertain, and the effect of debris critical heat flux on dry-out time is probably within this uncertainty, this effect was ignored in this study. In any case, as we will see, the thermal behavior of the debris is not very sensitive to the assumed debris uncovery (dry-out) time, at the values of this parameter which are expected in this accident sequence.

**Most of the free gas fission products will have escaped from the fuel before or when the channels disintegrate.

***Other materials, from control and safety devices, etc., would be found in the debris in an actual case, but they would constitute a very small fraction of the total and are ignored here.

****The models described here are also applicable to the events covered in boxes 37 to 39 of Figure 3, the behavior of core debris in the shield tank.

The methods used in these models and analyses are described in this section of the report.

4.6.1 Transient Thermal Behavior of Solid Debris

4.6.1.1 Characteristics of Debris

The disintegration of fuel channels under the severe temperature and mechanical and thermal stress conditions existing after calandria tube uncovery would obviously be a very complex and random process. It is not possible to predict the physical and geometric characteristics of the resulting debris with any confidence. The debris will consist of fragmented UO_2 particles, fractured pieces of oxidized Zircaloy with a spectrum of unknown shapes and sizes, and possibly re-solidified particles of previously molten Zircaloy. All that can be said is that the debris would probably form a porous layer of heated and unheated particles and larger fragments of different shapes and sizes. Some guidance on the thermal behavior of solid core debris is available in the literature from methods of analysis of core disassembly accidents in liquid-metal fast breeder reactors (e.g., 40). However, much of this information cannot be applied directly since it is based on prior core behavior and core characteristics which do not apply to the present problem.

4.6.1.2 Basic Heat Transfer Model and Property Values

The model developed to predict the transient thermal behavior of the debris recognizes the above facts. It is assumed that the debris forms a porous bed with the porosity (ratio of pore volume to total bed volume) and the average pore size to be specified as inputs to the computer program DEBRIS. In this way, the sensitivity of the thermal behavior of the debris to these important parameters can be evaluated and conclusions can be drawn using engineering judgment, as we will see.

In the model, the solid portion of the debris is assumed to be composed of a mixture of UO_2 and $Zr\ O_2$ in proportion to the quantities of UO_2 and Zircaloy originally in the core, allowing for the oxidation of the Zircaloy. The pores of the bed are assumed to be filled with heavy water vapor at atmospheric pressure.

Lacking any other information, the bed was assumed to be uniform throughout, i.e., it consists of a uniform distribution of averaged-size pores in a uniform mixture of UO_2 and $Zr\ O_2$.

The basic heat transfer model used in the analysis and incorporated in the program, DEBRIS, represents heat flow rates through the debris bed described above. The mechanisms of heat transfer considered are conduction through the solid material and conduction and radiation through the steam-filled pores.* The actual model developed assumes conduction through a heterogeneous, uniform mixture of material with a stipulated porosity and mean pore size, with the effective conductivity of the mixture accounting for these various mechanisms, as will be discussed later. Because of the many uncertainties involved in this analysis it was decided to assume a simple one-dimensional heat flow model rather than to attempt to allow for the actual three-dimensional heat flow paths to the curved bottom surface of the calandria and to the ends of the calandria. The one-dimensional model will be conservative in that it will predict higher temperatures in the bed at any time than those predicted by a three-dimensional model.

The depth of the one-dimensional debris bed was assumed to be equal to the distance from the surface of the actual debris bed to the calandria wall along the vertical centre-line of the calandria, i.e., to be equal to the maximum thickness of the actual bed. The bed depth is calculated in the program from the known geometry of the calandria and the assumed fraction of the fuel channels falling into the bottom of the calandria, FRCMAS (as used in MODBOIL), allowing for the volume occupied by the vapor-filled pores.

With the foregoing assumptions, an energy balance on a differential horizontal slice of the bed yields the following equation:

$$\frac{\partial^2 T}{\partial z^2} = \frac{1}{\alpha_B} \frac{\partial T}{\partial t} - \frac{q_{vB}}{k_B} \qquad (24)$$

In equation 24, k_B and α_B are the effective properties of the debris bed allowing for the mixture of UO_2 and $Zr\ O_2$ and the presence of steam-filled pores, accounting for radiation as well as conduction across the pores. The symbol q_{vB}

*Analysis showed that natural convection would not be a significant mechanism of heat transfer within the pores for the ranges of conditions considered likely. Also, the pore size range considered here results in short mean radiation beam lengths, which, coupled with the assumed atmospheric pressure of the steam, results in effectively no absorption of radiation by the steam in the pores.

represents the effective time-dependent volumetric heat source for the bed as a whole, allowing for the dilution effect of the structural material and for the porosity of the bed. As in IMPECC-Z and IMPECC-UCZ, the ANS heat source equation (41) was used to establish the heat source, but this value was reduced by a factor to account for the lack of contribution of gaseous fission products which have been lost from the debris. In DEBRIS, this factor is treated as an input value, but a value of 0.8 has been used in the study (42). The effects of structural material dilution and bed porosity on the volumetric heat source are allowed for as follows:

$$q_{vB} = q_v \left(\frac{V_u}{V_u + V_z}\right) (1 - \varepsilon_v) \qquad (25)$$

where q_v is the actual core-average volumetric heat source in the fuel material itself.

A key element in the analysis is to establish the appropriate value for effective bed thermal conductivity, k_B. This value was established assuming that the debris bed could be represented by a cubical pore structure. The effective thermal conductivity of such a structure, allowing for the same mechanisms assumed here, was established by the author in an investigation of high-temperature insulations for use inside a reactor pressure vessel for a high-temperature gas-cooled reactor (43).

The effective thermal conductivity for such a heterogeneous structure is given by:

$$k_B = (k_s + 4\sigma F_B \delta_p \bar{T}^3)\varepsilon_v^{1/3} + Fk_M (1 - \varepsilon_v^{2/3}) \qquad (26)$$

This equation was found to represent the thermal conductivity of fibrous insulation, with randomly-oriented fibres, at high temperatures, reasonably well ($\pm$ 20%), assuming F = 1.0 (43)*.

---

*Equation 26 is very similar in general form to an equation for the effective thermal conductivity of porous material developed by Ribaud (44):

$$k_{eff} = k_g \varepsilon_v^{1/3} + k_M(1 - \varepsilon_v^{2/3})$$

In equation 26, the radiation interchange factor F_B, for the assumed heterogeneous structure can be shown to be given approximately by:

$$F_B = \frac{3\varepsilon_B}{6 - \varepsilon_B} \tag{27}$$

where the emissivity of the debris surfaces, ε_B, was assumed to be a function of temperature:

$$\varepsilon_B = 0.7223 \times 10^{-3}\, T - 0.075 \tag{28}$$

for $T < 1073$ K

For $T > 1073$ K, the bed surface emissivity was assumed constant at 0.7.

Since the thermal conductivity of heavy water vapor in the required temperature range is not available, the thermal conductivity of ordinary water vapor was used for k_s. This assumption will not result in any significant errors in the analysis. The value of k_s as a function of temperature was taken from reference 19, and is represented in DEBRIS by a polynomial valid below 850 K. Above 850 K, k_s was extrapolated as a linear function of temperature, based on the dependence of k_s on temperature in the upper portion of the temperature range below 850 K.

The effective thermal conductivity of the solid debris, k_M, was assumed to be the volume-weighted average value of thermal conductivity for UO_2 and $Zr\,O_2$, assuming random orientation of layers of UO_2 and $Zr\,O_2$, and representing this random orientation by assuming 1/3 of the layers are perpendicular to the heat flow path and 2/3 are parallel to the heat flow path (45). The resulting value of k_M is given by:

$$k_M = \frac{1}{3}\, k_1 + \frac{2}{3}\, k_2 \tag{29}$$

$$\text{where} \quad k_1 = \frac{1}{\frac{V_u}{V_u+V_z}\frac{1}{k_u} + \frac{V_z}{V_u+V_z}\frac{1}{k_z}}$$

$$\text{and} \quad k_2 = k_u \frac{V_u}{V_u+V_z} + k_z \frac{V_z}{V_u+V_z}$$

Although thermal conductivities of irradiated UO_2 and of Zr O_2 vary with temperature, these variations were ignored in the analysis and mean values were used for the anticipated temperature ranges. The values used in the study were (46,47)

$$k_u = 3.0 \text{ W/mK}$$

$$k_z = 2.5 \text{ W/mK}$$

Justification for ignoring the variation of k_u and k_z with temperature is the large uncertainties in these values, especially at high temperatures, which are of the same order as the apparent variations. It should be noted that the decreases in k_u and k_z which might normally be expected at high temperatures are compensated by the increasing contribution of internal radiation effects and/or increasing electron conduction at these temperatures (44,45).

In the debris, there will be random, non-conforming contacts between fragments; these contacts will result in additional thermal resistances to heat flow. For a discussion of thermal resistance resulting from non-conforming contacts, see reference 48. The effect of these random contacts is accounted for by the factor F. This factor is an input value in the program, DEBRIS, and may be varied from 0 to 1.

To establish the value of α_B used in the analysis, values of the effective density, ρ_B, and effective specific heat, C_{pB}, of the debris are required, in addition to the value of k_B. The density of the solid material, ρ_m, is the volume-weighted average of the densities of UO_2 and Zr O_2. The effective density of the debris bed as a whole is given by

$$\rho_B = \rho_m(1 - \varepsilon_v) \tag{30}$$

where the density of the steam in the pores has been ignored since it is negligible compared to those of the solid materials.

The specific heat of the solid material, C_{pm}, is the mass-weighted average of the specific heats of UO_2 and Zr O_2. The effective specific heat of the debris

bed, C_{pB}, ignoring the negligible internal energy of the steam compared to that of the solid materials can be shown to be equal to C_{pm}.

Although there are considerable uncertainties in the model and the property values used to establish k_B, the thermal behavior of the debris is not very sensitive to variations in the various input parameters in equation 26, when these are varied over ranges that might be expected in the actual debris, and for the time periods that are likely to be encountered in the accident sequence being considered here, as we will see later. In particular, heat transfer rates and resulting thermal behavior are not very sensitive to variations in the parameters affecting heat flow rates in the solid fraction, including k_u, k_z and F, as will be shown later. Therefore, the predicted thermal behavior of the debris is probably less uncertain than might be expected from the large uncertainties in the properties and the configuration of the debris.

4.6.1.3 Boundary and Initial Conditions

Heat transfer from the upper surface of the debris bed is assumed to occur by radiation to the calandria wall above the bed, cooled by the shield tank water, and by natural convection to vapor above the bed, also eventually cooled by the calandria wall.

The radiation interchange factor, consistent with the simplified model of the debris bed, is given by

$$F_T = \frac{1}{\frac{1}{\varepsilon_T} + \frac{A_T}{A_{cs}} \left(\frac{1}{\varepsilon_{cs}} - 1\right)} \qquad (31)$$

The emissivity of the upper surface of the debris bed, ε_T, is assumed to be the same as that of the surfaces within the bed and so is given by equation 28. The emissivity of the calandria wall, ε_{cs}, is an input value to the program. A value of $\varepsilon_{cs} = 0.3$ was used in this study. The geometric ratio A_T/A_{cs} is calculated in the program. Note that this approach ignores absorption of radiation by the steam above the bed. Partial absorption of radiation would tend to increase the cooling rate of the top surface, but the higher average temperature of the steam than the calandria wall would tend to decrease the cooling rate. These tendencies compensate and so steam absorption of radiation from the upper surface of the bed was ignored.

The heat transfer coefficient for natural convection at the top surface of the bed is assumed to be given by the conventional correlation for turbulent natural convection from a large heated plate cooled on its upper surface (e.g., 26). Property values of the steam used to determine the natural convection heat transfer coefficient, in addition to thermal conductivity, are also provided as functions of temperature in the program DEBRIS. The mean steam temperature for natural convection cooling of the upper surface of the debris was assumed to be the arithmetic average of the calandria wall temperature and the upper surface of the debris. The calandria wall temperature is an input to the program. Its value was assumed to be that predicted by MODBOIL for nodes well above the debris just before the moderator completely boiled off. In all cases examined, this value was slightly above 100°C, so that a constant value of 105°C was used in the study.

Heat transfer from the bottom of the debris bed is by conduction through the calandria wall and then by natural convection or nucleate boiling to the shield tank water. Natural convection from the calandria wall is calculated for turbulent conditions around a large cylinder (e.g., 26). Although local natural convection heat transfer coefficients on the wall near the bottom of the calandria may deviate from those predicted in this manner, they will be of the correct magnitude and in any case, being quite large, they will not constitute the governing coefficients, so that results will be very insensitive to their actual values.

For nucleate boiling conditions, the Jens-Lottes correlation (32, eq. 14-7) is used to predict the heat transfer coefficients. Again, high accuracy is not needed in predicting the nucleate boiling coefficients because of their very large values. The program DEBRIS selects the appropriate heat transfer mechanism corresponding to the existing conditions at any time.

It should be noted that the method used to establish the boundary conditions at the bottom of the debris bed treats the calandria wall as a thermal resistance only, ignoring any energy storage effects in it. This assumption is justified because of its small heat capacity compared to that of the debris.

The debris bed is assumed initially to be at a uniform temperature equal to the weighted-average debris temperature calculated by MODBOIL at the time that

moderator boil-off is assumed to be complete. Similarly, the initial calandria wall temperature is assumed to be the average at this time for the calandria wall for the slices used in MODBOIL.

4.6.1.4 Computer Program DEBRIS

The analysis employing the heat transfer model and boundary and initial conditions described above has been incorporated in a computer program, DEBRIS, using an explicit finite-difference method.

In the program the debris bed is represented by ten nodes, with the first located at the upper surface of the bed and the tenth at the lower surface of the bed, i.e., at the interface between the debris bed and the calandria wall. Values of bed thermal conductivity are evaluated at the arithmetic average temperatures between adjacent nodes.

The time increment used in the program is an input value chosen by the user. To ensure that this choice does not result in mathematical instability resulting from the forward-difference technique used, the program incorporates a stability check at each time step. Should the stability criteria (considering both upper and lower surfaces) not be satisfied at each time step, the program prints out a message to this effect and stops the calculations.

A listing of the program, containing detailed comments and definitions of all variables, is given in Appendix D together with a sample output.

The major objectives of DEBRIS are to determine whether or not the debris will reach the melting point, under various conditions, and if so, how long does it take to reach this condition. Once melting begins anywhere in the debris, the analytical model is no longer valid, of course. The behavior of a molten pool is examined in the next section of this report.

4.6.2 Effect of Molten Pool of Core Debris on Calandria Wall

Should the solid core debris described in the previous section reach a sufficiently high temperature, it will begin to melt. Although, as we will see, complete melting of this debris is very unlikely under the range of conditions considered in this study, nevertheless, it is important to determine the possible effects on the calandria wall should a completely molten pool of

core debris be formed in the calandria. Therefore this question was investigated and the approach used and the models developed in the investigation are described in this section of the report.

There are two major aspects to this question: thermal behavior in the molten pool itself, specifically the heat fluxes from the upper and lower surfaces of the pool under various conditions, and the interactions between the molten pool and the calandria wall as a function of the effectiveness of the cooling of the wall. The ultimate questions to be answered are whether the calandria wall melts through completely and, if it does not, whether it can be expected to maintain its structural integrity.

4.6.2.1 Thermal Behavior of Heat-Generating Molten Pools

Prompted by the need to analyze severe accident sequences, particularly for liquid-metal fast breeder reactors, a number of studies have investigated the thermohydraulics and heat transfer characteristics of volume-heated pools (e.g., 24,40,49-54). A review of these references indicated that two situations must be considered:

a) Non-boiling pools
b) Boiling pools.

Experiments and analytical studies have shown that non-boiling conditions will occur in relatively shallow pools, but that boiling will occur at some point as the pool depth increases. Since we wish to consider the possible effects of various fractions up to 1.0 of the total core mass forming a molten pool, which could lead to the formation of a quite deep pool (maximum depth equal to one metre or more), we must consider both these situations.

In both of these situations, but particularly for boiling pools, there is considerable uncertainty about the behavior of the molten pool because of the complex nature of the mechanisms involved, the very great difficulty of undertaking experiments with molten pools using actual core materials and considerable uncertainty in property values of the molten and vaporized core materials. Nevertheless, sufficient information is available that estimates of the pool behavior under these conditions are possible, and, in particular, that answers can be provided with some confidence to the questions listed in section 4.6.1.4, as we will see.

Simplified models of pool behavior for both the above situations have been developed which nevertheless retain the essential features of molten pool behavior.

The most severe conditions for the calandria wall would be those in which the entire mass of any debris in the bottom of calandria would be molten, with no solidified crusts forming around the edges of the pool. As we will see later, these conditions will not arise and crusts would definitely form should a molten pool develop. However, to be conservative and to provide a simple model, it was assumed that the entire mass of whatever fraction of the total core mass accumulated in the bottom of the calandria would eventually form a molten pool. A boundary condition for these pools, whether boiling or not, was then assumed to be a constant temperature equal to the melting temperature of the core material. This assumption simplifies the analysis since only internal mechanisms of heat transfer within the pool need to be considered.

The model used in the analysis is a two-dimensional one, with heat flows from the pool towards the ends of the calandria being ignored. The model will thus represent the conditions near the centre of the calandria and will be conservative for conditions near the ends of the calandria.

4.6.2.1.1 Non-boiling Pools

For non-boiling conditions, the basic internal heat transfer mechanisms would be natural convection to the nominally-flat upper surface and to the curved lower surface of the pool (49,51,54). In addition, because of the very high temperatures which would exist in molten pools of core debris, internal thermal radiation is also an important mechanism of heat transfer to both surfaces (50,53).

For natural convection to the upper surface, the correlation of Kulacki and Goldstein (49) is used in the model:

$$Nu_u' = 0.960\ Ra_u^{0.228} \qquad (32)$$

where Nu_u', the natural convection Nusselt number for the upper surface, is:

$$Nu_u' = \frac{q_u'' \overline{Z}}{k(T_m - T_w)} \qquad (33)$$

and Ra_u, the Rayleigh number for the upper surface based on volumetric heat generation rate is:

$$Ra_u = \frac{g \beta q_v \bar{z}^5}{64 k \alpha \nu} \tag{34}$$

Experiments have shown that the natural convection heat transfer rate from a molten, heat generating pool to a cylindrical lower surface is significantly higher than that to a flat lower surface (51,52,54). The correlation of Mayinger, et al., (54) predicts natural convection heat transfer in a volume-heated molten pool to a cylindrical lower surface for different maximum pool depths, L_d. However, it is valid only to ratios of L_d/R down to 0.3. For lower values of L_d/R, Gabor, et al., (51) have shown that it overpredicts the heat transfer rate, but they do not present a correlation for this region. The author combined the predictions of the Mayinger correlation for $L_d/R > 0.3$ with the results of Gabor, et al., at $L_d/R = 0.25$ and 0.122 to develop a modified correlation which should be reasonably valid over the range of $0.122 < L_d/R < 1.0$:

$$Nu'_d = 0.54\, Ra_d^{0.18} \left(\frac{L_d}{R}\right)^{0.39} \tag{35}$$

where Nu'_d and Ra_d are given by equations 33 and 34 with L_d replacing $\bar{z}$.

Equation 35 predicts the average Nusselt number for heat flow to the lower surface of the pool. Local Nusselt numbers vary significantly over the surface (51). From reference 51, the maximum local Nusselt numbers on the lower surface, occurring at the upper corners of the pool, where the boundary layers on the lower surface begin to develop, are approximately twice the average values over the entire L_d/R range. Maximum local heat fluxes on the lower surface were calculated in this analysis on this basis.

The experiments of Stein, et al. (50), actually using molten UO_2, show clearly the need to allow for internal radiation heat transfer in such pools. In the present study, the approach recommended by Anderson (53) was used. In this approach, the total heat transfer rate, allowing for both natural convection

and internal thermal radiation, assuming an optically-thick medium,* is given by:

$$Nu = Nu' + \frac{4}{3\,N}\left(\frac{\theta_m^4 - 1}{\theta_m - 1}\right) \tag{36}$$

where Nu' is given by either equation 32 or 35.

In equation 36, N is a conduction-radiation coupling parameter given by:

$$N = \frac{k\,K_R}{4n^2\,\sigma\,T_w^3} \tag{37}$$

Values of K_R, the Rosseland absorption coefficient, and n, the index of refraction, of molten UO_2 used in the present study are given by Anderson (53) as:

$$K_R = 50\ cm^{-1}$$

$$n = 2.3$$

The analysis utilizes a steady-state heat balance between the heat generation rate in the molten pool and the heat flow rates over the upper and lower surfaces to establish the thermal conditions in the pool and the heat fluxes on the surfaces. The heat balance is given by

$$q_v = \left(q_u'' + q_d''\,\frac{\theta R}{w}\right)/\bar{z} \tag{38}$$

where q_u'' and q_d'' are the average upward and downward heat fluxes allowing for both natural convection and radiation.

The problem is treated as a steady-state problem although the decay heat source decreases with time. However, at the times in the accident sequence at which a molten pool might form the rate of change of the heat source with time is very slow, as we will see, and the problem may be treated as a quasi-steady state situation with good accuracy.

*Satisfied by layers of molten UO_2 as thin as 1 cm.

A difficulty in applying this analysis to predict the thermal behavior of a molten pool of core debris was the establishment of property values for the molten mixture. Anderson (53) gives two sets of property values for molten UO_2, to indicate the uncertainties in these values. No corresponding values for molten Zr O_2 could be found, and the validity of using conventional methods of liquid property value predictions (e.g., 55) under these circumstances is quite unknown. Therefore, property values used in this portion of the study are those of molten UO_2, as given by Anderson. Both sets of values have been used in the study to help establish sensitivities. The molten mixture volume, however, is calculated allowing for both UO_2 and Zr O_2 and the volumetric heat source is based on the mixture volume, i.e., the dilution effect of Zr O_2 is accounted for in establishing the volumetric heat generation rate.

4.6.2.1.2 Boiling Pools

As the depth of a molten heat-generating pool increases, for a given volumetric heat source, the pool internal temperature will eventually reach the saturation temperature and boiling will start.

Under boiling conditions, the upward heat flux at the pool boundary is basically that associated with the vapor reaching the surface (56). The downward heat flux can be predicted by the simple correlation of Gabor, et al., (51) for the average Nusselt number on a cylindrical surface. In both cases, internal radiation effects can be accounted for using the method of Anderson (53), as before.

The upward heat flux associated with the vapor reaching the surface is estimated in the following manner. A value is assumed for the pool-average void fraction, from which, assuming a churn-turbulent flow pattern with $C_o = 1.2$, the superficial vapor velocity at the surface of the pool, $j_{g\infty}$, is found from a prediction of pool-average void fraction as a function of $j_{g\infty}/v_\infty$ developed by Ginsberg, et al., (24) which has been confirmed experimentally. The assumed pool-average void fraction is also used to calculate the geometric parameters of the boiling pool (e.g., L_{db} and $\bar{z}_b$). From the superficial vapor velocity, the fraction of the volumetric heat source going to vapor formation is determined, from which the equivalent upwards heat flux and Nusselt number are found. The effect of internal radiation heat transfer is allowed for in the same manner as for non-boiling pools.

The downward heat flux is calculated by the correlation of Gabor, et al., (51) for the average Nusselt number on a cylindrical surface over an included angle of 60°:

$$Nu'_{db} = 35 \ (\pm 12\%) \qquad (39)$$

Gabor, et al., (51) show that variation of downward local heat flux over a cylindrical surface under boiling conditions is much less than that experienced under non-boiling conditions, so that local variation in this value was ignored for the boiling pool. Again, the effect of internal radiation heat transfer is allowed for in the same manner as for non-boiling pools.

With the average upward and downward heat fluxes established for the assumed pool-average void fraction, the heat balance is checked by equation 38, (with θ_b and w_b replacing θ and w). If the heat balance does not check within the desired accuracy* a new value of the pool-average void fraction is assumed and the calculations repeated. This procedure is continued until the heat balance converges to within the required accuracy.

The effects of the vaporized core material above the pool are considered in section 4.6.2.3.

4.6.2.1.3 Computer Program MOLTENPOOL

A computer program, MOLTENPOOL, has been developed to perform the calculations for the analysis of the thermal behavior of molten pools. The program uses either set of property values given by Anderson (53), at the choice of the user.

For the case of a boiling-pool, additional property values, namely, surface tension, vapor density and latent heat of vaporization, are needed. The values used are:

σ = 0.45 N/m or 1.37 N/m

ρ_g = 1.6 kg/m^3 or 1.0 kg/m^3

h_{fg} = 1.360×10^6 J/kg (set No.1.),
1.445×10^6 J/kg (set No.2.) or 2.09×10^6 J/kg

*A target accuracy of 1% was used in the study.

The first value of σ was taken from reference 57, for the oxide component of core melt, while the second was estimated from the data of Kazimi and Chen (58). The first value of ρ_g was estimated from generalized compressibility charts for vapors (55) and the second value was again obtained from the data of Kazimi and Chen (58). The values of h_{fg} were calculated by the method of Kistyakowsky (59), which was found to give reasonably accurate predictions of h_{fg} for uranium. Values of h_{fg} are given corresponding to sets No.1 and No.2 of Anderson's values, since Kistyakowsky's method gives h_{fg} as a function of the boiling point, which is different in each set. The other value of h_{fg} was once again obtained from Kazimi and Chen (58). Each set of vapor properties is combined with each set of liquid properties given by Anderson, so that four sets of property values are available in the computer program. In the study, results were obtained with each set of property values to explore the sensitivity of results to variations in property values.

The program has been used to investigate the thermal conditions in molten pools of core debris for a range of values of FRCMAS. The program print-out states whether the pool is boiling or not as well as providing the surface heat fluxes and other molten pool characteristics.

A listing and sample output of the program MOLTENPOOL are given in Appendix E, where the four sets of property values used are also given.

4.6.2.2 Interaction of Molten Pool with Calandria Wall

The interaction of a molten pool of core material with the calandria wall would be quite complex. A portion of the wall could melt and a crust of solid core material could form. During this process, a melt front would be propagating into the calandria wall and a solidification front would be propagating into the molten core material. Convection heat transfer would occur in the molten regions and conduction in the solid regions. Heat would continue to be generated in the solid crust. The solid crust could crack and permit molten material to flow into the cracks. In addition to the mathematical difficulties posed by such a system, there are considerable uncertainties in property values and their variation with temperature.

Because of the relative thinness of the calandria wall compared to its radius and because, as we will see, any crust that forms would also be relatively thin,

the curvature of the wall may be neglected and the problem treated as a one-dimensional system. The solid crust formed is assumed to remain stable in the present analysis.

A diagram of the syste to be analyzed is shown in Figure 8.

A review of the literature indicated four approaches that might be applicable to this problem, those of Yuen and Kleinman (60), Hakim (61), Nansteel and Wolgemuth (62) and El-Genk and Cronenberg (63).

Unfortunately, none of these approaches could be applied readily to the present problem for various reasons, such as being too restrictive (e.g., only one melting-solidification front or adiabatic boundary conditions), containing obvious errors or contradictions or having undefined terminology.

Therefore, an asymptotic approach was developed and used to establish the effects of the interaction of a molten pool with the calandria wall. In this approach, the transient behavior resulting from a molten pool contacting the calandria wall is ignored, but the ultimate steady-state conditions are established. The work of El-Genk and Cronenberg (63) shows that steady state conditions will ultimately be reached for a system like that considered here. Although no real steady-state would be reached here because of the decaying heat source, its rate of change is slow enough that quasi-steady-state conditions would eventually be reached. Although this approach will not enable predictions of the time behavior of wall melting and crust formation, it will enable us to determine whether the wall will melt through completely, or, if not, the fraction of wall actually melted and the thickness of crust formed. Therefore, it enables the questions posed earlier to be answered.

The analysis was applied to the system shown in Figure 8, consisting of a solid wall, a molten wall layer, a solidified crust of core materials and a molten layer of core materials.

The analysis employed the following assumptions:

a) constant property values apply (but appropriate average values for the temperature ranges concerned are used)

b) heat transfer on the outer surface of the calandria wall occurs by either natural convection or nucleate boiling

c) heat flow into the solid crust from the molten pool can be characterized by either a constant heat flux or by convection heat transfer in the pool with a designated pool temperature

d) no heat source exists in the solid crust. Obviously, this will not be the case but, as long as the crust is thin, this assumption will not result in a significant error (63).

e) The mechanism of heat transfer within the molten wall layer is conduction only. While some natural convection might develop in this layer, because of its thinness under anticipated conditions, considering the high viscosity of the melted wall material, no significant natural convection is expected.

f) Any crust formed is stable, i.e., it remains in position and does not develop cracks.

g) The interface temperature between the molten pool and the crust is the pool freezing temperature. This temperature is assumed constant in the analysis, although it will change slowly with time as the lower freezing point components of the molten core solidify and the composition of the remaining molten pool changes.

h) The interface temperature between the solid and molten wall layers is the wall material melting temperature.

With these assumptions, the analysis yields the following non-dimensional equations for the steady-state thickness of the remaining solid wall and the solidified crust:

$$\frac{\delta_w}{\delta_a} = \frac{1}{\phi} - \frac{1}{Bi_{ac}} \tag{40}$$

$$\frac{\delta_s}{\delta_a} = \frac{k_s}{k_w} \left\{ \frac{1}{\phi} \left(\frac{T_f - T_m}{T_m - T_c} \right) + \frac{k_w}{k_m} \left(\frac{1}{\phi} - \frac{1}{Bi_{ac}} - 1 \right) \right\} \tag{41}$$

where ϕ is the non-dimensional heat flow rate from the molten pool and Bi_{ac} is a Biot number based on the initial calandria wall thickness and the shield tank heat transfer coefficient. The parameter ϕ is defined in two ways, depending on the characterization of the heat flow rate from the molten pool.

For the case in which the heat flow rate from the pool is characterized by a convection heat transfer coefficient, h_b, and a designated pool temperature, T_b:

$$\phi = Bi_a \frac{T_b - T_f}{T_m - T_c} \tag{42}$$

where

$$Bi_a = \frac{h_b \delta_a}{k_w} \tag{43}$$

For the case in which the heat flow rate from the pool is characterized by a constant heat flux, q''_b :

$$\phi = \frac{q''_b \delta_a}{k_w (T_m - T_c)} \tag{44}$$

The parameter Bi_{ac} in equations 40 and 41 is defined by:

$$Bi_{ac} = \frac{h_c \delta_a}{k_w} \tag{45}$$

These equations permit conditions to be established for the cases of no wall melting, partial wall melting and complete wall melting.

Since, for no wall melting, $\delta_w/\delta_a \geq 1$, it can be readily shown that there will be no melting of the calandria wall when:

$$Bi_{ac} \geq \frac{\phi}{1 - \phi} \tag{46}$$

Similarly, since, for complete wall melting, $\delta_w/\delta_a \leq 0$, it can be shown that there will be complete melting of the calandria wall when:

$$Bi_{ac} \leq \phi \qquad (47)$$

For values of Bi_{ac} lying between the values defined by equations 46 and 47, there will be partial wall melting. Note that there will always be at least some melting of the calandria wall for values of the non-dimensional heat flux, ϕ, equal to, or greater than 1.0.

A map of the no-melting, partial-melting and complete melting regions for the calandria wall, as defined by equations 46 and 47, is shown in Figure 9.

Figure 9 may be used to determine whether any melting of the calandria wall would eventually occur for values of downward heat flux established for various conditions as described in section 4.6.2.1 and its sub-sections.

Should partial melting of the wall be predicted from Figure 9, equation 40 can be used to determine the remaining fraction of solid wall. To complete the assessment, equation 41 can be used to establish the thickness of solidified crust formed, whether partial melting of the wall occurs or not.

These assessments can be facilitated by plotting equations 40 and 41 for appropriate ranges of the various non-dimensional parameters. Figure 10 is a plot of equation 40 with δ_w/δ_a as a function of ϕ with Bi_{ac} as a parameter, ranging from 0.25 to 100,000.

Equation 41 can be plotted as $\frac{\delta_s}{\delta_a}\frac{k_w}{k_s}$ versus ϕ with Bi_{ac} as a parameter, in a similar fashion. However, for this plot two additional non-dimensional parameters are required:

$$\frac{T_f - T_m}{T_m - T_c} \quad \text{and} \quad \frac{k_w}{k_m} .$$

Values of these parameters can be readily calculated for the conditions of interest here. For a molten pool of the composition of core material, assuming as before that only UO_2 and $Zr\ O_2$ compose the core, the eutectic freezing temperature, T_f, for the concentration of UO_2 and $Zr\ O_2$ in the core is 2500°C, as determined from information in reference 64. The melting point of the austenitic stainless-steel calandria wall is 1430°C and the shield tank temperature is 60°C. The ratio k_w/k_m for austenitic stainless steel, according to Hakim (61) is 0.8.

Therefore values of these two parameters which are appropriate for the present problem are:

$$\frac{T_f - T_m}{T_m - T_c} = 0.8$$

$$\frac{k_w}{k_m} = 0.8$$

Equation 41 is plotted in Figure 11 for these values of the parameters.

Equation 41 for $\delta_s/\delta_a = 0$ is also plotted in Figure 9 to indicate the limit of the crust formation region. Note that no crust will ever form for $\emptyset \geq 2.0$ for the present conditions.

From Figures 9, 10 and 11, the predicted behavior of the calandria wall exposed to molten core material under various conditions can be readily established.

4.6.2.3 Interaction of Vaporized Core Material with Calandria Wall

In section 4.6.2.1.2, the behavior of a molten pool under boiling conditions was discussed. With a boiling pool of core debris, vaporized core material would be produced above the surface of the pool. In this section of the report, the behavior of the vaporized core material and, particularly, its interaction with the calandria wall are considered.

As pointed out earlier, in section 4.6.2, we will see later that complete melting of molten core debris is very unlikely; any molten pool formed would almost

certainly be overlaid with a frozen crust of core debris. Nevertheless, the stability of such a crust is quite uncertain, so that it is possible that some core material vapor would be present above the debris in the calandria in this accident sequence.

Virtually no information is available on the behavior of actual vaporized core material. The only reference found in a review of the literature was to a "cloudy haze" over a boiling pool of UO_2 (4, Appendix VIII, App.A, p.A-14), presumably an aerosol formed by particles entrained by the UO_2 vapor or perhaps by condensation within the vapor volume by radiation effects or by mixing with cooler gases or vapors. One of the significant unknown aspects of the behavior of vaporized core material is the effect of volumetric heat generation in core material vapor itself.

Thus, we cannot predict with great confidence the effects of vaporized core material in an accident sequence. However, by considering basic principles of vapor heat and mass transfer we can make estimates of the possible effects of core material vapor on the calandria wall and we can draw some useful conclusions.

The model used in the analysis assumes that the dense core material vapor will displace upwards the D_2O vapor normally present above the molten pool so that there will be a layer of UO_2 vapor formed above the boiling pool which will soon reach a quasi-steady-state equilibrium thickness* governed by a balance between the core material evaporation rate and the condensation rate of the core material vapor.

There obviously will be some contact and mixing between the D_2O vapor and the core vapor which will result in some volumetric condensation of the core material vapor. The resulting droplets may form a suspended aerosol with the larger ones falling back into the boiling pool. These effects and the effects of radiation from the core vapor and from the droplets to the cooled calandria wall are ignored in the model, and only direct condensation on the exposed calandria wall is considered. This assumption is conservative since it results in the heat transfer

*The assumption of quasi-steady-state is justified because the volumetric heat generation rate at this time will be decaying very slowly.

rate to the exposed calandria wall being higher than would actually be the case, which represents more severe conditions for the calandria wall.

With these assumptions, the mass balance on the UO_2 vapor is given by:

$$\rho_{gU} \frac{d V_{gU}}{dt} = 2 \rho_{gU} j_{g\infty} w_b L - \frac{\bar{h}_{cd} A_{cd} (T_{BPU} - T_{MPU})}{h_{fgU}} \quad (48)$$

where the calandria wall area exposed to core material vapor, A_{cd}, is given by:

$$A_{cd} = 2 R (\theta_g - \theta_b) L \quad (49)$$

Once again, we have ignored the ends of the calandria.

From equations 48 and 49, assuming quasi-steady-state conditions, as before, the extent of the calandria wall exposed to core material vapor under equilibrium conditions is given by:

$$\theta_g - \theta_b = \frac{j_{g\infty} w_b \rho_{gU} h_{fgU}}{R \bar{h}_{cd} (T_{BPU} - T_{MPU})} \quad (50)$$

The condensation heat transfer rate to the exposed calandria wall is calculated using a modified Nusselt-type analysis, assuming a laminar film of molten UO_2 is formed on the wall. The modified Nusselt analysis takes into account the formation of a laminar condensate film on a concave surface, and recognizes that a portion of the film will solidify when its temperature drops below the freezing point of the molten core material.

In the analysis, the volumetric heat source in the molten layer is ignored. This assumption is justified by the results of the analysis itself which show that the quasi-steady-state equilibrium thickness of the molten layer is about one millimeter for typical anticipated conditions, so that the additional heat flow rate through the layer because of its internal volumetric heat source is negligible.

The derivation of the equation for the average condensation heat transfer coefficient for the core material vapor, $\bar{h}_{cd}$, is given in Appendix F. It should be noted that the temperature difference across the condensed film is assumed in the derivation (and in equations 48 and 50) to be the difference between the boiling point and melting point temperatures of the core material. This assumption recognizes that a solidified sub-layer will form below the molten condensate layer and that the temperature at the interface between the molten layer and the solidified layer must be the melting point temperature.

It should also be noted that the derivation implies that θ_g will not exceed 90°, since the derivation is for an upward-facing concave surface. Nevertheless, the analysis can be assumed to apply also for θ_g greater than 90° because of the very high surface tension of the molten core material compared to most liquids, which would enable a falling film to adhere to the downward-facing part of the calandria wall for some distance above the calandria centre-plane.

The equation for $\bar{h}_{cd}$, as derived in Appendix F, is:

$$\bar{h}_{cd} = 0.707 \left[\frac{\rho_f^2 \, g \, h'_{fg} \, k_f^3}{\mu_f (T_{BPU} - T_{MPU}) R}\right]^{\frac{1}{4}} Q(\theta_g, \theta_b) \qquad (51)$$

where

$$Q(\theta_g, \theta_b) = \frac{1}{(\theta_g - \theta_b)} \int_{\theta_g}^{\theta_b} \frac{d\theta}{\frac{\tan(\theta_g/2)}{\left[\ln\left(\frac{\tan(\theta_g/2)}{\tan(\theta/2)}\right)\right]^{\frac{1}{4}}}} \qquad (52)$$

Equation 52 can be integrated numerically for any given values of θ_g and θ_b.

Under certain conditions, the power density in the boiling pool may be high enough that the pool vapor condensation rate on the exposed calandria wall surface, as calculated through equations 51 and 52, will not be enough to match the vapor generation rate; that is, equation 48 cannot be satisfied, in its steady-state form. Under these conditions, a large fraction of the calandria wall above the boiling pool will be concave downwards and there will be a greater tendency than

in other cases for the condensing film near the top of the calandria to separate from the wall under the force of gravity. Should this effect occur near the top of the calandria wall, drop-wise condensation would in effect be established in this region, which would result in a higher heat transfer coefficient over the affected area than would be predicted for film-type condensation using equations 51 and 52. Also, the length of the film in the direction of flow probably would be great enough in such cases for the film to become turbulent in the later stages, resulting in an increase in the average heat transfer coefficient over the exposed calandria wall. The model used in the analysis assumes that, under such conditions, the heat transfer coefficient is increased above the value calculated from equations 51 and 52 to the extent necessary to ensure that the condensation rate over the entire surface of the calandria above the boiling pool is sufficient to balance the evaporation rate from the pool, i.e., that equation 48 is satisfied.* This is considered to be a conservative approach, since, in reality in such cases, some of the core-material vapor may be expelled upwards through the relief ducts rather than condensing on the calandria walls. The resulting increased average heat transfer coefficient over the wall of the calandria above the boiling pool results in more severe conditions for the wall.

Of course, the basic conservative elements in the condensation analysis discussed earlier in this section also still apply in these cases.

A simplified analysis of the growth rate of the solidified sub-layer has been developed which again ignores the volumetric heat source in the sub-layer and also ignores the heat storage rate in the solidified layer. The first assumption is justified by the results of the analysis which show that the equilibrium thickness of the sub-layer, which is closely approached very rapidly (typically in less than five seconds) is quite thin, about five millimeters for typical anticipated conditions. The second assumption is also justified by the thin equilibrium sub-layer and the short time required to reach equilibrium thickness, so that the neglect of the rate of heat storage will not affect the overall heat flow rates significantly.

Since the heat flow rate into the solidifying layer is governed by the condensing heat transfer coefficient, which varies with position on the wall, the solidified

---

*For steady-state conditions

layer growth rate and equilibrium thickness will also vary with position. However, for the purposes of the present study, the analysis has been based on the average condensing heat transfer coefficient, and so yields predictions of average solidified layer growth rate and equilibrium thickness.*

With these assumptions, the boundary condition at the interface of the solidified layer and the molten layer, which gives the rate of growth of the solidified layer, is given by:

$$\frac{d\,\delta_s}{dt} = -\frac{\bar{h}_{cd}\,(T_{BPU} - T_{MPU})}{\rho_s \lambda} + \frac{U(T_{MPU} - T_c)}{\rho_s \lambda (1 + \frac{U\delta_s}{k_s})} \tag{53}$$

Integration of equation 53 yields the following implicit equation for δ_s at any time, t:

$$t = -\frac{\delta_s}{\beta_1} - \frac{\beta_2}{\beta_1^2}\ \ln\left\{\frac{\beta_3 - \beta_1(1 + \frac{U\,\delta_s}{k_s})}{\beta_3 - \beta_1}\right\} \tag{54}$$

where

$$\beta_1 = \frac{\bar{h}_{cd}\,(T_{BPU} - T_{MPU})}{\rho_s \lambda} \tag{55a}$$

$$\beta_2 = \frac{k_s (T_{MPU} - T_c)}{\rho_s \lambda} \tag{55b}$$

$$\beta_3 = \frac{U(T_{MPU} - T_c)}{\rho_s \lambda} \tag{55c}$$

$$U = \frac{1}{\frac{\delta_a}{k_w} + \frac{1}{h_c}} \tag{56}$$

*An analysis based on average conditions ignores, of course, local conditions near the leading edge of the condensing film, where the heat transfer coefficient will be higher than the predicted average value. The higher local heat transfer coefficient would increase the likelihood of calandria wall melting. However, three-dimensional heat conduction effects in the calandria wall in this region, also ignored in the analysis, would counteract the effects of the higher local heat transer coefficient.

From equation 53, the equilibrium thickness of the solidified layer can be established by setting $\frac{d\delta_s}{dt} = 0$.

The equilibrium thickness is thus:

$$\delta_{se} = \frac{k_s}{U} \left(\frac{\beta_3}{\beta_1} - 1\right) \tag{57}$$

Note that this analysis has implicitly assumed no melting of the calandria wall under the solidified sub-layer of core material (see the equation for U). The effects of wall melting under a solidifying crust on the stability of the crust at a large value of θ, where the molten wall material would tend to flow downwards, are quite unpredictable.

Since quasi-steady-state equilibrium conditions are reached so rapidly by the solidified sub-layer, the analysis described in section 4.6.2.2 can then be used to establish whether any melting of the calandria wall is likely to occur in the region over which core material vapor condensation occurs. A computer program, CONFILM, has been developed to perform this analysis. A listing of CONFILM and a sample output are given in Appendix G. The output of CONFILM contains statements as to whether no, partial or complete melting of the calandria wall would be expected.

Conclusions can then be drawn as to the integrity of the calandria wall when exposed to core material vapor.

4.7 Behavior of Fuel Channel Debris in Shield Tank

The event sequence diagram of Figure 3 considers the effects of calandria wall failure because of overheating (Box 31a).* The possible occurrence of calandria wall failure will be established by the analyses described in section 4.6.2. Should the calandria wall fail subsequent events in the shield tank are indicated in boxes 33 to 43c.

*Box 31a can be considered to represent also calandria wall failure from over-stressing at the conditions experienced in the accident sequence, even if the wall temperature is less than the melting temperature, since the subsequent events will be the same.

As discussed in section 4.4.2.7, and for similar reasons, as given in Appendix C, a vapor explosion may not occur in the shield tank should hot core debris enter it because of calandria wall failure so that the analyses and assessments covered by boxes 33 to 36 may not be required.

The quenching of hot debris in the shield tank (boxes 37, 37a and 38), the subsequent temperature history of the shield tank water (box 38a) and shield tank water boil-off, should it occur (boxes 40 to 43b), can be analyzed by using the same methodology used in MODBOIL for the similar events in the calandria.

Finally, the possible effects of core debris on the shield tank wall (boxes 38b, 38c, 43c and 45) can be analyzed using the methods developed in sections 4.6.1 and 4.6.2.

4.8 Interaction of Molten Core Material with Concrete

4.8.1 Probability of Molten Core Interaction with Concrete

Although, as we will see, it is virtually impossible in accident sequences S11 and S12 for molten core material to melt through the calandria wall, much less the shield tank wall, nevertheless, the possible interaction of molten core materials with concrete, which would occur if melt-through of the shield tank wall were to occur, were examined since these results were not available at the time this analysis took place. This interaction is covered in boxes 46, 47* and 51 of Figure 3. The analytical method developed can also be applied to the interactions between molten core materials and the underlying rock covered in boxes 53 and 54 of Figure 3.

The objective of this part of the study, given core material melt-through of the shield tank, is to predict whether molten core material could melt sufficiently far through the concrete floor of the base mat before solidifying to jeopardize the effectiveness of containment.

4.8.2 Behavior of Concrete Exposed to Molten Core Material

Information on the interactions of molten core material with concrete is given in references 57 and 65 to 69.

---

*Figure 3 indicates, in box 47, that the molten core mass would have to melt through a concrete roof to reach the FM duct. However, there is no concrete roof under the shield tank in Bruce-A so that this box should be ignored.

Gases and vapors are produced during the molten core-concrete interaction by de-hydration and by thermal decomposition. Reactions occur in three temperature regimes:

a) loss of free water, 30 - 250°C

b) loss of chemically-bound water, 380 - 550°C

c) loss of carbon dioxide, 680 - 1000°C

The total evolution of CO_2 depends on the type of aggregate, being less than 2% by weight in basaltic aggregate and more than 20% by weight in limestone aggregates. The rates of loss of water and CO_2 follow the usual Arrhenius equation form:

$$\frac{d\beta_g}{dt} = K_g \exp\left(-\frac{E_g}{R_o T}\right)(1 - \beta_g)^{n_g} \qquad (58)$$

Values of K_g, E_g and n_g for the three reactions listed above are given in reference 66.

The gases generated from the concrete, mainly CO_2 and H_2O, are chemically reduced by any metallic phase of the melt to H_2 and CO (66). However, in the accident sequences being studied, it is highly probable that all metallic phases would have been oxidized long before any molten material would begin to melt through concrete. Whether reduced or not, the gases produced, particularly non-condensibles, would contribute to containment pressurization.

Aerosols are generated at high rates during melt-concrete interactions, especially in the initial stages, with the aerosol concentration being proportional to the gas generation rate (66).

The gases released exert a strong influence on the melt/concrete interaction. The rise of the gas bubbles keeps the melt well-stirred, and hence close to isothermal, and also swells the melt pool.

The gases also tend to form insulating layers between the molten pool and the concrete surfaces. At the bottom of the pool, the gas layer thickness and the

heat transfer rate across it are governed by Taylor instability, similar to heat transfer in film boiling. At the sides of the pool, or beyond about 15° from the bottom of a pool with a curved (circular) lower surface, the heat transfer rate across the gas layer is governed by laminar and turbulent film behavior (66). Heat transfer from the interior of the molten pool to the gas layers is governed by gas-bubble-driven circulation, either indirect (bubble agitation) for steeply-inclined surfaces or direct (bubble injection) for horizontal or near-horizontal surfaces. Heat transfer rates within the pool under these conditions are much higher than those resulting from natural convection alone (65). However, it is very probable that the thermal resistance of the gas layers will be the governing resistance in almost all cases.

The gas bubble and film behavior directly governs the heat fluxes downward and sideways into the concrete. If these heat fluxes are high enough, the concrete will not only decompose, but will melt. Melting begins for both basaltic and limestone concrete at about 1100°C, in the cement; complete liquefaction depends on aggregate type and occurs at 1400°C $\pm$ 50°C (65,68). The latent heat of fusion of concrete is about 400 to 500 kJ/kg (65,68) and is small compared with the sensible heat at its liquidus point. However, as discussed later in this section, the latent heat of fusion used in the analysis must be an effective latent heat taking into account the energy required for the releases of free and chemically-bound water and of CO_2. Experiments have shown that the rate of concrete melting (erosion rate) is directly proportional to the heat flux at the melting interface (66).

Several detailed codes have been developed to predict the effects of melt-concrete interactions (e.g., 66,67). However, considering the improbability of the exposure of concrete to molten core materials in the accident sequences considered here, a simplified approach, based on a method developed by Peckover (67), was used in this study.

4.8.3 Analytical Model of Molten Core Material - Concrete Interaction

Experiments show that the shape of a molten pool melting into a miscible material, without gas formation, will depend on the distribution of the heat flux over the advancing melt front and on the difference in density between the melt pool and the underlying material (65). These experiments also show that the volume of the

melt pool is much less sensitive than its shape to the distribution of heat flux over its advancing surface. They also show that the volume of the pool at any time is also reasonably insensitive to the initial distribution of the debris, provided that it is compact (65).

Therefore, to calculate the maximum volume of the melt pool and the time taken to reach this volume, any reasonable assumption of pool shape and heat flux distribution may be assumed and a good approximation obtained. With this information, the likelihood of a molten pool melting through the concrete base mat and the times at which this event would occur can be estimated.

The most convenient assumption is that the molten pool grows downwards as a hemisphere with the melted material* being incorporated into the pool as it grows, thus diluting the volumetric heat source (65). The previously mentioned experiments show that the shape of the advancing pool roughly approximates a hemisphere when the density of the molten pool is relatively large compared to the underlying material, as would be the case here throughout the transient.

Implicit assumptions in this model are that the heat transfer rate from the molten pool to the concrete is uniform over the surface of the pool and that the melted concrete material is miscible with the molten core debris. The first assumption has been discussed above, and, while not actually true, results in a reasonable prediction of the growth of pool volume. The second assumption is valid provided that all metallic material in the core debris has been oxidized (65), which will certainly be the case as discussed earlier.

The effect of the re-inforcing rods in concrete on its thermal behavior under a molten pool has been shown to be negligible (65) and so is ignored in this analysis. Similarly, the effect of the steel liner on the FM duct floor has been ignored.

Four stages of molten pool growth can be identified:

---

*The gases formed are assume to be released, of course.

i) an early period when the pool grows rapidly and the pool temperature changes rapidly, with any heat conducted into the underlying solid concrete soon absorbed back into the pool by the advancing melt front. Almost all the heat generated in the pool goes into pool growth or into increasing the pool temperature above the melting point; very little net heat flows by conduction into the concrete.

ii) a period of "fast" melting-front growth after the initial pool temperature transient has decayed, but the melt front is still advancing rapidly, with still only a small fraction of total heat generated being conducted into the solid concrete.

iii) a period of conduction-dominated growth in which the advance of the melting front slows. At the end of this period, the maximum pool size is reached.

iv) a period of molten pool shrinkage as the heat source decays and heat is conducted into the solid concrete or re-frozen pool material.

The maximum radius of the molten pool, and the time at which this radius is reached, are governed by conditions in the third stage. In this stage, the molten pool, well-mixed by the generated gases and thermal and concentration gradient effects, will be at a uniform temperature essentially equal to the melting temperature of the concrete (65).

The geometry of the molten pool and surrounding concrete at a given time in the third stage is shown in Figure 12, in which the geometric symbols used in this analysis are defined.

A heat balance on the molten pool under the assumptions given previously can be written:

$$Q_o f(t) f_d \lambda' = (\rho\lambda)_C \, u_{mC} \, A_P - k_C A_P \left(\frac{\partial T_C}{\partial r}\right)_{r_o} \qquad (59)$$

In equation 59, the left hand side represents the fraction of the heat being generated in the pool at any time from fission product decay which flows downwards into the concrete. This term must account for the fraction of core debris that

could melt through the calandria and shield tanks and for the time taken for these processes as well as for the time to reach the third stage of concrete melting. The first term on the right hand side accounts for the effective energy required to melt the concrete and hence to advance the melt front. The second term on the right hand side represents the effective heat flow rate away from the melting front into the concrete.

Because of the evolution of gases and the different melting temperatures of the cement and the aggregate in the concrete there is not really a single melting front (65). Essentially, the penetrating front consists of a number of phase change* fronts propagating in close succession. This behavior can be assumed to be approximated by equation 59, if the phase-change front region is considered thin, provided that $(\rho\lambda)_c$ is interpreted as an effective latent heat per unit volume which includes the heat required to release the water vapor and CO_2 as well as to melt the cement and the aggregate and provided that the second term on the right hand side is interpreted as the effective heat flow rate away from the phase-change front region.

Within the solid concrete, the Fourier equation, written in symmetrical spherical co-ordinates in the frame of reference of the advancing melt front, is given by:

$$\frac{\partial \theta_C}{\partial t} = (u_{mC} + \frac{2\alpha_C}{r}) \frac{\partial \theta_C}{\partial x_C} + \alpha_C \frac{\partial^2 \theta_C}{\partial x_C^2} \qquad (60)$$

where θ_C is a non-dimensional temperature given by:

$$\theta_C = \frac{T_C - T_{C\infty}}{T_{Cm} - T_{C\infty}} = \frac{T_C - T_{C\infty}}{\Delta T_C} \qquad (61)$$

In stage 3, in the vicinity of the melt front (where $\theta_C = 1$), $x_C/r_o << 1$ so that $r \simeq r_o$ and $\frac{\partial \theta_C}{\partial t} \simeq 0$, as the melt front advances in a quasi-steady-state manner.

*Release of free water, release of bound water, release of CO_2, melting of cement, melting of aggregate.

Therefore equation 60 for the third stage can be written as:

$$(u_{mC} + \frac{2\alpha_C}{r_o}) \frac{\partial \theta_C}{\partial x_C} + \alpha_C \frac{\partial^2 \theta_C}{\partial x_C^2} = 0 \qquad (62)$$

A solution to this equation is given by

$$\theta_C = e^{-x_C/\delta(t)} \qquad (63)$$

Taking derivatives of equation 63 and substituting into equation 62, the following equation for $\delta(t)$ can be established:

$$\frac{1}{\delta(t)} = \frac{u_{mC}}{\alpha_C} + \frac{2}{r_o} \qquad (64)$$

At the maximum pool radius, $u_{mC} = 0$, so that:

$$\delta_m = \frac{r_{om}}{2} \qquad (65)$$

The boundary condition at the melting interface can be established from the heat balance, equation 59. From equation 61 and for conditions in the vicinity of the melt front in stage 3 we can write:

$$(\frac{\partial T_C}{\partial r})_{r_o} = \Delta T_C (\frac{\partial \theta_C}{\partial x_C})_o \qquad (66)$$

Substituting for $(\frac{\partial T_C}{\partial r})_{r_o}$ in equation 59, and solving for $(\frac{\partial \theta_C}{\partial x_C})_o$, we obtain:

$$(\frac{\partial \theta_C}{\partial x_C})_o = - \frac{q_{mC}''(t) - (\rho\lambda)_C u_{mC}}{k_C \Delta T_C} \qquad (67)$$

where $q_{mC}''(t)$ is the instantaneous heat flux from the molten pool into the concrete.

Taking the derivative of equation 63 and evaluating it at $x_c = 0$, equation 67 becomes:

$$\frac{1}{\delta(t)} = \frac{q_{mc}''(t)}{k_c \Delta T_c} - \frac{(\rho\lambda)_c u_{mc}}{k_c \Delta T_c} \tag{68}$$

Therefore, the value of $\delta(t)$ at the maximum pool radius is also given by:

$$\delta_m = \frac{k_c \Delta T_c}{q_{mc}''(t_m)} \tag{69}$$

Equation 69 suggests that the parameter δ_m can be considered as the thickness of a "thermal boundary layer" in the concrete.

The instantaneous heat flux from the pool at the maximum radius can be related to the initial reactor power, Q_o, by:

$$q_{mc}''(t_m) = \frac{Q_o f(t_m) f_d \lambda'}{2\pi r_{cm}^2} \tag{70}$$

In equation 70, $f(t_m)$ represents the relative power resulting from fission product decay heat at the time of maximum pool radius:

$$f(t_m) = f_o t_m^{-\alpha} \tag{71}$$

The paramter λ' represents two factors:

a) The fraction of original fuel mass which arrives at a concrete surface.

b) The fraction of fission products remaining in the fuel mass which arrives at a concrete surface.

From equations 65, 69 and 70, the maximum pool radius can be established:

$$r_{om} = \frac{Q_o f(t_m) f_d \lambda'}{4\pi k_C \Delta T_C} \tag{72}$$

To calculate r_{om} from equation 72, the time at which the maximum pool radius is reached, t_m, must be known. This time can be established by equating the total heat generated in the molten pool which does not escape upwards over the time in question to the total heat stored in the molten pool and in the concrete outside the pool at this time. This heat balance is expressed by:

$$\int_{t_i}^{t_m} Q_o f(t) f_d \lambda' \, dt = \frac{2}{3} \pi r_{om}^3 (\rho_C C_C \Delta T_C + (\rho\lambda)_C) + \int_{r_{om}}^{\infty} \rho_C C_C \Delta T_C \theta_C 2\pi r^2 \, dr \tag{73}$$

As we will see, the time at which molten pool formation could begin, t_i, would be of the order of one or two days. Such times are negligible compared to the times at which maximum molten pool radius would be reached. Therefore, we can set $t_i = 0$ as the lower limit of integration of the left hand side of equation 73.

To integrate the left hand side of equation 73, we substitute for f(t) in a manner similar to that given in equation 71 and we assume that f_d is constant at an average value during pool growth. To integrate the second term on the right hand side, we substitute for θ_C from equation 63.

Proceeding in this manner, we obtain the following equation for t_m:

$$t_m = \{1.055 \times 10^{-3} \frac{(\rho\lambda)_C}{(k_C \Delta T_C)^3} (1 + \frac{19}{4} S)(Q_o f_o f_d \lambda')^2 (1 - \alpha)\}^{\frac{1}{1+2\alpha}} \tag{74}$$

where S is the Stefan number:

$$S = \frac{\rho_C C_C \Delta T_C}{(\rho_C \lambda)_C} \tag{75}$$

Property values for concrete required to determine r_{cm} and t_m can be taken from references 57, 65 and 68.

An average value for f_d over the time to maximum pool radius can be estimated from a consideration of the pool internal and insulating gas layer heat transfer coefficients as given in references 57 and 66, as discussed earlier in this section, allowing for radiation heat transfer across the gas film.

4.9 Containment Pressurization

4.9.1 Causes of Containment Pressurization

In accident sequences S-11 and S-12, vapor would be discharged from the relief ducts following failure of the calandria rupture disks and the discharge would continue until all the moderator was expelled from the calandria. In addition, deuterium generated by the chemical reaction between Zircaloy and steam would also be released to the containment, while reducing the quantity of steam released. The pressurization of the containment which would result from this vapor and gas discharge must be estimated to establish whether containment failure would be expected to occur. This question is covered in boxes 21, 22, 29 and 32 of Figure 3.

Should molten core debris melt through the calandria wall into the shield tank additional vapor would be generated which would contribute to containment pressurization. See boxes 39 and 44 of Figure 3.

Finally, should molten core debris melt through the shield tank wall and interact with concrete, additional steam would be generated as would CO_2 from the decomposition of the concrete, as discussed in section 4.8*. The effects of this additional vapor and gas on containment are covered in boxes 48** and 52 of Figure 3.

4.9.2 Analytical Model of Containment Pressurization

Comprehensive computer codes such as PRESCON (70) and PATRIC (71) are available to calculate containment pressurization and fission-product behavior following

---

*It is possible that the steam and CO_2 could be reduced to D_2 and CO in passing through the molten pool should there be un-oxidized metallic material in the pool. However, this reduction is highly improbable as discussed in section 4.8.

**Box 48 should be ignored as a result of box 47 being ignored. See footnote on page 60.

a LOCA. In these codes, the containment volume, including the reactor vault, fuelling machine duct, fuelling machine servicing areas, pressure relief duct and manifold and vacuum building, is divided into a number of nodes. Transient momentum, mass and energy balances are used to establish flow rates between nodes and pressures and temperatures within nodes as functions of time after a LOCA. Discharge rates of two-phase mixtures from the primary heat transport system as a result of the LOCA are input values to the programs and are established from programs such as RODFLOW, FIREBIRD or SOPHT (e.g., 72). The codes allow for heat sources, such as piping, motors and electric lights, and heat sinks such as vault coolers, wall condensation and vacuum building dousing sprays, distributed appropriately among the nodes.

In the accident sequences studied here, the discharge rates will, in general, be much lower than those experienced in a large LOCA and will not begin until well after flow-rate and pressure transients from the initial LOCA will have essentially disappeared. Therefore, a much simpler model of containment pressurization was used here. Because of the relatively low average vapor and gas discharge rates from the calandria and shield tank or vapor and gas generation rates from interactions with concrete, the containment system pressurization rate will be low and we may treat it as a single node and assume that it is at a uniform pressure and temperature at any given time. Even during the expulsion surges from the calandria which occur momentarily following simultaneous multiple tube-row disintegrations, the maximum vapor discharge rates ($\approx$630 kg/s, as shown in section 5.2.4) are much lower than those which would occur early in a blowdown from a large ($\approx$25%) header break in a Bruce reactor unit (10).

The description of the model given here is, for convenience, based on pressurization of containment resulting from moderator expelled from the calandria, but it can be readily applied to the other causes of containment pressurization.

A simple computer program, BLDG, has been developed to predict containment pressure as a function of time in the accident sequences considered here. The model used is based on a model developed by the author and his colleagues some time ago (73). At each time step, the vapor, liquid and deuterium discharged to containment from the calandria are taken from the results of the appropriate

MODROIL run for the case being considered. The new mass and energy of the containment atmosphere are calculated from these quantities allowing for heat removal by the reactor vault coolers and condensation heat transfer on the containment boundaries. Condensation on other surfaces is ignored to compensate for ignoring other heat sources in the containment system. The capacity of the vault coolers at different steam temperatures is shown in Figure 13, taken from Bruce Design Manual DM-21-73120/67312, page 131. One hour after a large LOCA, the vault coolers may flood (10, p. 12.3.3.1.16), so that the heat removal rate by the vault coolers is set equal to zero after one hour. It is assumed that no dousing water remains available after the original LOCA so that this potential heat sink is ignored.

From the new energy and mass of the containment atmosphere, the new temperature is calculated by trial and error using Dalton's law, assuming that the vapor and non-condensibles are perfect gases and assuming perfect mixing among all atmospheric components. Knowing the new atmospheric temperature, the vapor pressure is known and the partial pressure of the non-condensibles and the total pressure can be calculated.

Initial conditions used in the analysis for calandria discharge are those predicted to exist in the containment at the time of initial moderator expulsion for the appropriate time after the initiating LOCA. Initial conditions are specified as input conditions in the program to permit its application to all causes of containment pressurization.

Further details of the analysis are given in Appendix H and a listing and sample output of BLDG are given in Appendix I.

5. RESULTS OF ASSESSMENT OF ACCIDENT SEQUENCES S11 AND S12: LOCA + LOECI + LOMCS

In this section of the report the results of the assessment of accident sequences S11 and S12 will be presented and discussed.

5.1 Heat Source to Moderator

Figure 14 shows the total heat flow rate to the moderator as a function of time established as described in section 4.3 (Box 6 of Figure 3). The peaks shown in the curve during the time that the heat source is increasing represent the rapid

discharges of stored energy from the pressure tubes as those in each group sag onto the calandria tubes. Only three peaks are evident, instead of the four expected, because the first peak, being relatively small was obscured in the computer plot. Figure 14 shows that the peak power to the moderator reaches about 88 MW some 18 minutes after the initial pipe rupture occurs. The power to the moderator drops to about 46 MW after 40 minutes. While the heat flow rate to the moderator given in Figure 14 is based on a constant moderator temperature of 80°C, the increase of moderator temperature in this accident sequence will have a negligible effect on the heat source to the moderator. The heat source shown in Figure 14 is valid as long as all the calandria tubes are effectively submerged.

The model assumes, in effect, that each pressure tube in a group sags over its entire length at the same moment onto a calandria tube. In actuality, of course, this would not be the case; sagging would occur initially at the hottest axial position on a pressure tube, near the channel mid-point. Sagging at other points would occur later as the local pressure tube temperature continued to rise, but, of course, it would be restricted at and near garter springs and in the vicinity of the ends of the channels. Also, not all pressure tubes in a group will begin to sag at the same moment. The model will thus be conservative in that the actual increase of heat flow rate to the moderator will be slower than that shown in Figure 14 and the peak heat flow rate will be less than 88 MW and will occur later.

5.2 Thermal-Hydraulic Behavior of Moderator and Thermal Behavior of Uncovered Fuel Channels

To study the behavior of the core under conditions of interest here requires the re-iterative use of the programs MODBOIL and IMPECC-UCZ as described in section 4.4.2.7 of this report. Initial runs were made with MODBOIL ignoring any channel disintegration to establish ranges of uncovery times and steam flow rates and temperatures to use in IMPECC-UCZ. Runs were then made with IMPECC-UCZ with ranges of these values to establish probable ranges of disintegration times for fuel channels in different slices using the disintegration criteria discussed in section 4.4.2.7 of this report. Disintegration times established in this manner were then used in MODBOIL to establish moderator expulsion rates and times for complete moderator expulsion from the calandria.

We will first consider results obtained for the thermal-hydraulic behavior of the moderator in the early part of accident sequences S11 and S12, i.e., before fuel channel uncovery, then we will consider results beyond this period, first assuming no disintegrations of uncovered channels and then allowing for disintegration of uncovered channels using the various disintegration criteria.

For the latter case, reference conditions have been established which are judged to represent the most severe probable conditions for the core in these accident sequences. These conditions are used to establish the reference-case core behavior. Then, the sensitivity of the core behavior to departures from these conditions is determined. From these results certain conclusions can be drawn as to the most probable behavior of the core during moderator expulsion in these accident sequences.

5.2.1 Moderator Behavior Before Channel Uncovery

SUBCOOL and MODBOILSUB have been run for conditions anticipated in a Bruce-A reactor unit for these accident sequences. The pressure over the moderator as a function of time from the beginning of the accident sequence is shown in Figure 15 for the case of complete mixing of the liquid moderator in the calandria. The predicted time to rupture disk failure is about 9.2 minutes after the initiation of the accident. Essentially the same result is obtained for the case of no mixing of the moderator. Both models predict that there will be no flashing of the moderator at the time of rupture disk failure since the bulk moderator temperature at this moment is below the saturation temperature corresponding to reactor vault pressure* at this time.

Liquid begins to spill from the relief ducts at about 9.4 minutes, again irrespective of the assumption about moderator mixing.

Since there are no significant differences between the important results for the cases of perfect mixing and no mixing of liquid moderator, it is immaterial which case is used as the basis for the analyses of the thermohydraulics of the moderator once boiling begins; in all later cases, perfect mixing of the liquid moderator is assumed before boiling begins.

---

*Assumed to be 101 kPa at this time.

With this assumption, bulk boiling is predicted to begin in the top moderator slice about 15.9 minutes into the accident sequence. As bulk boiling develops downwards from slice to slice, a very rapid generation of voids results, as can be seen in Figure 16. Figure 16 shows void profiles across the calandria at various times. At 15.6 minutes, the profile represents the sub-cooled void distribution about 20 seconds before bulk boiling begins in the top slice. At 16.5 minutes, bulk boiling is occurring in the top nine moderator slices with sub-cooled boiling still prevailing in the lower slices. At 19.8 minutes, bulk boiling has developed throughout the calandria, and the top row of tubes is about to become uncovered. Although not shown in Figure 16, bulk boiling is fully developed across the calandria by 17.6 minutes. Thus, in about 1.7 minutes, the average void fraction in the calandria has increased greatly, and a large fraction of the moderator mass has been expelled rapidly from the calandria, as can be seen in Figure 17. Figure 17 shows that the moderator mass in the calandria, about 302,000 kg just before bulk boiling begins, has decreased to somewhat less than 136,000 kg as bulk boiling becomes fully-developed, i.e., within about 1.7 minutes.

During this period, moderator is expelled from the calandria in sudden surges, as can be seen in Figure 18. The instantaneous discharge rates reach very high values, oscillating between values as high as 3400 kg/s and values as low as 750 kg/s. There are six such oscillations and the flow in the relief ducts chokes on each flow-rate surge. The oscillations can be explained as follows. The rapid rate of vapor generation as bulk boiling first develops expels fluid rapidly through the relief ducts. The choked-flow pressure drop resulting from the high flow rate of low-quality two-phase flow in the relief ducts increases the pressure in the calandria, which reduces the vapor generation rate. The flow rate from the calandria, and the accompanying pressure drop, decrease, decreasing the pressure in the calandria. The decreased pressure results in an increase in vapor generation rate and the cycle repeats. This process containues until the entire remaining moderator is undergoing bulk boiling.

The peak absolute pressure above the moderator reached during these oscillations is about 210 kPa, as can be seen in Figure 15. The absolute pressure at the bottom of the calandria at this moment is about 275 kPa. Since the calandria

walls remain well-cooled during this stage of the accident sequence, the integrity of the calandria is not jeopardized. After bulk boiling has been fully-established throughout the calandria, the flow oscillations disappear and the discharge flow rate decreases rapidly at first and then relatively slowly in a smooth manner.

The steam quality at the relief duct exits is quite low ($\leq$ 4%) during the flow oscillation period, but increases rapidly following this period to 100% at about 20 minutes, where it remains throughout the rest of this early part of the accident sequence. In effect, the discharge rate from the calandria is in quasi-steady-state equilibrium with the steam generation rate in the calandria at this time.

The behavior of the moderator before channel uncovery may be summarized as follows.

Prior to the onset of bulk boiling in the calandria, a small fraction of the moderator, about 6% to 7%, is expelled through the relief ducts by liquid swell and the onset of sub-cooled boiling. As bulk boiling develops in the calandria a large fraction of the moderator, over 50%, is expelled in less than two minutes by the rapid vapor generation rate; this expulsion occurs in a series of severe flow oscillations, but the integrity of the calandria is not threatened during this period. After bulk boiling is fully developed throughout the calandria the discharge rate drops rapidly at first and then more slowly and the discharge flow exit quality increases to 100%; moderator is now lost from the calandria by steam generation in a quasi-steady-state manner.

The behavior of the moderator in the early part of accident sequences S11 and S12 before channel uncovery, i.e., until after bulk boiling is fully established throughout the calandria and quasi-steady-state steaming is established, is of course, independent of conditions later in the accident sequences. In particular, these results are independent of any assumptions as to whether channel disintegration occurs or not and as to the nature and timing of channel disintegrations. Thus, the moderator behavior described in this section is common to all of the various subsequent scenarios considered in these accident sequences.

5.2.2 Moderator Behavior With No Channel Disintegration After Uncovery

Results have been obtained using MODBOIL under the assumption that no channel disintegration occurs after calandria tube uncovery. While such a situation is not realistic, the results obtained under this assumption establish a bounding condition and were used as one input to the re-iterative process with IMPECC-UCZ and MODBOIL to establish more probable long-term behavior of the moderator and fuel channels, as discussed earlier.

Figures 17 and 18 show the mass of moderator remaining in the calandria and the discharge rate from the calandria for the case of no-channel disintegration after calandria tube uncovery. Figure 18 shows that the discharge rate from the calandria continues to decrease steadily with time in this case, as quasi-steady-state steaming proceeds. As a result, as shown in Figure 17, the mass of moderator remaining in the calandria continues to decrease slowly and appears to approach an asymptotic value. The analysis shows that a steady-state mass of moderator remaining in the calandria (about 82,000 kg or about 25% of the initial moderator inventory) is reached about two hours after the start of the accident sequence. In this state, the eight lowest channel rows would still be well-cooled by the boiling liquid moderator and hence can be considered to be still "submerged". Row uncovery as a function of time is shown for this case in Figure 19.

An asymptotic condition in which the mass of moderator remaining in the calandria is constant and the discharge rate is zero is possible since the decaying heat input into the boiling moderator in the lower part of the calandria can be balanced by the condensation of the generated vapor on the walls of the calandria above the boiling moderator, which remain well-cooled by the shield tank water. In effect, the calandria tubes and calandria are acting in a reflux boiling mode.

Of course, as stated earlier, the assumption of no channel disintegration is not realistic so that these results represent a limiting case.

5.2.3 Thermal Behavior of Uncovered Fuel Channels

5.2.3.1 Method of Approach

To utilize IMPECC-UCZ in analyzing the thermal behavior of uncovered fuel channels requires knowledge of the time of uncovery of a calandria tube (i.e., the time at which steam cooling of the calandria tube begins), an average steam flow rate

and an average steam temperature. To establish representative values of these parameters, the results of MODBOIL runs with no channel disintegration, as described in the previous section, were utilized initially. From the results of IMPECC-UCZ runs with these parameters, criteria were established for fuel channel disintegration. Runs were then made using these criteria for fuel channel disintegration in MODBOIL, which resulted in different values of uncovery times and average steam flow rates for given rows of fuel channels, as well as different estimates of average steam temperatures. From these results, further runs with IMPECC-UCZ were made with extended ranges of the above three parameters to confirm or modify the fuel channel disintegration criterion.

The results obtained from the IMPECC-UCZ runs for the ranges of the three parameters studied are described in this section of the report.

5.2.3.2 Calandria Tube and Fuel Temperatures

The first runs with IMPECC-UCZ were made for the top row of channels for typical values of calandria tube uncovery time and steam flow rates predicted by MODBOIL*, assuming an average steam temperature of 100°C. Since we are dealing with the top row in this instance, uncovery times and initial steam flow rates are independent of channel disintegration, since there are no rows above this one whose disintegration could alter these values from those predicted by MODBOIL for no channel disintegration.

Typical results for the maximum calandria tube temperature as a function of time are shown in Figure 20 for an uncovery time of about 18 minutes and for two steam flow rates, 40.6 kg/s, typical of steam flow rates, at the moment of uncovery and 18.8 kg/s, representative of steam flow rates at later times. Figure 20 shows that higher peak temperatures of the calandria tube are predicted for the higher steam flow rate. Therefore, it is apparent that, at and near the peak temperatures, the Zircaloy-steam reaction rate is controlled by mass transfer and that the heating effect resulting from the higher mass-transfer rate with

*The values of uncovery times and steam flow rates used as input for these first IMPECC-UCZ runs were obtained from an earlier version of MODBOIL and do not agree exactly with more recent values obtained with the improved final version. However, the differences are not very significant and will not result in any meaningful differences in results obtained nor in conclusions reached, as we will see from the results of the parameter studies done using IMPECC-UCZ.

the higher steam flow rate predominates over the cooling effect resulting from the higher heat transfer rate under these conditions*. Later runs with IMPECC-UCZ confirmed this behavior, as we will see.

Using typical uncovery times predicted by MODBOIL with no channel disintegration, and the highest steam flow rates (at the moment of calandria tube uncovery) in each case, which will probably be conservative, IMPECC-UCZ runs were made for rows 4 and 12. These rows contain channels with the highest channel powers in the core, and the analysis has been done for the highest axial fuel element power rating in these rows under full-power pre-accident conditions, 40 W/cm. Again, a steam temperature of 100°C was assumed.

Figure 21 shows that the predicted calandria tube temperatures in each row exceed for several minutes the Zircaloy melting temperature of about 1750°C, as is also the case for row 1, as shown in Figure 20. However, the situation is not as clear-cut as it appears. Calculations of the energy per unit mass of tube above the melting point in each case and comparisons with the latent heat of fusion of Zircaloy show that there is insufficient energy for complete melting of the calandria tubes. Also, the temperature transient oxidizes the tube material to ZrO_2. The melting point of ZrO_2 ($\approx$ 2700°C) is considerably higher than the calculated peak temperatures reached in the transients. The results of the IMPECC-UCZ runs show that there will be considerable oxidation of the calandria tubes before their temperatures reach 1750°C in each case. Thus, complete melting of the calandria tubes would not be expected in these accident sequences. However, other mechanisms such as over-stressing, rapid creep or brittle fracture as well as superheating of the flowing steam would still lead to channel failure and disintegration. Thus, as stated in section 4.4.2.7, fuel channel disintegration is assumed to occur when the maximum temperature of the calandria tube reaches 1750°C. The rate of increase of calandria tube temperature is so rapid after tube uncovery, as shown in Figures 20 and 21, that large differences in the calandria tube temperature at which failure occurs would make very little difference in the predicted time to failure. Also, as we will see, the overall moderator behavior is quite insensitive to the assumed disintegration times for fuel channels.

---

*It is evident that the peak temperatures of the calandria tube reached in these transients are governed by the Zircaloy-steam reaction, since runs with this reaction rate set to zero, peak calandria tube temperatures fo approximately the lower dashed curve in Figure 20.

Therefore, we may conclude that the assumption that fuel channel failure occurs at a maximum calandria tube temperature of about 1750°C is a reasonable one for the present purposes.

Figure 22 shows the temperature histories of the hottest fuel elements in rows 1, 4 and 12 during these accident sequences for the same conditons* as those used to predict the calandria tube temperatures shown in Figures 20 and 21. In all cases, both the initial peaks, resulting from normal cooling by the moderator before the channel uncovers, and the second peaks, resulting from cooling by steam after calandria tube uncovery, are well below the UO_2 melting temperature of about 2800°C. Therefore, for these conditions, no fuel melting would be expected even if there is no channel disintegration.

To explore further the sensitivity of the peak calandria tube and fuel temperatures to steam flow rate, several additional runs were made with IMPECC-UCZ for row 12 for an uncovery time of 36.2 minutes. The results, shown in Figure 23, confirm that the predicted peak calandria tube temperatures increase with increasing steam flow rates up to the maximum value examined, ~125 kg/s. Figure 23 also shows, however, that the predicted peak calandria tube temperatures apparently reach a maximum in the neighborhood of a steam flow rate of 125 kg/s. Above this steam flow rate, the increased heat transfer rate as steam flow rate increases begins to predominate over the heating effect caused by the Zircaloy-steam reaction. Figure 23 also shows that the peak fuel element temperature is very insensitive to steam flow rate and is well below the melting point of UO_2 over the entire range of steam flow rates investigated.

The sensitivity of the peak calandria and fuel temperatures to fuel element power rating and to steam temperature was also examined, for a fixed steam flow rate. As shown in Figure 23, the predicted peak calandria tube temperature is reduced by less than 100°C by a reduction in FEPR from 40 W/cm to 12 W/cm., the lowest value expected, in an outer channel, for this row. Such an insensitivity to FEPR is to be expected since, as we have seen, the peak calandria tube temperatures are governed mainly by the Zircaloy-steam reaction rate.

---

*The maximum steam flow rate of 40.6 kg/s was used for row 1.

Also, as shown in Figure 23, the predicted peak calandria tube temperature is increased by about 150°C for superheated steam at 300°C compared to saturated steam at 100°C, so that peak calandria tube temperatures are somewhat sensitive to the assumed steam temperature, within this range.

Figure 23 also shows that the predicted peak fuel temperature is very insensitive to steam temperature, as expected. For an increase of steam temperature of 200°C, the peak fuel temperature is actually reduced about 16°C. This paradox can be explained by the different response times of the calandria tube and the fuel to changes in boundary conditions. As we will see in section 5.2.5, the heat flow rate from the calandria tube to the steam reaches a higher peak but also decreases much sooner for a steam temperature of 300°C than for a steam temperature of 100°C. Thus, at the time at which the fuel reaches its peak temperature, the average temperature of the calandria tube is lower for 300°C steam than for 100°C steam, resulting in the peak fuel temperature being marginally lower for 300°C steam than for 100°C steam.

Figure 23 also shows that the peak fuel temperature is quite sensitive, as expected, to initial FEPR, being about 1700°C for an FEPR of 12 W/cm compared to about 2150°C for an FEPR of 40 W/cm.

In MODBOIL, the average temperatures of the fuel and the solid and molten Zircaloy at the moment of channel disintegration are required, as input values, to permit the analysis of material quenching in the bottom slice of moderator. Typical values of these temperatures were obtained from IMPECC-UCZ for ranges of conditions at the times at which fuel channel disintegration is assumed to occur, i.e., when the calandria tube temperature first reaches 1750°C. Over representative ranges of FEPR (7 to 40 W/cm), steam flow rates (6.3 to 125 kg/s) and channel uncovery times (18.5 to 36.2 min.), the weighted average fuel temperatures obtained from IMPECC-UCZ at the predicted moments of channel disintegration, according to equation 16 as developed in section 5.2.3.3 of this report were within the range of 1600 to 1760°C. In all of these cases, the pressure tube temperatures were essentially equal to, or somewhat (within about 100°C) lower than, the calandria tube temperatures. That the fuel and pressure tube

temperatures are either equal to or below the calandria tube temperatures at the moment of disintegration results from the significant heating effect of the Zircaloy-steam reaction on the calandria tube. Since MODBOIL accommodates only single values of fuel and Zircaloy temperatures for all channels at the moment of disintegration, it was decided to assume that the temperatures of both fuel and Zircaloy are 1750°C at this time. From the IMPECC-UCZ results, this assumption is conservative. In cases in which a fraction of the Zircaloy is assumed to be molten, the temperature of the molten fraction is also assumed to be 1750°C at the moment of disintegration.

5.2.3.3 Prediction of Delay Time to Channel Disintegration

As discussed in section 4.4.2.7, the results of computer runs with IMPECC-UCZ were used to establish an approximate "empirical" equation to predict the time after calandria tube uncovery for the calandria tube temperature to reach 1750°C, which is taken as the condition for fuel channel disintegration, in the second option in MODBOIL. The equation developed, and incorporated into MODBOIL, is equation 16 of this report.

The runs used to establish equation 16 are listed in Table 2, where the values of key parameters are also shown. Assessment of the results indicated only a slight effect of steam flow rate within the range considered, so that this variable was not included in the correlation developed. This behavior can be explained by recognizing that the heating of the calandria tube as its temperature increases past 1750°C is governed in all cases by the Zircaloy-steam reaction rate, which, at this time, is governed by the solid-state diffusion rate of oxygen, not by the steam flow rate.

Least-squares curve fits of the time delay between uncovery and disintegration time, δt_d, in terms of time at uncovery and the fuel element power rating, yielded equation 16, which is repeated here for convenience:

$$\delta t_d(N) = 0.17 \left[\frac{t_{uc}(N)}{(FEPR(N))^{0.5}} \right]^{1.6} \text{min.} \qquad (16)$$

In considering the application of equation 16 to the prediction of fuel channel disintegration times, it should be recognized that the delay times predicted

Table 2: Data for IMPECC-UCZ Runs Used to Establish Equation for Fuel Channel Disintegation Times, Equation 16

Assumed Steam Temperature = 100°C

Row	FEPR, W/cm	t_{uc}, min.	$\dot{m}_g$, kg/s	δt_d, min.	Predicted δt_d, min.	% Error
1	27	18.4	52.9	1.20	1.29	+ 7.5
1	30	18.4	52.9	1.27	1.18	- 7.1
1	27	18.5	40.6	1.58	1.30	- 17.7
1	27	18.5	18.8	1.47	1.30	- 11.6
4	40	21.95	34.5	1.08	1.24	+ 14.8
12	40	36.2	12.7	2.80	2.77	- 1.1
12	12	36.2	12.7	7.72	7.26	- 6.0

RMS error = 10.8%

from MODBOIL cannot be more accurate than the minimum time step used in MODBOIL which was about 0.2 minutes in the runs listed in Table 2. Also, it is evident from the results of MODBOIL that differences of up to 0.5 minutes in disintegration times for given rows of fuel channels do not result in any significant differences in the predicted mass of moderator remaining in the calandria at any given time.

Equation 16, like any "empirical" equation, should not be applied outside the ranges of the variables, and the combinations of ranges of variables, used in developing it. These ranges are given in Table 2. In all cases considered in this study, the range of FEPR's is within that listed in Table 2. Also in all cases considered, row uncovery times were mainly within the range of values listed in Table 2, but some row uncoveries occur at times somewhat greater than the maximum value of 36.2 minutes. However, this extrapolation is not judged to introduce unacceptable uncertainties in the results, since, as we will see, the time to complete moderator expulsion is relatively insensitive to uncertainties in the disintegration delay time.

The steam flow rate assumed in IMPECC-UCZ is constant while the results of MODBOIL runs show that uncovered channels will be exposed to steam flow rates decreasing with time for the case of no channel disintegration. Steam flow rates for the case of no channel disintegation, are within the range of steam flow rates in Table 2, as can be seen from Figure 18.

For the case of cascading channel disintegration, large steam flow surges occur after each channel row, or group of channel rows, disintegrates, as we will see , but, by the time that additional rows are uncovered, the steam flow rate surge has disappeared, and uncovered rows are exposed only to moderate, steadily-decreasing steam flows. Furthermore, in most cases, these steam flow rates are within the range of steam flow rates in Table 2.

The observed insensitivity of delay time to steam flow rate indicates that equation 16 should be quite valid even for steam flow rates somewhat outside the range of Table 2.

Equation 16 was developed from runs of IMPECC-UCZ using a constant steam temperature of 100^{o}C, whereas the temperature of the steam flowing over an uncovered calandria

tube will increase with time. This effect is considered in the section 5.2.5 of this report.

5.2.4 Moderator Behavior With Channel Disintegration

5.2.4.1 Reference Conditions

As discussed in section 4.4.2.7, there are three options in MODBOIL to describe the disintegration behavior of fuel channels after uncovery of calandria tubes:

a) disintegration when the maximum calandria tube temperature reaches 1750°C, as predicted by equation 16 (normal failure)

b) disintegration at an arbitrary time, t, after uncovery

c) disintegration of all uncovered rows under a disintegrating row using either option a) or b) (cascading failure).

Analyses using MODBOIL have been completed using each of these criteria for channel disintegration. With channel disintegration, there are sudden surges in expulsion rate from the calandria as fuel channels disintegrate and drop to the bottom of the calandria and are quenched there. This behavior is illustrated in Figure 24, for the case of normal, cascading failure with complete disintegration of all channels in a row (FRCMAS = 1.0) and with 100% molten Zircaloy (FRMELT = 1.0) at the instant of disintegration. The temperatures of all fuel channel components at the moment of disintegration are assumed to be 1750°C, as explained earlier. These conditions are assumed to represent the most severe probable situation for channel disintegration and are termed the reference case conditions. Figure 24 shows that the peaks of the surges of moderator discharge rate, ~1760 kg/s, which is the maximum encountered, for the first peak, with a subsequent peak of about 630 kg/s, followed by several peaks of less than 250 kg/s, are less than those encountered as the moderator comes into bulk boiling. The first two of these surges result in choked flow conditions in the relief ducts. These surges are super-imposed on a gradually-decreasing mean flow rate, which is somewhat higher at any time than the expulsion rate for the limiting case of no channel disintegration. Examination of the computer outputs shows that the major surges occur as groups of disintegrating fuel channels drop into the moderator as would be expected but that significant flow surges also occur about 1.0 to 1.5 minutes later when the fuel pellets are quenched to the point at which nucleate boiling begins.

Times of channel uncovery and disintegration for this case are shown in Figure 25. The major flow surges shown in Figure 24 can be related to the channel disintegration times shown in Figure 25. We see that the top row of channels is uncovered at about 21 minutes and that the first channel disintegration occurs at about 23 minutes when the top three rows disintegrate simultaneously.

The maximum absolute pressure momentarily reached in the calandria, about 470 kPa, occurs at the peak of the second flow rate surge as shown in Figure 15. Although the peak flow rate in the first surge is much higher, the discharge quality is only about 10%, compared to 100% for the second surge, so that the peak calandria pressure is lower, about 400 kPa. Since the calandria walls are well cooled throughout the transient, it is not expected that momentary pressure surges of this magnitude would cause significant damage to the calandria. Also, it should be kept in mind that the assumption of instantaneous transfer of all the fuel channels in a given disintegrated row to the bottom slice of moderator will result in predicted flow rate and pressure surges greater than those that would be expected in an actual case. On the other hand, extensive fragmentation of the debris would result in larger surface-to-volume ratios than used in the analysis, which would produce flow rate surges greater than those predicted. Thus, these two assumptions tend to compensate for each other.

This analysis has been done assuming a constant pressure (101 kPa) in the reactor vault. Actually there will be a moderate increase in reactor vault pressure from an initial value of about 90 kPa over the period of moderator expulsion, with a peak of about 155 kPa being reached at the end of the expulsion period, for the reference conditions. See section 5.5. This variation in the reactor vault pressure will not have any significant effect on the moderator expulsion history nor on calandria pressure surges. One reason for this conclusion is that expulsion rate and pressure peaks occur under choked flow conditions, and are thus independent of the reactor vault back pressure.

Obviously, the moderator is expelled more rapidly from the calandria for the cases of channel disintegration than it would be if no channel disintegration occurred, as can be seen in Figure 26. For the reference case conditions, an asymptotic equilibrium level of moderator is not reached, and the moderator is completely

expelled from the calandria in about 48 minutes.

As discussed earlier, the weighted average fuel temperature at the moment of channel disintegration for the reference conditions will be 1750°C or less. Obviously, the fuel material will not be molten at this time and will be quenched rapidly as it falls into the moderator. Thus, no fuel melting is expected during this phase of the accident sequence. Since the Zircaloy fuel sheaths and pressure tube will have been oxidized before channel uncovery, and since a significant fraction of the calandria tube will have been oxidized by the time of channel disintegration, most of the Zircaloy will also not be molten when disintegration occurs and will be rapidly quenched in the moderator. Thus, almost all of the debris accumulating in the bottom of the calandria will fall as solid material* and all debris will remain in a solid state at least until all the moderator is expelled from the calandria. MODBOIL results show that average debris temperatures will be about 105°C to 110°C just before the last of the moderator is expelled from the calandria at about 48 minutes, and that only a few fuel channels (at an average temperature of about 1750°C) will remain intact at this time.

5.2.4.2 Sensitivity Assessment

The sensitivity of the results of the moderator expulsion analysis to the various parameters which affect it has been investigated. The predicted masses of moderator remaining in the calandria at any time for various assumed fractions of each channel row disintegrating (FRCMAS) are shown in Figure 27, for all Zircaloy assumed molten at the time of disintegration (FRMELT = 1.0). The same information is shown in Figure 28 for FRCMAS = 1.0 and for various values of FRMELT. In both cases all other conditions are the same as the reference conditions. Figure 27 shows that moderator expulsion is quite sensitive to the fraction of channel mass which disintegrates in each row; the behavior with FRCMAS = 0.1 is seen to approach the limiting condition for no channel disintegration, as would be expected. On the other hand, Figure 28 shows that moderator expulsion is not as sensitive to the fraction of Zircaloy which is molten at the moment of disintegration; this behavior results from the low latent heat of fusion of Zircaloy. Although the predicted time to complete expulsion is longer as FRMELT decreases, the general behavior of moderator expulsion is not affected greatly by variation in FRMELT.

*This conclusion is one of the main reasons that no vapor explosion is anticipated at this stage of this accident sequence. See Appendix C.

Obviously, there must be some delay time between the moment of calandria tube uncovery in a given row and the time of disintegration of the channels in that row. We have assumed that this delay time is given by equation 16, that is, that a fuel channel disintegrates when the maximum calandria tube temperature reaches approximately 1750°C. Since this hypothesis has no experimental verification, it is important to assess the sensitivity of the predicted moderator behavior to departures from this assumption. More severe effects would be expected to result if channels disintegrated sooner than predicted, so the MODBOIL option of an arbitrary disintegration delay time was used with the delay time set to zero. That is, channels are assumed to disintegrate as soon as they are uncovered*. Because of the earlier disintegration times, the weighted average fuel and Zircaloy temperatures at the moment of disintegration will be less than those associated with the reference disintegration criterion. Therefore, the effects of lower fuel and Zircaloy temperatures at the moment of disintegration are shown in Figure 29. Other input conditions are fixed at the reference values, except that the fraction of molten Zircaloy is set to zero for those cases in which the assumed Zircaloy temperature is below the nominal melting temperature of 1750°C.

Figure 29 shows that "instantaneous" disintegration would result in more rapid moderator expulsion if the initial fuel and Zircaloy temperatures are assumed to be the same as for the reference case, with all moderator being expelled by about 35 minutes rather than about 48 minutes, as in the reference case. Results are also shown in Figure 29 for combinations of fuel and Zircaloy temperatures of 1600°C/1100°C and 1400°C/900°C at the moment of disintegration. These values were chosen from the results of a number of runs of IMPECC-UCZ for reasonable ranges of the governing parameters that might occur during these accident sequences. Figure 29 shows for these more realistic ranges of initial fuel and Zircaloy temperatures, should channel disintegration occur immediately after uncovery rather than after delay times predicted by equation 16, that the mass of moderator remaining in the calandria at any time and the time to complete expulsion of moderator are not much different from those for the reference conditions.

---

*Actually, in MODBOIL, disintegration occurs at the next time step after uncovery, which is either 12 seconds or 24 seconds after uncovery in all cases.

5.2.5 Effect of Steam Superheating

Superheating of steam as it flows over uncovered calandria tubes is not accounted for in MODBOIL. The great sensitivity of the heat flow rate from an uncovered calandria tube to steam to parameters such as uncovery time, steam flow rate and steam temperature, as shown in Figure 30, as well as the variation of steam flow rate and temperature, would have made it extremely difficult to account for the effects of steam superheating. The effects of steam superheating on the behavior of uncovered fuel channels and on moderator expulsion are examined in this section of the report.

It is obvious that superheating of the steam as it flows over uncovered calandria tubes will result in the calandria tubes reaching the presumed failure temperature of 1750°C earlier than predicted by equation 16. We have seen in the previous section of the report that even the maximum possible earlier channel disintegration will not significantly affect the average rate of moderator expulsion. Nevertheless, the magnitude of the decrease in delay time was investigated to give a more complete insight into moderator expulsion in these accident sequences.

Figure 30, from the results of IMPECC-UCZ runs, shows that the heat flow rate from an uncovered calandria tube to steam flow increases to a maximum a few minutes after uncovery and then decreases rapidly. The maximum heat flow rate corresponds in every case to the time of completion of the Zircaloy-steam reaction on the calandria tube.

There are many uncertainties and difficulties in the calculation of the steam temperature at any time from heat flow rates such as those shown in Figure 30. Heat flow rates shown in Figure 30 are maximum values for a given channel where FEPR is a maximum and the pressure and calandria tubes are in contact. Heat flow rates would be lower at different axial positions and from channel-to-channel in a row particularly since channels will probably not uncover over their entire lengths at the same moment, nor will all channels in the same row uncover simultaneously. Steam flow rates would not be constant, as assumed in Figure 30, but are predicted by MODBOIL to decrease with time for a given group of uncovered channels. Steam flow rates would also not be uniform over the length of channels nor over all the channels in a given row. Also, as shown in Figure 30, superheating

would itself change the heat flow rate from a given row. The steam temperature at a given row would depend on the number of uncovered rows below it, the average heat flow and steam flow rates at these rows, the times of uncovery of these rows and the steam temperatures at these rows. Cooling of the superheated steam would also occur because of heat transfer to the calandria wall by radiation as well as by convection and condensation, and the overall cooling rate would increase as the steam temperature increased. In addition, any liquid droplets entrained in the steam flow would tend to be evaporated by heat flow from the steam, thus reducing its superheat.

Nevertheless, estimates were made of steam temperatures as a function of time for the reference conditions for moderator expulsion from the calandria. For each row in a group of uncovered channels, heat flow rates as a function of time were established from the curve, such as those shown in Figure 30, which was most appropriate considering the uncovery time, FEPR, average steam flow rate and average steam temperature.*

A major assumption used in this analysis was that the actual heat flow rate at any time was one-half that predicted from the appropriate curve of Figure 30. This assumption accounts for the effects of:

a) average heat flow rates from a channel being less than the maximum values
b) time spread for uncovery of a given channel and from channel-to-channel in a given row
c) cooling of the superheated steam at the calandria walls
d) evaporation of entrained liquid droplets.

It is assumed that these effects will outweigh the effects of non-uniform steam flow distribution.

The results of these calculations for the reference conditions are shown in Figure 31. Figure 31 gives the steam temperature leaving the uppermost intact row of each

*Exact correspondence of uncovery times, steam flow rates and temperatures was not attempted as this would have required an inordinate number of costly IMPECC-UCZ runs; the results in any case would have still been approximate since IMPECC-UCZ uses constant steam flow rates and temperatures rather than varying values.

group of uncovered tubes. The numbers of these rows are indicated in Figure 31. The peak steam temperatures for each group are reached just before all the uncovered rows in each group disintegrate. Following each peak, there are no uncovered channels for a short period, so that the steam temperature rapidly drops back to the normal saturation value, close to 100°C. Figure 31 shows that the peak temperatures, in general, are higher as the later groups disintegrate, because the maximum times of uncovery are generally longer for the lower rows. The predicted peak steam temperatures reached are moderate for three of the peaks, but reach values from 580° C to 1060° C for the other three peaks. Of course, these temperatures would not actually be reached since the rapidly increasing steam temperature would cause the uncovered channels to disintegrate earlier than predicted by equation 16.

Estimates using IMPECC-UCZ results and the temperature rises shown in Figure 31, indicate that the disintegration criterion temperature of 1750°C would actually be reached about 30 to 60 seconds earlier than indicated in Figure 31. With earlier disintegrations of this order, the peak steam temperatures encountered by the last two groups would be in the range of 400°C to 500°C.

These estimated time reductions for disintegration, are within the uncertainties of equation 16. Therefore, we may conclude that the use of equation 16 will not result in significant errors in predictions of disintegration times because of steam superheating.

Steam superheating can also increase the pressure drops in the relief ducts and hence can increase calandria pressure at certain times. This effect is considered in the next section where the effect of generated deuterium flow on relief duct pressure drop and calandria pressure is considered.

5.2.6 Effect of Deuterium Production in the Calandria

As stated in section 4.5.3, MODBOIL does not allow for the conversion of a fraction of the heavy water steam flow rate in the calandria to deuterium gas resulting from the Zircaloy-steam reaction on the calandria tubes. The deuterium gas produced by the reaction could affect the pressure drop through the relief ducts and hence the pressure in the calandria at certain times during the period of moderator expulsion from the calandria. The error introduced by the neglect

of the deuterium gas component of the discharge flow is estimated in this section of the report.

In section 4.5.3, the rate of growth of the Zr O_2 layer in the calandria tube is given by equations 20 or 23, depending on the mechanism governing the reaction rate. These equations have been incorporated into IMPECC-UCZ to predict the reaction rate and hence heat generation at any time. These equations can also be used to predict the rate of formation of Zr O_2 and hence the rate of formation of D_2 gas and the corresponding consumption rate of steam (D_2O vapor).

The rate of formation of D_2 gas per calandria tube, assuming uniform conditions along the length of the calandria tube, is given by

$$\frac{dm_{D_2}}{dt} = 0.0439\ 2\pi\ r\ L\ \rho_z \frac{dz}{dt} \qquad (76)$$

Similarly, the rate of steam (D_2O vapor) consumption is given by:

$$\frac{dm_{st}}{dt} = 0.395\ 2\pi\ r\ L\ \rho_z \frac{dz}{dt} \qquad (77)$$

The coefficients 0.0439 and 0.395 are the mass ratios of deuterium and steam, respectively, to zirconium, deduced from the chemical reaction equation. Equations 76 and 77 could be incorporated into IMPECC-UCZ to determine the rates of deuterium production and steam consumption at any time.

However, the existing version of IMPECC-UCZ does not include these equations, so that a hand calculation method has been used to establish the <u>average</u> deuterium gas production and steam consumption rates during the reaction period from the output of IMPECC-UCZ runs. In this method, the period of the reaction is determined as the time when the calandria tube temperature first reaches 1100°C until the time that the reaction is complete. The average rates of deuterium gas production and steam consumption per calandria tube are then established by

dividing the total mass of deuterium gas formed and steam consumed by the reaction of all the Zircaloy in a calandria tube by the period of the reaction. The rates established in this manner will over-estimate the actual rates in the early part of the reaction and will under-estimate them in the late part of the reaction. Also, the average rates established in this manner will over-estimate the actual average rates since they assume that conditions along a calandria tube are uniform at those corresponding to the maximum channel power position.

Results obtained in this way from the various IMPECC-UCZ runs are summarized in Table 3.

These results were applied to the reference conditions for moderator expulsion to establish the effect of deuterium gas production by the Zircaloy-steam reaction on relief duct pressure drop and calandria pressure. In this analysis, trial and error calculations, employing Dalton's Law and the relief duct pressure loss equation*, were used. The steam and deuterium gas were assumed to be at the same temperature, with the mixed vapor temperature at any time being taken from the results which are plotted in Figure 31.

Deuterium gas is generated only from uncovered calandria tubes after their temperatures have reached 1100°C. Therefore the most significant effect on calandria pressure will occur just before each group of channels disintegrates, when all the channels in a particular group are uncovered and the temperature of the vapor above the uppermost intact row has reached its maximum value.**

The results obtained are summarized in Table 4. Table 4 shows that the generation of deuterium from the Zircaloy-steam reaction has a negligible effect on calandria pressures throughout the moderator expulsion period. The actual effect would be even less than that indicated in Table 4, since the channel groups would disintegrate earlier, as explained in the previous section, when the vapor temperatures are lower than the values given.

---

*Note that, at all times when deuterium gas is being generated, there is only single-phase vapor flow in the upper part of the calandria and in the relief ducts.

**Note that deuterium gas production will not affect the pressure peaks in the calandria which occur after groups of channels disintegrate and when calandria tube debris is being rapidly quenched, halting the Zircaloy-steam reaction.

Table 3: Average Deuterium Gas Production Rates and Steam Consumption Rates From Uncovered Calandria Tubes Established From IMPECC-UCZ Runs

Row	$\dot{m}_g$, kg/s	t_{uc}, min.	TRS, °C	FEPR W/cm	$\bar{\dot{m}}_{D_2}$, kg/s	$\delta\bar{\dot{m}}_{st}$, kg/s
12	12.7	36.2	100	40	0.0029	0.026
12	63.0	36.2	100	40	0.0057	0.051
12	126.0	36.2	100	40	0.0064	0.058
12	12.7	36.2	100	12	0.0029	0.026
12	12.7	36.2	300	40	0.0039	0.035
1	40.6	18.5	100	7	0.0075	0.068
1	52.9	18.4	100	30	0.0077	0.069

Table 4: Maximum Effects of Deuterium Gas Production on Calandria Pressure. Reference Conditions

Channel Group	Rows	Conditions Just Before Group Disintegration		
		Vapor Temp. °C, Theoretical	Pressure, kPa abs. Uncorrected	Corrected
A	1 - 3	120	101.7	101.8
B	4 - 11	690	101.2	101.3
C	12 - 13	180	101.3	101.5
D	14 - 15	270	101.3	101.4
E	16 - 18	580	101.2	101.5
F	19 - 21	1060	101.2	101.8

Notes:

1. Uncorrected pressures are those obtained from MODBOIL results.
2. Corrected pressures allow for the flow of a mixture of vapor and deuterium gas, and the superheating of the mixture.

Therefore, we may conclude that deuterium gas production, allowing for vapor superheating, has a negligible effect on calandria pressure and hence moderator expulsion throughout the period of moderator expulsion.

5.2.7 Summary and Conclusions on Moderator Expulsion and Uncovered Fuel Channel Behavior

The behavior of the moderator before fuel channel uncovery has been summarized at the end of section 5.2.1.

The behavior of the moderator after fuel channel uncovery and the behavior of the uncovered fuel channels are summarized in this section and certain conclusions are drawn.

Calandria tube uncovery begins at about 21 minutes.

Reference conditions for the core behavior after calandria tube uncovery have been established as follows:

Channel disintegration criterion: Eq. 16.

Fraction of channel mass disintegrating in a row: 1.0

Fraction of molten Zircaloy at disintegration: 1.0

Average temperature of fuel at disintegration: 1750°C

Average temperature of Zircaloy (solid or molten) at disintegation: 1750°C

Uncovered channels disintegrate when struck by falling debris.

For the reference conditions, channel disintegration begins at about 23 minutes. The moderator will be completely expelled from the calandria about 45 to 50 minutes after the initial LOCA occurs. Sensitivity analyses indicate that uncertainties in the fuel channel disintegration time, including the effects of steam superheating, do not result in large uncertainties in the overall moderator expulsion time nor in disintegrated fuel channel behavior.

Deuterium gas generation from the Zircaloy steam reaction will have negligible effects on calandria pressure and moderator expulsion behavior.

Other studies have shown that there will be no fuel melting in a CANDU reactor following a LOCA with failure of emergency core cooling; this study shows that it is very probable that there will be no gross fuel melting, even with failure of the moderator cooling system, during the period that the moderator is being expelled from the calandria. At the end of this period, the fuel debris will be completely quenched and at a low average temperature. A small fraction of the Zircaloy in the core (i.e., part of the calandria tubes) may melt after channel uncovery, but all the Zircaloy debris will also be quenched and at a similar low temperature at the end of the period of moderator expulsion from the calandria.

Important conclusions that may be drawn from this part of the study include:

a) The integrity of the calandria will not be jeopardized during moderator heat up and expulsion.

b) Fission product release from the fuel will be quite limited until at least the end of moderator expulsion from the calandria, 45 to 50 minutes after the initial LOCA, since the fuel will remain in the solid state.

c) The release to containment of the small fraction of iodine fission products which may escape from the fuel will probably be delayed significantly by the water environment in the calandria (74,75).

d) The operators would have at least 20 minutes to provide an alternate heat sink before channel uncovery and disintegration begins. (However, severe fuel damage, although no melting, would have occurred earlier in the channels following the failure of the emergency cooling injection.)

e) While it is difficult to rationalize an assumption of less than 100% disintegration of uncovered fuel channels, should such be the case, significant reductions in average moderator expulsion rates and increases in times to complete expulsion would result.

f) Since it is likely that the fraction of molten Zircaloy at the moment of channel disintegration would be considerably less than 1.0, the times to complete expulsion of the moderator would be somewhat longer than that predicted for the reference conditions. However, the overall behavior of moderator expulsion would not be modified greatly from that predicted for the reference case, as can be seen from Figure 28.

g) Uncertainties in the delay times to disintegration will not affect the predicted moderator behavior significantly.

5.3 Thermal Behavior of Fuel Channel Debris in Bottom of Calandria

In section 4.6, the various computer programs and analytical methods used to establish the thermal behavior of the dried-out core debris in the bottom of the calandria were described. In this section of the report, the results of the application of these programs and methods to the study of accident sequences S11 and S12 are given.

5.3.1 Thermal Behavior of Solid Debris Bed in Bottom of Calandria

The assumptions, analytical methods and computer program, DEBRIS, used to establish the thermal behavior of solid debris are described in section 4.6.1. Here, we will discuss the results obtained for the conditions of accident sequences S11 and S12.

As in the consideration of the thermal-hydraulic behavior of the moderator, reference conditions were established for the thermal behavior of the solid debris. In this case, however, it was not possible to define readily all the reference conditions that would result in the most severe probable conditions experienced by the bed of solid debris. Thus, some of the reference conditions chosen for the solid debris bed behavior are more arbitrary than those used for the moderator behavior. Therefore, in this case, the sensitivity of the results to variations in the values of the key parameters was more extensively investigated than in the case of the thermohydraulic behavior of the moderator.

The chosen reference conditions are:

Initial time of bed dry out:	45 minutes
Initial bed temperature:	110°C
Fraction of total core mass in bed, FRCMAS:	1.0
Void fraction of bed, ε_v :	0.5
Average pore size of bed, δ_p :	0.03 m.
Contact conductance factor, F :	0.5

The bed dry out time of 45 minutes is consistent with the calculated time to complete moderator expulsion of 45 to 50 minutes established earlier and the initial bed temperature, 110°C, is also consistent with the results obtained

earlier. The value of FRCMAS = 1.0 is consistent with the value used for the reference conditions for the moderator analysis. Since these three parameters are not arbitrary, no extensive sensitivity study of their variations was made. The choice of 0.5 as the reference bed void fraction or porosity is arbitrary. The choice of 3 cm as the average void size is somewhat arbitrary but reflects a judgment that, since little or no melting of debris will occur before the formation of the debris bed, and that relatively large fragments of bundles or channels may constitute a significant fraction of the debris, the average pore size will probably be relatively large. Note that the reference pore size, 3 cm., is much larger than those typically used in the analysis of debris beds in fast breeder reactors (40). The selected reference condition contact conductance factor, 0.5, is arbitrary.

Figure 32 shows maximum, upper and lower surface temperatures of the debris bed as functions of time for the reference conditions. The maximum temperature in the bed reaches the melting point of Zr O_2, ~ 2700°C, at about 85 minutes after the bed re-heating starts, or about 130 to 135 minutes after the start of the accident sequence. The maximum temperature occurs on a plane slightly above the mid-plane of the debris. The upper and lower surface temperatures of the bed, 1290°C and 405°C respectively, are well below the melting point at this time. Heat fluxes from the upper and lower surfaces at the moment when melting starts are about 15.8 and 15.5 W/cm^2, respectively. From the low value of the heat flux on the lower surface into the shield tank water, it is obvious that critical heat flux* will not occur and the wall will remain well-cooled, up to the time that melting begins in the bed.

Temperature profiles across the bed at different times are shown in Figure 33. It can be seen that these profiles are relatively flat over most of depth of the bed.

The internal mathematical validity of the computer program was confirmed by calculating the overall heat balance at the time that the bed temperatures reach

*For the assumed shield tank water temperature of 60°C (sub-cooling of 40°C), the predicted critical heat flux for pool boiling of water at atmospheric pressure is about 280 W/cm^2 (76).

their predicted maxima. At this point, all bed temperatures are essentially constant with time, varying by less than one degree over a period of 20 minutes or so. Since the bed temperatures are not changing with time, the total rate of heat generation in the bed must equal the total heat flux away from the bed over the upper and lower surfaces. Making these calculations, it is found that the heat balance agrees to within 6% for the reference conditions, which gives reasonable confirmation of the internal mathematical validity of the method, considering the various assumptions and simplifications. Similar checks were made for each run and in all cases the heat balance errors were equal to or less than about 7%. Although the program is no longer physically valid at this maximum temperature point, since most of the predicted temperatures are well above the melting point at this time*, we may conclude that its mathematical validity is confirmed by the heat balance.

The sensitivity of predicted results to bed porosity was investigated. The predicted temperature histories for porosities of 0.1 and 0.8 compared to the reference porosity of 0.5 are also shown in Figure 32. It is hard to imagine porosities greater than 0.8 since the upper surface of the debris would then be above the mid-plane of the calandria, while porosities less than 0.1 are also difficult to imagine because of the very close packing of the debris which would then be required. It is obvious from Figure 31, that variation of the porosity over the range 0.1 to 0.8 has a negligible effect on predicted bed temperatures at any time, and on the predicted time to reach the melting point of the bed material. The insensitivity to porosity results from the fact that the effective pore conductivity is of the same magnitude as the effective solid conductivity, at least for the reference pore size of 0.03 m. This result is satisfying since bed porosity is certainly one of the major unknowns in the analysis. The results of a further examination of the effects of bed porosity are given later for other average pore sizes.

The sensitivity of the results to pore size for the reference bed porosity of 0.5 was investigated and the results are shown in Figure 34. It is evident that

*Except for the predicted upper and lower surface temperatures which are both well below the melting point.

uncertainties in average pore size over the range likely to be encountered will not reduce the time for the bed to reach the melting point significantly below 85 minutes (nor increase it much above 85 minutes). Figure 34 also shows that both the predicted upper and lower surface temperatures are well below the melting point, at the moment that melting begins in the bed over the entire range of pore size. Also, the bottom surface heat flux into the water shield is again well below the critical heat flux over the entire range of pore sizes when the bed melting point is reached. The same conclusions are drawn for bed porosities of 0.1 and 0.8, as can also be seen in Figure 34; it is obvious that the effects of bed porosity at different pore sizes are essentially the same as at the reference pore size. Probably the most important result of this part of the sensitivity study is the conclusion that uncertainties in either bed porosity or pore size will not reduce the estimated time to the initiation of melting in the debris bed below about 85 minutes.

While the important aspects of the thermal behavior of the bed are thus quite independent of the average pore size over a wide range of bed porosities, there are certain tendencies exhibited by the results which can be explained in terms of the various mechanisms involved. For a given porosity, the time to reach the melting point increases with pore size. As the pore size increases for a fixed porosity, the effective number of pores must decrease significantly, which will have the effect of reducing significantly the number of "radiation shields" within the debris, thus increasing the radiation contribution to the effective thermal conductivity of the bed. Thus, a longer time to reach the melting point results. The improved effective thermal conductivity of the bed also results in the observed higher surface heat fluxes and temperatures at the time that the melting point is reached.

The sensitivity of the important results to the contact conductance factor, F, was also investigated, with all other conditions at the reference values. The key results proved to be completely insensitive to values of F from 0.2 to 1.0, with the predicted time to reach the melting point varying by about 0.2%, while the surface temperatures and heat fluxes at the time the melting point is reached varied by about 7 to 8^{o}C and 0.5 W/cm^{2} respectively. It is obvious from these results that contact conductance effects do not constitute the governing thermal resistance in the bed so that bed thermal behavior is quite unaffected by the uncertainties in F.

Variation in the factor F is exactly equivalent to variation in the value of the effective thermal conductivity of the solid debris, k_M, as can be seen from equation 26. Therefore, the insensitivity of bed thermal behavior to variation in F means that it will also be insensitive to variation in k_M over a similar range, that is, to uncertainties in k_u, k_z and the geometry of the solid debris, as can be seen from equation 29.

Other cases were run using DEBRIS to assess the effects of later bed dry out times and smaller masses of debris on the predicted thermal behavior of the bed. These conditions are highly improbable for the accident sequences being examined, so the results will not be discussed in any detail here. As would be expected, later dry out times and smaller masses of debris resulted in longer times after dry out to reach the bed melting point. It was also shown that the debris mass would have to be less than about 35% of the actual core mass for no melting of the debris bed to occur.

Although, as has been pointed out, the analytical model is no longer valid after melting begins in the debris bed, in all cases run, the code predicts that the upper and, particularly, the lower surface temperatures are always well below the debris melting point, even when the maximum predicted temperatures in the bed reach their peak values and begin to decrease. This result suggests that a solid crust will be formed between the molten pool and the calandria wall at all times. This speculative result will be confirmed in the next section of this report.

From this study of the solid bed of debris in the bottom of the calandria, we can draw the following important conclusions:

a) Following dry out of the total core debris at about 45 to 50 minutes after the initiation of the accident sequence, the solid debris bed in the bottom of the calandria will heat up and will reach the melting point of ZrO_2 ($\sim 2700^{\circ}C$) about 85 minutes later, or about 130 to 135 minutes after the initiation of the accident.

b) Although uncertainties in bed porosity, average pore diameter and contact conductance parameter are large, none of these uncertainties have significant effects on the time to reach the debris melting point. In particular, the time to reach the bed melting point will not be reduced below about 85 minutes after dry out.

c) Up to the time that bed melting begins, bed upper and lower surface temperatures are well below the melting points of the debris.

d) Up to the time that bed melting begins, the lower surface heat flux into the shield tank water remains well below the critical heat flux value so that the calandria wall remains well cooled.

e) Considerable time is available to the operator after debris dry out to provide a means of cooling the debris to prevent fuel melting.

f) Fuel melting and hence large-scale release of fission products will not begin until about 135 minutes after the original accident occurs.

5.3.2 Thermal Behavior of a Molten Pool of Core Debris

As discussed in section 4.6.2, there are two major aspects of the question of the thermal behavior of a molten pool of core debris: the internal characteristics of heat generating molten pools and the interactions of a molten pool with the cooled calandria wall. As stated in section 4.6.2, the ultimate questions to be answered are whether the calandria wall melts through completely and, if it does not, whether it can be expected to maintain its structural integrity.

5.3.2.1 Internal Characteristics of a Molten Pool

The computer program, MOLTENPOOL, was used to establish the internal thermal characteristics of a molten pool of core debris, assuming that the entire mass of core material is molten.

Obviously, some time will be required for the transition from the bed of solid debris considered in the previous section to the completely molten pool considered in this section. A model for this transition period is very difficult to define since molten material, as it begins to form near the centre of the bed, will flow down through the pores of the bed where it will tend to freeze. As heating continues, the melting front will advance downwards and previously unmelted debris as well as the frozen material will begin to melt. In addition, solid material above the molten zone will fall into this zone and begin to melt. The rate of melting will depend on the timing and amounts of mass in the falls of material.

Thus, it is impossible to define the geometry of the solid and molten regions of the debris during this transition period in any simple fashion. There will be no single interface between the solid and molten material. Therefore, no attempt has been made to develop an analytical model of the bed for this period.

Because of the time required for this transition period, the volumetric heat source in the molten pool at the moment when all solid material (except for any thin crusts) becomes molten will be less than that at the beginning of the melting period because of fission product decay.

In the analysis of the molten pool, this decay is ignored and the pool heat source is assumed to be the same as that when debris bed melting begins. Thus, the results obtained in the present analysis will be conservative.

The results of this analysis are summarized in Table 5.

Table 5 shows that the predicted pool behavior depends significantly on the set of property values used. Using property value sets 1 and 2, the program MOLTENPOOL predicts that the pool will be undergoing boiling at the reference conditions, but, with property value sets 3 and 4, it predicts that it will not be boiling under these conditions.

To provide some additional perspective on molten pool behavior, certain important parameters are plotted as functions of pool mass (FRCMAS $\leq$ 1.0) in Figure 35 for property sets 1 and 2 and in Figure 36 for property sets 3 and 4. It should be remembered that the liquid property values are identical (Anderson's set No.1 (53)) for property value sets 1 and 2 and are also identical (Anderson's set No.2 (53)) for property value sets 3 and 4. Since only vapor properties differ between sets 1 and 2, there are no differences in predicted behavior until the pool mass is great enough that boiling of the pool begins. Since no boiling is predicted for property sets 3 and 4, there are no differences in predicted behavior over the entire range of pool mass.

Although, as can be seen from the property value data in Appendix E, the boiling point is considerably higher, 3720 K, for property value sets 3 and 4 than for property value sets 1 and 2, 3520 K, this difference in boiling points is not the sole cause of the significant difference in thermal behavior predicted for the different sets of property values. Figure 36 shows that the pool would not be predicted to boil when property value sets 3 and 4 are used even if the boiling point for these sets were 3520 K, the same as that for sets 1 and 2, instead of 3720 K.

Table 5: Results of MOLTENPOOL Analysis for Reference Conditions.
Total Mass of Core Material in Pool (FRCMAS = 1.0)
Time from Initiation of Accident Sequence = 135 min.

Property Value Set No.	1	2	3	4
Is Pool Boiling?	Yes	Yes	No	No
Nu_u	1557	1643	841	841
Nu_d	58.5	58.5	102	102
$\overline{q''_u}$, W/cm^2	110	116	118	118
$\overline{q''_d}$, W/cm^2	4.1	4.1	9.9	9.9
$q''_{d,max}$, W/cm^2	4.1	4.1	19.7	19.7
q_{vB}, W/cm^3	1.50	1.59	1.65	1.65
Void fraction	0.10	0.048	-	-
$j_{g\infty}$, m/s	0.74	0.81	-	-
Evaporation Rate, kg/m^{2}s	1.19	0.81	-	-

Examination of the property values in Appendix E, as well as the predicted results, shows that the differences in predicted pool behavior between Figures 35 and 36 can be attributed mainly to differences in liquid property values between sets 1 and 2 and sets 3 and 4, as the following argument shows.

While heat transfer from the pool to its surfaces is governed by both natural convection and internal radiation, as discussed in section 4.6.2.1.1, results indicate that the natural convection mechanism is dominant, with the radiation contribution to the total heat flux at a pool boundary typically being less than 20%. Therefore, we may base arguments on the pool thermal behavior mainly on the natural convection mechanism. Natural convection heat transfer from the pool is predicted by equation 32 for upward heat flow and by equation 35 for downward heat flow. From these equations and equation 33, the dependency of the heat fluxes on property values, using an average exponent of 0.2 in place of the upward equation exponent of 0.228 and the downward equation exponent of 0.18, is given by:

$$q'' \propto \left(\frac{\beta \rho^2 C_p}{\mu}\right)^{0.2} k^{0.6} \qquad (78)$$

Substituting liquid property values from Appendix E into equation 78, the ratio of the surface heat flux for property value sets 3 and 4 (Anderson set No.2) to that for property value sets 1 and 2 (Anderson set No.1), for a fixed geometry and temperature difference is calculated to be 3.33. Therefore, since property sets 3 and 4 produce better natural convection heat transfer than do property sets 1 and 2, higher pool temperatures are required to dissipate the same volumetric heat source with the latter sets than with the former sets. Therefore, higher pool temperatures are predicted for a given FRCMAS for property sets 1 and 2 and for sets 3 and 4, and, considering the lower boiling point for sets 1 and 2 than for sets 3 and 4, boiling is predicted for the former set, but not for the latter.

In spite of these uncertainties, Table 5 and Figures 35 and 36 show that, assuming the entire core mass to form the pool, the downward heat fluxes into the shield tank water are much lower than the predicted critical heat flux. The highest

downward heat fluxes predicted from the present analysis are 19.7 W/cm^2 at the upper corners of the non-boiling pool, for property sets 3 and 4, while the critical heat flux for the shield tank water at its assumed temperature of 60°C (sub-cooling of 40°C) would be about 280 W/cm^2 (76). Table 5 also shows that differences in vapor properties between property sets 1 and 2 do not result in any differences in predicted downward heat fluxes under boiling conditions, and these downward heat fluxes are less than those for the worst non-boiling conditions in any case.

Therefore, these results indicate that the calandria wall can remain well-cooled even if the entire mass of the core forms a molten pool in the calandria. Whether the calandria wall can survive this situation and retain its integrity is another question however, which is considered in the next section of this report.

5.3.2.2 Interaction of Molten Pool of Core Debris with Calandria Wall

There are two aspects of the interaction of a molten pool of core debris with the calandria wall. The first is the interaction of the liquid pool itself with the calandria wall while the second is the interaction of vaporized core material from a boiling molten pool with the calandria wall above the pool.

These aspects are considered in the next two sections of the report.

5.3.2.2.1 Interaction of Liquid Pool Itself with Calandria Wall

In section 5.3.1, we saw that the uncovered bed of solid debris in the bottom of the calandria would begin to melt near its centre about 135 minutes into the accident. We also saw that the results of the analysis implied that debris close to the calandria wall would not melt at all; however, since the analytical model is no longer valid once melting begins, this implication was speculative.

In this section, we will consider the interaction of a liquid pool of debris with the supporting calandria wall using the method developed in section 4.6.2.2, with the downward heat fluxes established in section 5.3.2.1 which are low enough that the calandria wall should remain well-cooled.

But, first of all, let us consider how the molten pool, and possibly a solidified crust, would form as the solid bed of debris melts. As molten material is formed,

it will tend to flow downwards through the pores of the debris until it refreezes as it approaches the well-cooled calandria wall. As pool heating continues, more of the central region of the debris melts and some of the refrozen debris will melt again and flow further downwards until it again refreezes. In this manner, most of the pool will eventually become molten and a solidified crust may form between the molten pool and the well-cooled calandria wall.

We can now apply the method of section 4.6.2.2 to this model of the pool, crust and well-cooled calandria wall, to establish whether or not any portion of the wall would melt. If so, the remaining thickness of solid wall will be determined so that we may draw conclusions as to whether or not the calandria wall would retain its structural integrity. Certain sensitivity calculations will also be done to provide more confidence in the conclusions.

From the results obtained in section 5.3.2.1, the predicted maximum downward heat flux from a molten pool of the entire core mass is 19.7 W/cm^2*. For the quasi-steady state model used for this analysis, the corresponding shield tank heat transfer coefficient can be established for either of the possible mechanisms of heat transfer from the calandria wall to the shield tank water, natural convection or sub-cooled nucleate boiling, using a conventional correlation for turbulent natural convection heat transfer (26, equation 7.25 and Table 2.1), and the Jens-Lottes equation (32) for sub-cooled nucleate boiling. In the latter case, the pressure was taken as two atmospheres to allow for the static head in the shield tank. For the given heat flux, the calculated natural convection heat transfer coefficient is 2020 W/m^2K while the calculated nucleate boiling heat transfer coefficient is 2570 W/m^2K. Therefore, the sub-cooled nucleate boiling mechanism will prevail, so that h_c = 2570 W/m^2K.

For these values of q''_b and h_c, the values of the non-dimensional heat flow parameter, ϕ, and the shield tank coolant Biot number Bi_{ac}, can be determined from equations 44 and 45, for the known calandria wall thickness, 0.0317 m, thermal conductivity - 16 W/mK, melting point, 1430°C, and shield tank water temperature, 60°C.

---

*This maximum heat flux occurs at the upper corners of the non-boiling pool, and is then actually at an angle of about 43° to the vertical. However, the model treats the wall and crust in a one-dimensional manner.

The calulated values are:

$$\phi = 0.285$$

$$Bi_{ac} = 5.10$$

From these values of ϕ and Bi_{ac}, equation 46 predicts that there will be no melting of the calandria wall by the molten pool of debris. Furthermore, Figure 9 indicates that the conditions to which the calandria wall is exposed ensure that it is very far from the melting point.

The solidified crust thickness which serves to protect the calandria wall from melting can be established from equation 41 or from Figure 11, using the values of the parameters $(T_f - T_m)/(T_m - T_c)$ and k_w/k_m given in section 4.6.2.2 and assuming a value of 2.5 W/mK to represent the thermal conductivity of the solidified crust, k_s. The predicted crust thickness, established in this manner, is:

$$\delta_s = 0.023 \text{ m.}$$

This result confirms one of the basic assumptions: that the crust will be thin, so that the one-dimensional analysis used is justified. Also, the assumption that all the core debris forms the molten pool is seen to be reasonable since only a relatively small mass will form the solidified crust.

As a further assurance that the calandria wall is far from conditions that could initiate wall melting, an analysis was done using equation 40 (or Figure 10) in which the heat flux from the pool was assumed to be increased above the maximum predicted value of 19.7 W/cm^2. The value of h_c was also increased, corresponding to the increased heat flux, with h_c calculated using the Jens-Lottes nucleate boiling correlation. This analysis showed that the heat flux from the pool would have to be about 100 W/cm^2 before any melting of the calandria wall would occur. A plot of the fraction of unmelted wall against downward heat flux from the molten pool is shown in Figure 37. Figure 37 shows that at least half the wall would remain solid for heat fluxes as high as 200 W/cm^2.

We may conclude with considerable confidence that the interaction of the molten pool of core debris with the calandria wall supporting it will result in the formation of a solidified crust which will serve to protect the wall from melting under all conditions that may be encountered in these accident sequences. The conditions to which the wall is exposed are such that it would require an increase of about a factor of five in the heat flux from the molten pool before any melting of the wall would occur.

We conclude from this analysis that the calandria wall under the molten pool surface will retain its integrity since it is well cooled by the shield tank water, with the actual heat flux being far below the critical heat flux, and it is well protected from direct contact with the molten pool by the solidified crust.

Therefore, if the molten pool properties are represented by property value sets 3 and 4, so that there is no boiling of the pool, we can conclude that the integrity of the calandria will not be jeopardized by the formation of the molten pool, particularly since the total mass of the core debris is only about 70% of the moderator mass initially in the calandria. Calculated hoop and beading stresses in the calandria wall under these conditions are very low, about 6.9 MPa (~1000 psi).

However, if the pool properties are represented by property value sets 1 and 2, so that boiling of the pool would be expected to occur, we cannot yet conclude that calandria integrity would be assured. Although the maximum downward heat flux in this case is only about 4.1 W/cm^2, so that the integrity of the wall under the pool surface is assured, the condensation of vaporized core debris on the calandria wall above the surface of the boiling pool may jeopardize the wall. This question is examined in the next section of this report.

5.3.2.2.2 Interaction of Vaporized Core Material with Calandria Wall

The method described in section 4.6.2.3 to predict condensing film behavior on the calandria wall above a boiling pool of molten core debris has been incorporated into a computer program, CONFILM, a listing of which is given in Appendix G. In this section of the report, the results of the application of this program to accident sequences S11 and S12 are presented.

As we saw in section 5.3.2.1, boiling of the molten pool of core debris is predicted only for property value sets 1 and 2. Therefore, only these sets of property values were considered in this part of the study.

The results obtained for the reference case, FRCMAS = 1.0, are summarized in Table 6. The predicted condensation heat flux is not very sensitive to the differences in property values and is well below the critical heat flux for the shield tank water which is about 280 W/cm^2, as indicated earlier. Therefore, the calandria wall above the boiling pool surface will remain well-cooled in the presence of the condensing film of vaporized core material.

From the values of ϕ and Bi_{ac} established for the two sets of property values, we conclude from the criterion of equation 46 that there will be no melting of the calandria wall under the condensing film, as stated in Table 6. Either set of property values predicts, from equation 57, that a solidified crust about 1.0 cm. in thickness will form under the condensing film to protect the calandria wall.

Therefore, we conclude that if boiling of the molten pool of core debris occurs, the heat fluxes resulting from the condensation of the vaporized core debris on the calandria wall will be low enough to avoid critical heat flux on the outer surface of the calandria wall, and so will ensure that it continues to be well-cooled, and will not cause any melting of the calandria wall. This conclusion is independent of uncertainties in the vapor property values.

Therefore, considering the conclusions drawn in the previous section as well as in this section, it is highly probable that the calandria will retain its structural integrity even when all the core mass forms a molten pool in these accident sequences, irrespective of whether the pool boils or not.

5.4 End Point for Accident Sequences S11 and S12

The analyses of the various stages of accident sequences S11 and S12 have resulted in the conclusion that moderator will be expelled from the calandria between about 45 to 50 minutes after the original LOCA occurs, that the fuel channels will disintegrate and form a quenched bed of solid debris which will begin to heat up after all the moderator has been expelled and that the solid

Table 6: Condensation of Vaporized Core Debris on Calandria Wall.
Accident Sequences S11 and S12
Reference Conditions

Property Value Set	1	2
FRCMAS	1.0	1.0
Superficial vapor velocity at surface of pool, m/s	0.744	0.814
Condensation heat transfer coefficient, W/m^2K	1220	1310
Condensation heat flux at calandria wall, W/cm^2	49.1	52.5
ϕ (See eq. 44)	0.65	0.687
Bi_{ac} (See eq. 45)	10.8	11.5
δ_s, m	0.0103	0.0100
Calandria Wall Melting?	No	No

debris bed will start to melt some 135 minutes into the accident. A molten pool of heat-generating core debris will form, but, because of uncertainty in pool property values, it is not possible to determine whether the pool will undergo boiling or not. However, the analyses show that, irrespective of whether boiling of the pool occurs or not, the calandria wall will remain well cooled as long as the shield tank cooling system continues to operate. The calandria wall will be protected by a solidified crust both below the surface of the molten pool and above the surface under a condensing film of vaporized core debris should boiling of the molten pool occur.

Therefore, we may conclude with good confidence that the calandria will retain its structural integrity throughout these accident sequences as long as the shield tank cooling system continues to function. Eventually, as the fuel heat source decays, the molten pool would gradually re-solidify, over a long period. Calculations with MOLTENPOOL show that the molten pool would begin to re-solidify at about 50 hours, assuming property values are given by sets 1 and 2 and at about 84 hours, assuming property values are given by sets 3 and 4. The differences in predicted times to solidification are consistent with the better liquid transport properties in property value sets 3 and 4 compared to those in sets 1 and 2. Therefore, since no further damage is anticipated, the containment of the mass of the core within the calandria, with its gradual cooling and re-solidification marks the end-point of accident sequences S11 and S12. That is, the end point for this accident sequence is indicated by boxes 31a and 31b of the analytical flow chart of Figure 3. The calandria wall temperature is well below the melting temperature and is decreasing slowly as the heat source decays.

To complete the assessment of these accident sequences, we must assess the potential effects on containment of these accident sequences, box 32 of Figure 3. The results of this assessment are presented in the next section of the report.

5.5 Containment Pressurization and Effects in Accident Sequences S11 and S12

The discharge rate from the calandria as a function of time has been established in section 5.2.4, as shown in Figure 24 for the reference conditions. Figure 24 shows the total flow rate of vapor and liquid D_2O from the calandria. As discussed in section 5.2.6, deuterium gas from the Zircaloy-steam reaction on the calandria tubes will be produced at intervals during moderator expulsion

from the calandria as groups of channel rows become uncovered. The consumption of steam in the Zircaloy-steam reaction will actually result in small decreases in the total mass expulsion rates from the calandria during these intervals below the rates shown at these times in Figure 24. The program, BLDG, was used to establish the pressure history in containment resulting from these accident sequences. Input data for the reference case were established as described below.

The vapor and liquid discharge rates as functions of time for the reference case were taken from the output of MODBOIL for this case. The vapor discharge rates were reduced appropriately during the periods of deuterium gas expulsion and the gas expulsion rates during these periods were established from the analysis described in section 5.2.6. Since these accident sequences end with the core debris contained in the calandria, as discussed in section 5.4, there is no interaction of molten core material with concrete and no evolution of CO_2 is encountered, so that no allowance for CO_2 gas flow was made.

The volume of the containment used in the analysis included that of the reactor vault, the fuelling machine duct, the central service area, the pressure relief duct and manifold and the vacuum building, for a total volume of 114,050 m^3(77). Initial conditions in containment were a pressure of 90 kPa and a temperature of 90°C. These conditions are typical of those which exist in the reactor vault at the time after a large header break that discharge from the calandria relief ducts begins (10,11). Note that the assumed initial conditions are conservative in that they ignore the much lower atmospheric temperature that would exist in the vacuum building at this time (10,11).

Results for the reference conditions are shown in Figure 38 where the containment pressure and temperature are plotted against time. The pressure history before relief duct discharge begins is taken from Fig. 12.3.3-32 of the Bruce-A Safety Report (10). It can be seen that the absolute pressure reaches a maximum of about 155 kPa at about 48 minutes after the start of the accident. The predicted temperature of the containment atmosphere at this time is about 99°C. Thus, the maximum predicted pressure difference across the containment boundary in these accident sequences is about 54 kPa or about one-half atmosphere.

This predicted peak pressure difference is about the same as the containment design pressure difference (~50 kPa) and is well below the test pressure difference (~80 kPa) (10,11). This peak pressure difference would not cause any containment failure (e.g., 78) and the leak rate at this time would be lower than the design value at the test pressure.

Free, gap-inventory, fission products will begin to escape to the primary system, and thence to containment when the fuel sheaths begin to fail early in the accident sequence. As the fuel channels disintegrate following calandria tube uncovery, further release of gap-inventory fission products would be expected, but the actual build-up of radioactivity in containment would probably be delayed because of the solubility of iodine in the remaining moderator, given the probable appropriate water chemistry conditions (74,75).

Major releases of the fission products bound in the fuel matrix would not be expected until the fuel begins to melt. As we have seen, fuel melting will not begin until about 135 minutes after the initial LOCA occurs. By this time, the pressure and temperature of the containment atmosphere will have decreased below their peak values, as shown in Figure 38, with the containment pressure being about 130 kPa absolute. Therefore, since the pressure peak experienced will not have damaged containment and since major fission product release from the fuel will not occur until the containment pressure is fairly close to atmospheric, it appears that there would not be a major release of fission products to the environment in accident sequence S11 at least, in which no containment impairment is assumed. Whether significant releases from containment would occur in accident sequence S12, because of open ventilation dampers, failed air-lock door seals, failure of dousing, etc., is not known, although it should be noted that the pressure differential across the containment boundary in many cases would be very low when significant fission product releases from fuel would be expected to occur. Nothing further can be said since the analysis of fission product behavior and dispersion in and from containment was not a part of this study.

To assess the sensitivity of containment pressurization to the assumed disintegration behavior of uncovered fuel channels, BLDG was also run for conditions in which instantaneous disintegration of fuel channels at the moments

of their uncovery is assumed to occur, with the fuel and Zircaloy temperatures at these moments at 1600°C and 1100°C respectively. The results of this run are also shown in Figure 38. It can be seen that the containment pressure at any time in this case is somewhat less than that predicted for the reference conditions, with the peak pressure being about 135 kPa in this case compared to 155 kPa in the reference case.

Further sensitivity studies were made to establish the importance of condensation on the containment boundaries and of the containment volume assumed to be effective.

Figure 39 shows the predicted containment pressure for the reference conditions but ignoring condensation on the boundaries. The pressure at any time is only slightly higher than that predicted allowing for boundary condensation with the peak absolute pressure being about 163 kPa instead of about 155 kPa. Thus, the results are very insensitive to boundary condensation, because of the low values of effective boundary heat transfer coefficient resulting from the large fraction of non-condensibles present in containment.

To establish the sensitivity of the predicted containment pressure to the estimated deuterium produced from the calandria tubes under the reference conditions for these sequences, a run with BLDG was made for these conditions but ignoring deuterium production. The resulting containment pressures at any time are almost identical to those for the reference conditions, so that the curve in Figure 39 for the reference conditions equally well represents the pressure history for the conditions which ignore deuterium production. For example, the predicted peak containment pressure for these conditions is about 156 kPa compared to 155 kPa for the reference conditions. The slightly higher pressure for the conditions without deuterium production results from the fact that deuterium generation results in reduction of steam discharge from the calandria, as discussed earlier.

Shown in Figure 39 is the predicted containment pressure when the containment volume assumed to be effective is reduced below the total available volume.

For example, it might be assumed that the pressure relief valves to the vacuum building might fail to re-open during this second pressurization of containment. The predicted peak absolute pressure for an effective volume equal to that of the reactor vault, fuelling machine duct, central servicing area and manifold, i.e., ignoring the vacuum building, is about 215 kPa ($\Delta p \approx 114$ kPa). This predicted peak pressure difference is about 34 kPa (~5 psi) above the test pressure, but no catastrophic failure of containment would be expected under this condition (78). Somewhat greater leakage of fission products from containment than for the reference case would be expected later in the accident sequences under this condition. However, since the Bruce-A PRV's operate on the basis of differential pressure between the manifold and the vent duct, it is difficult to imagine that <u>all</u> of the PRV's would fail to re-open following the second pressurization of containment during these accident sequences. Note that, because of the relatively slow re-pressurization during moderator expulsion from the calandria, even one PRV would be adequate to ensure that the vacuum building volume would be "available".

The total mass or deuterium gas generated from the calandria tubes during these accident sequences is very small, ~78 kg. The maximum incremental increase in the volume fraction of deuterium in the containment corresponding to this mass is about 0.64%, well below the flammability limit. Therefore, it is evident that the additional deuterium released from the calandria tubes in these accident sequences will not result in conditions leading to deuterium deflagration or detonation. Thus, these mechanisms will not present any additional threat to containment integrity during these accident sequences.

These sensitivity studies indicate that the containment pressure history shown in Figure 38 for the reference conditions is probably quite realistic for these accident sequences. If anything, because of assumptions in the analysis, it is probably somewhat conservative.

From this assessment, we may add the following conclusions for accident sequences S11 and S12 to those given in section 5.4:

a) there will be no damage to containment caused by these accident sequences,

b) iodine fission product release from disintegrating fuel will probably be delayed by iodine solubility in the remaining moderator,

c) no major release of bound fission products from containment will occur in accident sequence S11 since the containment pressure will be quite close to atmospheric when significant releases of bound fission products from the fuel begin because of fuel melting,

d) it is uncertain whether a major release of fission products from containment would occur in accident sequence S12 since, although it is assumed that containment is impaired in this sequence, there may be only a small pressure difference across the containment boundary when significant releases of bound fission products from the fuel begin.

A summary of the analysis and results of accident sequences S11 and S12 is given in reference 114.

Although the analysis has been based on LOCA conditions in which pressure tubes sag onto calandria tubes, the general behavior of the moderator and core would probably not be greatly different for LOCA conditions in which the pressure tubes balloon into contact with the calandria tubes. In this case moderator would probably be expelled more rapidly from the calandria, but subsequent behavior would be similar to that in the present case. In the judgment of the author, the core material would still be contained within the calandria, there would be no consequent failure of containment and there would be no significant release of fission products from containment, at least for an unimpaired containment.

6. ASSESSMENT OF ACCIDENT SEQUENCES S13 AND S14: LOCA + LOECI + LOMHS

6.1 Introduction

As pointed out in section 3.2, these accident sequences are similar to accident sequences S11 and S12, except that fuel channels would be uncovered much more rapidly and fuel melting would probably occur earlier. Therefore, it was judged to be unnecessary to develop a separate analytical flow chart for these accident sequences, since Figure 3 could again be used as a guide. Also, almost all of the analytical tools necessary to analyze these accident sequences have already

been developed in the analysis of accident sequences S11 and S12, so that only the one new analytical model required for these sequences, the prediction of moderator discharge rate through a ruptured pipe, is described here.

6.2 Initiation of Accident Sequences S13 and S14

For these accident sequences, it was again assumed that the size and location of the primary system pipe rupture causing the LOCA results in late stagnation conditions, so that, with failure of emergency cooling injection, pressure tubes sag onto the calandria tubes at pressure tube temperatures of 1000°C. In these accident sequences, it is assumed that a moderator outlet pipe from the calandria, the largest single pipe (12", 0.305 m, dia.) in the moderator circuit, also fails simultaneously.

The sequence of events following these initiating events is similar to those for accident sequences S11 and S12, as noted earlier, and most of the analytical models needed have been developed for S11 and S12 and are described in sections 4.3 to 4.9. The one additional analytical model required for S13 and S14 is described in the next section.

6.3 Moderator Discharge Rate Through Ruptured Outlet Pipe

6.3.1 Description of Accident Sequences

In these accident sequences, it is assumed that a guillotine rupture of a 0.305 m moderator outlet pipe occurs simultaneously with the LOCA. The rupture is assumed to occur outside the shield tank, since there would be no drainage from the calandria if the rupture occurred in the part of the pipe contained within the shield tank. Thus, the moderator is discharged through approximately 11 metres of pipe, most of which is horizontal, with two 90°-elbows and one 45°-elbow*. It is estimated that the highest point in the moderator outlet pipe outside the shield tank is about 1.2 metres below the bottom of the calandria*. It is assumed that the rupture occurs at this point.

Following the outlet pipe rupture, moderator will be discharged at a rate governed by the pressure over the moderator, compared to the reactor vault pressure, and the static head of the moderator above the pipe rupture elevation.

*Information from Bruce-A Design Manual OM-21-32110/63210.

The relief-duct rupture disks are intact for at least the early part of these accident sequences, so that the pressure above the moderator surface will decrease rapidly from its initial value as the gas volume over the moderator expands as the moderator level drops. The gas pace pressure will fall until it reaches the saturation pressure of heavy water corresponding to the bulk average temperature of the moderator. The pressure over the moderator will then remain constant for a period, as moderator flashes into the vapor space as the moderator level continues to fall, assuming the rupture disks remain intact.

As the moderator level drops, calandria tube rows will be uncovered and the fuel, pressure and calandria tube temperatures will start to rise rapidly. Eventually, fuel channels will disintegrate and fall into the rapidly draining moderator. The quenching of the debris will cause a steam generation surge from the moderator which may or may not result in relief-duct rupture disk failure, depending on the timing of fuel channel disintegrations and the number of channels disintegrating at any one time. If the rupture disks do not fail, the increased pressure over the moderator resulting from the steam generation will increase the discharge rate and decrease the time required to empty the calandria. If the rupture disks do fail, the pressure over the moderator will drop almost immediately to the reactor vault pressure and will tend to remain relatively close to this pressure subsequently, even following further uncovered fuel channel disintegrations, since pressure rises following such disintegrations will be limited by the rapid increase in gas-space volume as liquid is driven more rapidly from the broken pipe.

In either case, all the moderator will eventually be lost from the calandria in a relatively short time compared to that required for complete moderator expulsion in the cases of the loss of moderator cooling system accident sequences, about 48 minutes for the reference case.

Following complete loss of moderator from the calandria, the models developed for accident sequences S11 and S12 can be used for further analyses of the present accident sequences, provided appropriate initial conditions are used.

6.3.2 Analytical Model for Moderator Discharge Through Pipe Break

The program MODBOIL could have been modified to allow for liquid discharge from a broken moderator outlet pipe, quenching of debris and vapor generation under

sub-cooled moderator conditions and to establish whether the relief duct rupture disks would fail and the subsequent effect on discharge times. However, assessment of the problem indicated that simpler hand calculations would provide reasonable upper and lower limits on the total time required for complete moderator discharge in this case. Therefore, this simpler approach was employed.

A diagram of the model used in this analysis is shown in Figure 40. In this model, we first ignore the effect of the presence of the calandria tubes in the calandria on moderator volume. Because the overall moderator discharge period is relatively short and since cooled moderator flow into the calandria may continue for some time, at least, after the pipe rupture, the moderator temperature is assumed to be constant at its initial value, taken as 80°C, in these accident sequences, until channel disintegration occurs.*

The mass flow rate from the calandria can be expressed in terms of the change in liquid level by:

$$\dot{m}_m = \rho_f L w_m \left(\frac{-dz_m}{dt}\right) \tag{79}$$

The mass flow rate from the calandria can also be expressed by equating the pressure losses of the flow through the broken moderator outlet pipe to the driving head:

$$(p_i - p_\infty) + \rho_f \frac{g}{g_c} (z_m + z_o) = K_T \frac{\rho_f}{2g_c} \left(\frac{\dot{m}_m}{\rho_f A_p}\right)^2 \tag{80}$$

In equation 80, K_T is the total loss coefficient for flow in the broken moderator outlet pipe, including inlet, pipe friction, elbow and outlet losses.**

---

*Also, for a significant fraction (1/4 to 1/3) of the transient considered here, the heat flow rate from the calandria tubes to the moderator will be very low since blowdown will still be occurring in the fuel channels. After EOB, the heat flow rate from the calandria tubes to the moderator will continue to be quite low for some time, until pressure tubes begin to sag onto the calandria tubes. Even after pressure tube sagging occurs, the heat flow rate to the moderator from the calandria tubes will remain relatively low for the period of concern here. These conclusions are reached from an examination of IMPECC outputs for relevant conditions.

**Pressure losses in the calandria itself are negligible.

For high Reynolds number flow in large, smooth pipes, with allowance for two 90°-elbows and one 45°-elbow, the estimated value of K_T, from information in reference 79, is:

$$K_T \simeq 3.0$$

It is more convenient to express the moderator height in terms of y_m rather than z_m (Figure 40), where:

$$y_m = z_m - R \tag{81}$$

Eliminating $\dot{m}_m$ by combining equations 79 and 80, substituting for z_m by equation 81 and expressing w_m in terms of y_m from Figure 40, we obtain:

$$-\phi_m \, d\left(\frac{y_m}{R}\right) = \frac{A_p^2}{R^2 L}\left(\frac{g_c}{2\rho_f K_T}\right)^{1/2} dt \tag{82}$$

where ϕ_m is given by:

$$\phi_m = \left[\frac{1 - \left(\frac{y_m}{R}\right)^2}{p_i - p_\infty + \rho_f \frac{g}{g_c} R \left(1 + \frac{y_m}{R} + \frac{z_o}{R}\right)}\right]^{1/2} \tag{83}$$

Equation 82 cannot readily be integrated, even for p_i constant, except for the simple case in which $p_i = p_\infty$ and $z_o/R = 0$*. Therefore, equation 82 was solved for desired conditions using numerical methods.

The volumetric discharge rate from the calandria through the broken pipe can, however, be calculated analytically, since:

---

*In this case, equation 82 can be integrated to give a total drainage time of:

$$t_e = 2.667 \frac{R^{3/2} L}{A_p}\left(\frac{K_T}{g}\right)^{1/2} \tag{84}$$

$$\dot{V}_f = w_m \left(\frac{dy_m}{dt}\right) \tag{85}$$

Therefore, the volumetric discharge rate of the moderator is given by:

$$\dot{V}_f = A_p \left(\frac{2g_c}{\rho_f K_T}\right)^{\frac{1}{2}} \left[p_i - p_\infty + \rho_f \frac{g}{g_c} R \left(1 + \frac{y_m}{R} + \frac{z_o}{R}\right)\right]^{\frac{1}{2}} \tag{86}$$

It is assumed that the only effect of the presence of the calandria tubes on the moderator discharge rate is to reduce the calandria volume in a homogeneous manner. This simplification means that all the above equations still apply with the calandria radius reduced to an equivalent radius, R_e, the radius of a calandria without calandria tubes with a volume equal to the free volume of the actual calandria. For a Bruce-A reactor unit:

$$R_e = 0.94\ R \tag{87}$$

Therefore, the volume occupied by the calandria tubes will not have a significant effect on the drainage of moderator from the calandria in a typical CANDU reactor.

Equation 86 shows that, when p_i is less than p_∞, i.e., for the conditions expected during the early part of this accident sequence, the quantity in square brackets in equation 86 can equal zero when y_m is low enough, i.e., the volumetric discharge rate from the calandria would be predicted to stop. This situation would occur when the external reactor-vault pressure was just balanced by the pressure over the moderator plus the static head of the moderator. However, in reality moderator discharge from the calandria would not cease, even if there were no channel disintegrations to cause pressure surges which would upset this equilibrium. It is very unlikely that the pipe break would be upward-facing, so that, should the equilibrium condition be approached, Taylor instability at the break would result in the establishment of two-phase slug counter-flow in the moderator outlet pipe. Slugs of air would travel through the pipe from the break to the calandria, and up through the calandria to the moderator surface where they would enter the

gas-vapor space to replace the volume of moderator being discharged. Moderator would continue to discharge through the pipe break, flowing around the counter-flowing air slugs in the moderator outlet pipe. Such a slug-counter-flow regime would set a lower limit to the discharge rate from the calandria.

A simple model of the slug-counter-flow regime in a vertical pipe can be used to establish this lower limit discharge rate. The void fraction in the slug-flow regime in a vertical pipe is given by (22, Chapter 10):

$$\langle\alpha\rangle = \frac{\dot{V}_g}{1.2(\dot{V}_f + \dot{V}_g) + A_p\, v_{s\infty}} \tag{88}$$

where $v_{s\infty}$, the slug rise velocity in a vertical circular pipe, is given by:

$$v_{s\infty} = 0.345\left[\frac{g\, d(\rho_f - \rho_g)}{\rho_f}\right]^{\frac{1}{2}} \tag{89}$$

In this case, the time-averaged volumetric air flow rate, at the moderator surface, must be equal and opposite to the time-averaged volumetric liquid flow rate at this point. Because of the effect of the static head of the moderator, the average volumetric flow rate of the air in the discharge pipe will be less than that at the surface of the moderator in the ratio of $p_i/(p_i + \rho_f \frac{g}{g_c} z_m)$, ignoring temperature changes of the moderator.

Therefore, the relationship between the liquid and gas volumetric flow rates in the moderator outlet pipe is:

$$\dot{V}_g = -\frac{p_i}{p_i + \rho_f \frac{g}{g_c} z_m}\, \dot{V}_f = -r_p\, \dot{V}_f \tag{90}$$

From equations 88 and 90, the average moderator volumetric discharge rate under these conditions is given by:

$$\dot{V}_f = - \frac{A_p \, v_{s\infty} \langle \alpha \rangle}{1.2(1 - r_p) \langle \alpha \rangle + r_p} \qquad (91)$$

Equation 91 can be used to establish an ultimate lower limit to the moderator discharge rate from the broken pipe, for a given value of the void fraction in the moderator outlet pipe.

Another factor which would ensure that discharge continued from the calandria when equation 86 predicts a zero discharge rate, in the absence of channel disintegration, would be the in-leakage of the reactor-vault gas atmosphere through reactivity control mechanism and instrumentation penetrations through the top of the calandria.

6.3.3 Criterion for Channel Disintegration

As pointed out earlier, the heat flow rate to the moderator from the calandria tubes will be quite low during most of these accident sequences compared to the heat flow rate in accident sequences S11 and S12. Therefore, to estimate the temperature history of fuel channels, particularly after their uncovery, the conservative assumption is made that, after EOB, no heat is transferred from the channels to the moderator nor to the gas-vapor space above the moderator. This is a reasonable limiting assumption since, as we will see, there is not much time for heat flow from sagged pressure tubes through the calandria tubes to the liquid moderator, even for the lower rows, because of the rapid discharge of moderator, and since, before the first rows disintegrate there will be no significant steam flow over uncovered calandria tubes and thus no significant cooling of the calandria tubes and fuel channels. Thus, the temperature history of the fuel after EOB is established conservatively assuming adiabatic conditions. It is also assumed that the temperatures of the pressure tube and calandria tube are essentially the same as that of the fuel at any given time after EOB, which will again be conservative, but, at the same time, not very unrealistic considering the adiabatic assumption. Before the first channel disintegration, no Zircaloy-steam reaction is assumed to occur on uncovered calandria tubes, since there is no flow of steam over the tubes.

As for the previous accident sequences, it will be assumed that channel disintegration will occur when the calandria tube temperature (i.e., in this

case again, the fuel temperature also) reaches 1750°C. It will also be assumed again that a disintegrating row will cause disintegration of all lower uncovered rows, as in the reference case for accident sequences S11 and S12.

Based on the foregoing model, the rate of temperature rise of the fuel, and thus the pressure and calandria tubes, is given by:

$$\frac{d\,\bar{T}_{Fa}}{dt} = \frac{\dot{Q}_{gz}}{37\ \rho_u (\frac{\pi}{4} d_p^{\,2})\ C_{pu}} \qquad (92)$$

where $\dot{Q}_{gz}$ as a function of time can be taken directly from the output of an IMPECC run for the appropriate FEPR.

For any row of tubes, equation 92 can be used to determine $\bar{T}_{Fa}$ as a function of time from appropriate IMPECC runs, using the EOB weighted-average fuel temperature as the initial temperature. From this information, the times for row disintegration can be established, accounting for the assumption that all uncovered rows will disintegrate if struck by a higher disintegrating row.

7. RESULTS OF ASSESSMENT OF ACCIDENT SEQUENCES S13 AND S14: LOCA + LOECI + LOMHS

7.1 Heat Source to Moderator

As explained in the previous section, the heat source to the moderator is ignored in these cases, except for the quenching of disintegrated fuel channels. The validity of this assumption will be demonstrated later.

7.2 Discharge of Moderator from Calandria

For the assumed moderator temperature of 80°C, the saturation pressure of heavy water is 46 kPa (6.7 psia). For the initial gas space volume of 170 ft^3 (4.8 m^3) and pressure of 101 kPa (14.7 psia), the volume of the gas space when its pressure equals the saturation pressure of the moderator is about 270 ft^3 (7.7 m^3) assuming adiabatic expansion of the gas phase and ignoring the partial pressure of the water vapor in the gas volume. It can be readily shown that the moderator level would be at $y_m/R = 0.945$ when this gas-space volume is reached.*

*The very small initial liquid volume in the relief ducts (5.9 ft^3, 0.167 m^3) is ignored in this calculation.

If the gas-space pressure is assumed to be constant at the saturation pressure of the moderator, the time for the moderator level to reach $y_m/R = 0.945$ can be calculated* from equation 82 to be about 5 seconds. Since the gas-space pressure will really be higher than the saturation pressure during this period, the actual time to reach y_m/R will be less than 5 seconds, so that this period may be ignored in the analysis.

Integrating equation 82 numerically, the time for the moderator level to reach a given value of y_m/R was determined for a constant value of p_i equal to 46 kPa and a constant value of p_∞ equal to 101 kPa.** The results are shown in Figure 41. Equation 86 predicts that there would be no further moderator discharge after the moderator level reaches $y_m/R = 0.056$, i.e., just below the horizontal mid-plane, as shown in Figure 41 by the dashed portion of the curve. Of course, as discussed earlier, this asymptotic condition is not realistic. We will now establish a more realistic behavior for the latter part of the moderator discharge.

The times of uncovery of the various calandria tube rows for the early part of the transient (y_m/R positive) are indicated on the discharge curve in Figure 41. Figure 41 shows that the top row would become uncovered at about 50 seconds, i.e., before the end of blowdown. Once EOB is reached, the fuel in the top row would heat up adiabatically, as assumed. From equation 92, and the total heat generation rate (including heat generation by the Zircaloy-steam reaction in the coolant channel) at the maximum power position in the top row of fuel channels as predicted in an appropriate IMPECC run, the time at which the fuel reaches a temperature of 1750°C, and thus the assumed time for disintegration of the top row, is about 410 seconds. From Figure 41, the top nine rows of channels are uncovered by this time, so that with the assumption of cascading failure, all these rows drop into the remaining moderator at this moment.

Without modifying the MODBOIL program as discussed earlier, it is impossible to establish whether the resulting steam generation surge would break the rupture

*The very small initial liquid volume in the relief ducts (5.9 ft^3, 0.167 m^3) is ignored in this calculation.

**The reactor vault pressure undergoes a short-lived (<30 sec.) transient above P_{atm} in the early stages of the initiating LOCA (10), but this pressure transient is ignored here, which is a conservative assumption.

disks on the relief ducts, and then to establish the subsequent discharge behavior of the remaining moderator. However, it is possible to establish probable upper and lower limits for the discharge rate of the moderator following this initial surge of steam generation by setting upper and lower limits for the pressure over the moderator after this time. Should the rupture disks not break, the maximum pressure over the moderator could not exceed about 234 kPa (34 psia or about 20 psig) following this initial steam surge. If the rupture disks do not break on the first steam surge, they are unlikely to do so on subsequent steam surges because of the probable fewer channel rows disintegrating at any one time and the rapidly increasing vapor volume available as the moderator discharge continues. Therefore, a constant pressure of 234 kPa (34 psia) was assumed over the moderator after the first steam surge to establish an upper limit for the moderator discharge rate and a lower limit for the time required for total discharge of the moderator from the calandria.

If the rupture disks do break, the pressure over the moderator would drop rapidly to that of the reactor vault as vapor discharged through the relief ducts and liquid moderator was expelled more rapidly through the pipe break. Subsequent channel disintegrations and resulting steam surges would probably not increase the pressure over the moderator greatly above the reactor vault pressure because of the continuing rapid discharge of the liquid moderator from the broken pipe. Therefore, a constant pressure equal to the reactor vault pressure, taken as 101 kPa at this time, was assumed to exist over the moderator surface to establish a lower limit for the moderator discharge rate and an upper limit for the time required for total discharge of the moderator from the calandria.

With these assumptions, equation 82 was numerically integrated for values of p_i = 234 kPa and 101 kPa respectively, starting at t = 410 seconds, i.e., $y_m/R \simeq 0.22$, to determine the upper and lower limits for the moderator level as a function of time after the first group of fuel channels disintegrate.

The results are also shown in Figure 41. Figure 41 shows that the predicted maximum and minimum times for total discharge of the moderator from the calandria are about 980 seconds (16.3 minutes) and 680 seconds (11.3 minutes) respectively.

This range of probable discharge times is considerably less than the total calculated discharge time for the reference case for accident sequences S11 and S12 (≈48 minutes), confirming the expected results for the present accident sequences.

The predicted volumetric discharge rates of the moderator during these accident sequences are shown in Figure 42 for the same conditions as in Figure 41. Figure 42 shows that the minimum discharge rate at any time is about 7.3 ft^3/s (0.21 m^3/s), at $y_m/R = -1.0$ for $p_i = 101$ kPa. This predicted minimum discharge rate is well above the ultimate lower limit established by equation 91 for slug counter-flow conditions in the moderator outlet pipe, which is about 1.3 ft^3/s (0.036 m^3/s) for a representative void fraction of 0.8. Thus, we conclude that the discharge rate from the calandria will not be governed by the slug counter-flow mechanism at any time during these accident sequences.

Therefore, we may conclude that the moderator will be completely discharged from the calandria between approximately 11 and 17 minutes in accident sequences S13 and S14, irrespective of whether the rupture disks fail or not.

7.3 Behavior of Fuel Channel Debris

We have seen that the moderator will have been completely discharged from the calandria at a time approximately with the limits of 11 and 17 minutes after the initial LOCA. The upper nine rows will have disintegrated at about 7 minutes and will probably have been completely quenched by the time that the last of the moderator is discharged from the calandria even for the shortest discharge times, based on the quenching behavior predicted by MODBOIL for accident sequences S11 and S12 (i.e., the group of eight rows is quenched within one minute after disintegration under the reference conditions).

In the remaining time after the first group of channels disintegrates, some other rows will also disintegrate and will be at least partially quenched before all the liquid moderator is expelled. However, particularly for the shortest probable moderator discharge times, many of the lower tubes will not have been quenched, and may still be intact by the time that the calandria has been completely drained. Therefore, at the end of the discharge period, there will be a debris bed at the

bottom of the calandria, the lower portion of which will have been completely quenched to temperatures around 105°C to 110°C, with the upper portion at higher temperatures, depending on the degree of quenching. Above the bed there may be still a few rows of intact channels, which however will disintegrate within a few minutes, and will obviously not be quenched at all. Therefore, we may assume that within a few minutes of the emptying of the calandria, all the fuel channels will have disintegrated and will have formed a debris bed with a temperature gradient from about 100°C at the bottom to about 1750°C at the top.

However, to be conservative, it is assumed for the reference cases for these accident sequences that initial temperature of the debris bed is 1750°C throughout.

Because of the uncertainty in the moderator discharge times, cases were run using the program DEBRIS for initial times outside the probable range of discharge times as well as within it; initial times of 5, 10, 15 and 20 minutes were used. Note that the assumption of a uniform initial temperature of 1750°C for the debris bed becomes particularly conservative for the 20-minute discharge time.

Other conditions assumed for the reference-case debris bed are the same as those used for the reference conditions for the previous accident sequences, as listed in section 5.3.1. Thus, the debris bed conditions assumed for the present accident sequences are:

Initial time of bed dry-out:	5, 10, 15 or 20 minutes
Initial bed temperature:	1750°C
Fraction of total core mass in bed, FRCMAS:	1.0
Void fraction of bed, ε_v:	0.5
Average pore size of bed, δ_p:	0.03 m
Contact conductance factor, F:	0.5.

The program DEBRIS was then used to determine the time required after dry-out for the debris bed to reach the melting point of Zr O_2, 2700°C. The results are shown in Table 7. The results shown for bed dry-out times of 10 and 15 minutes should be considered more representative of actual conditions than those for 5 and 20 minutes, from the analysis of moderator discharge. The times to reach

Table 7: Characteristics of Solid Debris Bed in Bottom of Calandria at Initiation of Melting. Accident Sequences S13 and S14

Initial average temperature of debris: 1750°C

FRCMAS = 1.0

ϵ_v = 0.5

δ_p = 0.03 m

F = 0.5

Bed dry-out time, min.	5	10	15	20
Overall time to reach M.P., min.	23.6	30.7	37.3	43.7
Temperature of bed at calandria wall, °C	480	466	450	438
Temperature of upper surface of bed, °C.	1420	1399	1385	1367
Heat flux into shield tank water, W/cm^2	24.3	22.9	22.0	21.3

Note that the temperatures of the bed at the calandria wall, the upper surface of the bed and the heat flux into the shield tank water are the values existing at the time of initiation of bed melting.

the initiation of melting in the debris bed are, of course, much shorter for these accident sequences than for accident sequences S11 and S12, and depend significantly on bed dry-out time.

However, the results show that, even for the shortest dry-out time, the bed temperature next to the calandria wall is very low and is well below the calandria wall melting point. Furthermore, the heat flux into the shield tank water is again well below the critical heat flux value for the shield tank water, 280 W/cm^2, as given in section 5.3.2.1. Even at the upper corners of the debris bed where the temperature next to the wall and the heat flux into the shield tank water will be the highest, the bed temperature must be significantly below the calandria wall melting point of 1430°C, since the maximum temperature of the upper surface well away from the corners is about 1420°C for the shortest dry-out time, and lower for longer dry-out times.

Therefore, we can conclude that the calandria wall would remain intact and well-cooled even for the very short bed dry-out times and conservatively-high initial temperature assumed for these accident sequences.

Furthermore, the margins between the bed temperatures next to the calandria wall and its melting temperature and between the heat fluxes into the shield tank water and the critical heat flux are so large that variations in the reference-case debris bed parameters ε_v, δp and F over the wide ranges considered in the sensitivity study of section 5.3.1 will not jeopardize the integrity of the calandria wall, as deduced from the results of that sensitivity study.

Therefore, we conclude that, for accident sequences S13 and S14, as for accident sequences S11 and S12, the calandria wall will retain its integrity and will contain the core debris at least up to the time that melting begins in the debris bed in the bottom of the calandria.

The analysis of moderator discharge indicated that the minimum bed dry-out time would be about 11 minutes. Therefore, in further analysis of these accident sequences, a bed dry-out time of 10 minutes has been assumed for the reference case.

From Table 7 we see that debris bed boundary conditions at the initiation of melting are quite insensitive to dry-out time, with only the time to reach melting being sensitive to this parameter. In particular, there is no drastic change in debris bed behavior at assumed dry-out times less than 11 minutes. Therefore the use of a bed dry-out time of 10 minutes as the reference case is quite reasonable.

7.4 Thermal Behavior of Molten Pool of Core Debris

7.4.1 Internal Characteristics of the Molten Pool

The computer program, MOLTENPOOL, was used to establish the internal thermal characteristics of the molten pool, as for the cases of accident sequences S11 and S12. As in the previous cases, the transition period from the initiation of melting in the debris bed to the time that the debris bed becomes completely molten is ignored and the decay of the pool heat source in this period is also ignored. The results obtained will again be conservative because of these assumptions.

The results obtained are shown in Table 8, for the reference case for these accident sequences (bed dry-out time of 10 minutes) with the initial melting time rounded off to 30 minutes from the time of 30.7 minutes shown in Table 7.

Table 8 shows that the predicted pool behavior again depends significantly on the set of property values used, as in accident sequences S11 and S12. With property value sets 1 and 2, the pool is predicted to boil, but with property values sets 3 and 4, no boiling is predicted, again as in the previous accident sequences.

The reasons for the differences in predicted behavior with property sets 1 and 2 (boiling) and property sets 3 and 4 (no boiling) were discussed in section 5.3.2.1.

Again, in spite of the uncertainties resulting from the different sets of property values, Table 8 shows that the predicted downward heat fluxes are much lower than the predicted critical heat flux for the shield tank water on the calandria wall. The highest heat fluxes into the shield tank water predicted for the present conditions are 29.5 W/cm^2 at the upper corners of the non-boiling pool,

Table 8: Results of MOLTENPOOL Analysis for Accident Sequences S13 and S14.

Total Mass of Core Material in Pool (FRCMAS = 1.0)
Time from Initiation of Accident Sequence = 30 minutes

Property Value Set No.	1	2	3	4
Is Pool Boiling?	Yes	Yes	No	No
Nu_u	2135	2333	926	926
Nu_d	58.5	58.5	110	110
$\overline{q''_u}$, W/cm^2	150.5	164.5	181	181
$\overline{q''_d}$, W/cm^2	4.1	4.1	14.8	14.8
$q''_{d,\,max}$, W/cm^2	4.1	4.1	29.5	29.5
q_{vb}, W/cm^3	2.11	2.26	2.53	2.53
Void fraction	0.17	0.11	-	-
$j_{g\infty}$, m/s	1.06	1.18	-	-
Evaporation Rate, kg/m^2s.	1.69	1.18	-	-

for property sets 3 and 4, while the shield tank CHF would be about 280 W/cm^2, as indicated in section 5.3.2.1.

Once again, we conclude that the calandria wall would remain well-cooled even with the entire core forming a molten pool in the calandria. Again, we must consider, in the next section, whether the calandria wall can survive this situation.

7.4.2 Interaction of Molten Pool with Calandria Wall

Again, we will consider the two aspects of the interaction of a molten pool of core debris with the calandria wall:

a) the interaction of the liquid pool itself with the wall
b) the interaction of vaporized core debris with the wall above the molten pool.

7.4.2.1 Interaction of Liquid Pool Itself with Calandria Wall

We saw, in section 7.3, that the bed of solid debris in the bottom of the calandria would begin to melt near its centre about 30 minutes after initiation of the accident for the reference condition of bed dry-out time of 10 minutes. We also saw that the debris close to the wall would not melt and that the wall would remain well-cooled up to the time that melting of the debris began. As in section 5.3.2.2.1, we must now assess the interaction of the liquid pool with the supporting calandria wall, using, again, the method described in section 4.6.2.2, and the downward heat fluxes established in section 7.4.1.

The predicted maximum "downward" heat flux from a molten pool of the entire core mass, as given in Table 8, is 29.5 W/cm^2, at the upper corners of the non-boiling pool, as predicted using property value sets 3 and 4. With this heat flux, sub-cooled nucleate boiling would occur on the outer surface of the calandria wall in the shield tank water, as can be deduced from the results in section 5.3.2.2.1. The calculated nucleate boiling heat transfer coefficient, using the Jens-Lottes equation as before, is 3790 W/m^2K.

For these values of q''_b and h_c, the parameters ϕ and Bi_{ac} can be determined, as before, from equations 44 and 45 and the appropriate wall and shield tank conditions. The calculated values are:

$$\phi = 0.427$$
$$Bi_{ac} = 7.51$$

From these values of ϕ and Bi_{ac}, equation 46 predicts that there will be no melting of the calandria wall by the molten pool of debris. The solidified crest thickness for the present conditions, determined from equation 41 or Figure 11, is:

$$\delta_s = 0.015 \text{ m.}$$

Previous analysis, as described in section 5.3.2.2.1, showed that a heat flux from the molten pool would have to be about 100 W/cm^2 before any melting of the wall would occur. Thus, the present results show that the calandria is still far from melting conditions for these accident sequences.

We can conclude for accident sequences S13 and S14 as for S11 and S12 that the calandria wall under the molten pool surface will remain intact since it is well cooled by the shield tank water and is well protected from direct contact with the molten pool by the solidified crust.

Again, we can conclude that if the molten pool properties are such that no boiling of the pool occurs, the integrity of the calandria will not be threatened by the formation of a molten pool of the entire mass of the core. However, as before, if boiling of the pool occurs, we must examine the effect of the condensation of vaporized core debris on the calandria wall above the molten pool before we can conclude that the calandria will retain its integrity under all conditions of molten-pool formation.

7.4.2.2 Interaction of Vaporized Core Material with Calandria Wall

As in accident sequences S11 and S12, the program CONFILM was used to investigate the behavior of a condensing film of core debris on the calandria wall above the boiling pool, for property value sets 1 and 2, since boiling of the pool is predicted only for these property values.

The results obtained for the reference case, FRCMAS = 1.0, are summarized in Table 9. The predicted condensation heat flux is, again, not very sensitive to the differences in property values and is again below the critical heat flux

Table 9: Condensation of Vaporized Core Debris on Calandria Wall. Accident Sequences S13 and S14. Reference Conditions.

Property Value Set	1	2
FRCMAS	1.0	1.0
Superficial vapor velocity at surface of pool, m/s	1.06	1.18
Condensation heat transfer coefficient, W/m^2K	1930*	1950*
Condensation heat flux at calandria wall, W/cm^2	77	78
ϕ (See eq. 44)	1.01	1.02
Bi_{ac} (See eq. 45)	16.5	16.7
δ_s, m	0.00517	0.00505
Calandria Wall Melting?	Slight	Slight
δ_w, m	0.0289	0.0285

*Heat transfer coefficient allows for assumed drop-wise condensation near top of calandria, and for turbulent film effects.

for the shield tank water which is about 280 W/cm^2, as established earlier. Therefore, the calandria wall above the boiling pool surface will again remain well-cooled in the presence of the condensing film of vaporized core material.

However, in these cases, the evaporation rate from the molten pool is so high that the condensing heat transfer coefficient on the wall above the boiling pool has been increased above the value predicted for laminar film condensation to allow for assumed drop-wise condensation on the wall near the top of the calandria and turbulent film condensation near the bottom of the film. The resulting averaged conditions on the calandria wall give values of ϕ slightly over 1.0, which, as noted in section 4.6.2.2, means that, some slight melting of the calandria wall will occur, as indicated in Table 9. Table 9 shows that the unmelted wall thickness is predicted to be over 28 mm, compared to an original thickness of 31 mm, so that less than 3 mm of the wall thickness is predicted to melt, on the average, or less than 8% of the original wall thickness. This occurs in spite of the predicted formation of a thin (about 5 mm thick) solidified crust of core debris on the wall.

As pointed out in section 4.6.2.3, the effects of wall melting under a solidifying crust at large values of θ, are quite unpredictable. Therefore, for molten pool property values which result in the prediction of pool boiling in accident sequences S13 and S14, it is not possible to draw firm conclusions as to the integrity of the calandria wall above the boiling pool, from the foregoing analysis. However, considering the conservative elements in the analysis, the somewhat arbitrary increase of the condensing heat transfer coefficient to ensure that the condensation rate on the calandria wall equals the evaporation rate from the pool* and the very small predicted thickness of molten wall layer, it is still quite probable that the integrity of the calandria wall above the boiling pool will be maintained in accident sequences S13 and S14, in the judgement of the author.

Therefore, considering the results given in section 7.4.2.1 as well as those given in this section, it is highly probable that the calandria wall, being well cooled

*If film condensation only is assumed for these conditions, about 40 to 60% of the vapor is estimated to condense on the calandria walls, with the rest assumed to be released into the relief ducts. No melting of the calandria wall is predicted in this case.

by the shield tank water, will retain its structural integrity in accident sequences S13 and S14 even when the entire core mass forms a molten pool in the calandria, whether the pool boils or not. However, the confidence in this conclusion is not quite as great as that for accident sequences S11 and S12 because of the predicted tendency for a small percentage of calandria wall melting above the pool surface, should boiling of the pool occur, together with the unknown behavior of the protective solidified crust over a thin molten layer on a downward facing wall.

7.5 End Point for Accident Sequences S13 and S14

As in section 5.4 for accident sequences S11 and S12, we may conclude with reasonable confidence that the calandria will retain its structural integrity throughout accident sequences S13 and S14 as long as the shield tank cooling system continues to function.

Again, as the fuel heat source decays, the molten pool would gradually re-solidify over a long period. As before, the times to re-solidification would range from about 8 or 9 hours to about 50 hours, depending on the molten pool property values.

Therefore, since no further damage is anticipated, the end-point of these accident sequences is again defined by the containment and re-solidification of the mass of the core within the calandria, again indicated by boxes 31a and 31b of the analytical flow chart of Figure 3, with the calandria wall well-cooled and with its temperature decreasing slowly as the heat source decays.

Again, to complete the analysis of these accident sequences, we must assess the potential effects on containment of these accident sequences, as is done in the next section.

7.6 Containment Pressurization and Effects in Accident Sequences S13 and S14

In these accident sequences, moderator is lost from the calandria by liquid drainage only for about the first seven minutes after the initiation of the accident sequence. See Figure 41. During this period, there will be no expulsion of vapor from the calandria, so that there will be no additional pressure rise in the containment above that resulting from the initial LOCA and LOECI.

After the first group of channels drops into the remaining moderator, at 410 seconds, moderator discharges from the calandria in either of the two limiting scenarios discussed in section 7.2, one with intact rupture disks and the other with broken rupture disks.

For the case of intact rupture disks, steam generation surges within the calandria as groups of channels drop into the liquid moderator serve to expel the liquid more rapidly through the broken moderator outlet pipe, with the vapor being contained within the calandria. Therefore, there will be practically no expulsion of vapor from the calandria during this portion of the discharge so that again there will be no additional pressure rise in the containment above that for the LOCA plus LOECI. Therefore we can conclude that, should the rupture disks remain intact during these accident sequences, there will be no increase in containment pressure above that expected during this period in a large LOCA accompanied by failure of ECI. The containment will obviously survive in this case. In accident sequence S14, releases from containment could be greater than those in the above dual failure, of course, depending on the nature of containment impairment. Assessment of such additional releases is not a part of this study.

For the case of failed rupture disks, steam generation surges as subsequent groups of fuel channels drop into the moderator will result in vapor expulsions to containment through the relief ducts, with consequent effects on containment pressure. Since MODBOIL has not been modified to permit analysis of the calandria discharges in these accident sequences, as explained in section 7.2, the effects of these expulsions on containment pressure cannot be predicted quantitatively. However, the rates of these vapor expulsions will probably be less in general than those predicted for accident sequences S11 and S12, because of the rapidly increasing vapor volume in the calandria resulting from the discharge of the liquid moderator through the broken moderator outlet pipe and the total vapor discharge will certainly be less than in the previous accident sequences. Therefore the incremental pressure-rise history in S13 and S14 resulting from vapor discharge will be less than that in accident sequences S11 and S12. Although the total discharge will occur over a shorter period and, in general, earlier than in S11 and S12, the nominal containment pressure resulting from the LOCA

plus LOECI only,at the time period of this total discharge is essentially atmospheric (10, Fig. 12.3.3-32). Therefore, we conclude that the peak pressure rise resulting from vapor discharge from the calandria should the rupture disks fail will be less than that for accident sequences S11 and S12. Once again, the integrity of the containment will not be threatened.

Whether the rupture disks fail or not, debris melting will not begin until at least 30 minutes after the initial LOCA. Therefore significant releases of bound fission products from the fuel will not begin before this time. Considering the lower peak pressures expected in these accidents compared to those in S11 and S12 (zero incremental Δp for rupture disks intact) and the shorter and earlier total discharge period, the containment pressure will not be much greater than atmospheric when major releases of bound fission products from the fuel begin.

Therefore, since the pressure peak experienced will not have damaged containment and since major fission product releases will only occur when the containment pressure is relatively close to atmospheric, it can be concluded that there would not be a major release of fission products to the environment in accident sequence S13 at least, in which no containment impairment is assumed. Whether significant releases would occur in accident sequence S14 is not known, but, as in S12, in many cases the pressure difference across the containment boundary will be quite low when significant fission product releases from fuel would be anticipated.

Therefore, we may conclude for accident sequences S13 and S14 that:

a) there will be no damage to containment caused by these accident sequences
b) no major release of bound fission products from containment will occur in accident sequence S13
c) no large pressure difference may exist across the containment boundary when significant releases of bound fission products begin from the fuel in accident sequence S14.

8. GENERAL CONCLUSIONS

In this report, we have investigated in some detail the thermohydraulic and heat transfer aspects of severe accident sequences in a Bruce reactor unit involving the loss of the moderator cooling system (S11 and S12) and loss of the moderator heat sink (S13 and S14) following a large LOCA and failure of emergency coolant injection.

In this investigation, we have attempted to model physical behavior of core components and the moderator on a physically-sound basis, as far as possible. However, because of the general lack of experimental information on core component behavior, physical phenomena and property values under the extreme conditions encountered in the accident sequences, there are considerable uncertainties in many aspects of the analyses and, inevitably, informed judgement has played an important role in the assessments. To compensate to some extent for the uncertainties, sensitivity studies of the more important aspects of the accident sequences have been made. The sensitivity studies permit more confidence to be placed on the overall results than would be apparent from an examination of the uncertainties in the individual physical parameters and in the behavior characteristics of the different stages of the accident sequences.

A number of computer programs have been developed in the course of the investigation. These programs have been designed to facilitate sensitivity studies, in general, and to permit improvements in the analyses as more experimental information, such as given in references 80-82, becomes available.

The results of the assessments indicate that the very low-probability accident sequences studied would cause, eventually, gross melting of the core. However, core melting would not begin until about 135 minutes into accident sequences S11 and S12 and about 30 minutes into accident sequences S13 and S14. In all cases, the molten core would be contained within the calandria, as long as the shield tank water cooling system remains operational. Eventually, sometime in the period from 8 to 50 hours after the initiation of the accident, the molten core would re-solidify within the calandria.

In effect, the calandria in a CANDU reactor would act as an inherent "core-catcher" in the unlikely event of such very severe accidents as those examined here.*

The assessments also indicate that the accident sequences studied will not result in any consequential damage to containment, nor result in any significant

*See reference 40 for information on core-catchers in LMFBR's.

increases in fission product releases from containment above those that would otherwise occur since containment pressure when gross fuel melting begins will be quite close to atmospheric.

In the judgement of the investigator, the many uncertainties in the parameters involved are not likely to change these major conclusions to any marked extent.

In general, we may conclude that there will be no serious impacts on public health resulting from the severe accident sequences studied here, at least for the cases in which there is no impairment of containment.

Finally, of course, it is re-emphasized that the accident sequences studied are highly improbable. While no estimates of the probabilities of these accidents have been made as part of this study, it is judged that, for a reactor designed, built and operated according to established Canadian safety requirements, the probability of such accident sequences will be significantly less than 10^{-7} per year, and hence, should the recommendations of reference 83 be accepted, such accident sequences would not need to be considered in the safety analysis required for licensing of a reactor in Canada.

REFERENCES

1. Rogers, J.T.
Thermal and Hydraulic Behavior of CANDU Cores Under Severe Accident Conditions. Report to the AECB. Dept. of Mech. and Aero. Engineering, Carleton University. AECB INFO- Feb., 1982

2. Rogers, J.T.
Loss-of-Coolant Accidents with Impaired Emergency Coolant Injection with and without Additional Heat Sinks. Report to the AECB. Dept. of Mech. and Aero. Engineering, Carleton University. AECB INFO-0061 Feb., 1981

3. Rogers, J.T., T.C. Currie, J.C. Atkinson and R. Dick
Analysis of Effects of Calandria Tube Uncovery Under Severe Accident Conditions in CANDU Reactors. Proc. Fourth Annual Conf., Canadian Nuclear Society, Montreal, Que. June, 1983

4. -
Reactor Safety Study. An Assessment of Accident Risks in US Commercial Nuclear Power Plants, WASH-1400 Oct., 1975

5. -
The German Risk Study Summary. Federal Minister of Research and Technology Aug., 1979

6. Levine, S., and F. Stetson
Applying the Lessons of PRA - An American Perspective. Nuclear Engineering International, 29, p. 38 Jan., 1984

7. Meneley, D.A., and W.T. Hancox
LOCA Consequence Predictions in a CANDU-PHWR. Paper 145, IAEA International Conference on Nuclear Power Experience, Vienna Sept., 1982

8. Rogers, J.T.
CANDU Moderator Provides Ultimate Heat Sink in a LOCA. Nuclear Engineering International, 24, 280, p.38 Jan., 1979

9. Rogers, J.T., and T.C. Currie
Analysis of Transient Dry-Patch Behavior on CANDU Reactor Calandria Tubes in a LOCA with Late Stagnation and Impaired ECI. Proc. International Meeting on Thermal Nuclear Reactor Safety, Chicago, Ill. Sept., 1982

10. -
Bruce Generating Station-A
Safety Report. Ontario Hydro Revised, 1978

11. Bruce Generating Station NK29
Design Manuals. Ontario Hydro

12. Rogers, J.T., and T. Currie
A Model for Thermal Analysis of a CANDU Fuel Channel Following a LOCA with Delayed ECC Flow. Paper presented at: CNA International Conference, Ottawa, June 1978. Also, report of: Dept. of Mechanical and Aeronautical Engineering, Carleton University, Ottawa, May, 1978

13. Rogers, J.T.
Studies of Loss-of-Coolant and Loss-of Regulation Accidents, 1977-1979. Report to the AECB. Dept. of Mech. and Aero. Engineering, Carleton University, AECB No. 1199 Oct., 1979

14. Hancox, W.T.
Whiteshell Nuclear Research Establishment, Pinawa, Man., Personal Communication July, 1980

15. Elliott, J.N.
Tables of Thermodynamic Properties of Heavy Water. AECL-1673 Jan., 1963

16. Irvine, H.S.
Some Thermodynamic Properties of Saturated and Compressed Heavy Water. CGE Report R67CAP15 March 1, 1967

17. Rosta, P.Z.
Specific Heat and Enthalpy of Liquid Heavy Water. AECL-3689 Nov., 1971

18. Meyer, C.A., R.B. McClintock, G.J. Silvestri and R.C. Spencer, Jr.
ASME Steam Tables 1967 2nd Ed. Thermodynamic and Transport Properties of Steam. American Society of Mechanical Engineers 1968

19. Collier, J.G.
Convective Boiling and Condensation. McGraw-Hill 1972

20. Rogers, J.T., J.C. Atkinson and R. Dick
Analysis of Moderator Expulsion from a CANDU Reactor Calandria Under Severe Accident Conditions. ASME Paper 84-HT-16. Presented at 22nd U.S. National Heat Transfer Conference, Niagara Falls, N.Y. Aug., 1984

21. Saha, P., and N. Zuber
Point of Net Vapor Generation and Vapor Void Fraction in Sub-cooled Boiling. Proc. Fifth Int. Heat Transfer Conference, Tokyo, Vol.IV, p.175 Sept., 1974

22. Wallis, G.B.
One-Dimensional Two-Phase Flow. McGraw-Hill 1969

23. Levy, S.
Forced Convection Sub-cooled Boiling: Prediction of Vapor Volumetric Fraction. Int. J. Heat and Mass Transfer, 10, 951 July, 1967

24. Ginsberg, T., O.C. Jones and J.C. Chan
Flow Dynamics of Volume-Heated Boiling Pools. ASME 79-HT-102 Aug., 1979

25. Zuber, N., and J.A. Findlay
Average Volumetric Concentration in Two-phase Flow Systems. J. of Heat Transfer, 87, 453 Nov., 1965

26. Holman, J.P.
Heat Transfer, 5th ed., McGraw-Hill 1980

27. Barns, G.M.
Two-Phase Pressure Drop Calculations. How and Why.
CGE Report R67CAP30 July, 1967

28. Dukler, A.E., and Y. Taitel
Flow Regime Transitions for Upward Gas Liquid Flow:
A Preliminary Approach Through Physical Modelling. NUREG-0162 Jan., 1977

29. Breen, B.P., and J.W. Westwater
Effect of Diameter of Horizontal Tubes on Film Boiling Heat Transfer.
AIChE Preprint No.19, 5th U.S. Nat. H.T. Conf., Houston 1962

30. Bromley, L.A.
Heat Transfer in Stable Film Boiling.
Chem.Eng. Progress, 46, 221 1950

31. Bradfield, W.S.
On the Effect of Sub-cooling on Wall Superheat in Pool Boiling.
J. of Heat Transfer, 89, 3, 269 Aug., 1967

32. McAdams, W.H.
Heat Transmission, 3rd Ed., McGraw-Hill 1954

33. Rogers, J.T.
Falling Film Flow, Heat Transfer and Breakdown on Horizontal Tubes.
Report to the AECB. Dept. of Mechanical and Aeronautical Engineering,
Carleton University, AECB INFO-0060 Nov., 1980

34. Levich, V.G.
Physicochemical Hydrodynamics. Prentice-Hall 1962

35. Parker, J.D., and R.J. Grosh
Wall Temperature Variation for Mist Flowing Through Tubes with
Constant Heat Flux. ASME 62-HT-47 Aug., 1962

36. Jakob, M.
Heat Transfer, Vol. II. Wiley 1957

37. Urbanic, V.F., and T.R. Heidrick
High Temperature Oxidation of Zircaloy-2 and Zircaloy-4 in Steam.
Journal of Nuclear Materials

38. Heidrick, T.R.
Zirconium-Water Reaction Rates at High Temperatures.
WNRE-226-1 March, 1975

39. Dhir, V.K.
On the Coolability of Degraded LWR Cores. Nuclear Safety,
24, 3, p.319 May-June, 1983

40. Costa, J.
In-Vessel Post Accident Heat Removal. Chapter 17 in Nuclear Reactor Safety Heat Transfer. O.C. Jones, ed. Hemisphere Publishing Corp. 1981

41. American Nuclear Society Standard ANS-5.1
Assessed for CANDU in:
Whittier, A.C.
CANDU Channel Decay Power, AECL-5704 Jan., 1977

42. Jansen, and Stepnewski
Nuclear Technology Jan., 1973

43. Rogers, J.T.
Unpublished Internal Notes and Design File.
General Atomic, San Diego, Calif. 1959

44. Ribaud, G.
Thermal Conductivity of Porous and Pulverulent Materials - A Theoretical Study. Chaleur et Industrie, 201, p.35 1937
NRC Technical Translation TT-801 1965

45. Rogers, J.T.
Heat Transfer Course 1961-62. Part 1. Conduction.
Canadian General Electric Co. Ltd. 1962

46. Tong, L.S., and J. Weisman
Thermal Analysis of Pressurized Water Reactors.
An AEC Monograph. American Nuclear Society 1970

47. -
Heat Transfer Data Book, 515.22, p.8.
General Electric Co. 1979

48. Currie, T.C., and J.T. Rogers
Contact Heat Transfer Between Non-Conforming Surfaces.
Report to the AECB. Dept. of Mechanical and Aeronautical Engineering, Carleton University. AECB INFO-0017 Jan., 1980

49. Kulacki, F.A., and R.J. Goldstein
Thermal Convection in a Horizontal Fluid Layer with Uniform Volumetric Heat Sources. J. Fluid Mech., 55, Part 2, 271 1972

50. Stein, R.P., L. Baker, Jr., W.H. Gunther and C. Cook
Heat Transfer from Heat Generating Molten UO_2: Interpretations of the Available Experimental Data. ASME Paper 79-HT-115 Aug., 1979

51. Gabor, J.D., L. Baker, Jr., J.C. Cassulo, D.J. Erskine and J.G. Warner
Heat Transfer to Curved Surfaces from Heat Generating Pools.
ASME Paper 79-HT-113 Aug., 1979

52. Greene, G.A., O.C. Jones, Jr., N. Abuaf and C.E. Schwarz
Heat Removal Characteristics of Volume-Heated Boiling Pools with Inclined Boundaries in Bubbly Flow Regime. ASME Paper 79-HT-99 Aug., 1979

53. Anderson, E.A.
Radiative Heat Transfer in Molten UO_2 Based on the Rosseland Diffusion Method. Nuclear Technology, 30, p.65 July, 1976

54. Mayinger, F., M. Jahn, H.H. Reineke and U. Steinbrenner
Examination of Thermohydraulic Processes and Heat Transfer in a Core Melt. BMFT RS 48/1. Institut fur Vehrfahrenstechnik der T.U. Hannover 1976

55. Gambill, W.R.
Estimate Engineering Properties, Parts I-VI. Series of articles in Chemical Engineering 1957-1959

56. Kazimi, M.S.
The Potential for Fuel Boiling Under Decay Heat Conditions. Proc. Third Post-Accident Heat Removal Information Exchange, Argonne Nat. Lab., Nov. 2-4, 1977, p.377. ANL-78-10 1978

57. Alsmeyer, H., and M. Reimann
On the Heat and Mass Transport Processes of a Horizontal Melting or Decomposing Layer Under a Molten Pool. Paper in Nuclear Reactor Safety Heat Transfer. ASME Publication 1977

58. Kazimi, M.S., and J.C. Chen
Void Distribution in Boiling Pools with Internal Heat Generation. Nucl. Sci. and Eng., 65, 17 1978

59. Gambill, W.R.
Estimate Engineering Properties. Part III. Latent Heat of Vaporization, Fusion and Sublimation. Chemical Engineering Dec., 1957

60. Yuen, W.W., and A. Kleinman
Application of a Variable-Time-Step Finite-Difference Method for the One-Dimensional Melting Problem Including the Effect of Sub-cooling. Heat Transfer - San Diego, 1979. AIChE Symposium Series, Vol.75, p.120 1979

61. Hakim, S.J.
Simultaneous Freezing and Melting in Finite Media. Nucl. Sci. and Engineering, 72, 129 1979

62. Nansteel, M.W., and C.H. Wolgemuth
An Investigation of a Two-Phase, Moving Boundary System, With Convection at the Solid-Liquid Interface. Heat Transfer - San Diego, 1979. AIChE Symposium Series, Vol.75, p.112 1979

63. El-Genk, M.S., and A.W. Cronenberg
Stefan-Like Problems in Finite Geometry. Heat Transfer - San Diego, 1979. AIChE Symposium Series, Vol.75, p.69 1979

64. Hofmann, P., and C. Politis
The Kinetics of the Uranium Dioxide-Zircaloy Reactions at High Temperatures. J. of Nucl. Mat., 87, p.375 1979

65. Peckover, R.
Ex-Vessel Post-Accident Heat Removal. Chapter 18 in:
Nuclear Reactor Safety Heat Transfer.
O.C. Jones, Ed.
Hemisphere Publishing Corp. 1981

66. Powers, D.A., and J.F. Muir
Melt/Concrete Interactions: The Sandia Experimental Program,
Model Development, and Code Comparison Test.
Paper presented at: Seventh Water Reactor Safety Research
Information Meeting, Gaithersburg, Md. Nov.5-9, 1979

67. Peckover, R.S.
Thermal Moving Boundary Problems Arising in Reactor Safety Studies.
UKAEA Report. CLM-P562 Aug., 1978

68. Corradini, M.L.
A Transient Model for the Ablation and Decomposition of Concrete.
Nuclear Technology, 62, 263 Sept., 1983

69. Peckover, R.S.
Post Accident Heat Removal. UKAEA Report. CLM-P518 1978

70. Elliott, J.N. and G. Odlozinski
PRESCON, a Fortran Program for Predicting Containment Transients
Following Pipe Breaks. AECL TDAI-48 May, 1971

71. -
Ontario Hydro PATRIC Engineers' Manual. OH Report 79113 To be issued

72. Chang, C., and J. Skears
SOPHT - A Computer Model for CANDU-PHWR Heat Transport Networks
and Their Control. Nucl. Technology, 35 Oct., 1977

73. Pauls, R.E.
BLDGPT - A Shared-Time Computer Program for Predicting the Containment
Building Pressure - Temperature Response to Loss-of-Coolant Accidents.
CGE Report R69PP6 (AECL Power Projects Peterborough) Dec.8, 1969

74. -
Realistic Estimates of the Consequences of Nuclear Accidents.
Series of Papers in Nuclear Technology, 53,2 May, 1981

75. Lemire, R., J. Paquette, D. Torgerson and D. Wren
Iodine Behavior in Containment. Proc. Second Annual Conf.,
Canadian Nuclear Society, Ottawa June 10, 1981

76. Rogers, J.T.
Critical Heat Flux on CANDU Reactor Calandria Tubes.
A Study for AECL Power Projects Nov., 1972

77. Pauls, R.E.
Personal Communication. Ontario Hydro July 28, 1983

78. MacGregor, J.G., D.W. Murray and S.H. Simmonds
Behaviour of Prestressed Concrete Containment Structures. A Summary of Findings. Report to the AECB. U. of Alberta, Dept. of Civil Engineering, AECB INFO-0031 May, 1980

79. Idel'chik, I.E.
Handbook of Hydraulic Resistance. Israel Program for Scientific Translation. USAEC and US Nat. Sci. Foundation, AEC-tr-6630 1966

80. Rosinger, H.E.
A Study of the Pellet/Clad (Uranium Dioxide/Zircaloy-4) Interaction at 1373 K and 1473 K. AECL-7785 Feb., 1983

81. Hadaller, G.I., G.H. Archinoff and E. Kohn
CANDU Fuel Bundle Behaviour During Degraded Cooling Conditions. Proc. Fourth Ann. Conf., Canadian Nuclear Society, Montreal June 15, 1983

82. Rosinger, H.E.
The Severe Fuel Damage Program at WNRE: Status and Future Direction. Atomic Energy of Canada Ltd., WNRE-556 Feb., 1984

83. Advisory Committee on Nuclear Safety
Recommended General Safety Requirements for Nuclear Power Plants. ACNS-4. Atomic Energy Control Board, INFO-0116 July, 1983

84. Thompson, T.J., and J.G. Beckerley
The Technology of Nuclear Reactor Safety, Vol.2, Reactor Materials and Engineering. MIT Press 1973

85. Currie, T.C., and J.T. Rogers
Heat Transfer Between Contacting Non-conforming Surfaces with Application to CANDU Reactor Safety Analysis.
Heat Transfer in Nuclear Reactor Safety, p.313.
S.G. Bankoff and N.H. Afgan, editors.
Hemisphere Publishing Corp., Washington, D.C. 1982

86. Currie, T., and J.T. Rogers
Experimental and Numerical Studies of Heat Transfer Through Areas of High Ellipticity. ASME Paper No.84-HT-85
Presented at US National Heat Transfer Conference, Niagara Falls, N.Y. Aug., 1984

87. Williams, L.G.
Report of the NII Specialist Study Group Set Up to Review the Molten Fuel Coolant Interaction Phenomenon. Health and Safety Executive Nuclear Installation Inspectorate. United Kingdom March, 1980

88. Bankoff, S.G.
Vapor Explosions: A Critical Review. Proc. Sixth Int. Heat Transfer Conference, Toronto, Ont., Vol.6, p.355 Aug.7-11, 1978

89. Bankoff, S.G.
Vapor Explosions. Chap. 20 in: Nuclear Reactor Safety Heat Transfer
O.C. Jones, Ed.
Hemisphere Publishing Corp. 1981

90. Becker, K.M.
Steam Explosions in Light Water Reactors.
Translation of
KTH-NEL-27, Royal Inst. of Technology, Stockholm Feb., 1980

91. -
Report of Group of Experts on Reactor Safety Implications of FCI
Phenomena (Based on Review "Steam Explosions and Reactor Safety"
by A.J. Briggs). CSNI, Nuclear Energy Agency, OECD June, 1982

92. Corradini, M.L., D.V. Swenson and R.L. Woodfin
Analysis of Containment Failure Due to Steam Explosions Following a
Postulated Core Meltdown in a Light-Water Reactor.
Nuclear Safety, 23, 1, 21 Jan.-Feb., 1982

93. Fauske, H.K.
On the Mechanism of Uranium Dioxide-Sodium Explosive Interactions.
Nucl. Sci. and Engineering, 51, 95-101 1973

94. Henry, R.E., and H.K. Fauske
Energetics of Vapor Explosions
ASME Paper 75-HT-66 Aug., 1975

95. Board, S.J., R.W. Hall and R.S. Hall
Detonation of Fuel Coolant Interactions.
Nature, Vol.254, No.5498, 319-321 March, 1975

96. -
A Study of the Causes of Molten Metal and Water Explosions.
Joint Standing Committee on Health, Safety and Welfare in Foundries.
Health and Safety Executive, UK 1977

97. Corradini, M.L.
Phenomenological Modeling of the Triggering Phase of Small-Scale
Steam Explosion Experiments. Nucl. Sci. and Engineering,
78, 154-170 1981

98. Drumheller, D.S.
The Initiation of Melt Fragmentation in Fuel-Coolant Interactions.
Nucl. Sci. and Engineering, 72, 347-356 Dec., 1979

99. Tong, L.S.
Memo to R.B. Minogue, Director, Office of Nuclear Regulatory Research,
USNRC. Technical Review Meeting on Steam Explosions May 24, 1982

100. Gilby, R.L.
Reaction of Molten UO_2 with Water.
BNWL-362 1967

101. Amblard, M., et al.
Contact Effect Between UO_2 and Sodium and Molten UO_2 and Water
EURFNR-811 1970

102. Benz, R., et al.
Melt-Water Interactions in Tank Geometry: Experimental and Theoretical Results. Report at 4th CSNI Specialist Meeting, Bournemouth, UK April, 1979

103. Bird, M.J., and R.A. Millington
Fuel Coolant Interaction Studies with Water and Thermite Generated Molten Uranium Oxide. Report at 4th CSNI Specialist Meeting, Bournemouth, UK April, 1979

104. Saito, M.
Third Specialist Meeting on Sodium/Fuel Interactions in Fast Reactors. Paper SNI 6/11, Tokyo 1976

105. Higgins and Schultz
USAEC Report IDO-28000 April, 1957

106. Nelson, L.S., and L.D. Buxton
Steam Explosion Triggering Phenomena: Stainless Steel and Corium-E Simulants Studied with a Floodable Arc Melting Apparatus.
NUREG/CR-0122, Sandia National Labs. 1978

107. Nelson, L.S., et al.
Steam Explosion Triggering Phenomena, Part 2. Corium-A and Corium-E Simulants and Oxides of Iron and Cobalt Studied with a Floodable Arc Melting Apparatus. NUREG/CR-9633 1980

108. Dhir, V.K., and G.P. Purohit
Sub-cooled Film Boiling Heat Transfer from Spheres.
Nucl. Eng. and Design, 47, 49 1978

109. Theofanous, T.G., and M. Saito
An Assessment of Class 9 (Core Melt) Accidents for PWR Dry Containment Systems. Nucl. Eng. and Design, 66, p.301 Sept., 1981

110. Hicks, E.P., and D.C. Menzies
Theoretical Studies on the Fast Reactor Maximum Accident.
Proc. Conf on Safety, Fuels and Core Design in Large Fast Power Reactors. ANL-7120 Oct., 1965

111. Judd, A.M.
Appendix 1, Section A.1.1.1, of reference 87

112. Rogers, J.T.
Laminar Falling Film Flow and Heat Transfer Characteristics on Horizontal Tubes. Can. J. Chem. Eng., 59, 213 April, 1981

113. Uchida, H., A. Oyama and Y. Togo
Evaluation of Post-incident Cooling Systems of Light Water Power Reactors. Proc. Third Int. Conf. on Peaceful Uses of Atomic Energy, 1964, Vol.13, p.93-104 1965

114. Rogers, J.T.
A Study of the Thermo-hydraulic Aspects of the Failure of the Moderator Cooling System in a Severe Accident Sequence in a CANDU Reactor. Paper accepted for the Fifth International Meeting on Thermal Nuclear Reactor Safety, Karlsruhe, FRG Sept.9-13, 1984

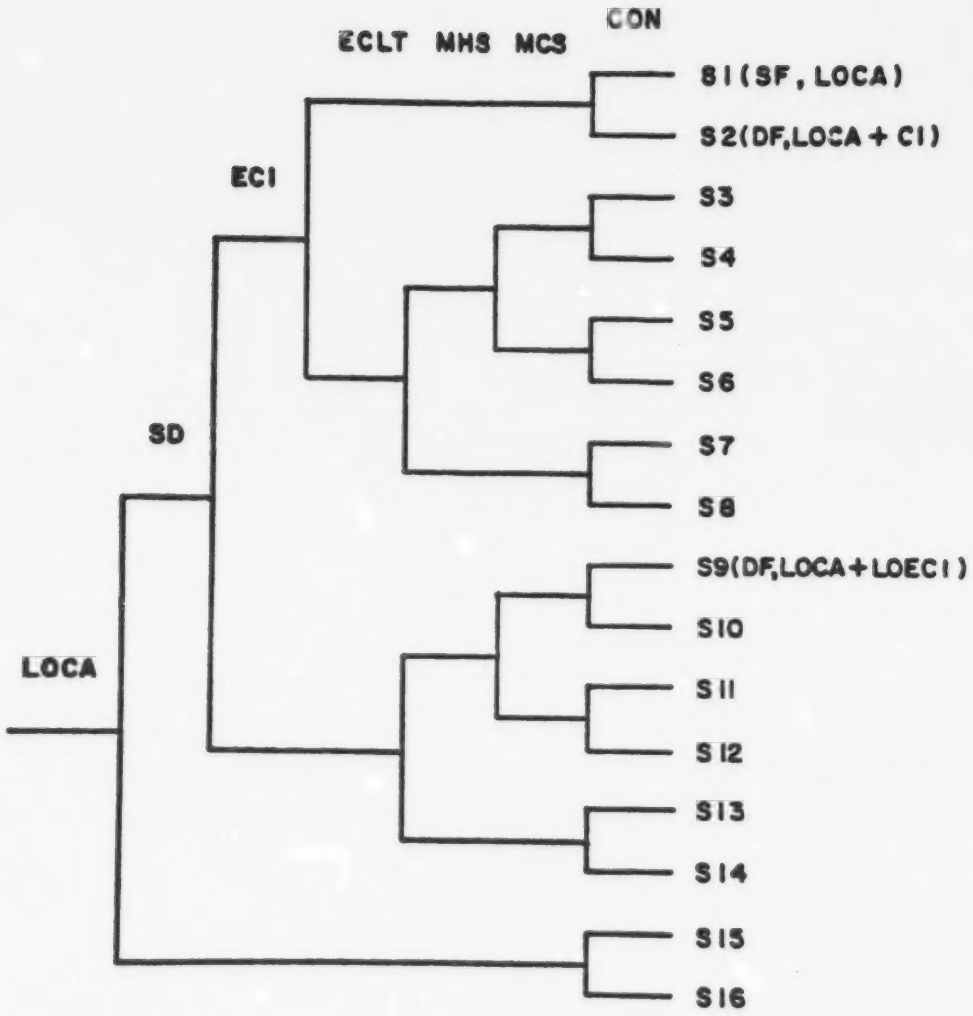

FIG. 1 CANDU LOCA FUNCTIONAL EVENT TREE, ACCIDENT SEQUENCES

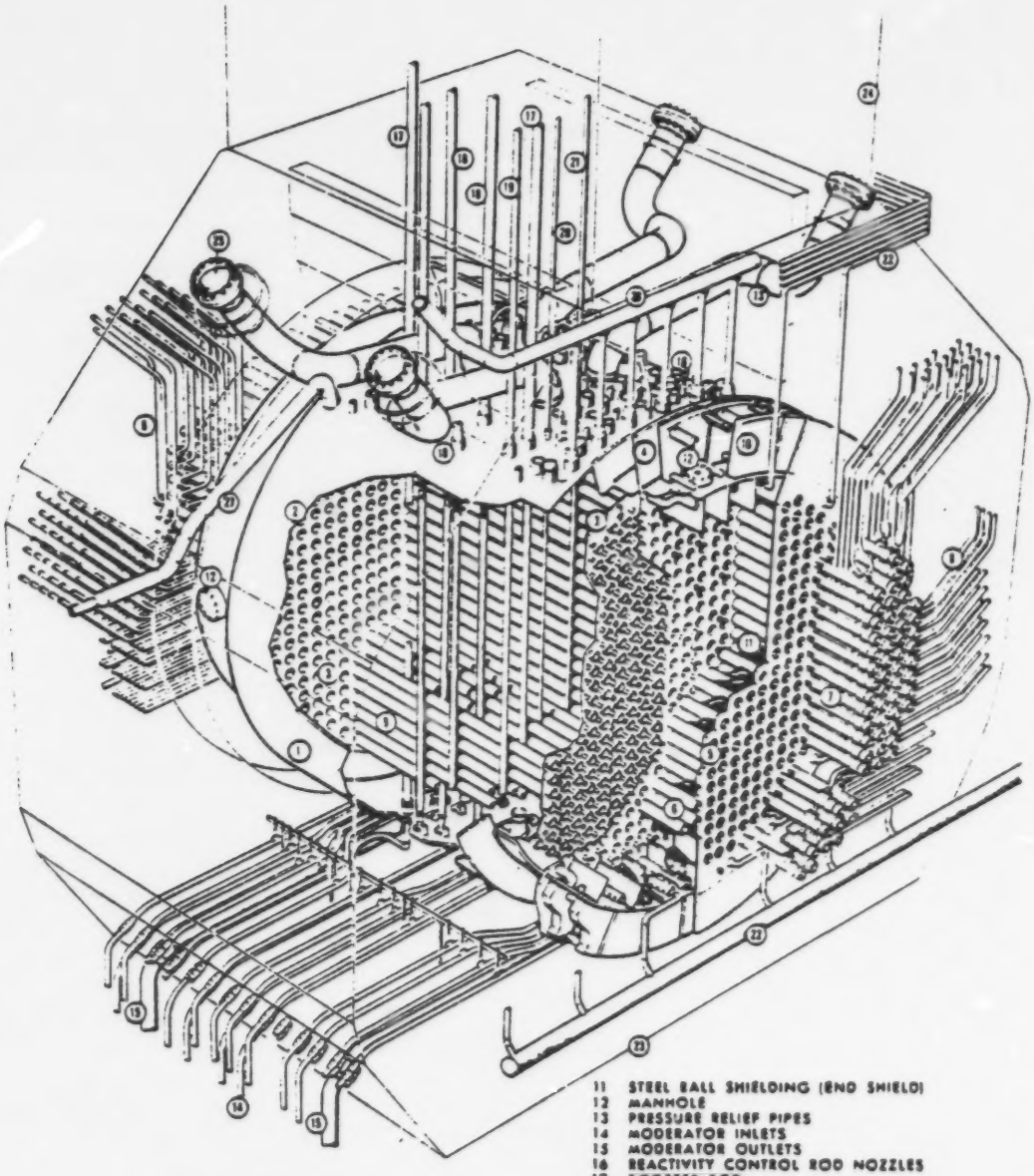

1 CALANDRIA
2 CALANDRIA SHELL
3 CALANDRIA SIDE TUBE SHEET
4 BAFFLE PLATE
5 FUELLING MACHINE SIDE TUBE SHEET
6 LATTICE TUBE
7 END FITTINGS
8 FEEDERS
9 CALANDRIA TUBES
10 SHIELD TANK SOLID SHIELDING
11 STEEL BALL SHIELDING (END SHIELD)
12 MANHOLE
13 PRESSURE RELIEF PIPES
14 MODERATOR INLETS
15 MODERATOR OUTLETS
16 REACTIVITY CONTROL ROD NOZZLES
17 BOOSTER ROD
18 SHUT-OFF ROD
19 ZONE CONTROL ROD
20 FLUX MONITOR
21 FLUX MONITOR AND POISON INJECTION
22 END SHIELD COOLING PIPING
23 SHIELD TANK
24 SHIELD TANK EXTENSION
25 RUPTURE DISC ASSEMBLY
26 MODERATOR INLET HEADER
27 MODERATOR OVERFLOW

FIG. 2 CANDU REACTOR ISOMETRIC DIAGRAM

FIG. 3 ANALYTICAL FLOW CHART FOR ACCIDENT SEQUENCES S11 AND S12

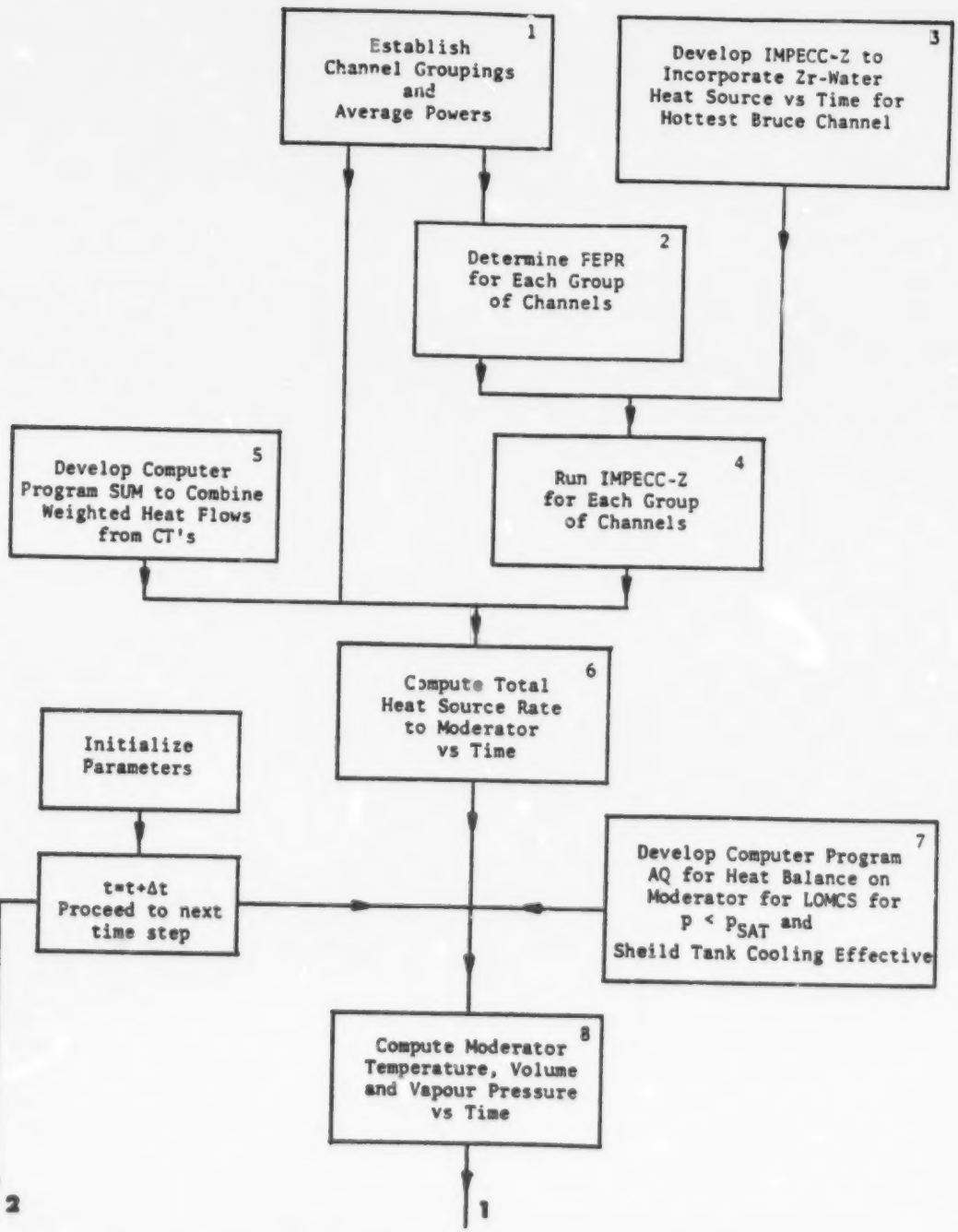
1
Establish Channel Groupings and Average Powers
3
Develop IMPECC-Z to Incorporate Zr-Water Heat Source vs Time for Hottest Bruce Channel
2
Determine FEPR for Each Group of Channels
5
Develop Computer Program SUM to Combine Weighted Heat Flows from CT's
4
Run IMPECC-Z for Each Group of Channels
6
Compute Total Heat Source Rate to Moderator vs Time
Initialize Parameters
t=t+Δt Proceed to next time step
7
Develop Computer Program AQ for Heat Balance on Moderator for LOMCS for p < P_SAT and Sheild Tank Cooling Effective
8
Compute Moderator Temperature, Volume and Vapour Pressure vs Time
2
1

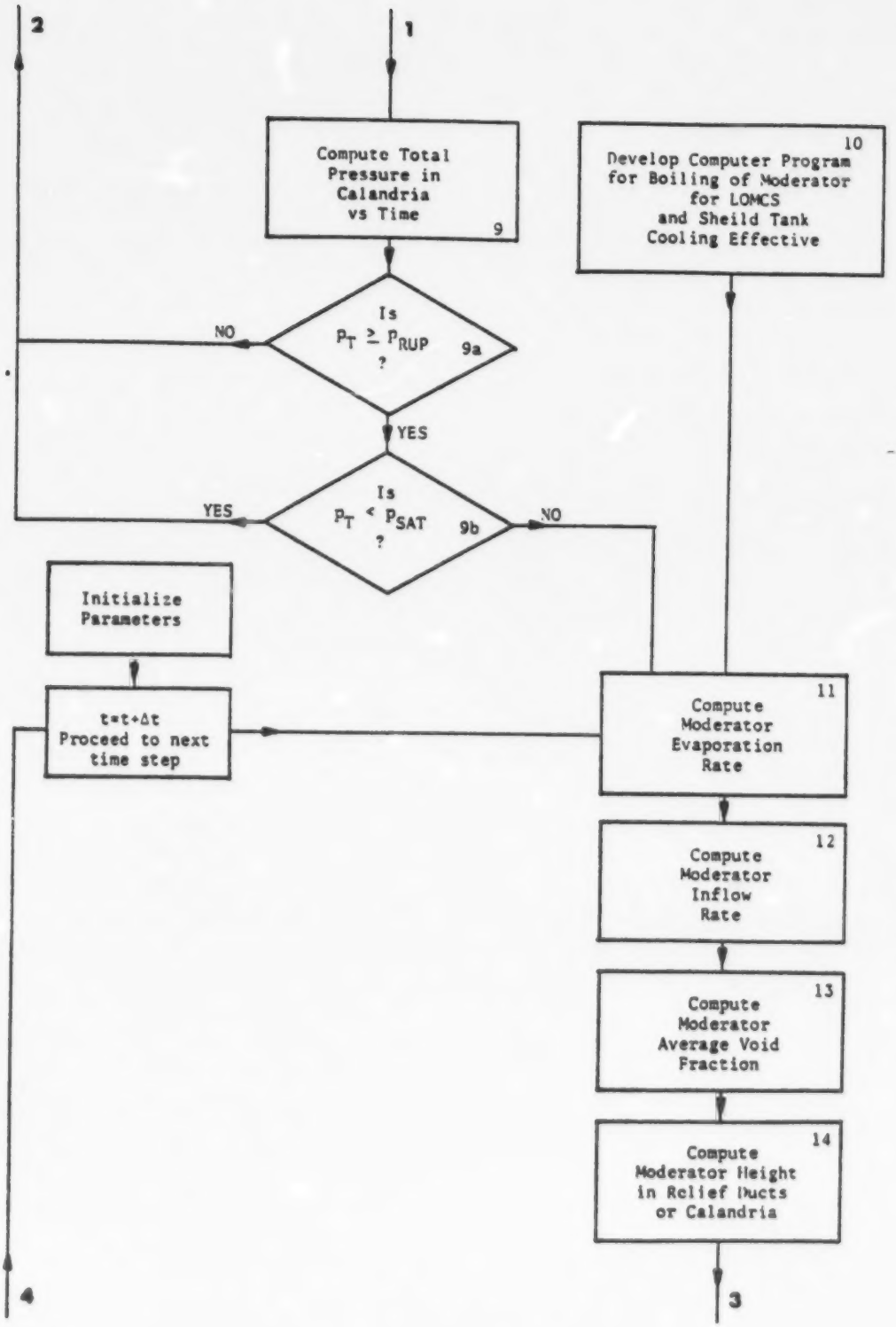
2
1
Compute Total Pressure in Calandria vs Time
9
10
Develop Computer Program for Boiling of Moderator for LOMCS and Sheild Tank Cooling Effective
Is $P_T \geq P_{RUP}$?
9a
NO
YES
Is $P_T < P_{SAT}$?
9b
YES
NO
Initialize Parameters
t=t+Δt Proceed to next time step
11
Compute Moderator Evaporation Rate
12
Compute Moderator Inflow Rate
13
Compute Moderator Average Void Fraction
14
Compute Moderator Height in Relief Ducts or Calandria
4
3

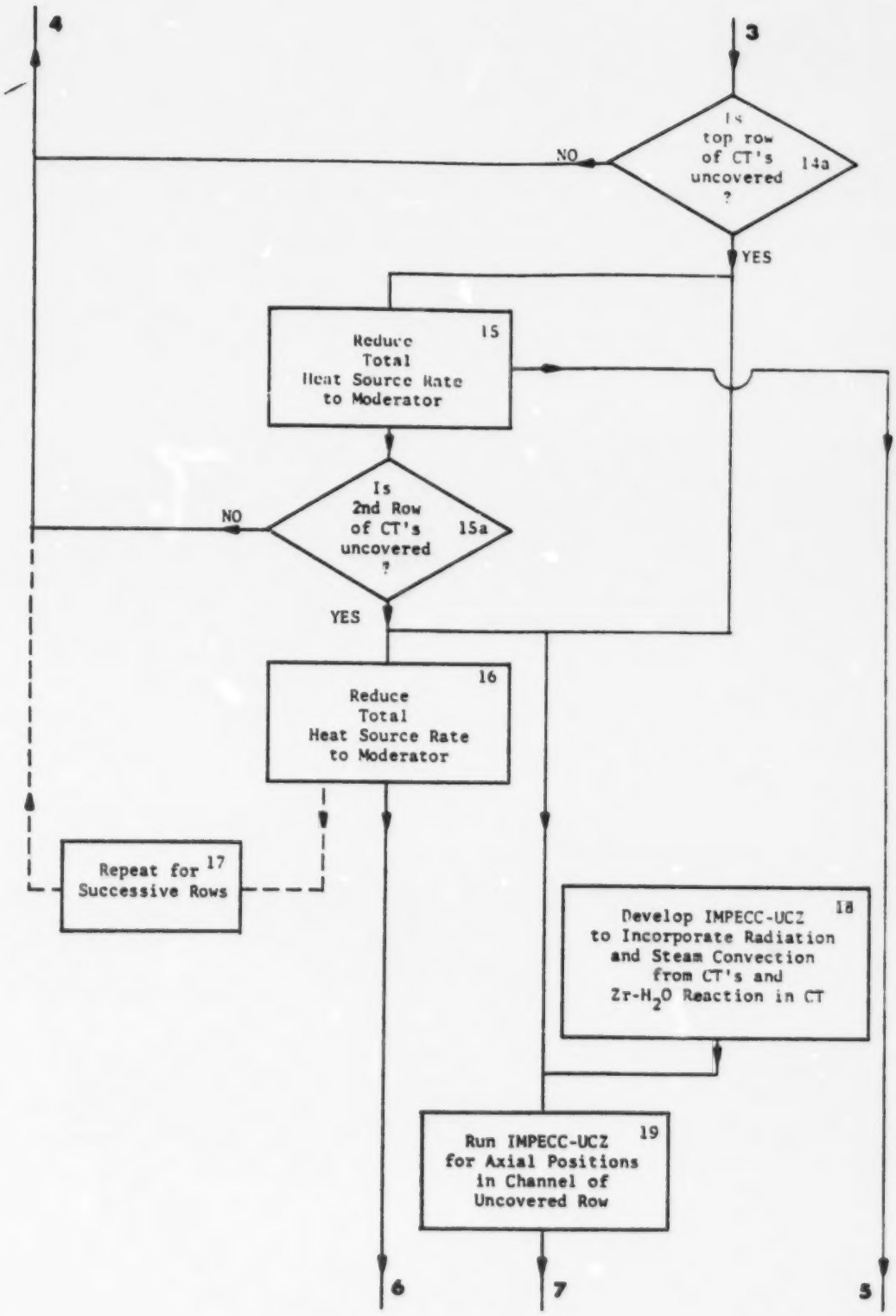
4
3
Is top row of CT's uncovered ? 14a
NO
YES
Reduce Total Heat Source Rate to Moderator 15
Is 2nd Row of CT's uncovered ? 15a
NO
YES
Reduce Total Heat Source Rate to Moderator 16
Repeat for Successive Rows 17
Develop IMPECC-UCZ to Incorporate Radiation and Steam Convection from CT's and Zr-H_2O Reaction in CT 18
Run IMPECC-UCZ for Axial Positions in Channel of Uncovered Row 19
6
7
5

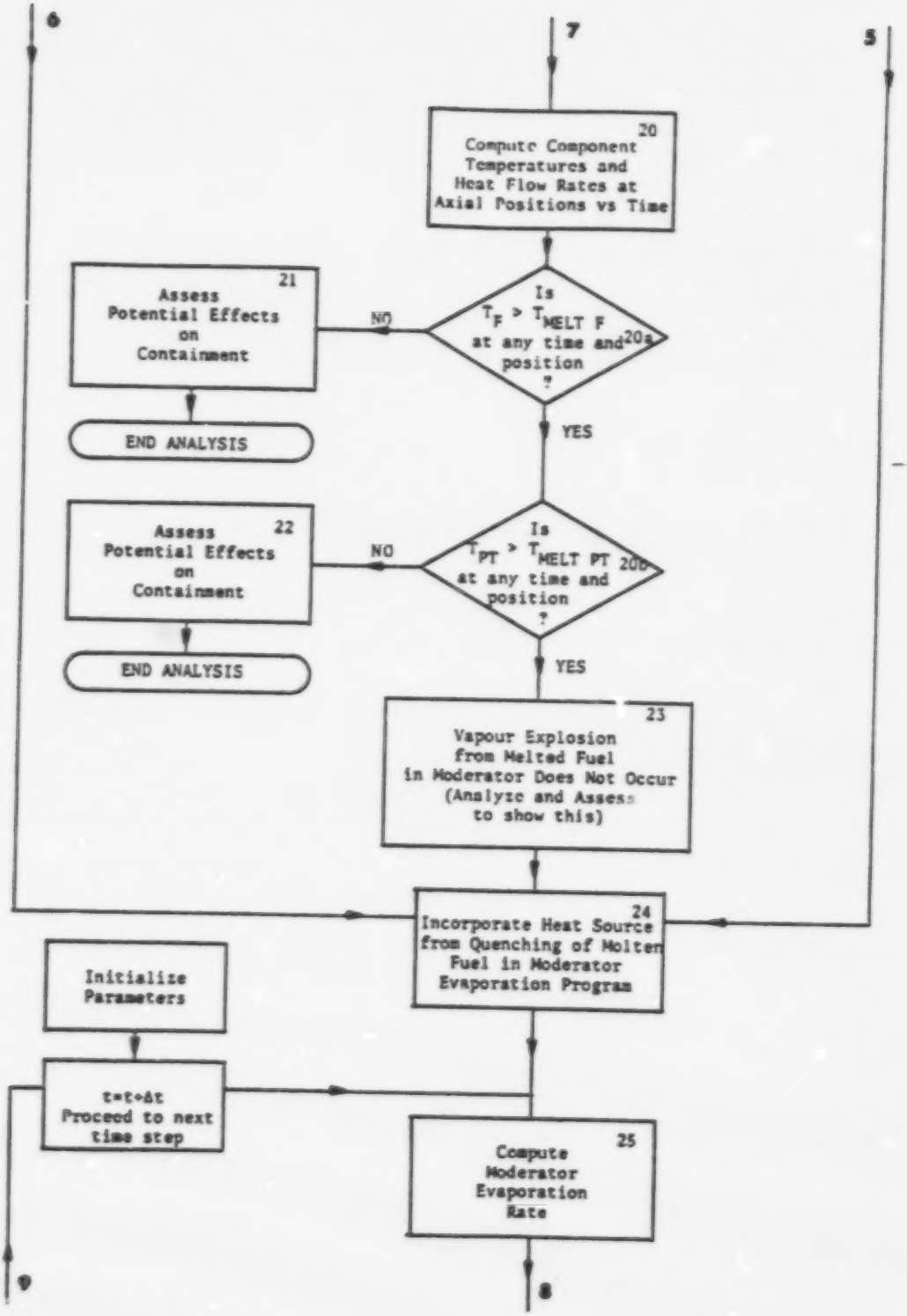
6
7
5
20
Compute Component Temperatures and Heat Flow Rates at Axial Positions vs Time
21
Assess Potential Effects on Containment
NO
Is $T_F > T_{MELT\ F}$ at any time and position ?
20a
END ANALYSIS
YES
22
Assess Potential Effects on Containment
NO
Is $T_{PT} > T_{MELT\ PT}$ at any time and position ?
20b
END ANALYSIS
YES
23
Vapour Explosion from Melted Fuel in Moderator Does Not Occur (Analyze and Assess to show this)
24
Incorporate Heat Source from Quenching of Molten Fuel in Moderator Evaporation Program
Initialize Parameters
t=t+Δt Proceed to next time step
25
Compute Moderator Evaporation Rate
9
8

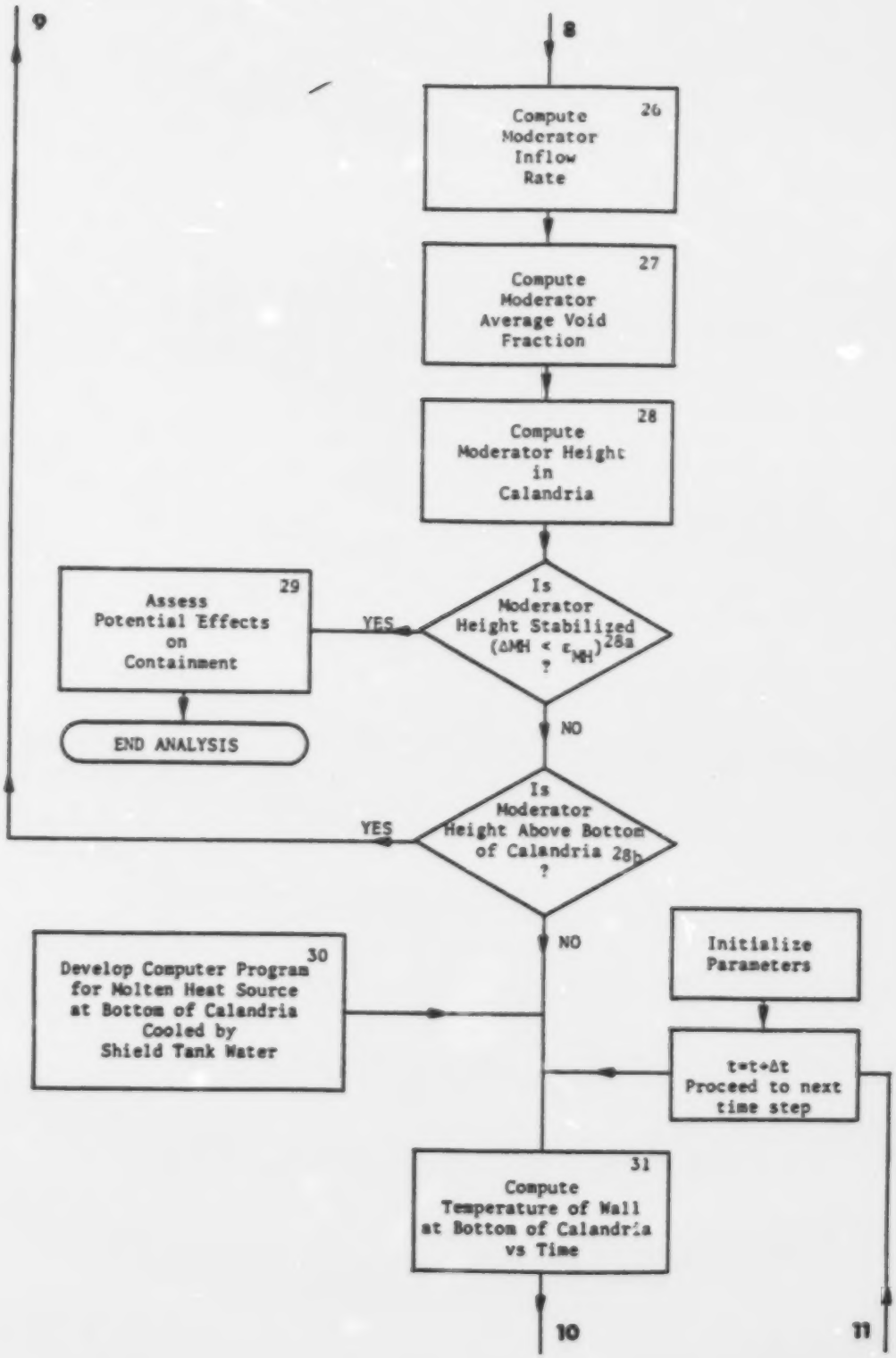
9
8
Compute Moderator Inflow Rate
26
Compute Moderator Average Void Fraction
27
Compute Moderator Height in Calandria
28
Is Moderator Height Stabilized ($\Delta MH < \epsilon_{MH}$) ?
28a
YES
Assess Potential Effects on Containment
29
END ANALYSIS
NO
Is Moderator Height Above Bottom of Calandria ?
28b
YES
NO
Develop Computer Program for Molten Heat Source at Bottom of Calandria Cooled by Shield Tank Water
30
Initialize Parameters
t=t+Δt Proceed to next time step
Compute Temperature of Wall at Bottom of Calandria vs Time
31
10
11

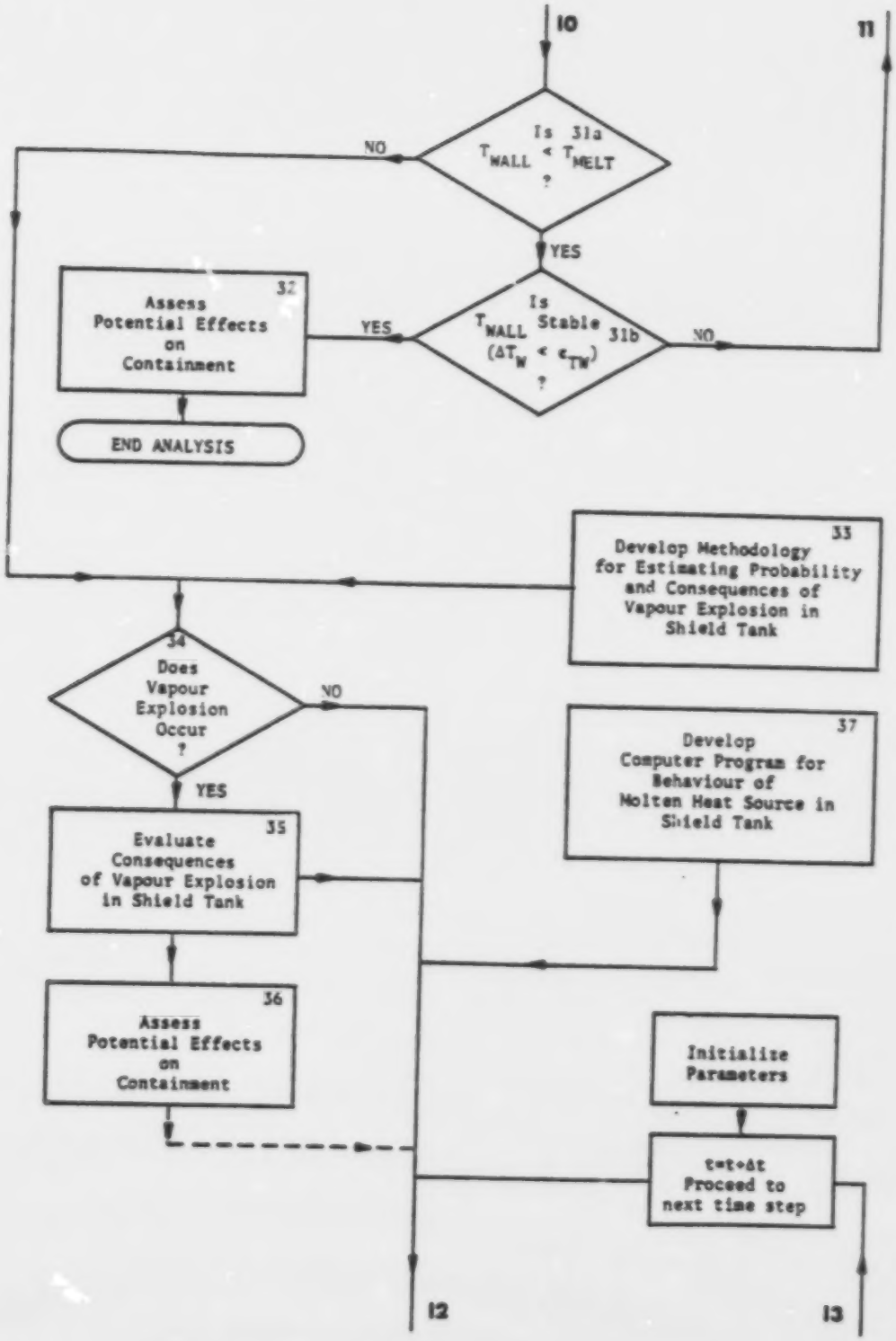
10
11
Is 31a
$T_{WALL} < T_{MELT}$
?
NO
YES
Is
T_{WALL} Stable 31b
$(\Delta T_W < \epsilon_{TW})$
?
YES
NO
32
Assess
Potential Effects
on
Containment
END ANALYSIS
33
Develop Methodology
for Estimating Probability
and Consequences of
Vapour Explosion in
Shield Tank
34
Does
Vapour
Explosion
Occur
?
NO
YES
35
Evaluate
Consequences
of Vapour Explosion
in Shield Tank
36
Assess
Potential Effects
on
Containment
37
Develop
Computer Program for
Behaviour of
Molten Heat Source in
Shield Tank
Initialize
Parameters
t=t+Δt
Proceed to
next time step
12
13

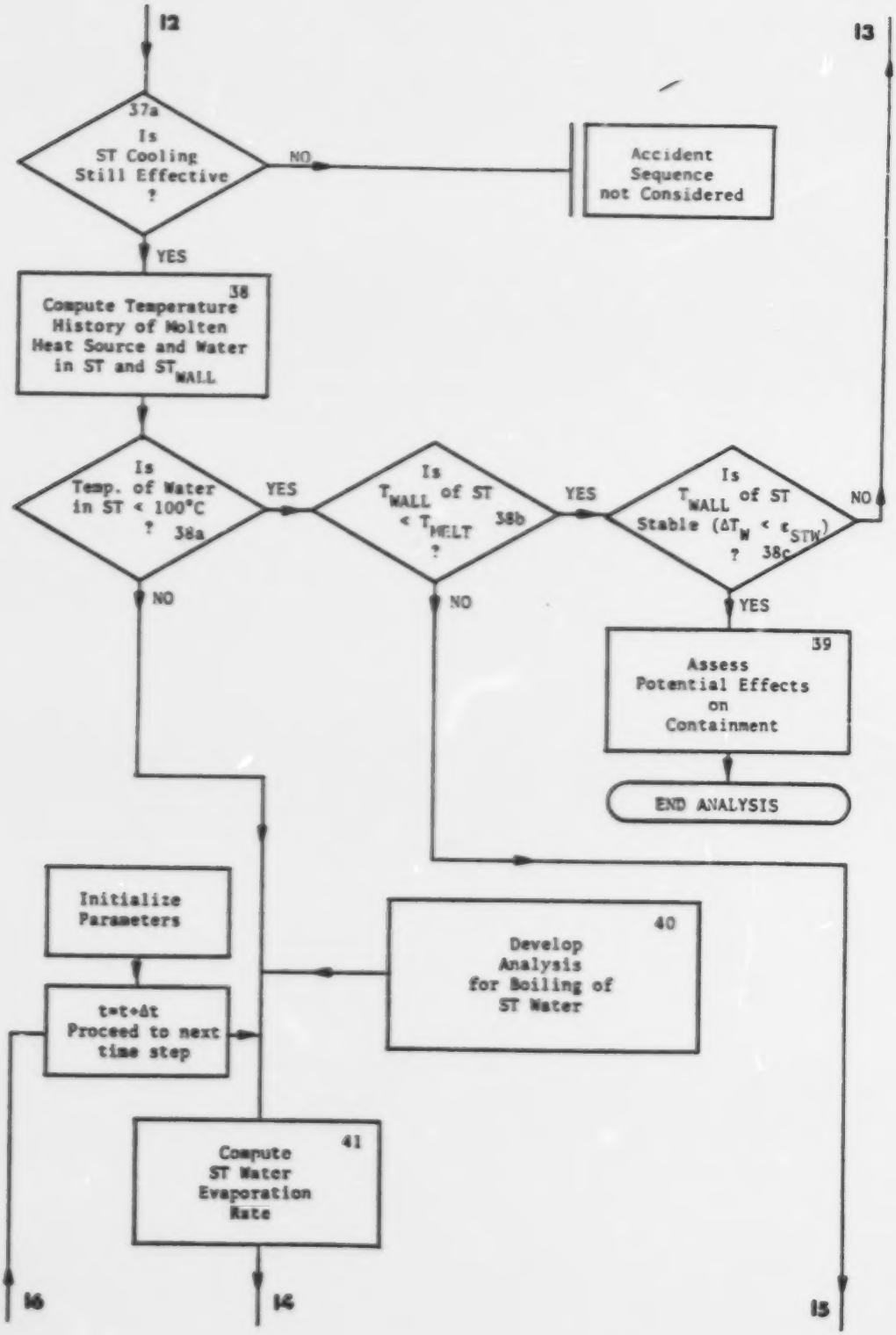
12
13
37a
Is ST Cooling Still Effective ?
NO
Accident Sequence not Considered
YES
38
Compute Temperature History of Molten Heat Source and Water in ST and ST_{WALL}
Is Temp. of Water in ST < 100°C ? 38a
YES
Is T_{WALL} of ST < T_{MELT} ? 38b
YES
Is T_{WALL} of ST Stable ($\Delta T_W < \epsilon_{STW}$) ? 38c
NO
NO
NO
YES
39
Assess Potential Effects on Containment
END ANALYSIS
Initialize Parameters
40
Develop Analysis for Boiling of ST Water
t=t+Δt Proceed to next time step
41
Compute ST Water Evaporation Rate
16
14
15

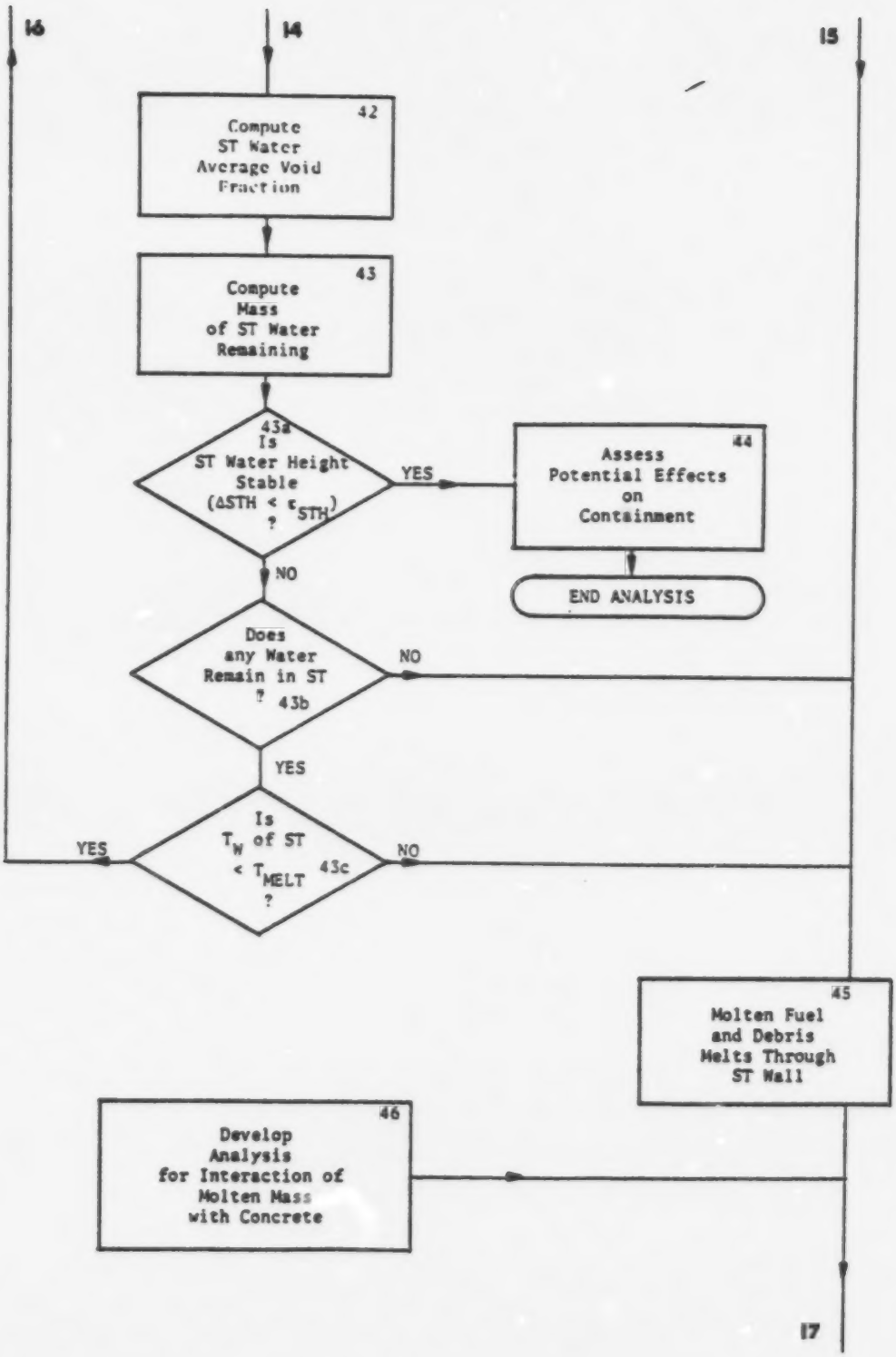
16
14
15
42
Compute ST Water Average Void Fraction
43
Compute Mass of ST Water Remaining
43a
Is ST Water Height Stable ($\Delta STH < \epsilon_{STH}$) ?
YES
44
Assess Potential Effects on Containment
END ANALYSIS
NO
Does any Water Remain in ST ? 43b
NO
YES
Is T_W of ST $< T_{MELT}$? 43c
YES
NO
45
Molten Fuel and Debris Melts Through ST Wall
46
Develop Analysis for Interaction of Molten Mass with Concrete
17

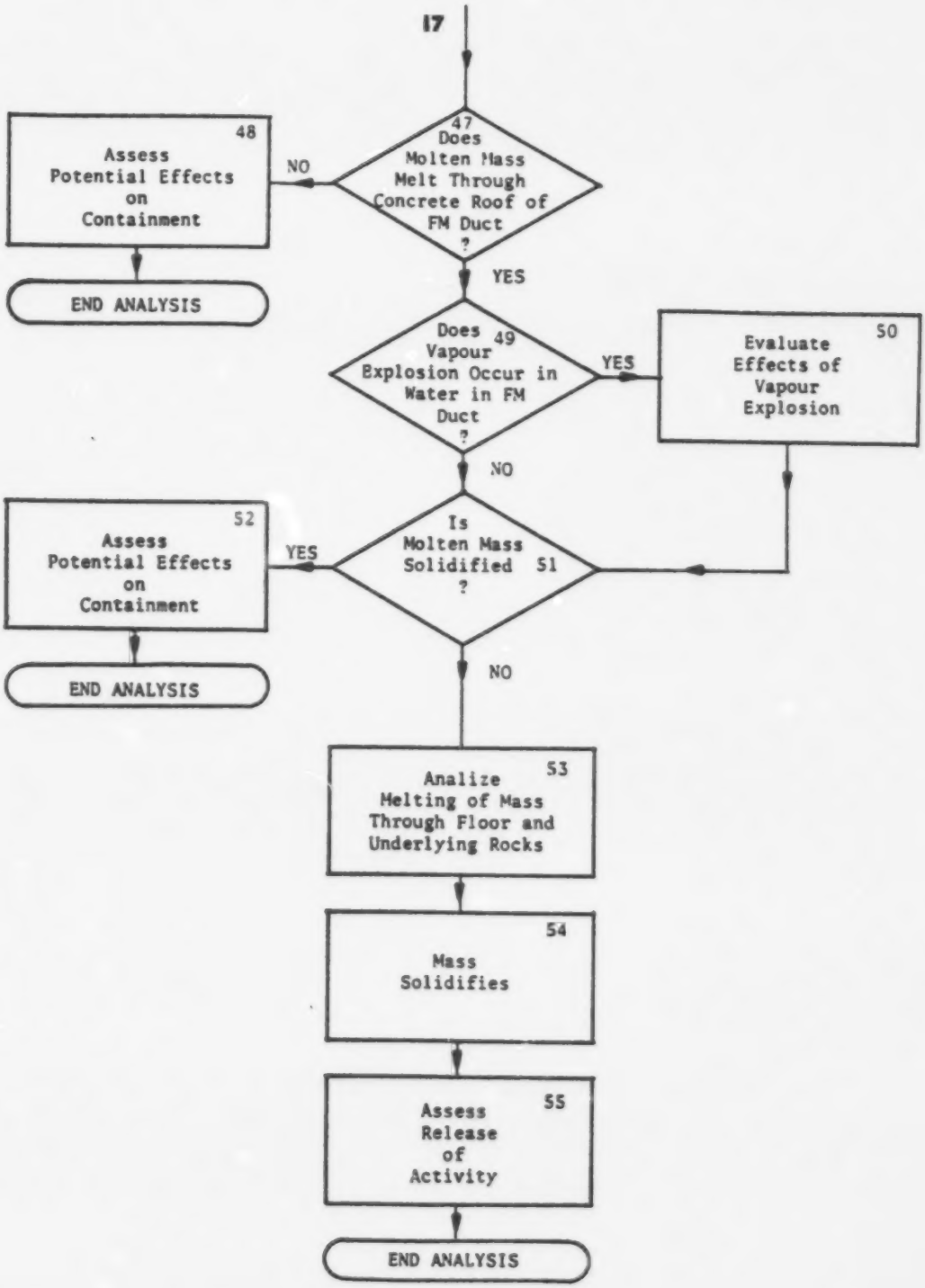
17
47
Does Molten Mass Melt Through Concrete Roof of FM Duct ?
NO
48
Assess Potential Effects on Containment
END ANALYSIS
YES
Does Vapour Explosion Occur in Water in FM Duct ?
49
YES
50
Evaluate Effects of Vapour Explosion
NO
Is Molten Mass Solidified ?
51
YES
52
Assess Potential Effects on Containment
END ANALYSIS
NO
53
Analize Melting of Mass Through Floor and Underlying Rocks
54
Mass Solidifies
55
Assess Release of Activity
END ANALYSIS

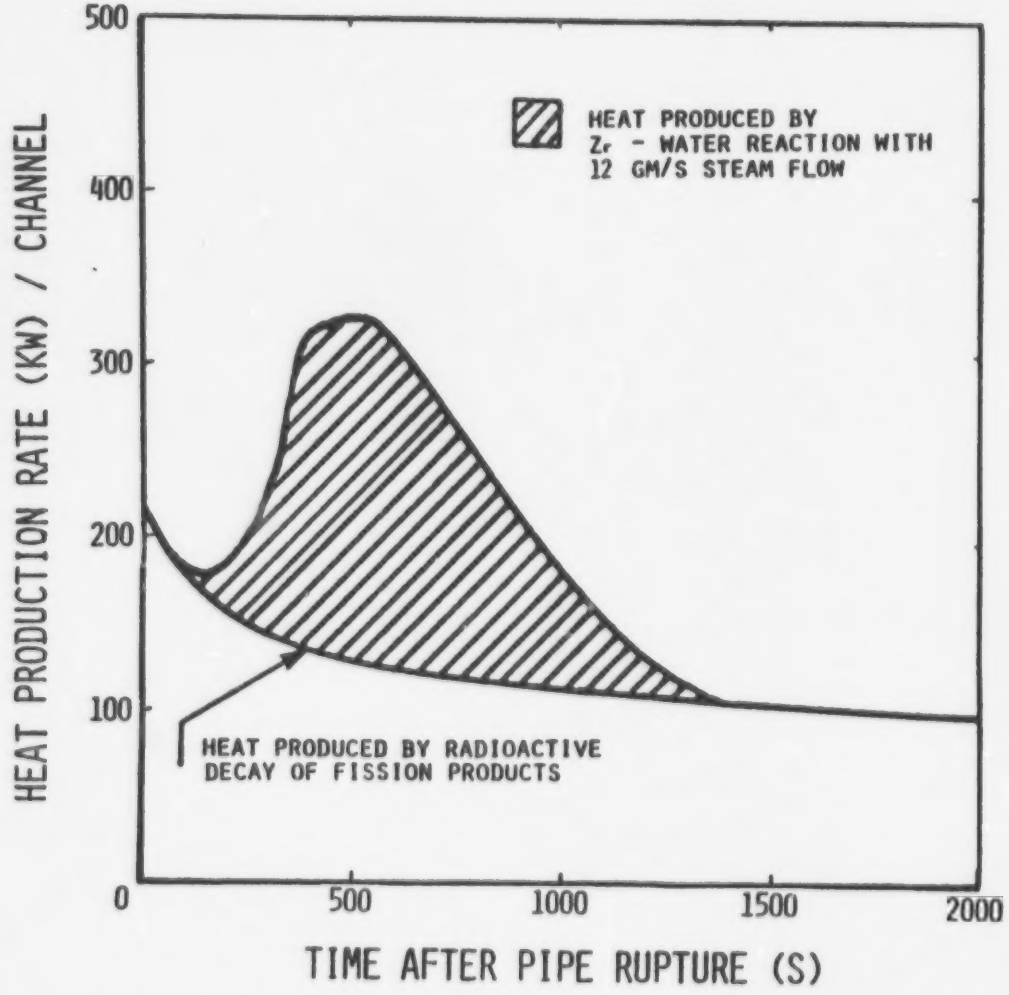

FIG. 4 HEAT PRODUCTION RATE BY ZIRCALOY-WATER REACTION.
BRUCE MAXIMUM POWER CHANNEL CONDITIONS.

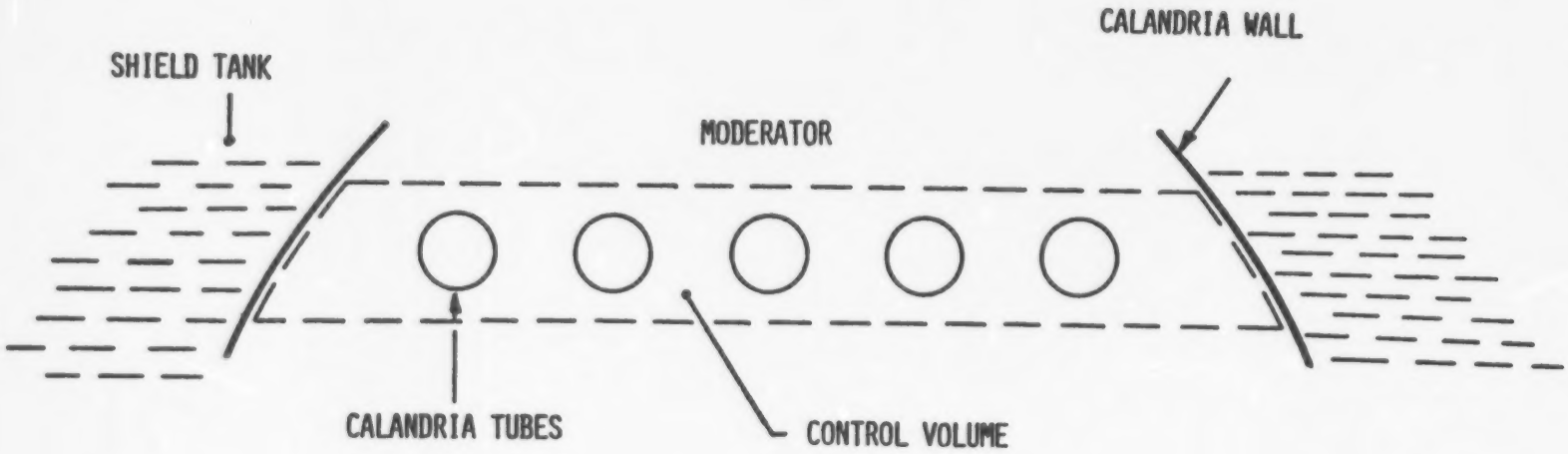

FIG. 5 CONTROL VOLUME USED IN MODBOIL

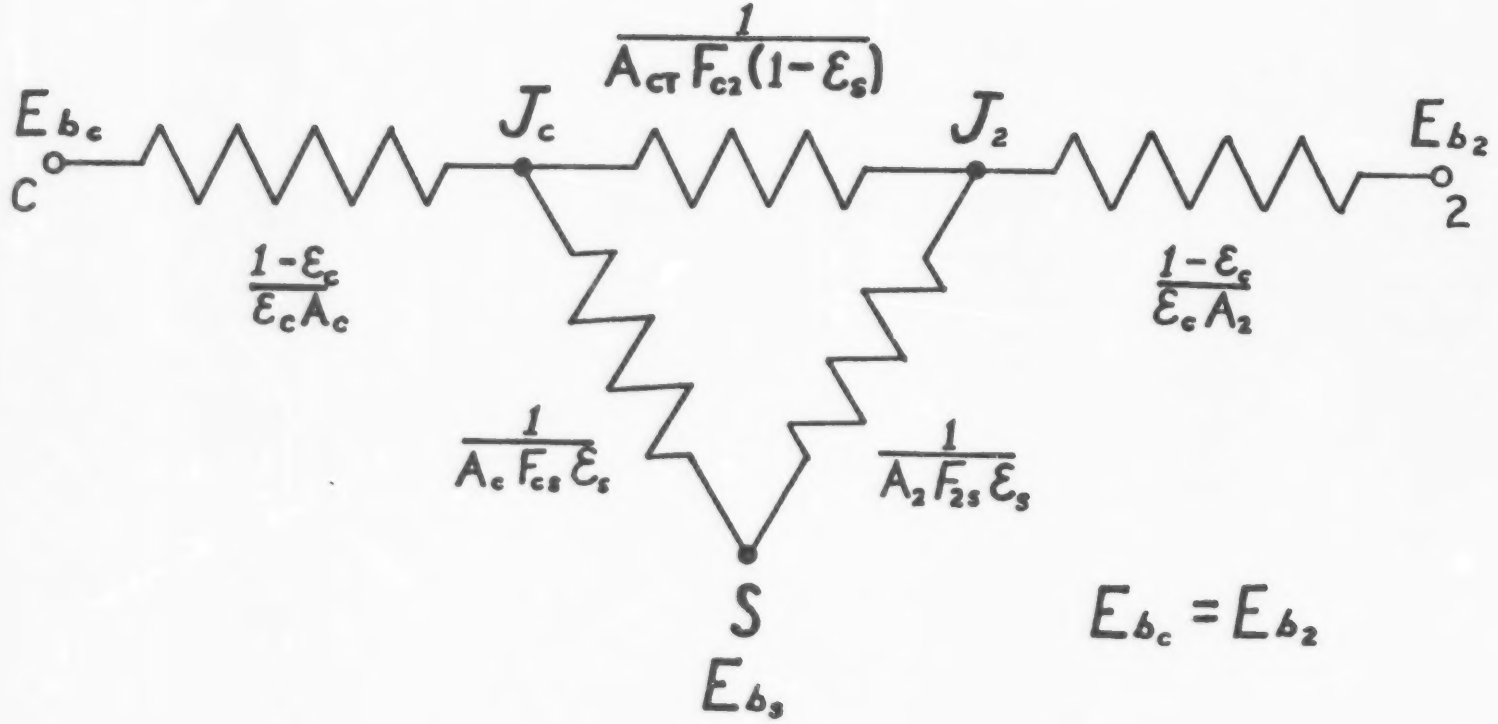

FIG. 6 NETWORK DIAGRAM FOR RADIATION HEAT TRANSFER FROM UNCOVERED CALANDRIA TUBE

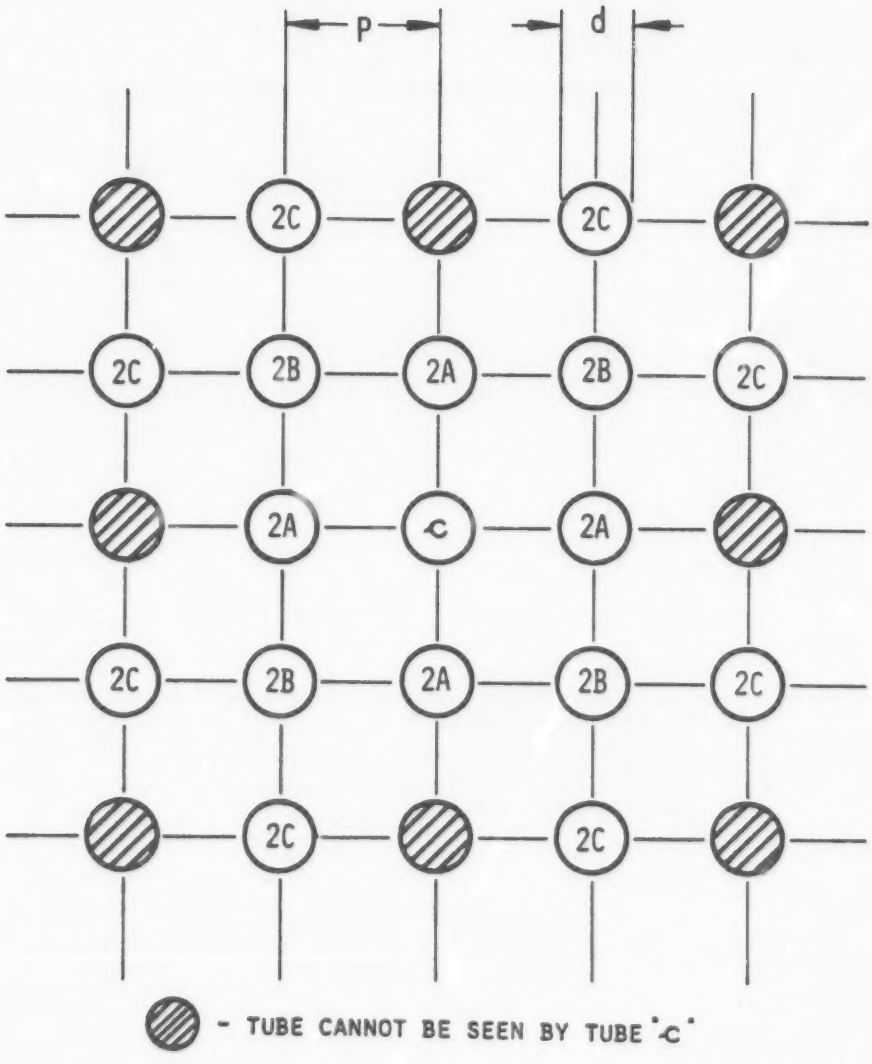

FIG. 7 DETERMINATION OF CONFIGURATION FACTOR FOR CALANDRIA TUBES

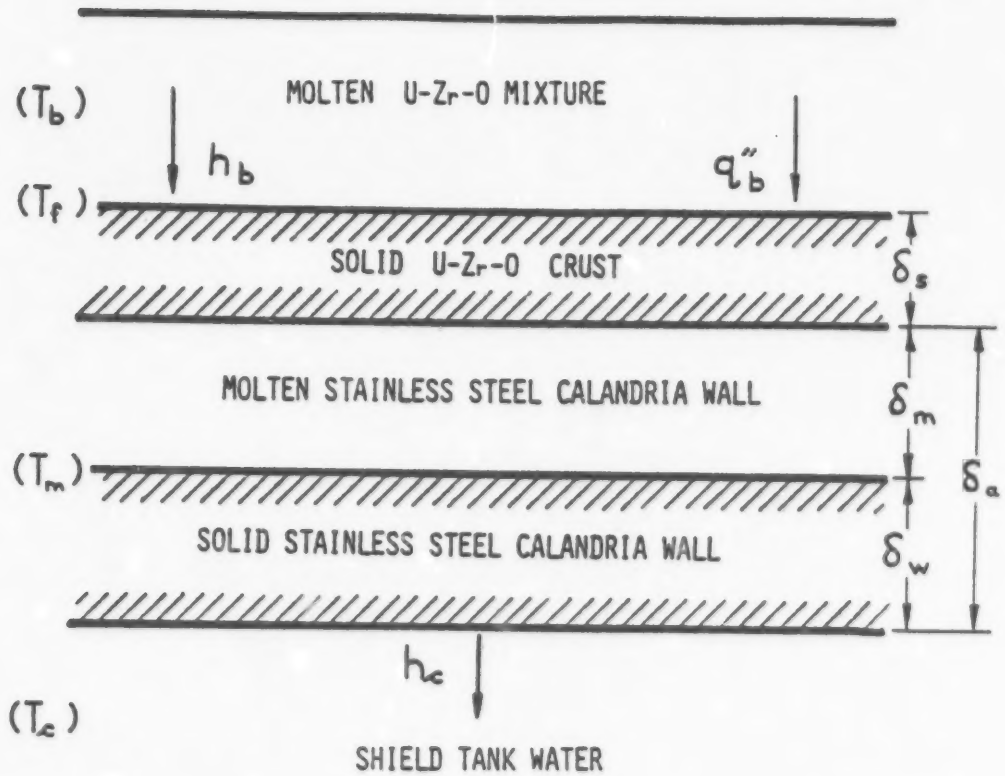

FIG. 8 ANALYTICAL MODEL FOR MOLTEN MATERIAL ON CALANDRIA WALL

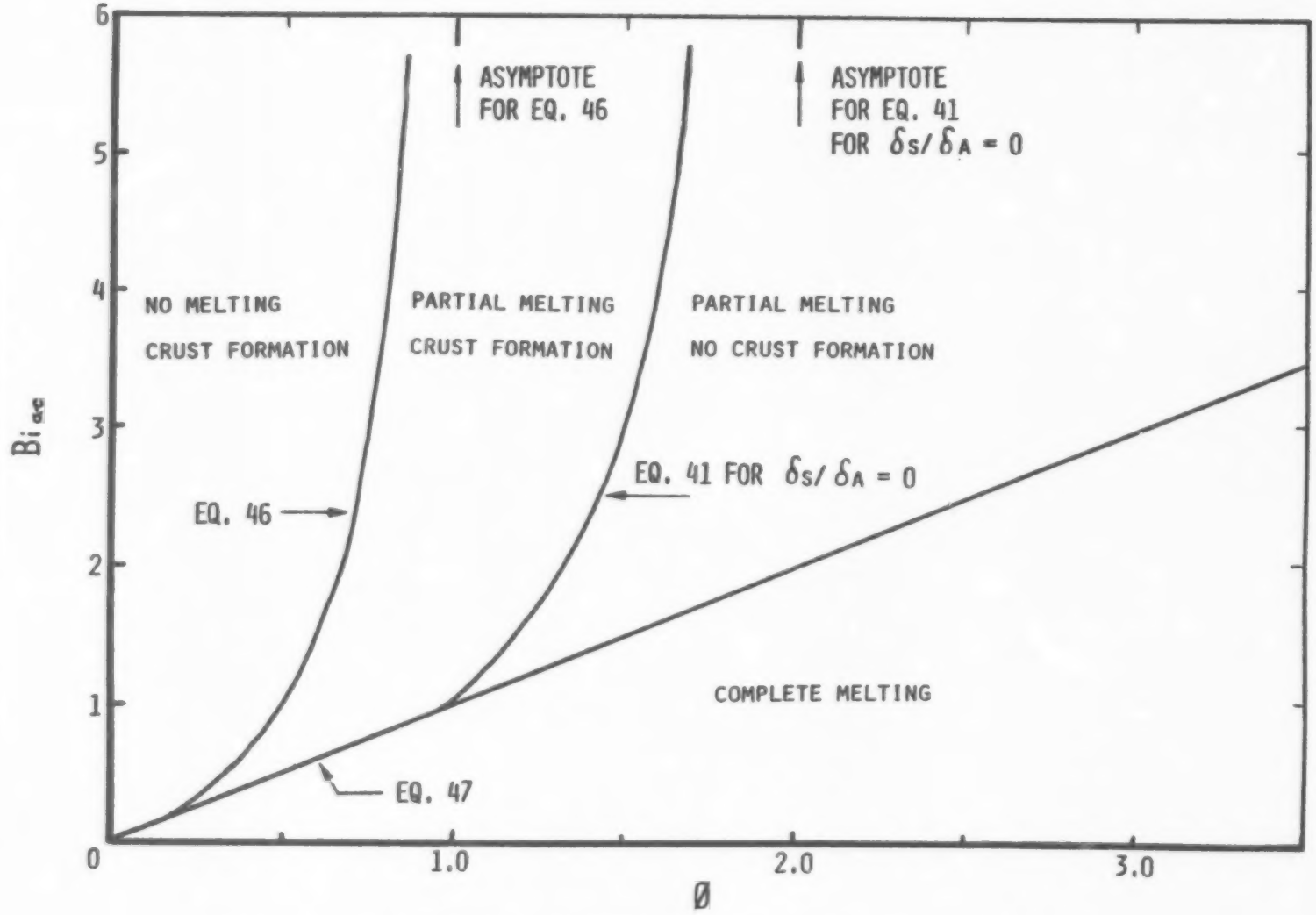

FIG. 9 MAP OF CONDITIONS FOR MELTING OF CALANDRIA WALL

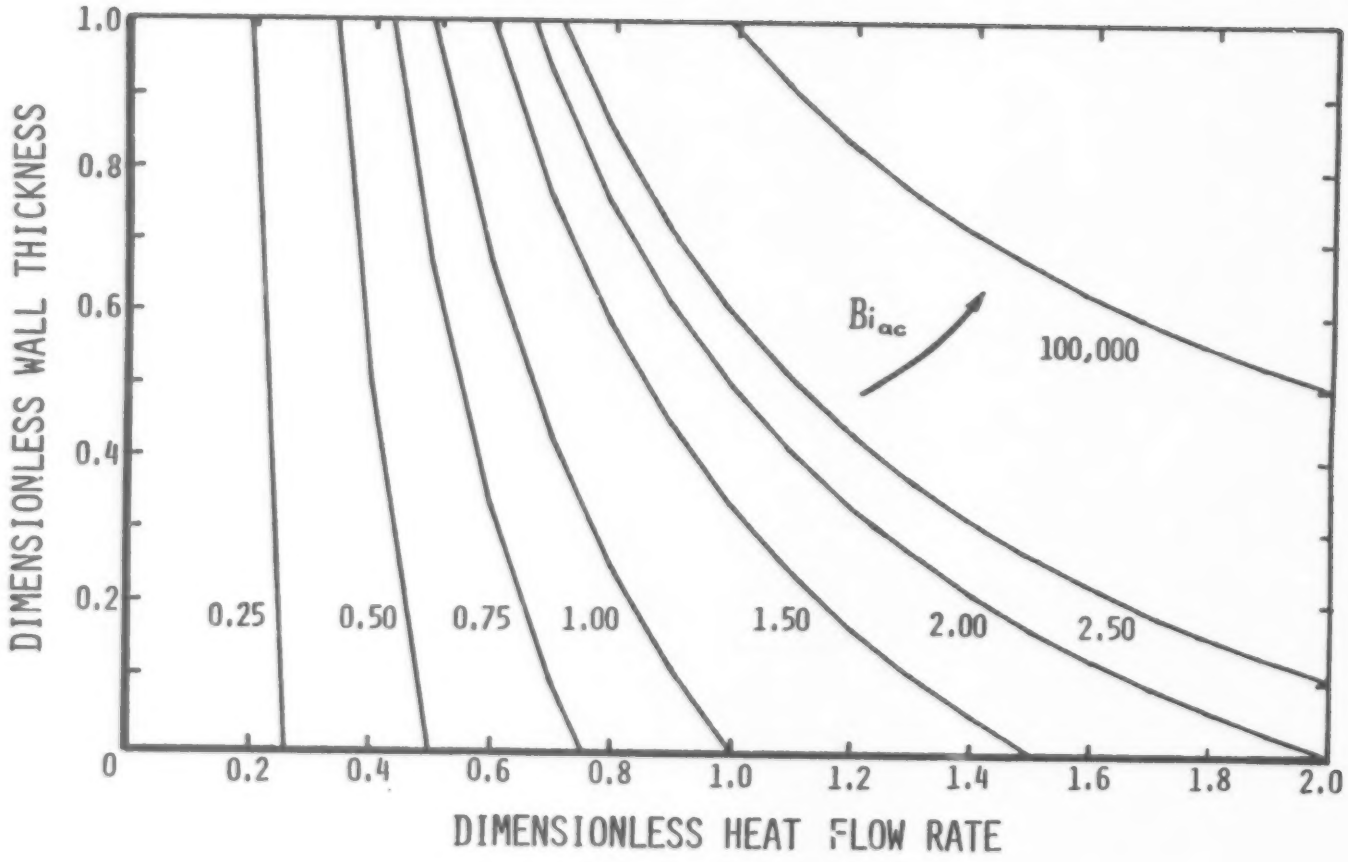

FIG. 10 NON-DIMENSIONAL UNMELTED WALL THICKNESS DIAGRAM

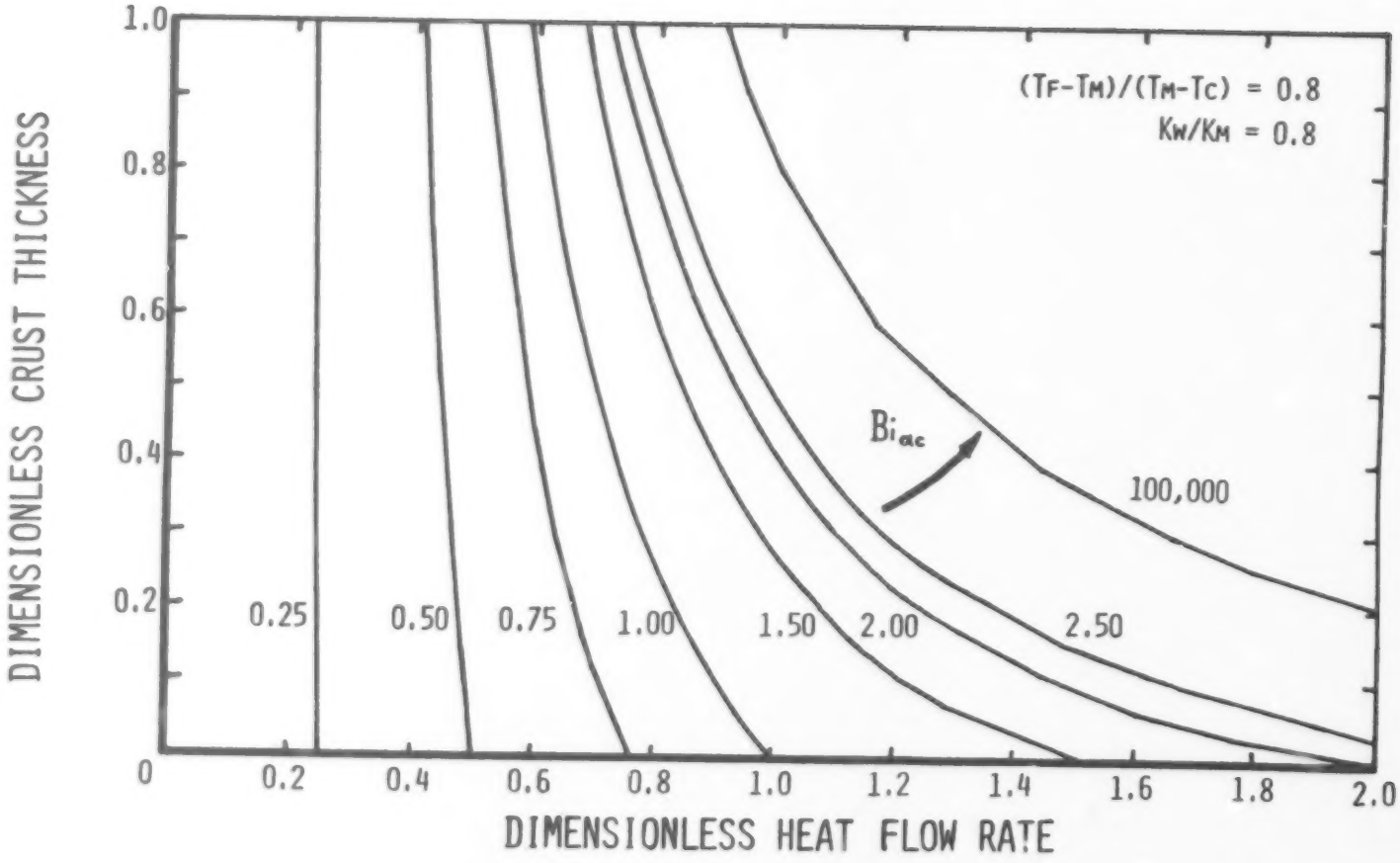

FIG. 11 NON-DIMENSIONAL SOLIDIFIED CRUST THICKNESS DIAGRAM

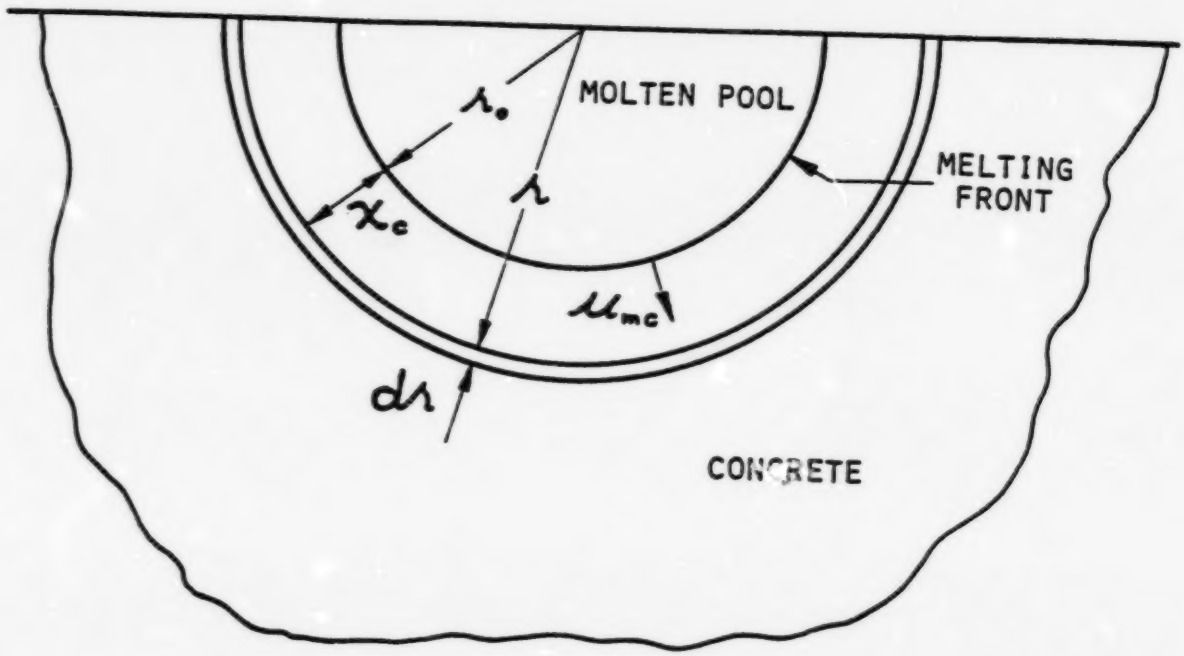

FIG. 12 GEOMETRY OF MOLTEN POOL OF CORE MATERIAL AND MELTED CONCRETE

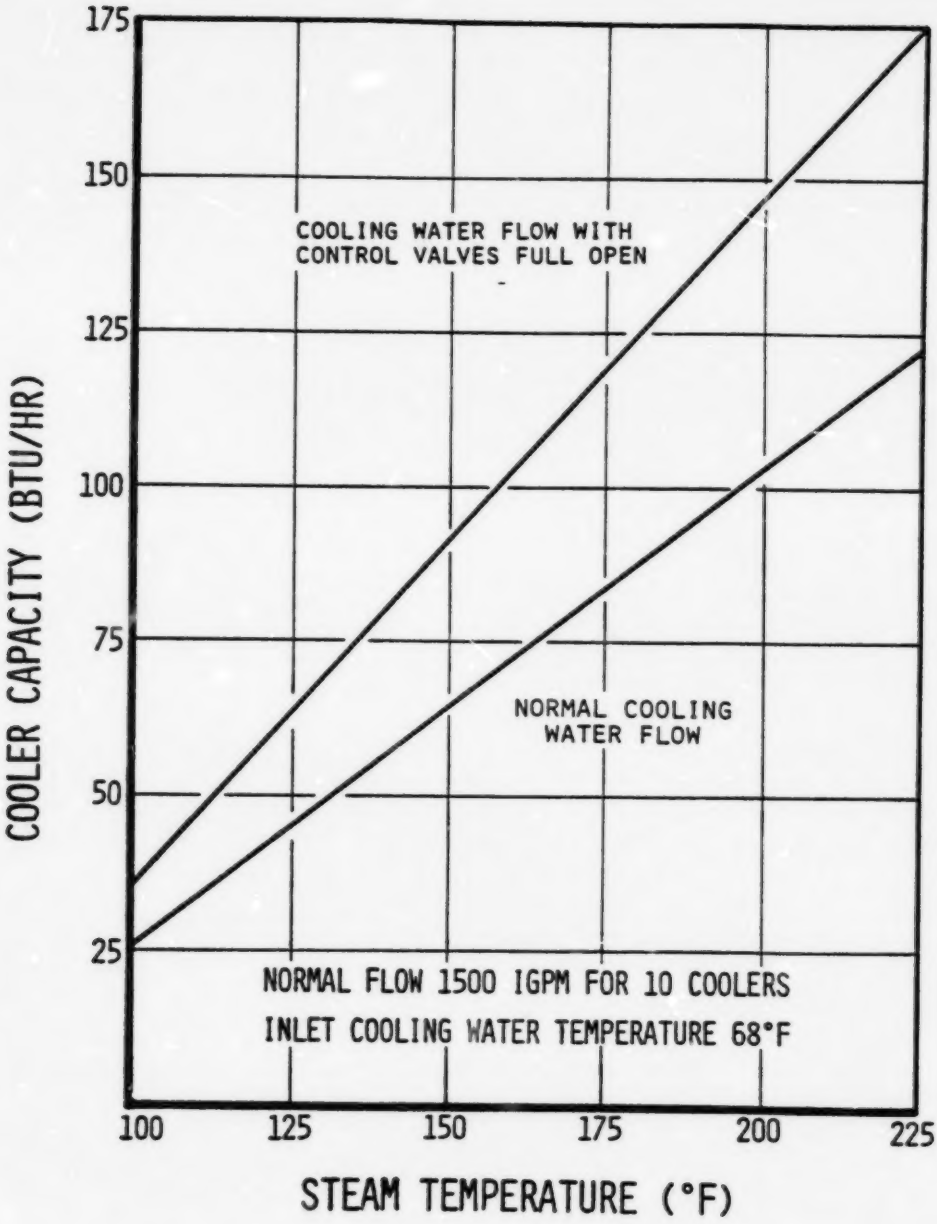

FIG. 13 BRUCE REACTOR VAULT COOLER CAPACITY TO CONDENSE STEAM VS. STEAM TEMPERATURE

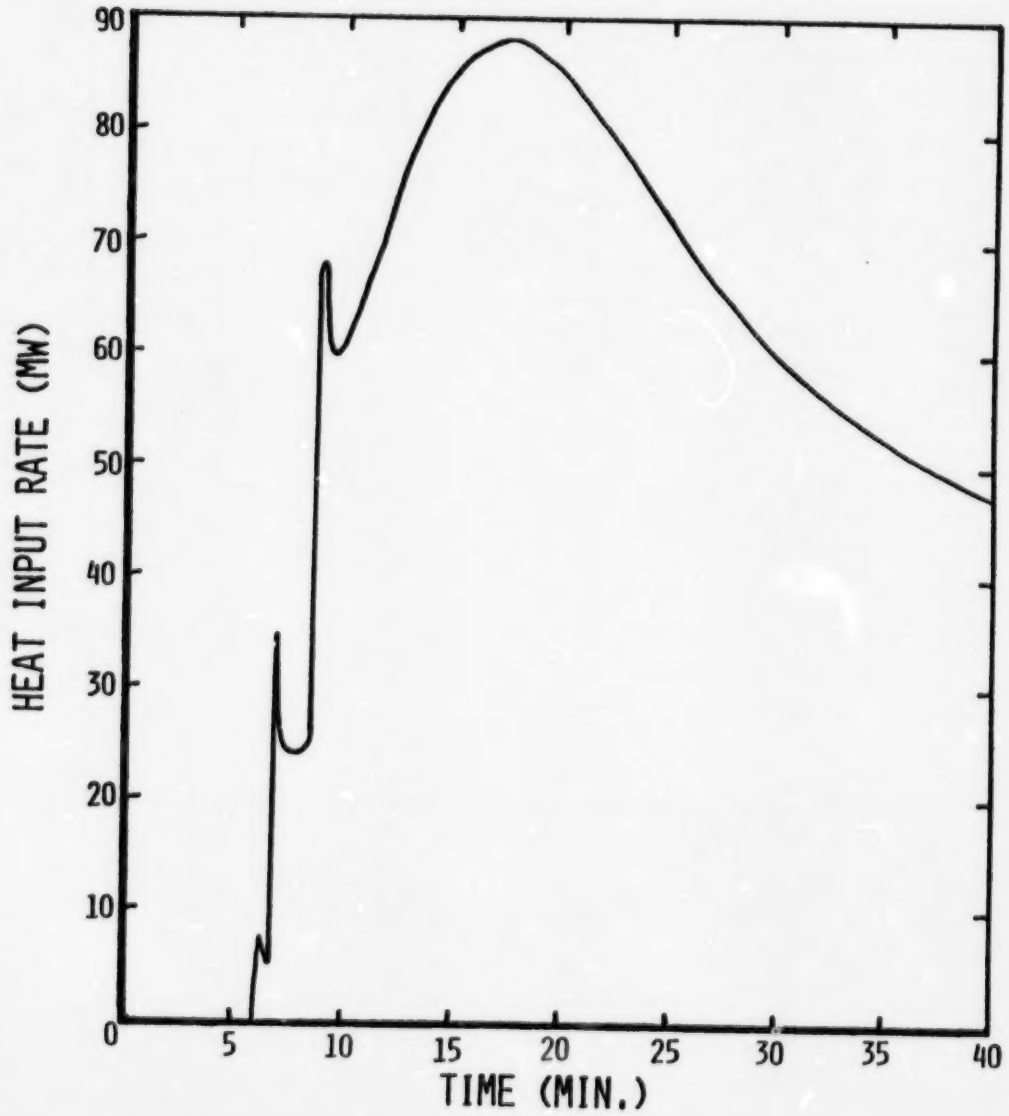

FIG. 14 TOTAL HEAT INPUT RATE TO MODERATOR. BRUCE-A UNIT

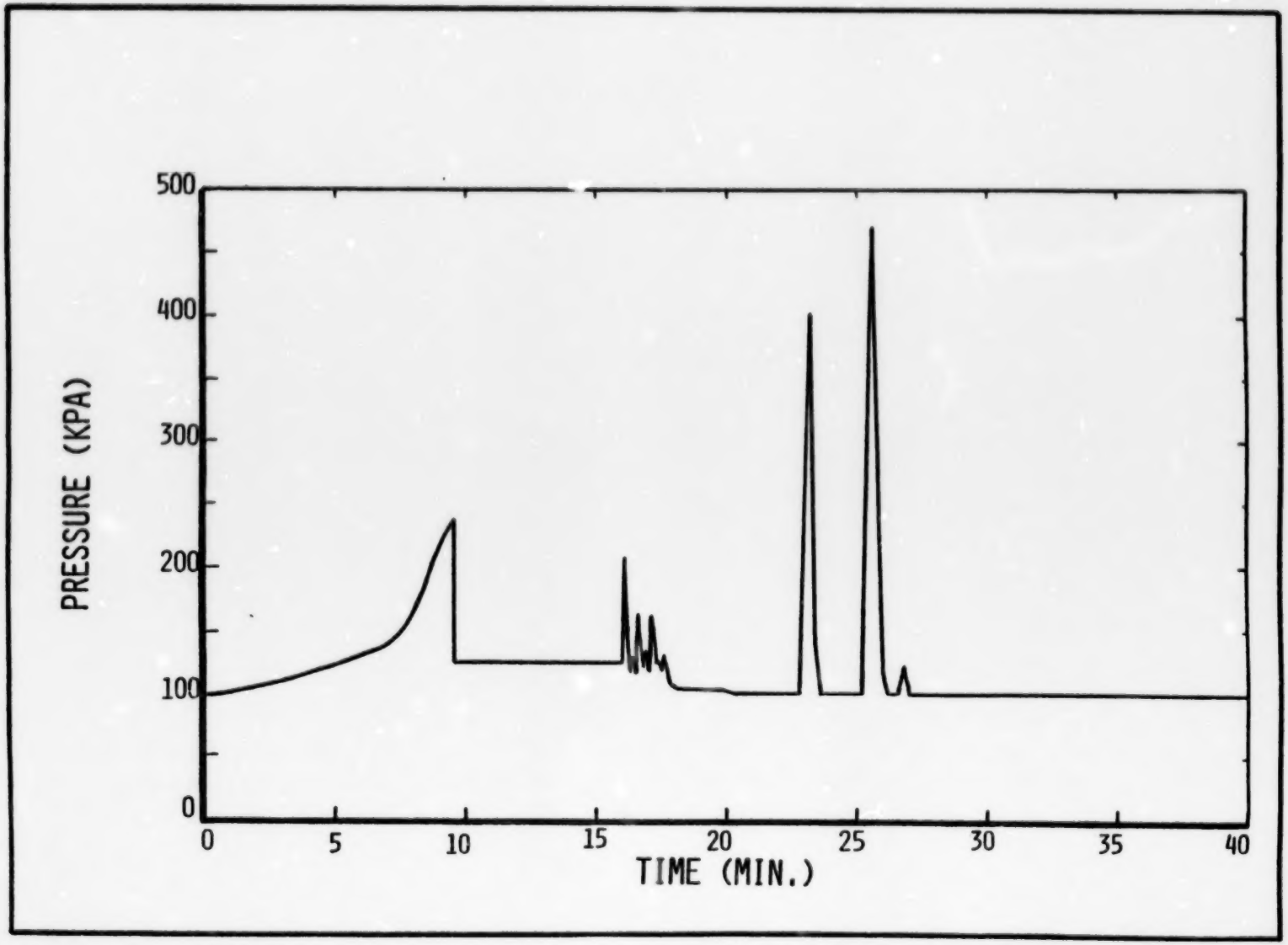

FIG. 15 CALANDRIA PRESSURE AT BASE OF RELIEF DUCTS REFERENCE CONDITIONS

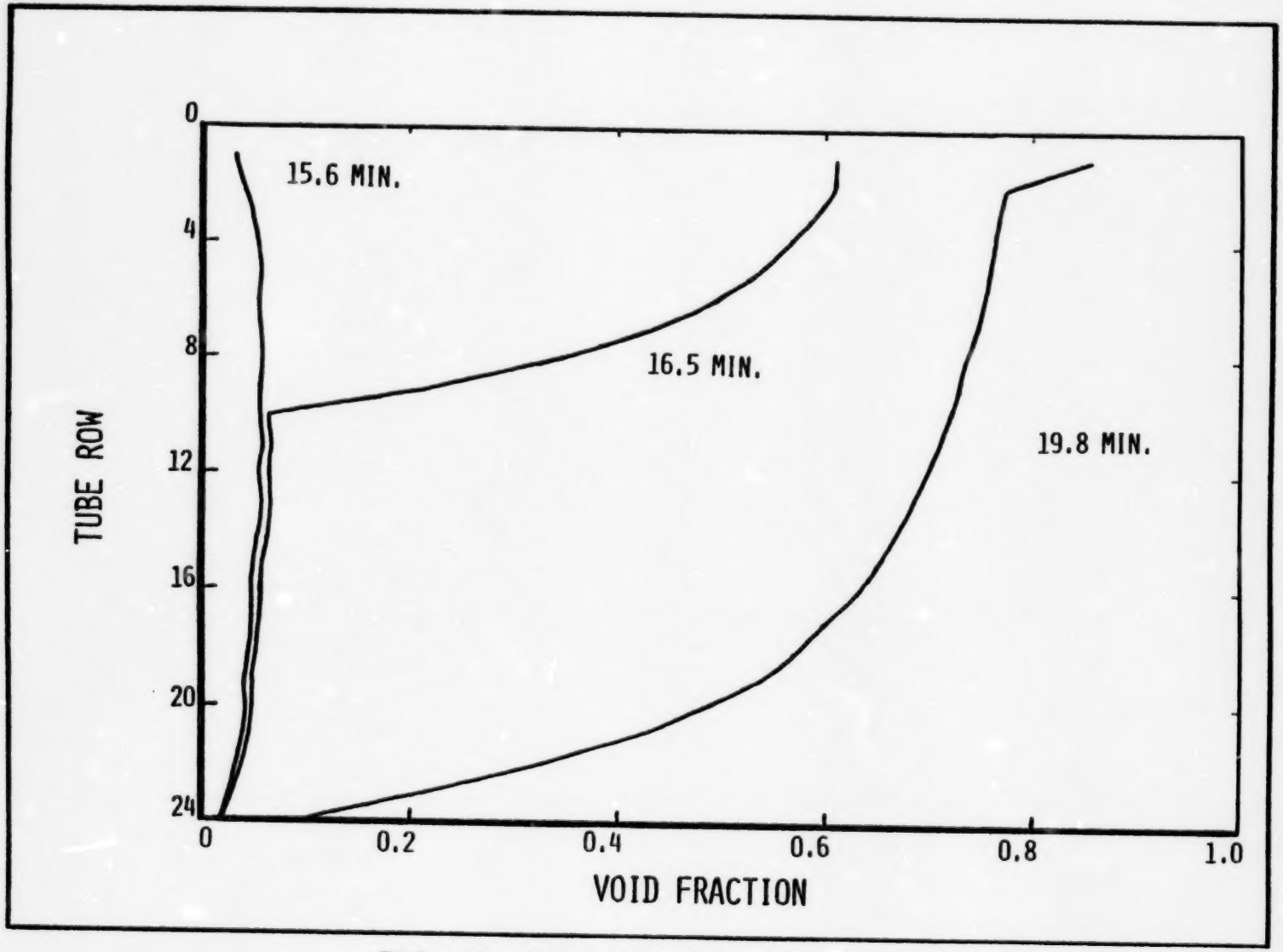

FIG. 16 VOID PROFILES ACROSS CALANDRIA

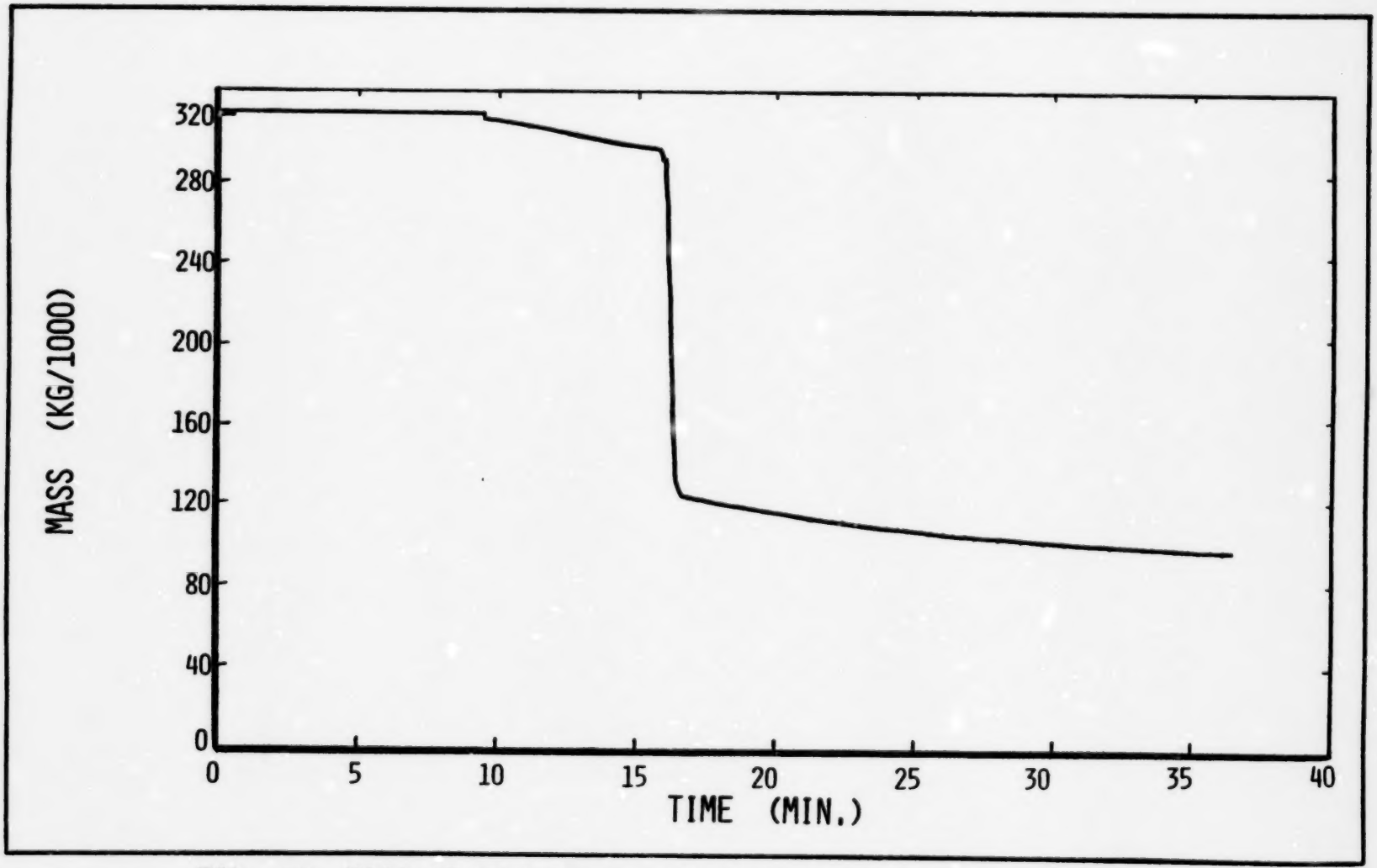

FIG. 17 MASS OF MODERATOR REMAINING IN CALANDRIA VS. TIME.
NO CHANNEL DISINTEGRATION.

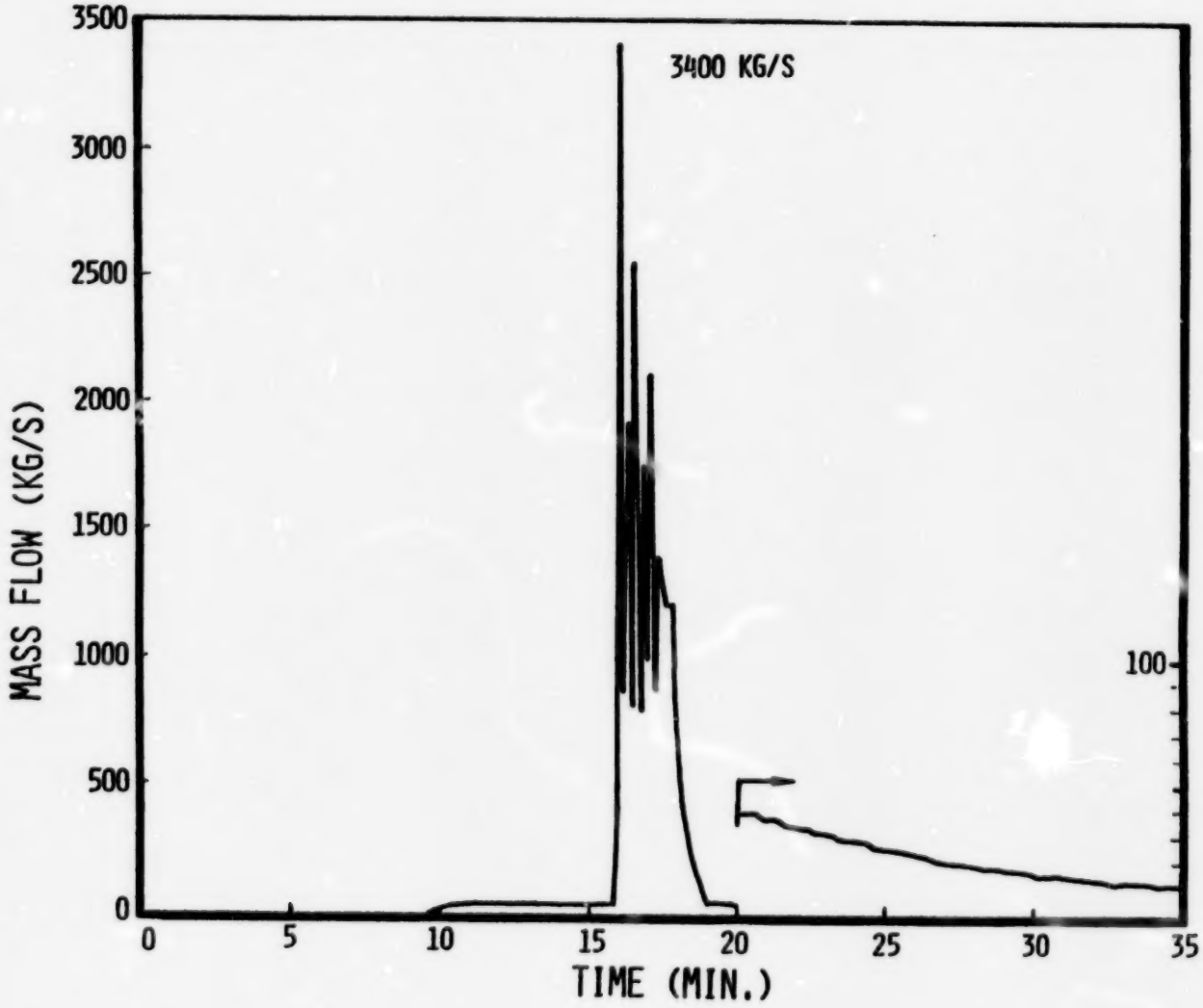

FIG. 18 MODERATOR EXPULSION RATE. NO CHANNEL DISINTEGRATION.

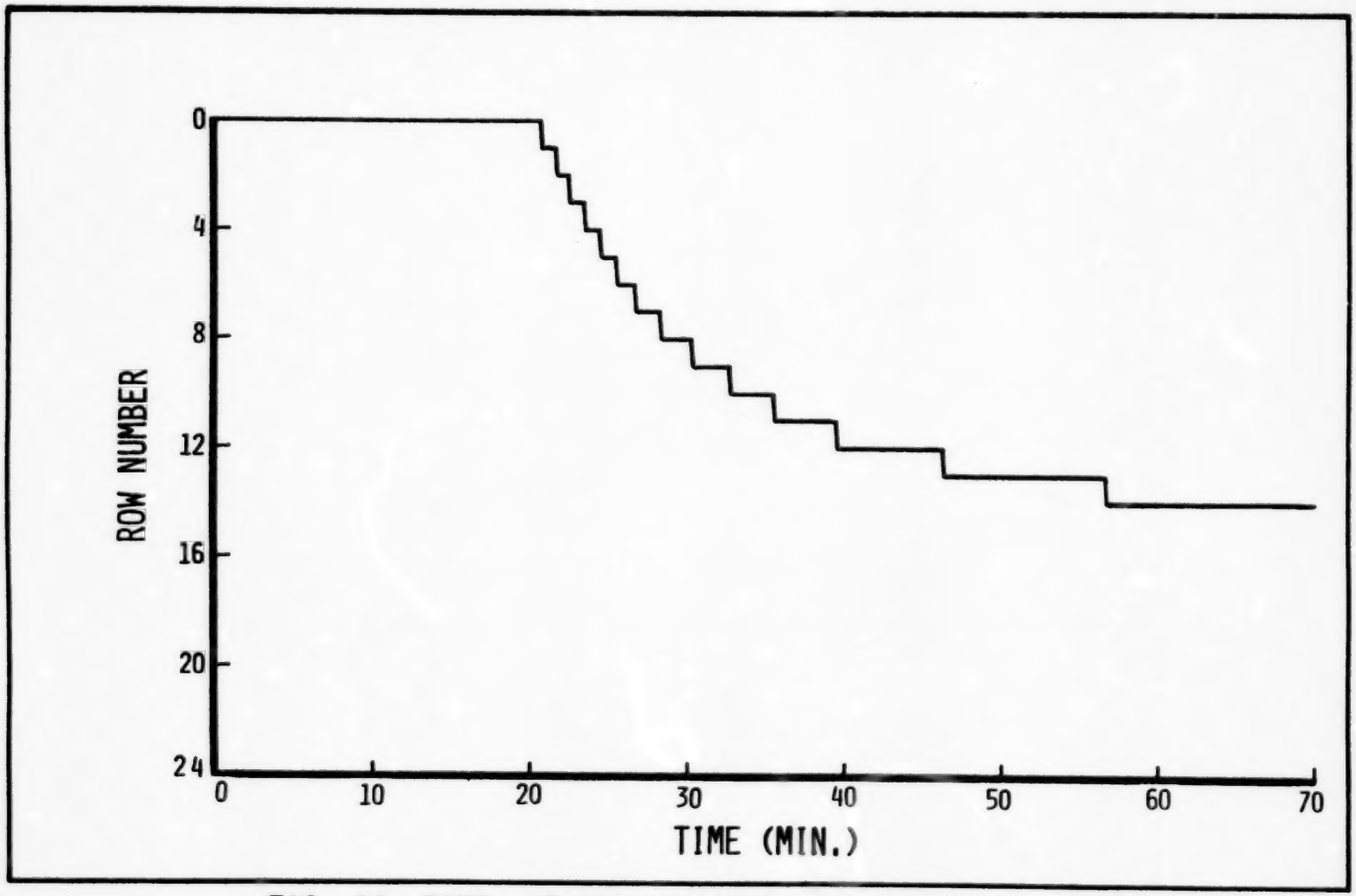

FIG. 19 TIMES OF ROW UNCOVERY, NO CHANNEL DISINTEGRATION

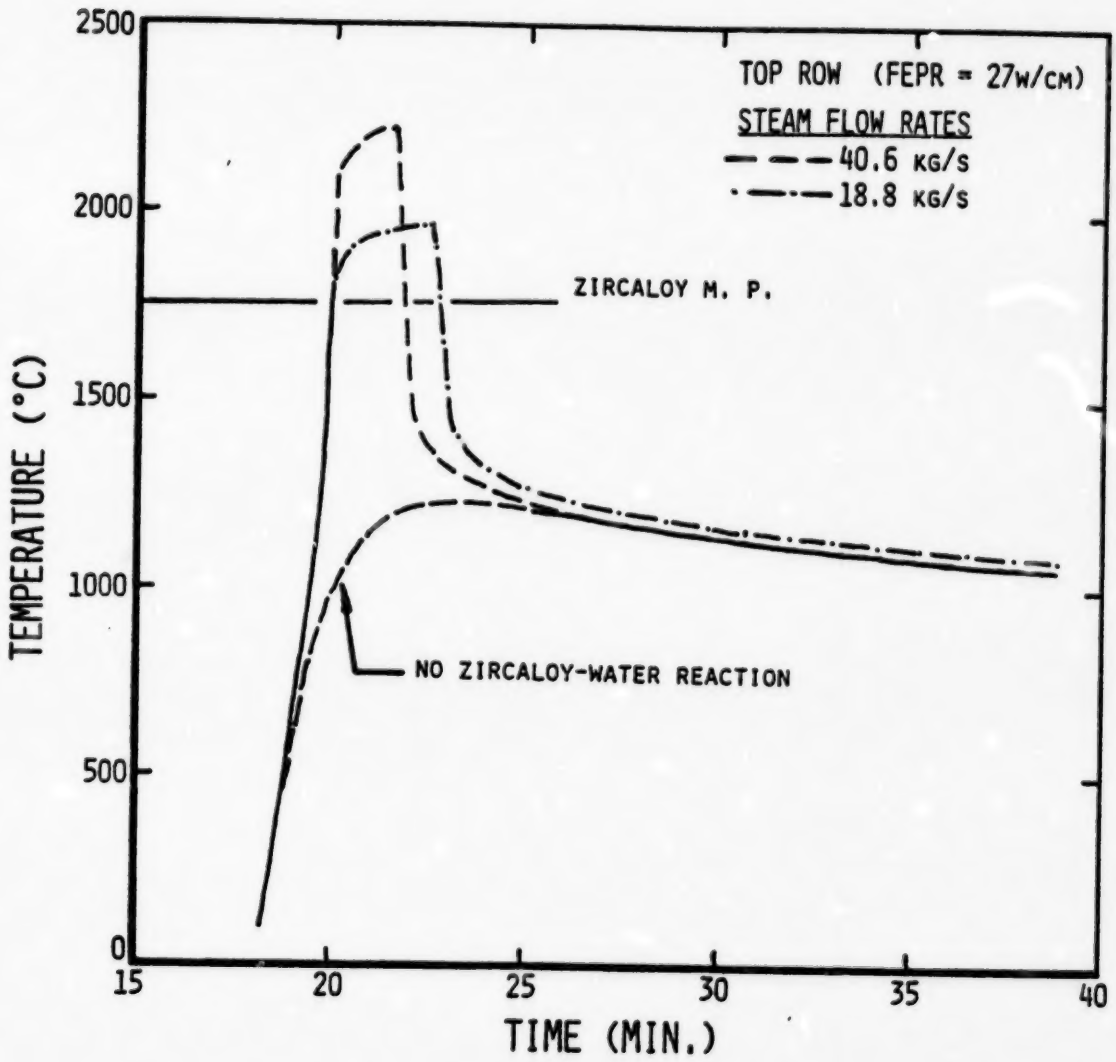

FIG. 20 MAXIMUM CALANDRIA TUBE TEMPERATURES FOR TOP ROW

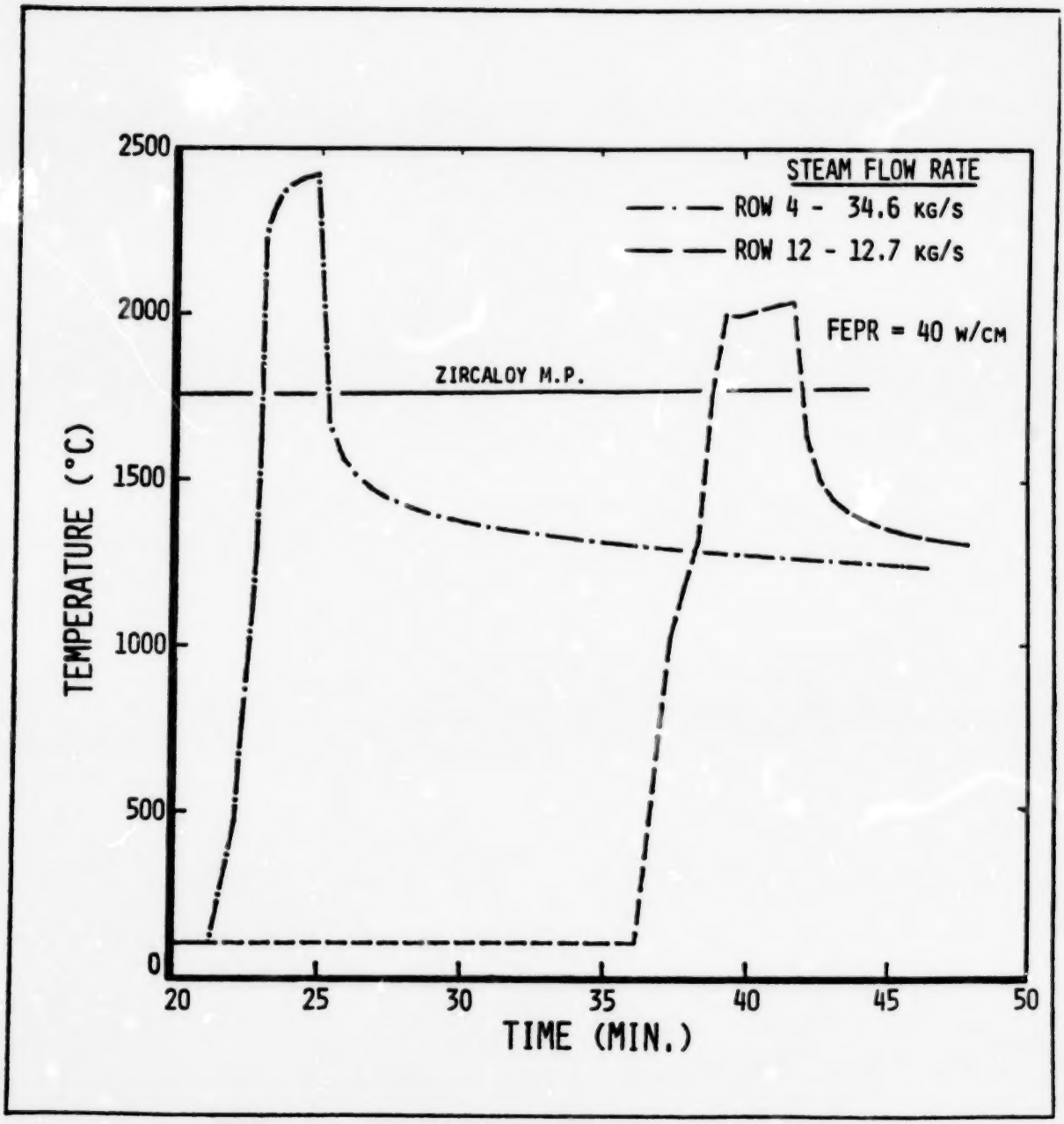

FIG. 21 MAXIMUM CALANDRIA TUBE TEMPERATURES FOR ROWS 4 AND 12

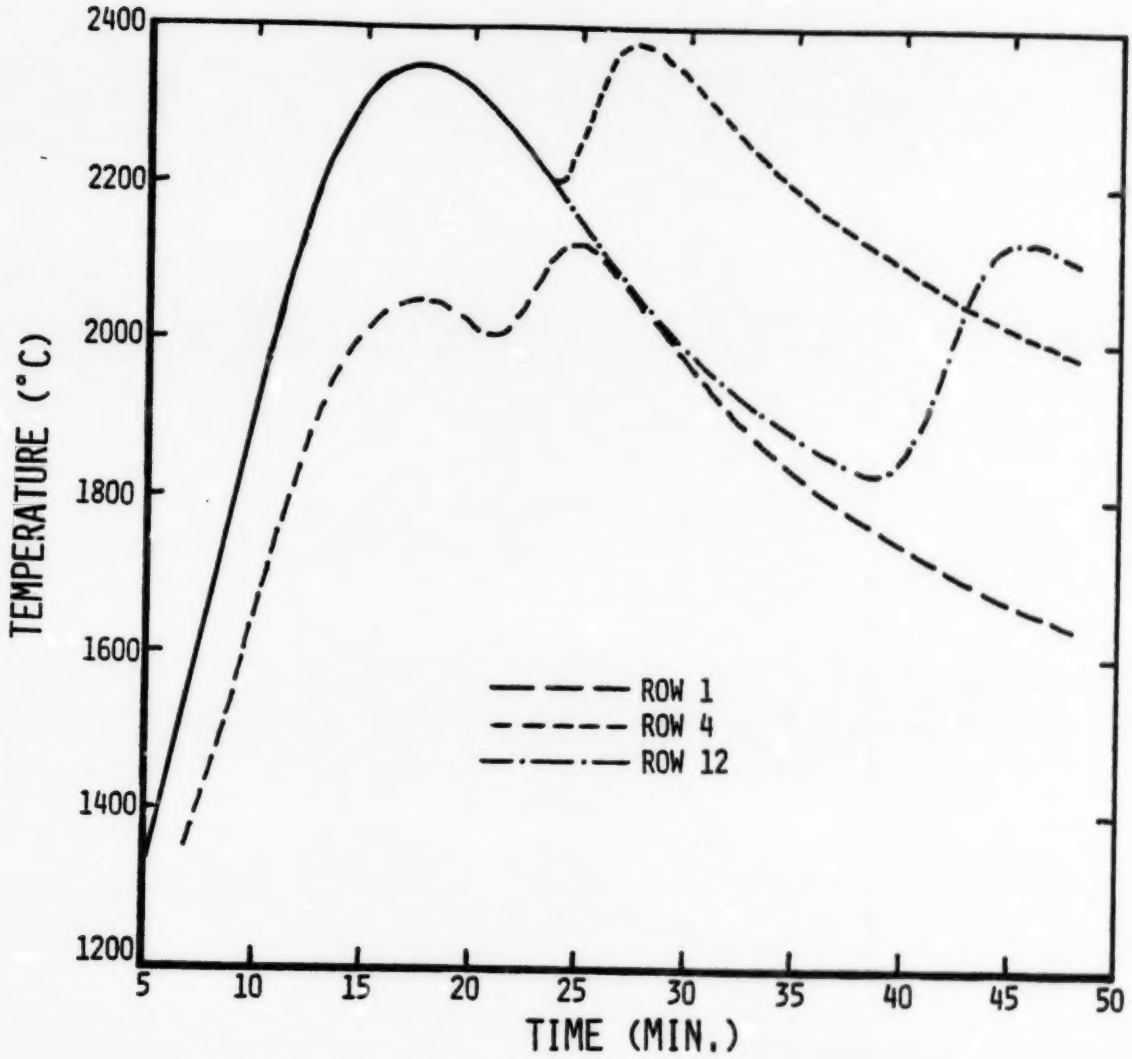

FIG. 22 MAXIMUM FUEL TEMPERATURES IN DIFFERENT ROWS

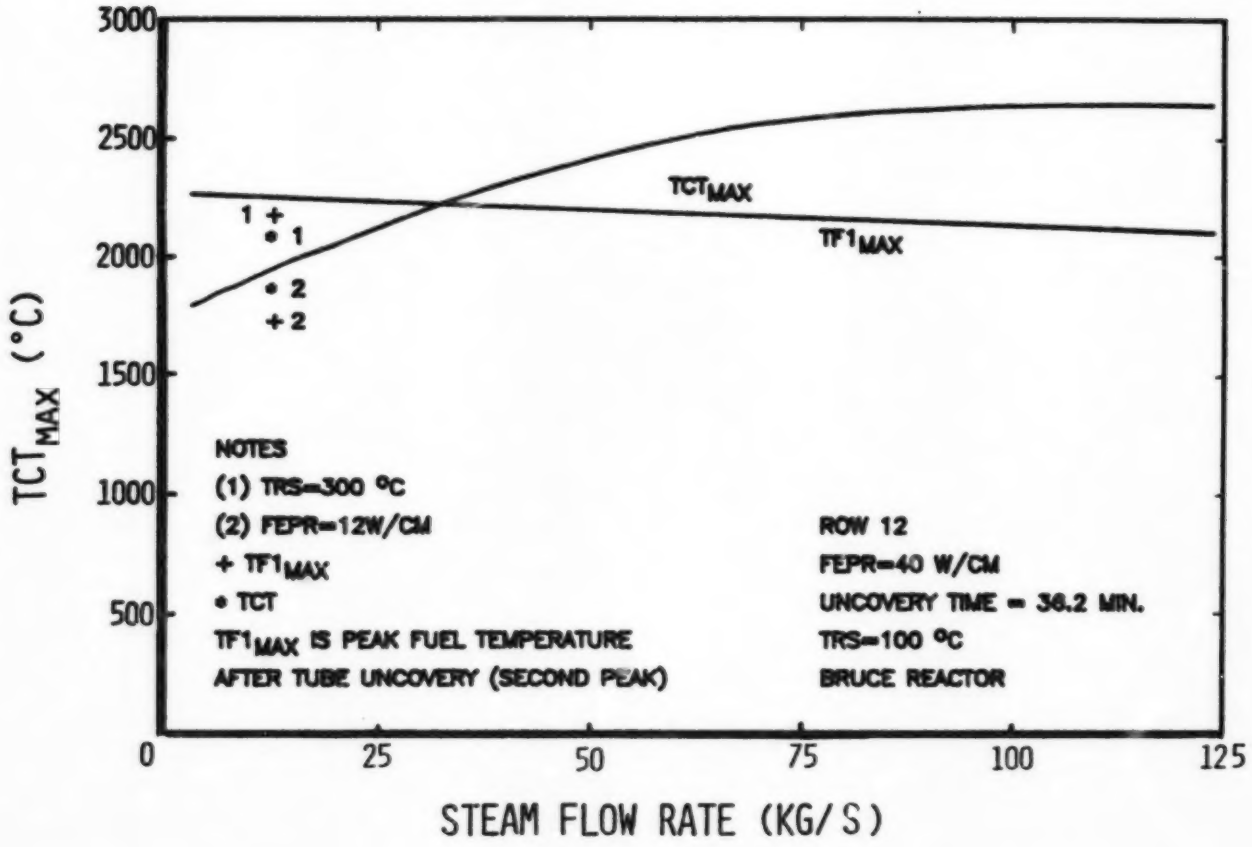

FIG. 23 MAXIMUM FUEL AND CALANDRIA TUBE TEMPERATURES. SENSITIVITY STUDY RESULTS.

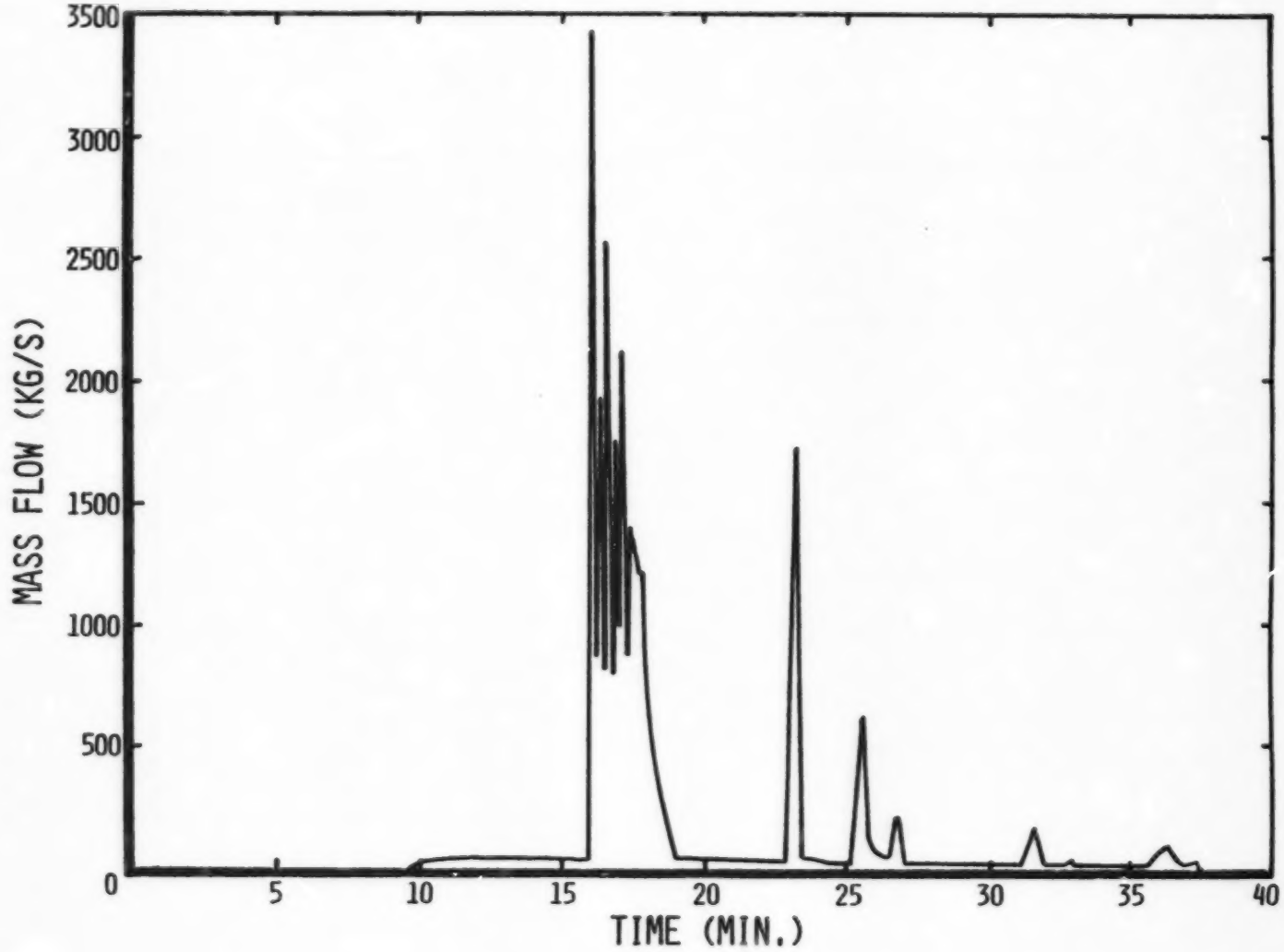

FIG. 24 MODERATOR EXPULSION RATE. REFERENCE CONDITIONS

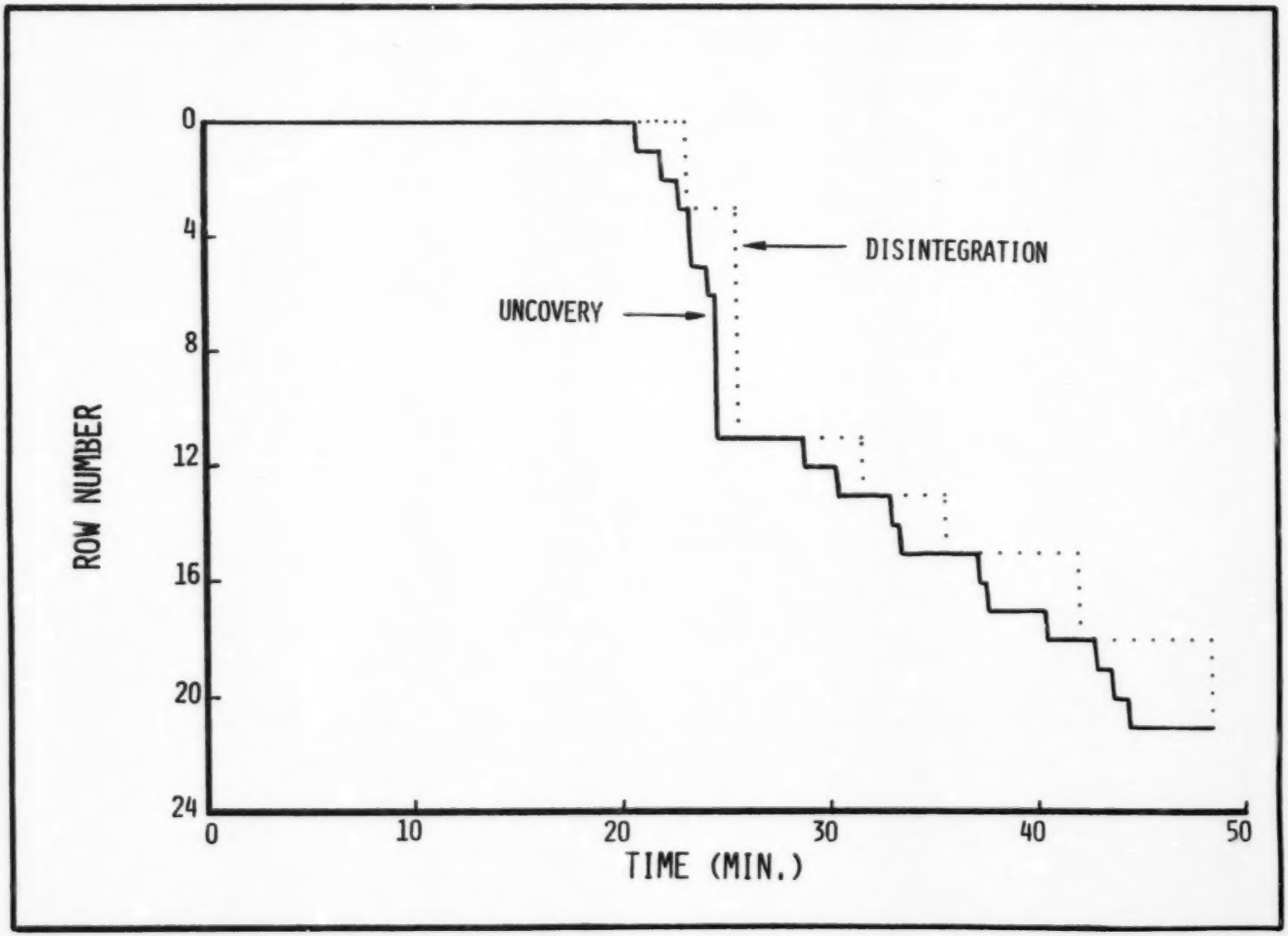

FIG. 25 TIMES OF ROW UNCOVERY AND DISINTEGRATION, REFERENCE CONDITIONS

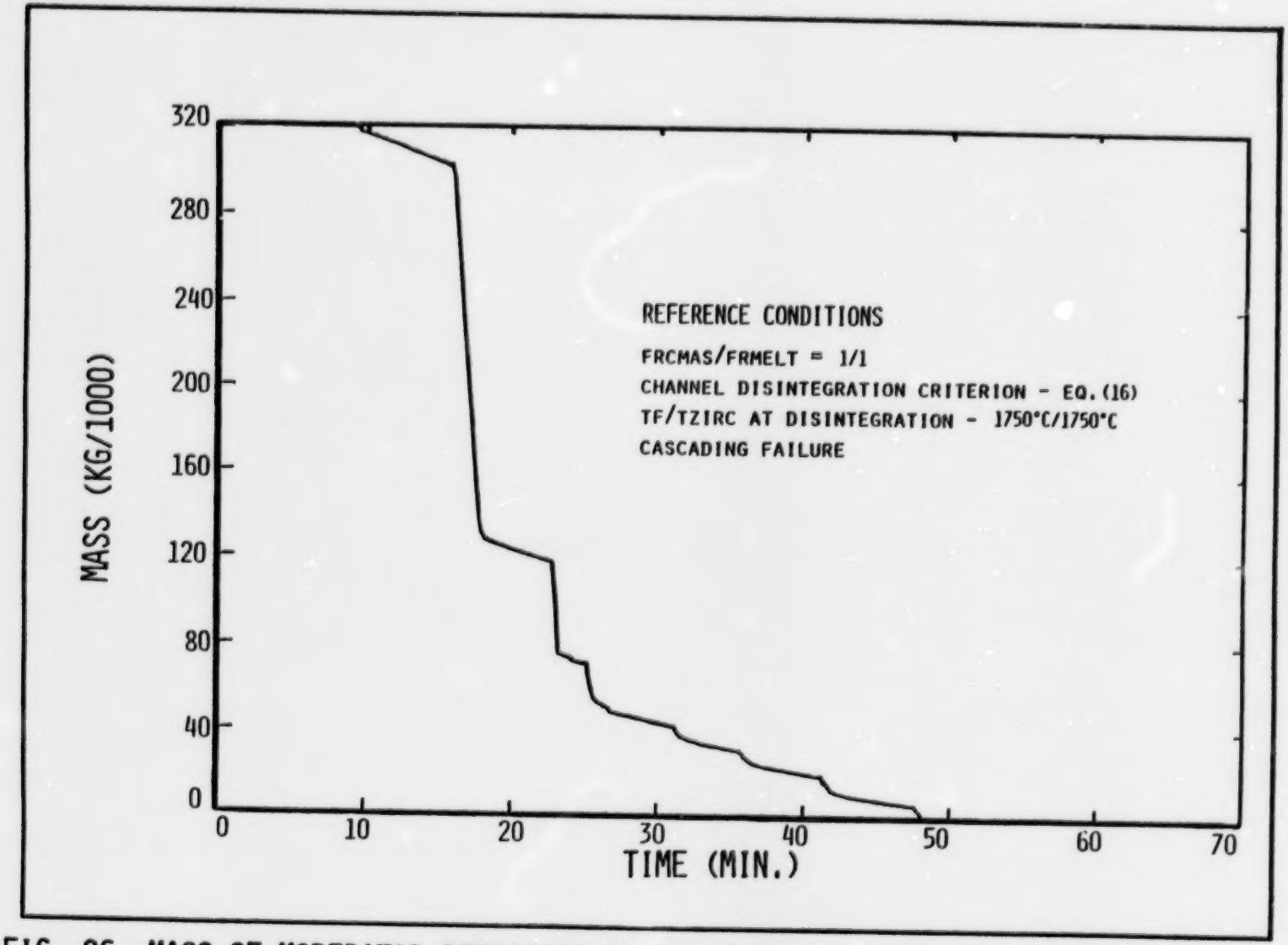

FIG. 26 MASS OF MODERATOR REMAINING IN CALANDRIA VS TIME REFERENCE CONDITIONS

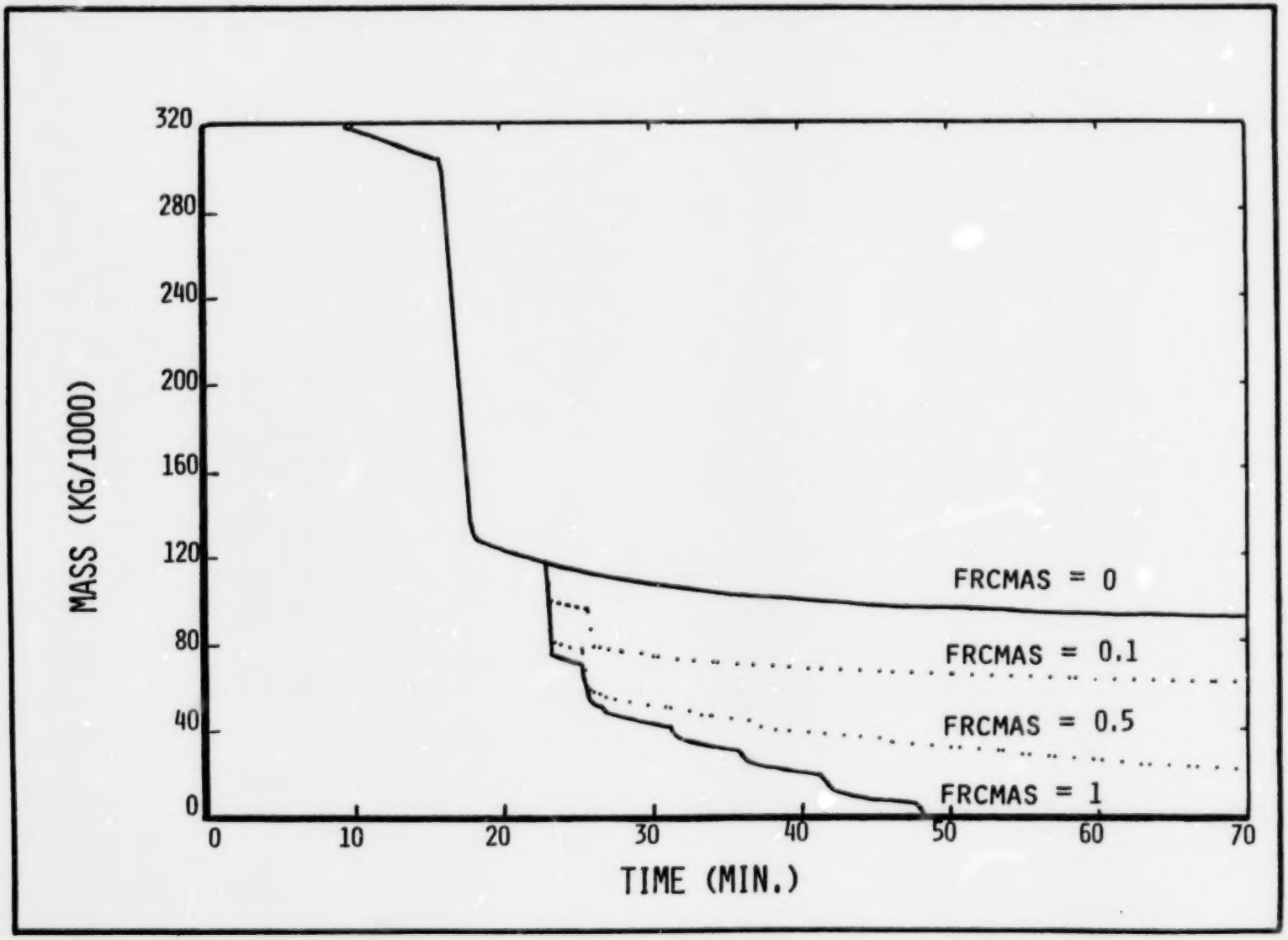

FIG. 27 EFFECT OF FRCMAS ON MODERATOR REMAINING IN CALANDRIA

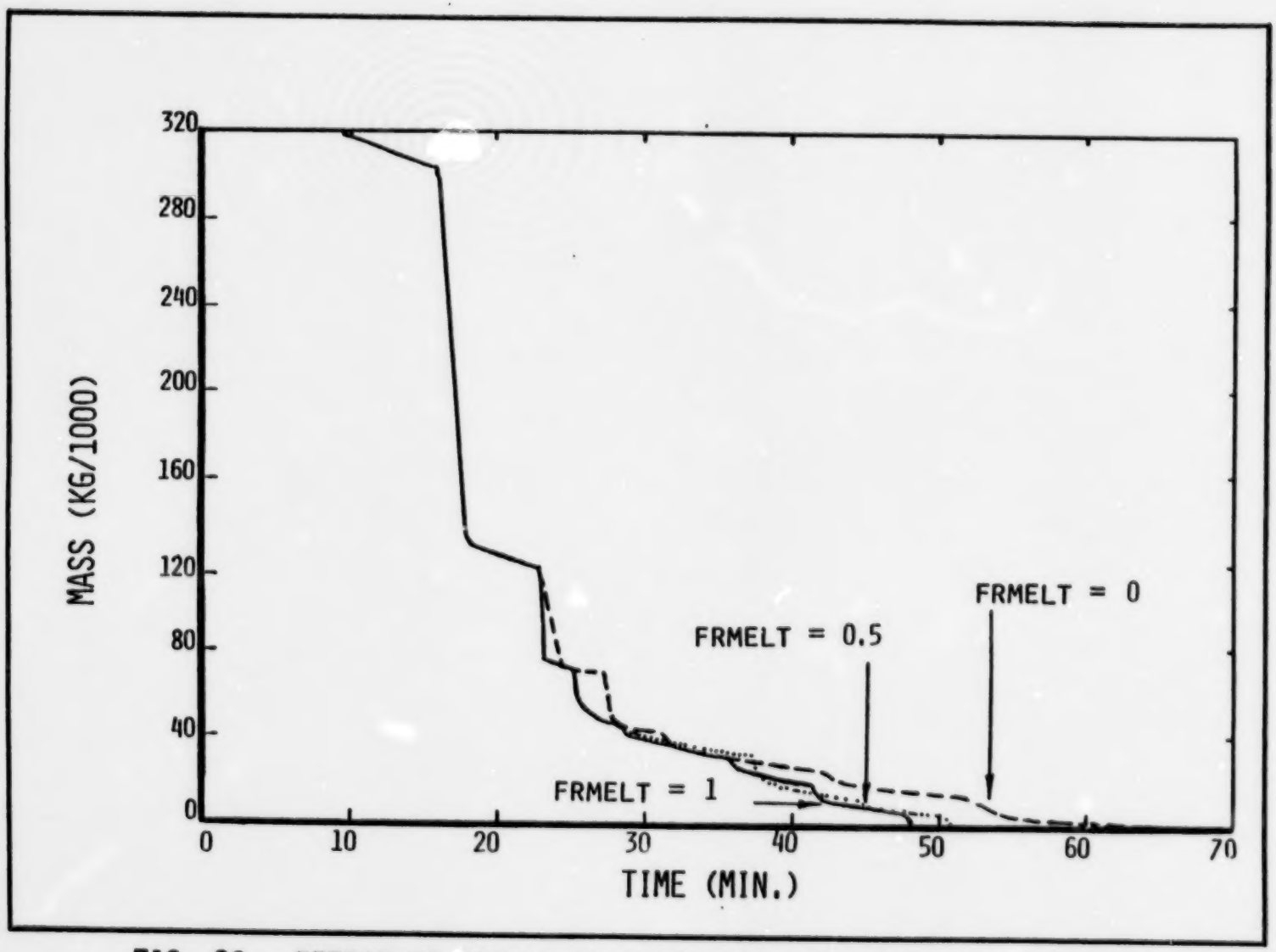

FIG. 28 EFFECT OF FRMELT ON MODERATOR REMAINING IN CALANDRIA

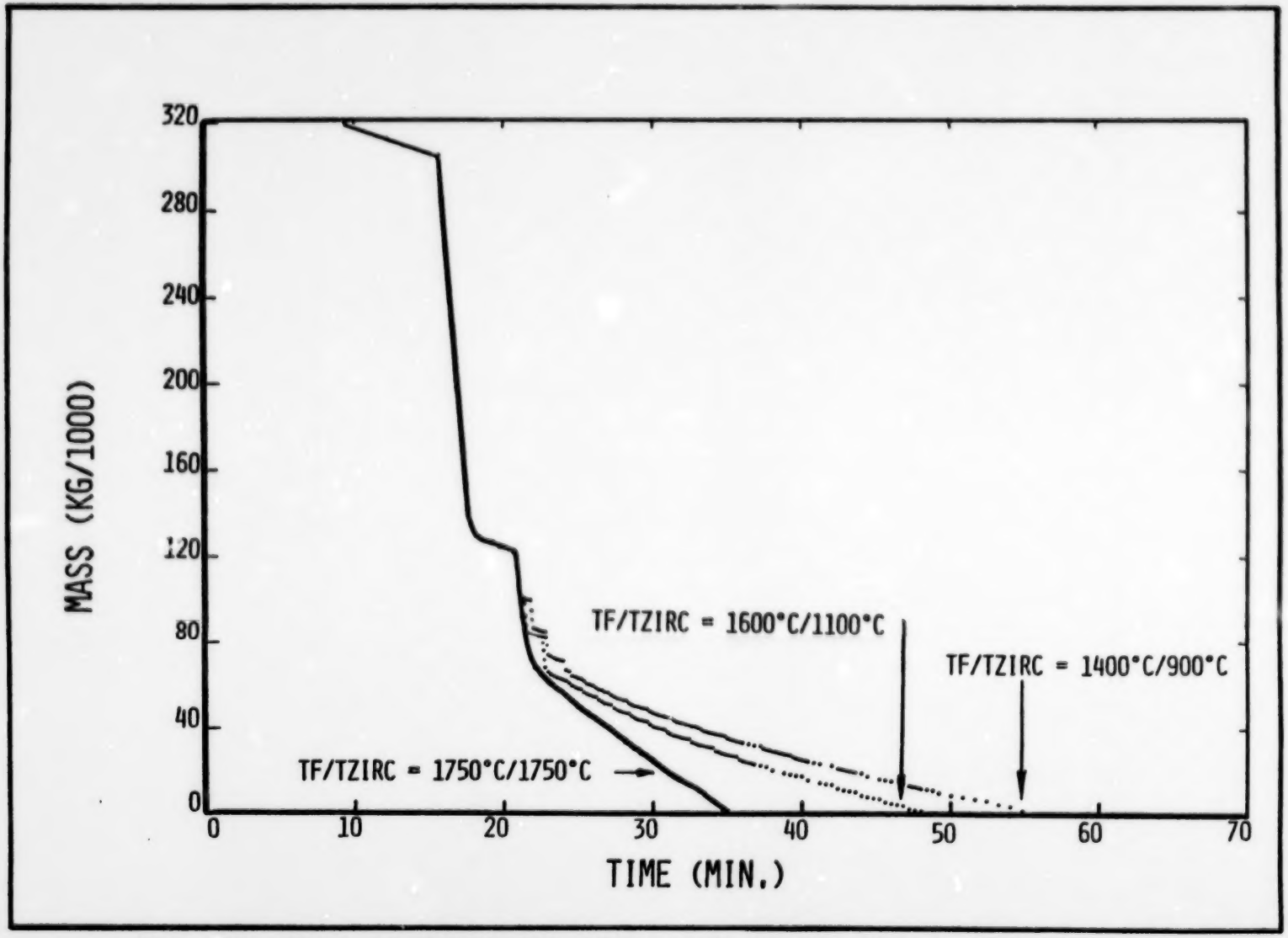

FIG. 29 MASS OF MODERATOR REMAINING IN CALANDRIA WITH INSTANTANEOUS DISINTEGRATION. EFFECTS OF DEBRIS TEMPERATURE.

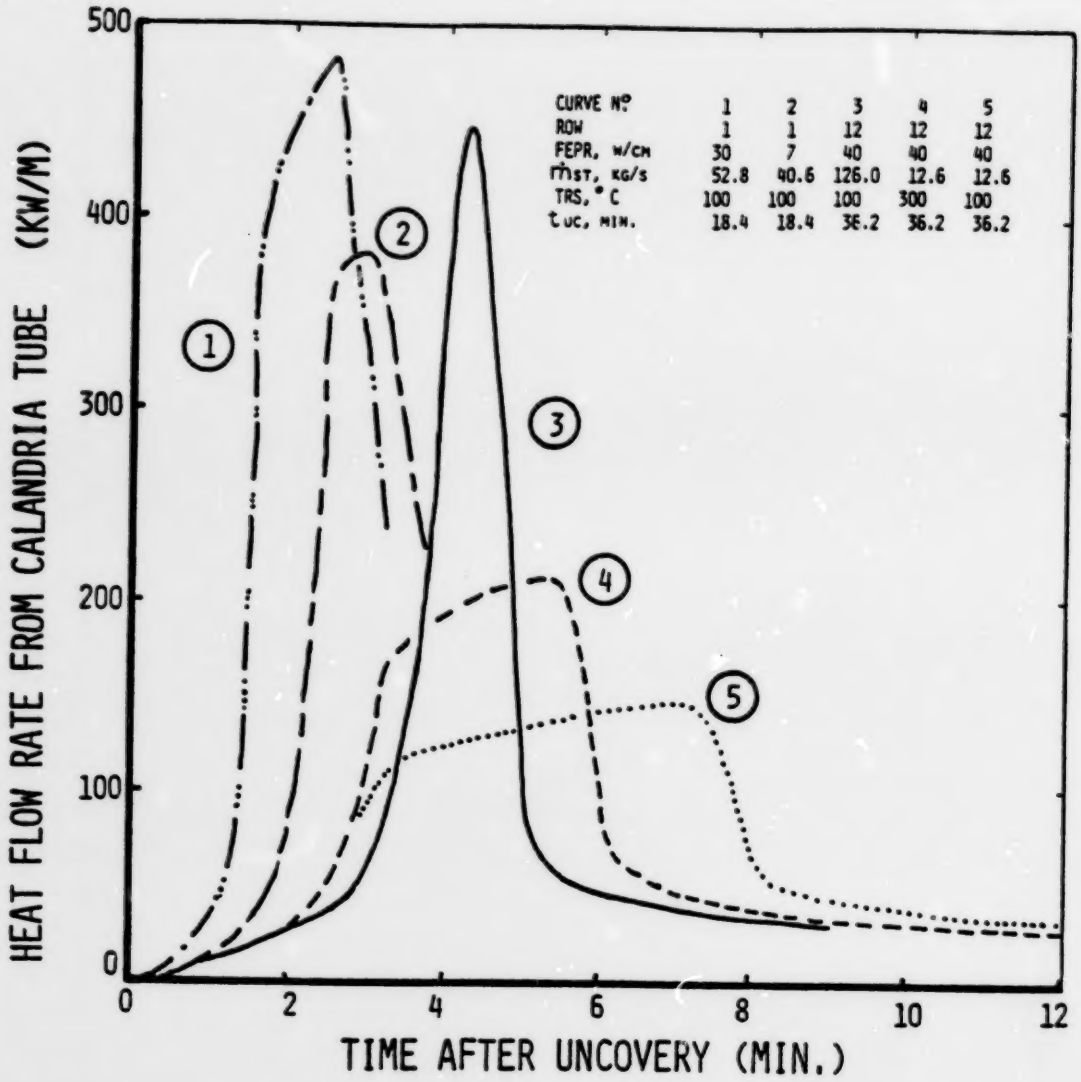

FIG. 30 HEAT FLOW RATES FROM UNCOVERED CALANDRIA TUBES TO STEAM FLOW FOR VARIOUS CONDITIONS.

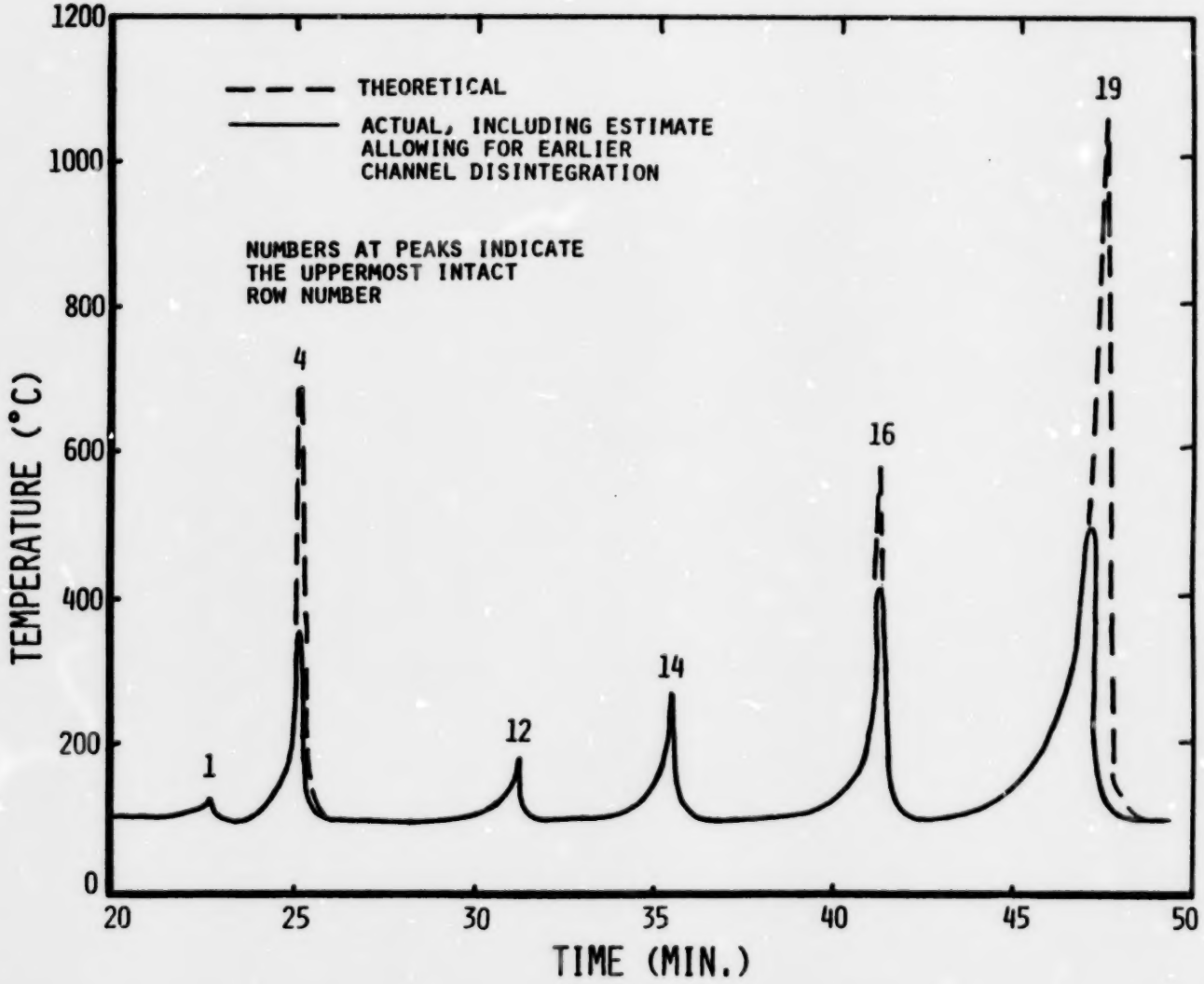

FIG. 31 ESTIMATED STEAM TEMPERATURE AT UPPERMOST ROW OF INTACT TUBES

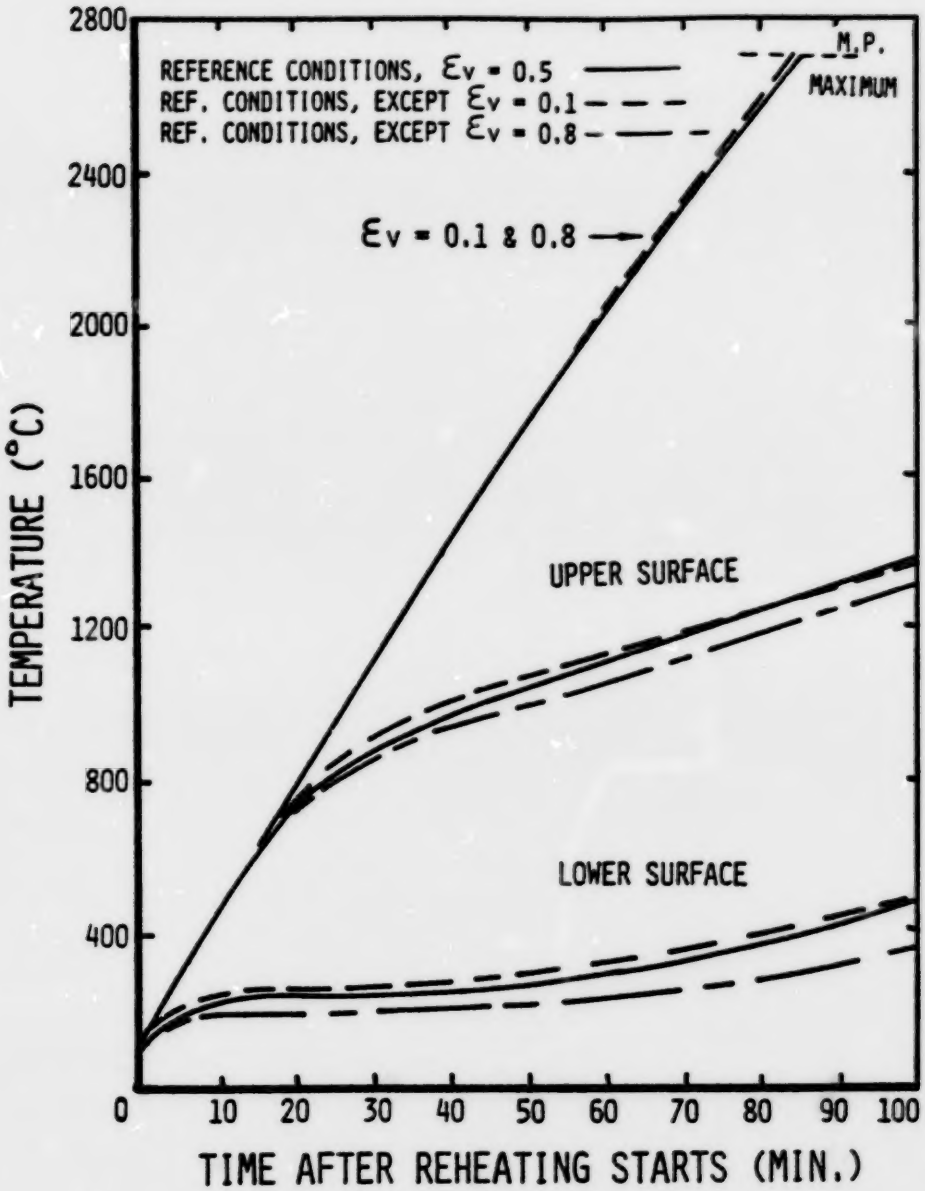

FIG. 32 TEMPERATURES IN POROUS BED OF SOLID CORE DEBRIS

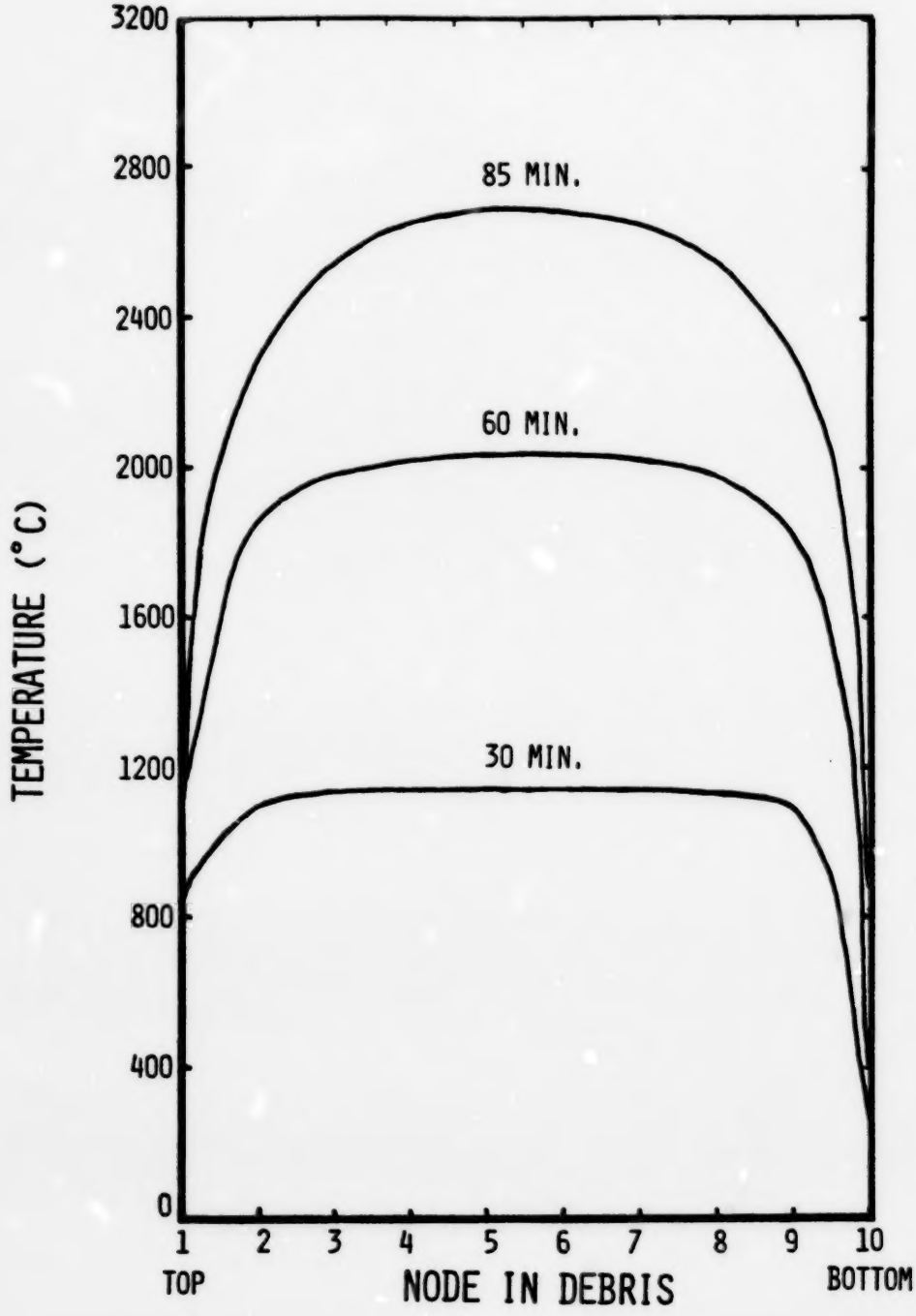

FIG. 33 TEMPERATURE PROFILES ACROSS POROUS BED OF SOLID CORE DEBRIS. REFERENCE CONDITIONS

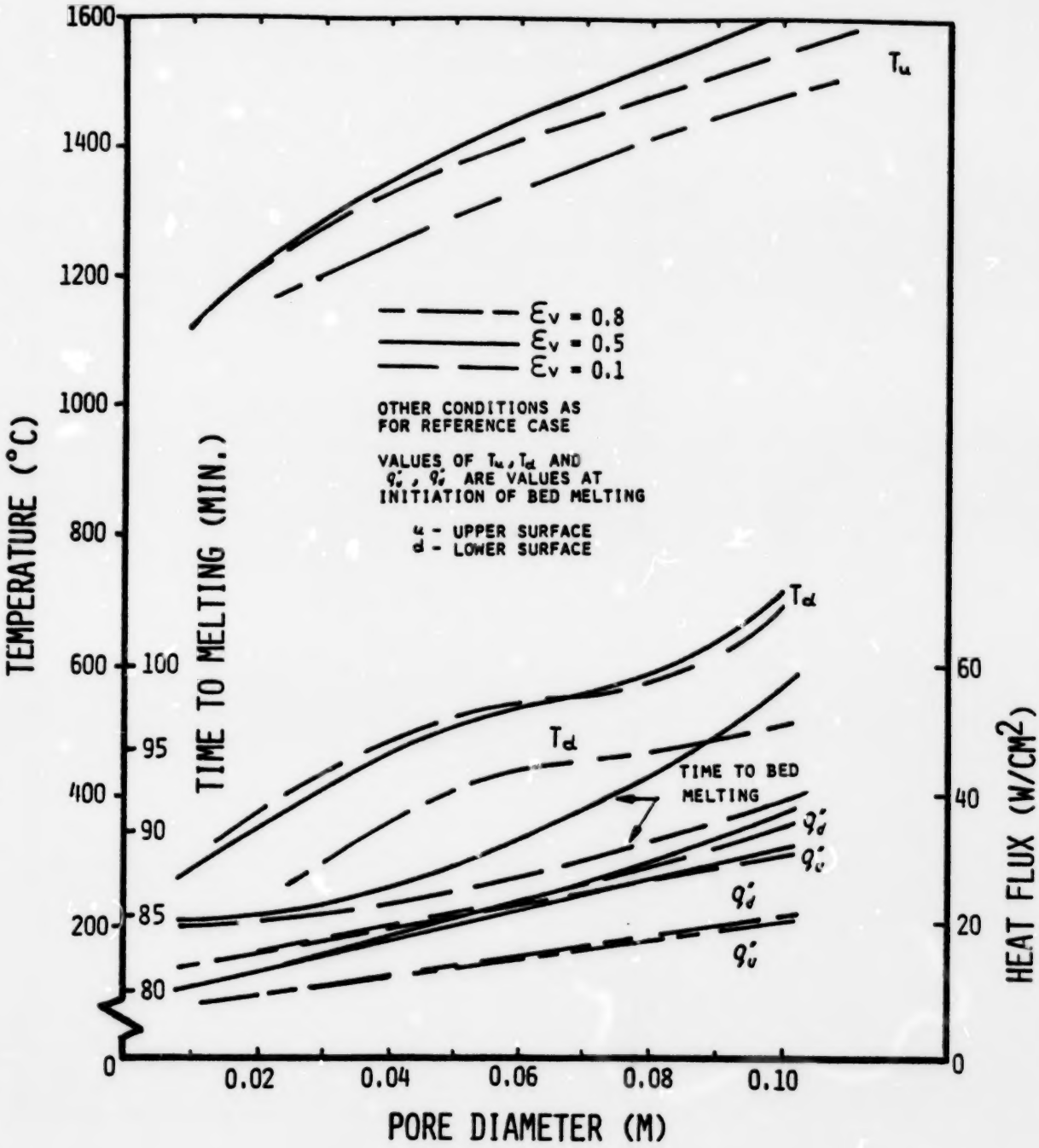

FIG. 34 EFFECT OF PORE SIZE ON CHARACTERISTICS OF POROUS DEBRIS BED

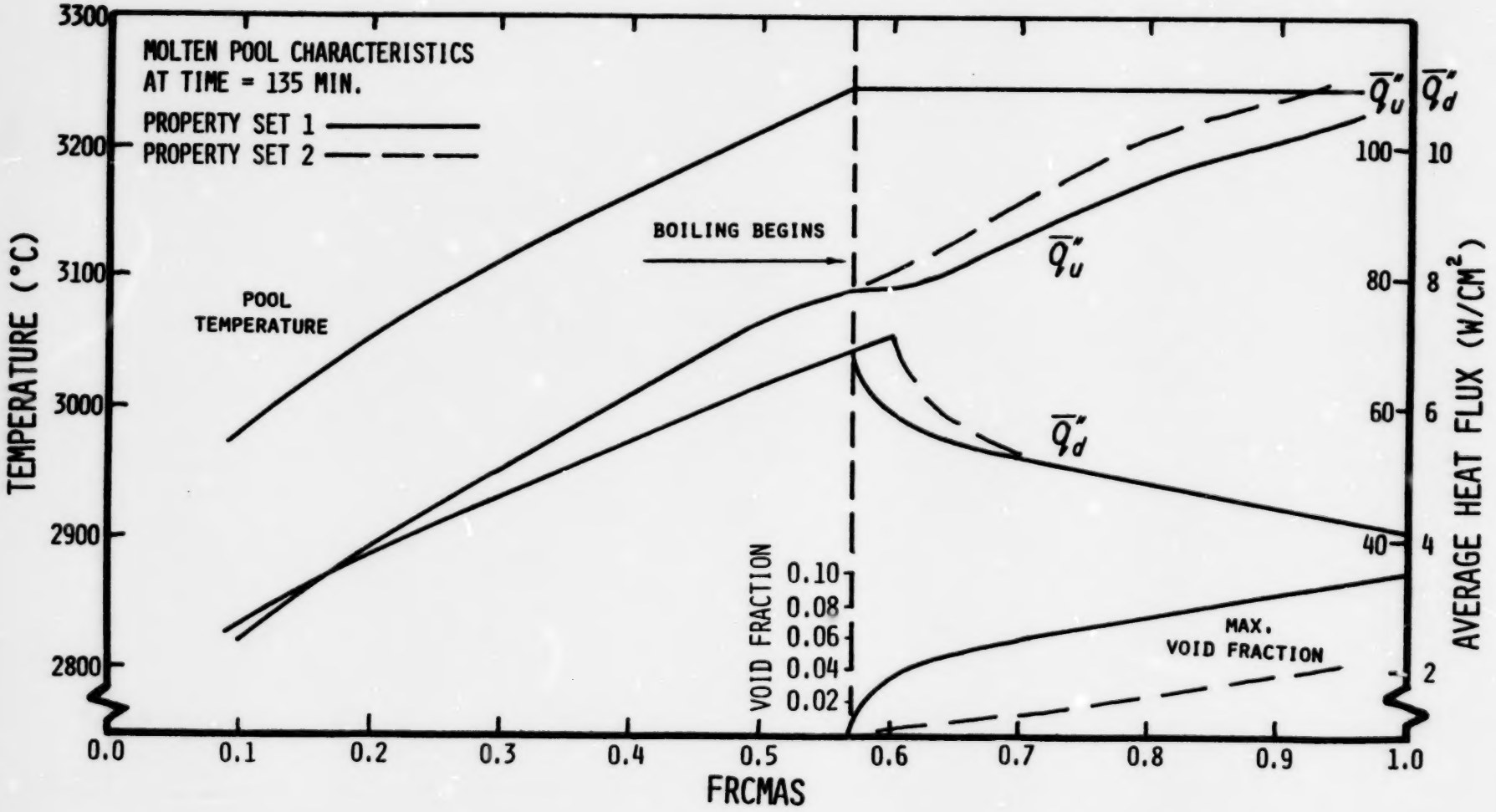

FIG. 35 CORE DEBRIS MOLTEN POOL CHARACTERISTICS FOR PROPERTY SETS 1 AND 2

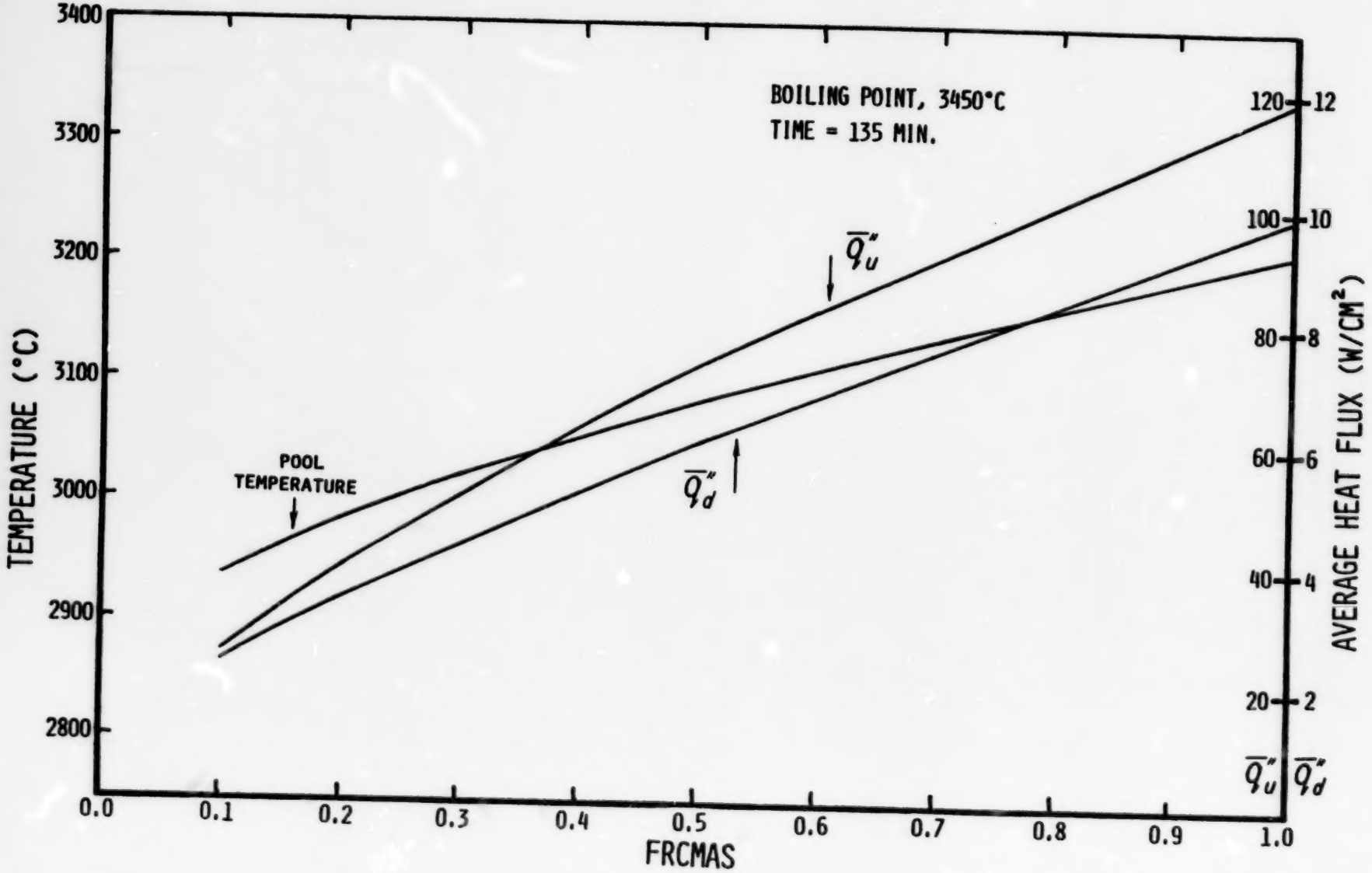

FIG. 36 CORE DEBRIS MOLTEN POOL CHARACTERISTICS FOR PROPERTY SETS 3 AND 4

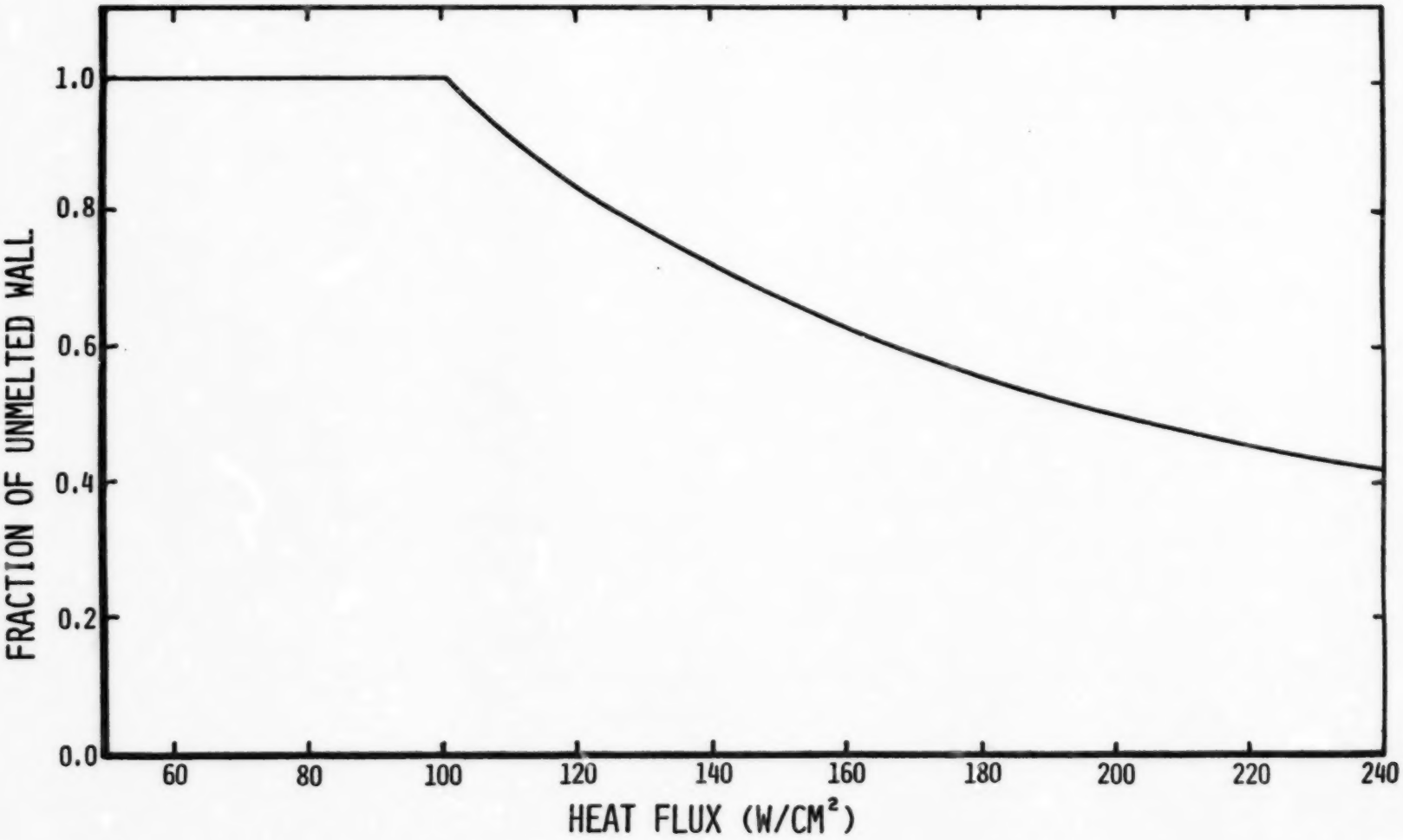

FIG. 37 EFFECT OF HEAT FLUX FROM CORE DEBRIS MOLTEN POOL ON CALANDRIA WALL

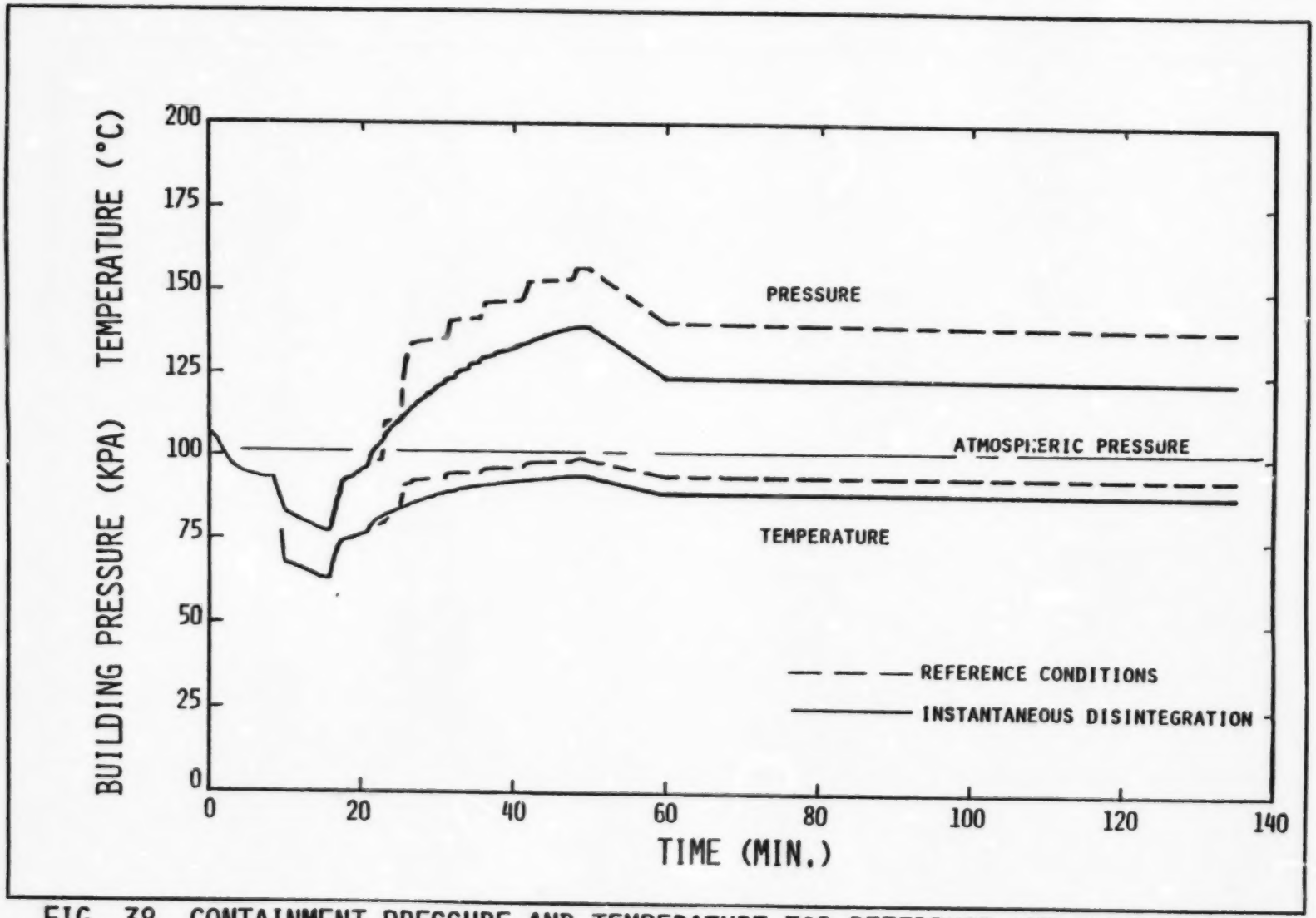

FIG. 38 CONTAINMENT PRESSURE AND TEMPERATURE FOR REFERENCE AND INSTANTANEOUS DISINTEGRATION CONDITIONS.

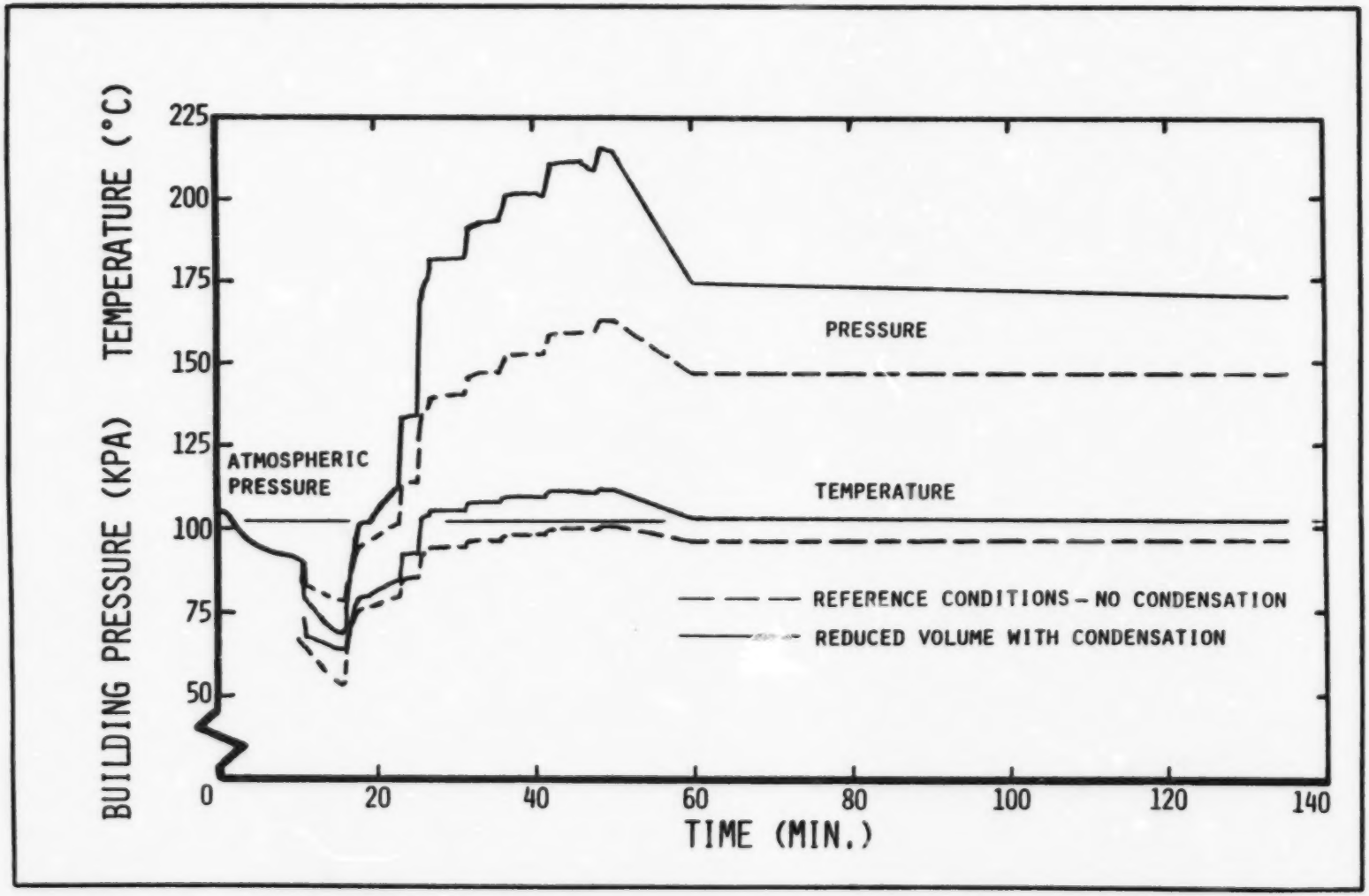

FIG. 39 CONTAINMENT PRESSURE AND TEMPERATURE SENSITIVITY STUDY RESULTS.

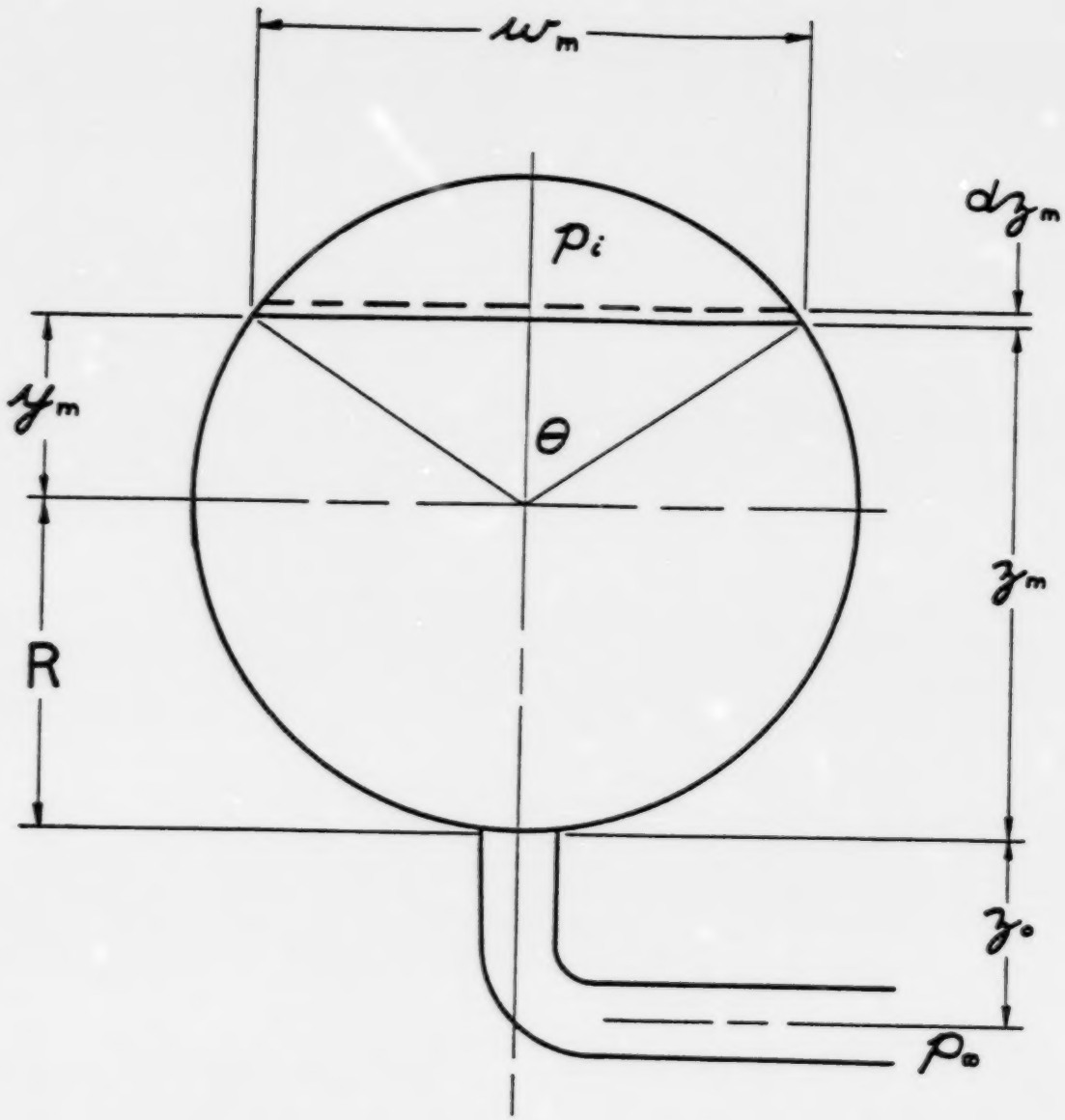

FIG. 40 MODEL FOR MODERATOR DRAINAGE FROM CALANDRIA. ACCIDENT SEQUENCES S13 AND S14

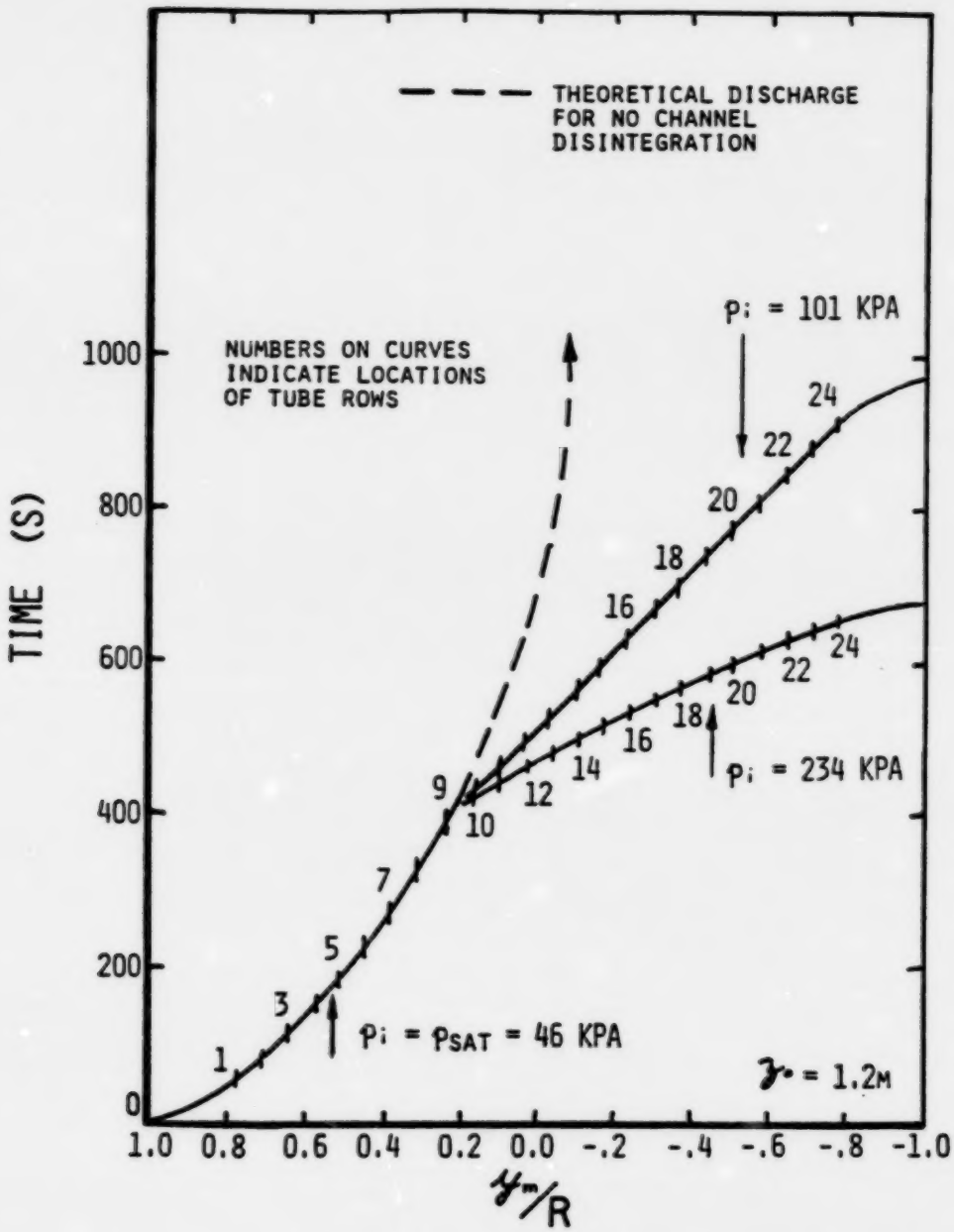

FIG. 41 MODERATOR LIQUID LEVEL IN CALANDRIA. ACCIDENT SEQUENCES S13 AND S14

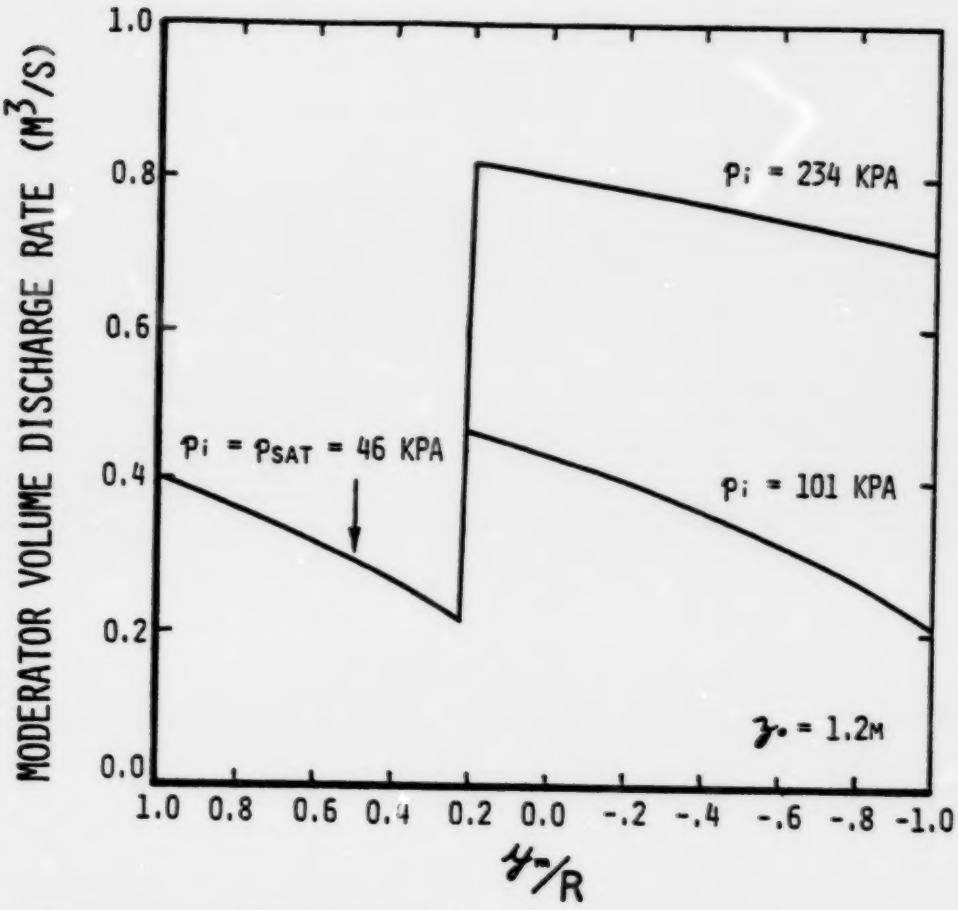

FIG. 42 VOLUMETRIC DISCHARGE RATES FROM CALANDRIA. ACCIDENT SEQUENCES S13 AND S14

ACKNOWLEDGEMENTS

The work described in this report was undertaken for the Atomic Energy Control Board under contract OSU82-0079.

Considerable additional support for the work was provided through NSERC Research Grant A6342.

The significant contributions of research associates T.C. Currie, J.C. Atkinson and R. Dick to the work are gratefully acknowledged.

Assistance was also provided from time to time during the course of the project by undergraduate students E. Antecol, G. Sanderson and B. Ham.

Sincere thanks are extended to Mrs. Ruth Thomas for the painstaking job of typing the report.

The advice of Dr. F.R. Campbell and his colleagues on the AECB staff was helpful in the original definition of the accident sequences.

Thanks are extended to W.T. Hancox and H.E. Rosinger of WNRE and to D.A. Meneley and R.E. Pauls of Ontario Hydro for information provided.

The author sincerely thanks W.T. Hancox, H.E. Rosinger and their colleagues at WNRE for the opportunity to discuss this work during a visit to WNRE in April, 1983.

POOR

QUALITY

ORIGINAL